Programmable logic construction kit for massive qualitative analysis of neuronal networks with an application to machine olfaction

Thesis submitted for the degree of

Doctor of Philosophy

at the University of Leicester

by

Ruben Guerrero

Department of Engineering

University of Leicester

Supervisor:

Dr. Tim C. Pearce

January 2009

abstract

Programmable logic construction kit for massive qualitative analysis of neuronal networks with an application to machine olfaction,
RUBEN GUERRERO-RIVERA

In this thesis, a construction kit for the implementation of neuronal networks on Field Programmable Gate Arrays (FPGA) is presented. The utility of this technology for the implementation of neuronal networks becomes apparent when we show that is possible to perform hyper-real time operation, a feature which allows neuronal networks designers to analyse in great detail the dynamics of their networks through the means of a comprehensive behavioural analysis.

Additionally, the construction kit presented here is used to implement a biologically inspired version of the mammalian olfactory bulb based on previous work by T. C. Pearce et al. (2005). The results we obtain show that tasks such as identification, classification and segmentation of odours are successfully performed by the olfactory bulb model. We illustrate the practical utility of the model by including experiments using real odour information.

Finally, a comprehensive behavioural analysis is performed by means of a massive exploration of the characteristics of the response of the model as it was subjected to different conditions of certain parameters. Results show that as the stimulating input approaches the trained input (target odour), the response tends to reach an attractor. This comprehensive analysis, made it possible to observe the effects of the training on the model response.

To God.

To my wife Lizda whose unconditional support made this possible.

To my kids: Itzel, Gilda, Jaydy and Luken whose smiles make my life happier.

Contents

List of Figures

List of Tables

Acknowledgements

There is undoubtedly one person whose help and support was determinant during my Ph.D., I am talking about Dr. Tim C. Pearce, my supervisor, a person who knows how to be a friend, a supervisor and a motivation, many thanks!.

Great thanks goes to my beautiful wife Lizda and adorable kids Itzel, Gilda, Jaydy and Luken, for their unfaltering support and enthusiasm.

Thanks also goes to my parents and parents in law. I would never end listing all the things I am grateful for.

I am thankful to my friends Serge, Kwok, Hannah, Juan, Carlos and Matias for all those happy times and especially for those Friday movies and chickens we shared together.

I would like to thank the researchers of Tufts University lead by Dr. D. Walt, who kindly agreed to supply their data for testing the olfactory bulb.

Finally, thanks to CONACYT, my sponsor, whose contribution made possible my Ph.D. along these years.

Publications

Peer reviewed articles

Guerrero-Rivera, R., Morrison, A., Diesmann, M., and Pearce, T. C. (2006). Programmable Logic Construction Kits for Hyper-Real-Time Neuronal Modeling. Neural Computation (2006), 18 pp. 2651-2679.

Guerrero-Rivera, R., and Pearce, T. C. (2007). Attractor-based pattern classification in a spiking FPGA implementation of the olfactory bulb. 3rd International IEEE EMBS conference on neural engineering (2007).

Chapter 1

Introduction

1.1 Research problem and justification.

Over the years, a variety of techniques for modelling neuronal networks have been developed (Wijekoon & Dudek, 2008; Balzera, Takahashia, Ohtaa, & Kyuma, 1991; Nabet, Darling, & Pinter, 1992). As the necessity for implementing larger networks increases (Siwei & Zhen, 1998; Nakamura, Sawai, & Sugiyama, 1992; Kazuki, Yoshihiro, & Sei, 1990), current implementation approaches present serious limitations. For instance the hardware requirements needed to process the information utilized and generated by the model become more significant (Andonie, Chronopoulos, Grosu, & Galmeanu, 2005). Additionally, the insufficient speed of existing approaches results in considerable processing time and hence longer waiting periods until results become available. There is thus a need for new approaches to the implementation of neural network-based applications. We

therefore ask the following questions:

- Can we implement neuronal networks using existing technologies so that hyper real-time performance can be achieved?
- If so, would such an approach also result in benefits for the analysis of neuronal networks?

Answering these questions favourably would put us in a position to offer a better way to design, develop and implement (relatively) complex neuronal networks.

In this thesis, we first prove that is possible to come up with a programmable logic construction kit for neuronal modelling which offers hyper real-time performance, flexibility and re-usability. Next we are interested in using this kit to both solve an existing open problem and demonstrate its advantages over other technologies.

For a suitable example application for the proposed construction kit for neuronal modelling, we turn to the field of the bioengineering. More precisely, the selected application involves the olfactory sense. Apart from allowing us to enjoy and distinguish odours, this sense also helps us take critical decisions such as avoiding dangerous environments (due to the presence of toxic substances), or classifying odours based on their molecular structure and concentrations. Additionally, risky activities such as the search for drugs or explosives unavoidably rely on the detection of substances. It is therefore of great interest to develop a device capable of carrying out the duties of the olfactory sense (detection and classifi-

cation) without human intervention. Leaving the humans out of risky activities (such as the ones mentioned above) would considerably reduce unnecessary exposure to potentially dangerous situations. For these reasons, we choose a simplified model of the olfactory bulb (the central part of the olfactory sense) as an example application using our construction kit for neuronal modelling.

If successful, our olfactory bulb model could in principle be used in a variety of applications. Among these we can mention:

- Safety: Gas detection (Kish et al., 2005).
- Food industry: Bacteria detection (Alocilja, Ritchie, & Grooms, 2003), coffee classification (Pardo & Sberveglieri, 2002).
- Military: Explosives detection (King, Horine, Daly, & Smith, 2004).
- Wine and beer industry: Identifying and classifying wines according to chemical concentrations (Lozano et al., 2006; Rodriguez-Mendez et al., 2004), and monitoring the flavour of beers (Pearce, Gardner, Friel, Bartlett, & Blair, 1993).

The example application presented in this thesis builds upon previous research done in the Bioengineering Laboratory of the University of Leicester by Dr. Tim C. Pearce and Dr. Carlo Fulvi-Mari (Pearce et al., 2005), whose simplified model of the olfactory bulb is implemented using the construction kit for neuronal modelling described here.

We should stress that it is important not only to be able to effectively detect and classify odours, but equally to perform it in real time, meaning that odour identification should be accomplished within the first seconds after it was initially detected. This is where the FPGA stands out from other integrated circuits: due to its inherent capability for parallel processing circuits, it permits the implementation of systems at high speeds.

Finally, we will show that a comprehensive behavioural analysis of the model, only possible due to the hyper real-time performance of the neuron model, can be used to gain a better understanding of the dynamics of the circuit.

1.2 Outline of the thesis

Chapter 2 reviews the foundations of the neuron. The morphology of a neuron is revised here, and some important concepts such as reversal potentials and ion channels are introduced. The Hodgkin-Huxley and Integrate and Fire models are reviewed. Finally, a description of the olfactory bulb is given in this chapter.

Chapter 3 details the programmable logic construction kit for neuronal modelling developed in this investigation. We show how the simplest of the linear ODE (ordinary differential equation) solvers can be used to formulate an exact calculation of the Integrate and Fire model and the synapse model. The synapse and soma models are discussed separately and a Register Transfer Level (RTL) description of the implementation is given. Both models are combined to

form the overall model of a neuron, the main processing element of the olfactory bulb. Other topics such as axonal delays and Spike-Timing Dependant Plasticity (STDP) are tackled here.

Chapter 4 introduces the olfactory bulb model starting from the connection of the neurons to proceed to show some results which include a comparison between the model response and its respective exact solution. The Hebbian learning algorithm is also reviewed here, as well as the integration of the model with external devices (PC), which forms the basis for subsequent experiments. This chapter finishes by showing an odour classification experiment, in which the ability of the model to distinguish between two odours becomes apparent.

Chapter 5 presents an application of the olfactory bulb model using real odour information obtained in Tufts university (USA). Specifically, this chapter provides solutions to an identification problem and a classification task. The capabilities of the olfactory bulb model to 1) detect a target odour and 2) discriminate odours are demonstrated with real data.

Chapter 6 exemplifies the most important advantage of the construction kit presented in chapter 3: the ability to perform a comprehensive analysis of the behaviour of the network under study. This feature is demonstrated by a broad behavioural analysis of the olfactory bulb which is carried out by investigating of the effects of 1) the input on the olfactory bulb and 2) the synaptic weights on the response of the model. This chapter is perhaps the most important one in

the thesis, since the advantages of the proposed model over other approaches are evidenced by the two experiments presented here. Finally, chapter 7 concludes the thesis.

Chapter 2

Foundations

2.1 The basic neuron

A neuron in its more general form is made up of a dendritic tree (with synapses that act as input terminals), a soma (cell body) and an axon (output terminal). Synapses are where an axon from a presynaptic neuron connects with the dendrite of a postsynaptic neuron (Figure 2.1), however, there is no physical connection between them, there is rather a very small gap called the synaptic cleft (Kandel, Schwartz, & Jessel, 2000). Once a spike is generated in the presynaptic neuron, this travels along its axon, and when the action potential reaches the ends of the axon, a chemical process gives rise to a release of a neurotransmitter which travels toward the dendritic terminal, passing across the synaptic cleft. On the other side, at the dendrite of the postsynaptic neuron, a group of receptors detects the presence of the neurotransmitter, activating special channels which permit the

influx and efflux of ions contained in the surroundings of the neurons and within the plasma membrane of the cell. This causes a synaptic current which results in a change in the membrane potential. Multiple occurrences of action potentials could increase the membrane potential in such a way that if it exceeds a threshold value (threshold potential) the postsynaptic neuron fires, emitting a spike which travels to further neurons (McCormick, 1998). This results in the membrane potential resetting to a certain level of voltage called the after-hyperpolarization potential. After an action potential is generated, there is a period where the neuron is not able to emit any spike, which is known as "absolute refractory period". This is followed by the "'relative refractory period"' during which although it is not impossible to emit another spike, it requires large input for the neuron to fire an action potential (Levitan & Kaczmarek, 1997). In the nervous system, thousands of neurons are interconnected forming a complex network, all of them communicated by mean of spikes governed by the same dynamics (Dayhoff, 1990).

2.1.1 Reversal Potential

A neuron is surrounded by a semi-permeable plasma membrane which isolates the internal part of the cell from the external environment. The neuron is enclosed by this membrane, which contains protein pumps and channels, determining the electronic and chemical properties of the cell by means of influx and efflux of ions. Internally, the neuron contains ions of several chemicals at different concentrations than the existing in the surrounding extracellular fluid of the neuron (Figure 2.2),

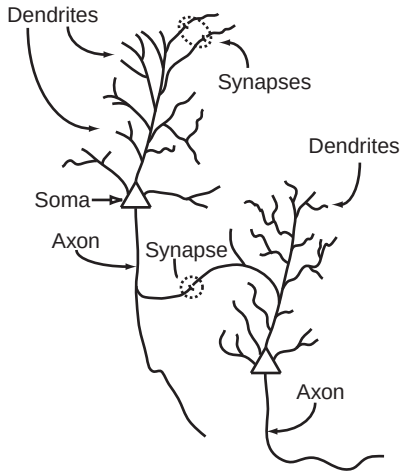

Figure 2.1: Neuron elements. Sketch of the different elements of a neuron, dendrites are joined to the soma while axons leave from the soma toward other dendrites. Connections between dendrites and axons form a synapse (dotted circles), adapted from Gerstner & Kistler, 2002.

on the outside, sodium, calcium and chloride exist in much higher concentrations, by contrast, potassium ions have higher concentrations on the inside (McCormick, 1998).

From electrical theory, we know that wherever a charge movement is present, a voltage difference is caused. This voltage is called the "Nernst potential" and is calculated by the formula (Hille, 2001)

$$\Delta u = \frac{kT}{q} \ln \frac{[S]_o}{[S]_i}, \tag{2.1}$$

where k is the Boltzmann constant, T the temperature, q is the static charge of the considered ion, and, $[S]_o$ and $[S]_i$ the ionic concentration outside and inside the membrane respectively.

At equilibrium, the Nernst potential (reversal potential in the context of the

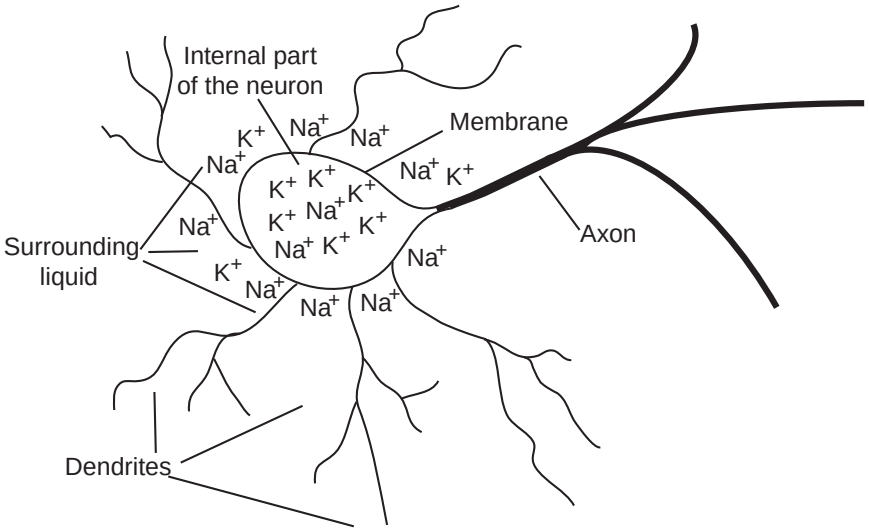

Figure 2.2: The internal part of the neuron contains more potassium ions than the surrounding fluid. Conversely, sodium ions are more common in the surrounding fluid than within the neuron. Besides sodium and potassium, other ionic concentrations (not shown) are present on the neuron, and together they form up the electrochemical properties of the neuron.

neuron) due to sodium ions is around 62 mV regarding the surrounding liquid. In the same way, the reversal potential of the potassium is around -103 mV, at body temperature (37°C). When the voltage difference is either above or below the reversal potential, then an ionic flux is induced to counteract this situation (McCormick, 1998).

Apart from sodium and potassium, there are more different types of ions around the neuron. Altogether, they contribute to settle the membrane potential between -60 mV and -75 mV, consequently, pumps and channels actively transport ions from (to) the neuron to (from) the surrounding liquid. The membrane potential at equilibrium is called "resting potential" and is an important value in modelling neurons (Hille, 2001).

2.1.2 Ion channels

The neuron can be seen as being controlled by a set of input and output currents, that runs through the many channels of the neuron. Several types of channels have been identified in neurons, and each type has special characteristics that control the ionic flux into/from the neuron. The most common types of channels used in neural modelling are: sodium channels (Na^+), potassium channels (K^+) and calcium channels (Ca^+). Channels are a very important part of the neuron because they are responsible of many special characteristics of the neuron such as postinhibitory rebound and adaptation.

2.1.2.1 Sodium channels

Apart from the sodium channel described by (Hodgkin & Huxley, 1952d) there is a persistent sodium current found in neurons from the mammalian CNS. This non-inactivating sub-threshold sodium current (I_{NaP}) is activated about -10 mV to the transient sodium current, where few voltage-gated channels are activated, and neuron input resistance is high. I_{NaP} adds to synaptic current, increasing effectiveness of digital depolarizing synaptic activity (Crill, 1996).

2.1.2.2 Potassium Channels

Voltage and ion-gated ion channels determine how the synaptic currents are integrated into a pattern of action potentials. Potassium channels are very diverse and control aspects of membrane excitability such as the delay in spiking response

to sustained synaptic input, the frequency of action potentials and the degree of accommodation within a burst (Kuenzi & Dale, 1998). The rapidly inactivating outward current (I_A) is a type of potassium current. Depolarizing voltages from -90 mV elicits a low threshold inactivating outward current I_A, as well as a higher threshold current, which is composed of non-inactivating and slowly inactivating components. The latter typically with bi-exponential decay (Banks, Haberly, & Jackson, 1996).

2.1.2.3 Calcium channels

Voltage-dependent calcium channels play a dual role in the CNS, they couple electrical activity to calcium influx, and they contribute to membrane properties that determine the precise nature of excitability in different cell types (Talley et al., 1999). Several different voltage-gated calcium channels have been described in neurons. Biophysical criteria effectively separate low-voltage-activated (LVA) from high-voltage-activated (HVA) calcium currents (Talley et al., 1999).

LVA calcium currents activate at hyper-polarizing potentials and inactivate rapidly relative to HVA currents (Lorenzon & Foehring, 1995). LVA channels can be activated by small depolarizations of the plasma membrane, as they are rapidly inactivated, they are also called T-type channels, where T stands for transient (Perez-Reyes, 2003). Functional roles for T currents include generation of low-threshold spikes that lead to burst firing, promotion of intrinsic oscillatory behaviour, boosting of calcium entry and synaptic potentiation (Huguenard, 1996).

HVA calcium channels are slowly inactivated ($\tau \approx 2000$ ms), thus, HVA Ca^{2+} channels are also called L-type channels, where L stands for long lasting (Perez-Reyes, 2003). L-type calcium channels activation is potentiated by strong depolarizations (Kammermeier & Jones, 1997). Activation of L-type Ca^{2+} channels plays a role in the increased firing rate in some type of neurons (Filosa & Putnam, 2003).

In many neurons, the activation of voltage-gated calcium channels during the action potential leads to a prolonged after-hyperpolarization (AHP) lasting several seconds. the AHP causes spike frequency adaptation and is a major determinant of cell excitability (Martinez-Pinna, Davies, & McLachlan, 2000). Long lasting AHPs are attributed to the activation of a calcium-dependent potassium current channel (Constanti & Sim, 1987).

2.1.3 Synapses

Information flows from one neuron to the next at specialized points of contact known as synapses, which provide a unidirectional flow of information from the presynaptic to the postsynaptic neuron (Stevens & Zhu, 2003).

Synapses come in two different types, chemical and electrical, which, chemical are by far the most abundant. These use a chemical neurotransmitter that is released to the postsynaptic receptors that either open an ion channel or activate a G-protein coupled receptor (Gibson & Connors, 2003). Synaptic communication between neurons involves conversion of a presynaptic electrical signal (the action

potential), into a chemical signal (the neurotransmitter) and then back into an electrical signal (the postsynaptic potential) (Nicoll, Frerking, & Schmitz, 2000).

According with the reversal potential, synapses with reversal potential less than the threshold for action potential generation are called inhibitory, while those with reversal potentials above the action potential threshold are called excitatory (Dayan & Abbott, 2001). Synaptic currents generated by an action potential are given by (Tan, Zhang, Merzenich, & Schreiner, 2003).

$$I_{syn}(t) = g_{syn}(t)[u(t) - E_{syn}], \tag{2.2}$$

where $g_{syn}(t)$ is a time dependent function of the synapse conductance, E_{syn} is the reversal potential of the synapse which value depends on the type of synapse, $u(t)$ is the membrane potential and $I_{syn}(t)$ is the current induced by a presynaptic spike.

2.1.3.1 Excitatory synapses

Glutamate is the main excitatory neurotransmitter in the mammalian CNS, and mediates neurotransmission across most excitatory synapses (Kemp & McKernan, 2002). Glutamate usually acts on two distinct classes of receptors, a non-N-methyl-D-aspartate receptor (non-NMDA) and NMDA receptors (Edmods, Gibb, & Colquhoun, 1995).

Channels activated by NMDA are controlled by both the presence of amino

acid and a voltage-dependent channel which is blocked by concentrations of magnesium ions [Mg^{2+}] (Jahr & Stevens, 1990a). Magnesium concentrations inhibit the activation of the channels at hyper polarized potentials in such a way that channels are completely closed below -80 mV, however, at higher membrane potentials, channels start to conduct. The voltage-dependent gating properties of NMDA-receptor channels are given by (Jahr & Stevens, 1990b)

$$g_\infty(u, [Mg^{2+}]_o) = \frac{1}{1 + \frac{e^{\alpha u}[Mg^{2+}]_o}{\beta}}, \tag{2.3}$$

where $\alpha = 0.062$ mV, $\beta = 3.57$ mM and $[Mg^{2+}]_o$ is the extracellular concentration in mM.

The NMDA synaptic currents are modelled by a conductance function consisting of three terms: the maximal conductance $\bar{g}_{NMDA}$, the time course of the current following the activation of the synapse and the voltage-dependence of the magnesium block $[Mg^{2+}]_o$ (Gabbiani, Midtgaard, & Knopfel, 1994). The conductance function is given by

$$g_{\mathrm{NMDA}}(t) = \bar{g}_{\mathrm{NMDA}} 1.358 (e^{-\frac{(t-t^{(f)})}{\tau_{\mathrm{decay}}}} - e^{-\frac{(t-t^{(f)})}{\tau_{\mathrm{rise}}}}) g_\infty, \tag{2.4}$$

with $\tau_{\mathrm{rise}} = 3$ ms and $\tau_{\mathrm{decay}} = 40$ ms.

On the other side, non-NMDA receptors show a faster response than NMDA receptors (Silver, Traynelis, & Cullcandy, 1992). Non-NMDA receptors can be further subdivided into AMPA receptors and Kainate receptors (Frerking, Malenka,

& Nicoll, 1998), which, AMPA receptors are the most generalized type of non-NMDA receptors. synaptic currents caused by AMPA receptors are modelled by (Gabbiani et al., 1994)

$$g_{\mathrm{AMPA}}(t) = \bar{g}_{\mathrm{AMPA}} 1.273 (e^{-\frac{(t-t^{(f)})}{\tau_{\mathrm{decay}}}} - e^{-\frac{(t-t^{(f)})}{\tau_{\mathrm{rise}}}}), \tag{2.5}$$

with $\tau_{\mathrm{rise}} = 0.09$ ms and $\tau_{\mathrm{decay}} = 1.5$ ms.

2.1.3.2 Inhibitory synapses

γ-Aminobutyric acid (GABA), which is synthesized from glutamic acid (Awapara, Landua, Fuerst, & Seale, 1950) constitutes the primary inhibitory neurotransmitter in the CNS (Graham & Kado, 2003). GABA acts on two pharmacologically distinct types of receptors, GABA_A and GABA_B (Jensen, & Mody, 2001). Activation of GABA_A receptors by synaptically released GABA increases membrane chloride conductance, producing an early inhibitory postsynaptic potential (IPSP). In contrast, GABA_B receptors increases membrane potassium conductance producing a late IPSP (Mott, Xie, Wilson, Swartzwelder, & Lewis, 1993).

The alpha function $kte^{-\frac{t}{\tau}}$ is often used as a standard model for the conductance response of GABA_A and GABA_B receptors to synaptic inputs (Bernard, Ge, Stockley, Willis, & Wheal, 1994), however exponential decays and beta functions are also used to model inhibitory conductances (Gerstner & Kistler, 2002b), &

Kistler, 2002 according with the models

$$g_{syn}(t) = \sum_f \bar{g}_{syn} e^{-\frac{(t-t^{(f)})}{\tau}}, \tag{2.6}$$

where $\bar{g}_{syn}$ is the maximum conductance, and

$$g_{syn}(t) = \sum_f (\bar{g}_{fast} e^{-\frac{(t-t^{(f)})}{\tau_{fast}}} + \bar{g}_{slow} e^{-\frac{(t-t^{(f)})}{\tau_{slow}}}), \tag{2.7}$$

whose conductance is made up of a fast and a slow component.

2.1.4 Neuron models

There are many different models used to reproduce the behaviour of a neuron, some of them treat with great detail several dynamics of the neuron, while others gather the most relevant characteristics of the neuronal behaviour and these are reflected in the model. Among the most popular neuron models are the Hodgkin-Huxley neuron model and the integrate and fire model.

2.1.4.1 Hodgkin-Huxley model

The Hodgkin-Huxley model originates from the experiments carried out on the giant axon of a squid ((Hodgkin & Huxley, 1952b), (Hodgkin & Huxley, 1952a), (Hodgkin & Huxley, 1952c), (Hodgkin & Huxley, 1952d)). Three different currents were identified by Hodgkin-Huxley: a sodium, a potassium and a leaky current made up of chloride and other ions ((Hodgkin & Huxley, 1952b), (Hodgkin

& Huxley, 1952c)). The results obtained show that the electrical behaviour of the membrane can be represented by the electrical network shown in Figure 2.3 ((Hodgkin & Huxley, 1952d)).

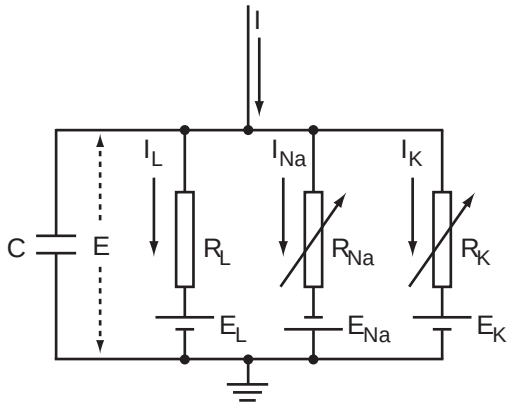

Figure 2.3: Equivalent electric diagram of the Hodgkin-Huxley model. The semi-permeable characteristic of the membrane is characterized by a capacitance (C), the voltage dependent sodium and potassium channels are represented by a variable resistance, while the leakage is represented as a constant resistance. Reversal potentials are characterized by batteries (Hodgkin & Huxley, 1952d).

The capacitance arises from the semi-permeable membrane surrounding the neuron. The two variable resistors correspond to the voltage dependent sodium and potassium channels. The batteries are equivalent to the reversal potentials and finally the fixed resistor corresponds to the leakage channel. Currents can be carried through the membrane either by changing the value of the membrane potential or by inducing an ionic current into the network (Hodgkin & Huxley, 1952d). Ionic currents come from the difference in ionic concentration at the neuron, and by the potential difference across the membrane, thus, current is zero at equilibrium potential, which is when the membrane potential is equal to the

resting potential (Hodgkin & Huxley, 1952b). Ionic currents are defined in terms of conductances given by (Hodgkin & Huxley, 1952a)

$$g_x = \frac{I_x}{[u(t) - E_x]}, \tag{2.8}$$

where I_x is the ionic current, and E_x is the resting potential of the x ion. A formal assumption used to describe sodium and potassium variable conductances are (Hodgkin & Huxley, 1952d)

$$\begin{aligned} g_{Na} &= \bar{g}_{Na} m^3 h, & (2.9) \\ g_k &= \bar{g}_k n^4, & (2.10) \end{aligned}$$

where g_{Na} and g_K are the variable conductances of the channels. Typical values are defined in Table 2.1 (Gerstner & Kistler, 2002b), m and n are the activation variables for the sodium and potassium respectively, and h is the inactivation variable for the sodium given by (Hodgkin & Huxley, 1952d)

$$\begin{aligned} m' &= \alpha_m(u)(1-m) - \beta_m(u)m, \\ n' &= \alpha_n(u)(1-n) - \beta_n(u)n, & (2.11) \\ h' &= \alpha_h(u)(1-h) - \beta_h(u)h, \end{aligned}$$

x	$E_x\,(mV)$	$g_x\,(mS/cm^2)$
Na	50.0	120.0
K	-77.0	36.0
L	-54.4	0.3

Table 2.1: Typical values of reversal potentials and conductances in the Hodgkin-Huxley model (Gerstner, & Kistler, 2002).

m, n and h represent the ionic concentration in a certain place (e.g. inside the neuron), while $(1 - n)$ represents the ionic concentration somewhere else (e.g. outside the neuron). α_x determines the rate of ion transfer from outside to inside, while β_x represents the ion transfer in the opposite direction (Hodgkin & Huxley, 1952d). α_x and β_x are defined in Table 2.2 (Gerstner & Kistler, 2002b).

x	$\alpha_x(u(t)/mV)$	$\beta_x(u(t)/mV)$
n	$\frac{(0.1-0.01u(t))}{\left(e^{(1-0.1u(t))}-1\right)}$	$0.125e^{-\frac{-u(t)}{80}}$
m	$\frac{(2.5-0.1u(t))}{\left(e^{(2.5-0.1u(t))}-1\right)}$	$4e^{-\frac{-u(t)}{18}}$
h	$0.07e^{-\frac{-u(t)}{20}}$	$\frac{1}{\left(e^{(3-0.1u(t))}+1\right)}$

Table 2.2: Definition of the functions α_x and β_x found by Hodgkin-Huxley to fit the dynamics of their model with the data (Gerstner, & Kistler, 2002).

Analysing the equivalent circuit (Figure 2.3), when a current is induced in the circuit, from the Kirchoff's law for currents we have that

$$I(t) = I_{cap}(t) + \sum_j I_j(t). \tag{2.12}$$

The current of the capacitor can be substituted by

$$I_{cap}(t) = C\frac{du}{dt}. \tag{2.13}$$

Rearranging the equation (2.12):

$$C\frac{du}{dt} = -\sum_j I_j(t) + I(t), \tag{2.14}$$

where C accounts for the membrane capacitance; u for the membrane capacitance and $\sum_j I_j$ for the sum of all the ionic currents of the neuron. Rewriting the equation using the formulas given for ionic currents, the Hodgkin-Huxley model becomes

$$C\frac{du}{dt} = -[g_{Na}m^3h(u(t) - E_{Na}) + g_K n^4(u(t) - E_K) + g_L(u(t) - E_L)] + I(t), \tag{2.15}$$

here, E_{Na}, E_K and E_L are the resting potentials of the sodium, potassium and the leakage channel, their values are given in the Table 2.1.

The Hodgkin-Huxley model accounts for several characteristics of the neuron, therefore constitutes a detailed neuron model of the giant axon of the squid, and is widely used in modelling neurons.

2.1.4.2 Integrate and fire model

The integrate and fire model is the simplest neuron model which mimics certain properties of a neuron (Feng & Brown, 2004). Consequently, they are easier to understand and analyse. In the integrate and fire model, the membrane potential starts from the resting state, rising or lowering according with the synaptic input, when the voltage reaches a certain threshold ϑ, the neuron fires an action potential and resets the membrane voltage to the resting state (Koch, Mo, & Softky, 2003).

In its simplest form, an integrate and fire neuron i consists of a resistor R in parallel to a capacitor C driven by an external current I_i (Figure 2.4). the voltage u_i across the capacitor is interpreted as the membrane potential. The voltage scale is chosen so that $u_i = 0$ is the resting potential. The membrane potential u_i in between action potentials is given by (Gerstner & Kistler, 2002a),

$$\tau_m \frac{du_i(t)}{dt} = -u(t) + RI_i(t), \tag{2.16}$$

where $\tau_m = RC$ is the time constant of the membrane. Networks combining integrate and fire neurons with synaptic plasticity carry out powerful computations that are not easily solved using traditional approaches (Spruston & Kath, 2004).

In this model, the active properties of the neural membrane responsible for spike generation are not explicitly taken into account, only the passive membrane properties are incorporated in the equation (Hansel, Mato, Meunier, & Neltner, 1998). A variant of the integrate and fire model based on Hodgkin-Huxley model

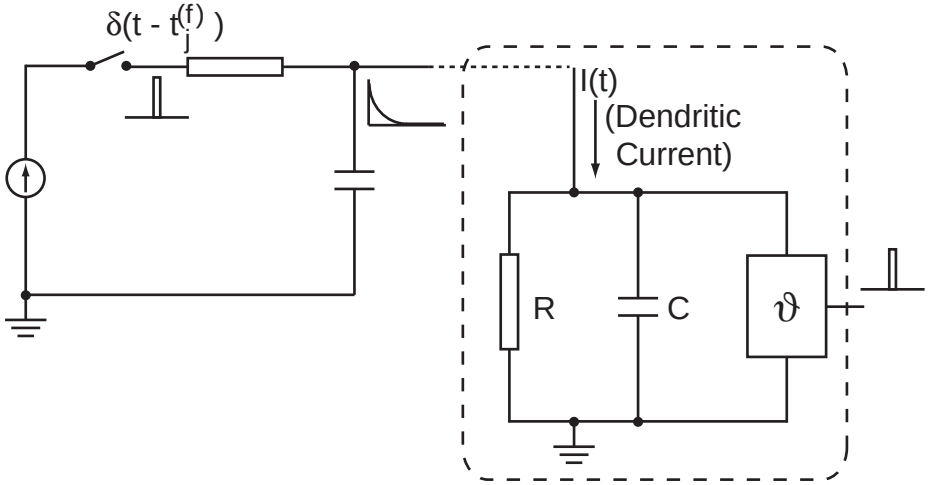

Figure 2.4: Schematic diagram of the integrate and fire model. The integrate and fire model (dotted square) receives dendritic current from the synapse (An exponential decay in this case), which is integrated by the RC circuit; the resulting membrane potential is compared against a threshold potential (ϑ), whenever the membrane potential is below the threshold potential, the integration should continue, once the membrane potential exceeds the threshold, a spike is generated and the membrane voltage is reset to the resting potential (adapted from Gerstner) .

equations captures conductances changes due to action potentials, which has a determinant influence on electro-physiological behaviour (Destexhe, 1997).

2.1.5 Learning algorithms

Changes in the synaptic connections between neurons are widely believed to contribute to memory storage, and the activity dependent development of neural networks. These changes could occur through correlation-based, or Hebbian plasticity (Rossum, Bi, & Turrigiano, 2000). Unless changes in synaptic strength across multiple synapses are coordinated appropriately, the level of activity in a neural circuit can grow or shrink in an uncontrolled manner (Abbott & Nelson, 2000), & Nelson, 2000.

Hebbian learning rules rely on two critical mechanisms, activity dependent synaptic modification according to Hebbian rules, and a mechanism that forces synapses to compete with one another so that when some synapses to a given post-synaptic neuron are strengthened, others are weakened (Song, Miller, & Abbott, 2000).

2.1.5.1 Hebbian learning

The Hebbian learning algorithm employs a rate-based Hebbian rule to train a network, in such a way that the activity of the pre-synaptic and post-synaptic cells serves as a base for the calculation of the new weights in the network. As a consequence, the new weights should increase the activity of some neurons while inhibiting the activity of others. The calculation of the new weights under the Hebbian learning algorithm is based on the firing rates of each cell.

The firing rate is defined by a temporal average. The mean firing rate v of a cell, is the number of spikes $n_{sp}(T)$ fired by that cell, and which occur in the time T (Gerstner & Kistler, 2002b), this is given by the equation

$$v = \frac{n_{sp}(T)}{T}, \tag{2.17}$$

where the mean firing rate is expressed in Hz.

Dr.Hebb's description of the fundamental principle of learning (Hebb, 1949) states that correlation between the firings of pre and postsynaptic neurons drive

changes in the transmission efficacy (Maass & Bishop, 1999). The activity of a given neuron i is measured by means of its firing rate v_i, which is related to the membrane potential u_i by a nonlinear monotonically increasing function g (Gerstner & Kistler, 2002a) is:

$$v_i = g(u_i). \tag{2.18}$$

The Hebbian learning rule use firing rates of both the postsynaptic cell and the presynaptic cell to calculate the amount of change of the synaptic weight. The synaptic change is obtained by the equation (Gerstner & Kistler, 2002a):

$$\frac{d}{dt} w_{ij} = c \cdot v_i \cdot v_j, \tag{2.19}$$

where v_i and v_j are the firing rates of the postsynaptic and presynaptic cells respectively, c is a parameter which in order to adhere to the Hebbian learning rule has to satisfy $c > 0$.

2.1.5.2 Spike-Timing-Dependent Plasticity (STDP)

Spike-timing-dependent plasticity (STDP) is a learning model which forces synapses to compete with each other for control of the timing of postsynaptic action potentials, and this, by itself, can lead to competitive Hebbian synaptic modification (Song & Abbott, 2001). STDP relies on the spike-timing from both presynaptic and postsynaptic cells to calculate the extent of change of the synaptic strength of the postsynaptic cell. In STDP, the firing order is also important

since it determines the sign of the synaptic change. That is, the spike-timing defines the amount of change of the synaptic strength, whereas, the order of spiking between pre and postsynaptic cells determines if the synaptic change should be added (rewarded) or substracted (punished).

The amount of synaptic modification $F(\Delta t)$ is calculated according to the following equations (Song et al., 2000)

$$F(\Delta t) = A_+ e^{\frac{\Delta}{\tau_+}} \quad if \Delta t < 0, \tag{2.20}$$

or

$$F(\Delta t) = -A_- e^{\frac{-\Delta}{\tau_-}} \quad if \Delta t \geq 0, \tag{2.21}$$

where A_+ and A_- determine the maximum amount of synaptic modification. τ_+ and τ_- determine the ranges of pre to post synaptic interspike intervals over which synaptic strengthening and weakening occur.

In addition to STDP, there are other learning algorithms based on Hebbian plasticity such as synaptic scaling, synaptic redistribution (Abbott & Nelson, 2000), & Nelson, 2000), asymmetric Hebbian plasticity (Gutig, Aharonov, Rotter, & Sompolinsky, 2003), and the method proposed by (Soto-Trevino, Thoroughman, Marder, & Abbott, 2001), where the regulation of synaptic inhibition plays an important role.

2.2 The olfactory bulb

Enjoying a nice meal, perceiving the delicate smell of a perfume or differentiating between an orange and coffee would not be possible without the olfactory sense. Smelling is not just a sense to enjoy life more, but could also be the difference between life or death, hence the importance of being able to decode odour information.

2.2.1 Olfactory bulb background

The olfactory coding starts at the olfactory epithelium (Cang & Isaacson, 2003), which is a patch of about 5 cm^2 located above and behind the nose (Figure 2.5). Dendrites of the olfactory sensor neurons (also known as olfactory receptor neurons - ORNs) extend to the surface of the olfactory epithelium (Belluscio, Lodovichi, Feinstein, Mombaerts, & Katz, 2002). There, several cilia (5 - 20) protrude and are bathed by a mucosa which creates a favourable environment for odour molecules to bind special receptors to the cilia of the ORNs (Kandel et al., 2000). Each ORN expresses a single type of odorant receptor (Uchida, Takahashi, Tanifuji, & Mori, 2000; Usrey, 2002), as depicted in Figure 2.6, where different colours represent different types of ORNs. The olfactory bulb receives the odour molecule information through axons of the sensory neurons (Mori, Nagao, & Yoshihara, 1999).

Axons of ORNs converge into spherical structures called glomeruli (see Fig-

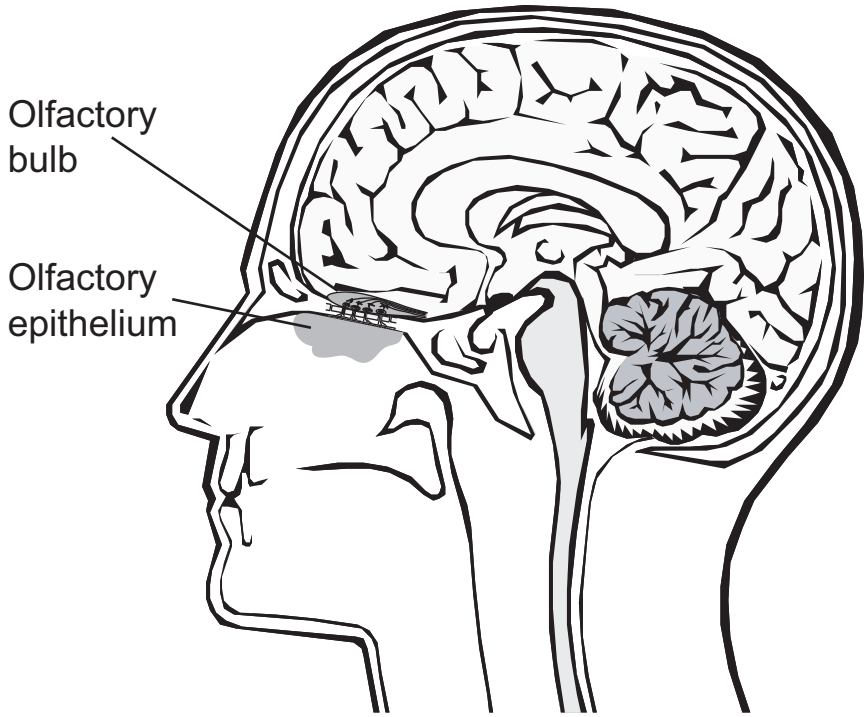

Figure 2.5: Location of the olfactory epithelium and the olfactory bulb in humans.

ure 2.6); each glomerulus contains axons of ORNs expressing the same odorant receptor (Friedrich, 2006). Odour stimulation results in activation of patterns of glomeruli distributed across the surface of the main olfactory bulb (Schoppa & Urban, 2003). In the glomerulus, axons from ORNs synapse with dendrites of mitral and tufted cells (Kosaka & Kosaka, 2004), see Figure 2.7. In addition, periglomerular neurons form dendrodendritic inhibitory synapse onto mitral and tufted cells (Mizrahi & Katz, 2003). Mitral cell axons convey olfactory input to higher brain centres such as the piriform cortex (Isaacson & Strowbridge, 1998), where information is thought to be decoded (Kandel et al., 2000). The excitability of mitral and tufted cells determines the ease with which olfactory sensor information is conveyed from the receptor cells to the cortex (Smith & Jahr, 2002).

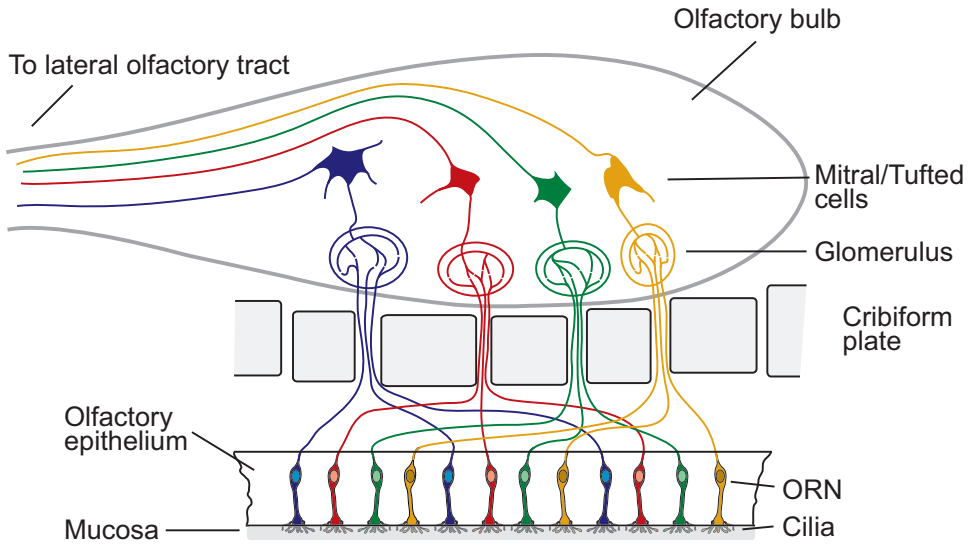

Figure 2.6: Schematic representation of the mammalian olfactory bulb.

Mitral cells also receive inhibitory input from local interneurons, the granule

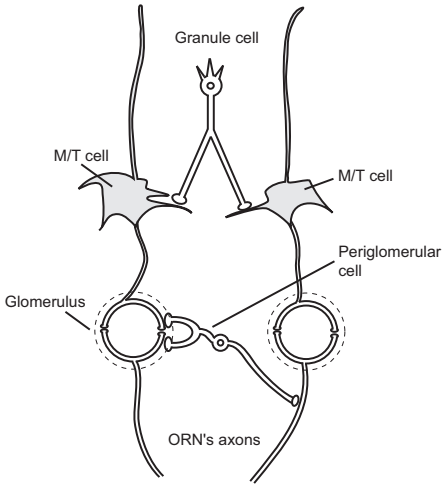

Figure 2.7: Synaptic connections of ORNs onto mitral/tufted cells and dendrodendritic connections between periglomerular cells.

cells (Segev, 1999). Granule cells are axonless inhibitory interneurons that provide the main source of interaction between the principal excitatory neurons of the bulb, the mitral and tufted cells (Egger, Svoboda, & Mainen, 2003). Therefore, the activity of mitral and tufted cells is regulated by dendrodendritic synaptic contacts with periglomerular cells and granule cells. Periglomerular cell dendrites mostly mediate interactions between cells affiliated with the same glomerulus (intraglomerular interactions), whereas granule cells mostly mediate interactions between mitral and tufted cells projecting to many different glomeruli (interglomerular interactions), (Schoppa & Urban, 2003).

The unusual synaptic arrangement found in the olfactory bulb causes different types of responses between granule cells and mitral cells. Mitral dendrites synaptically excite granule dendrites, and granule dendrites then synaptically inhibit mitral dendrites (self-inhibition), as well as inhibiting other mitral and tufted

cells (lateral inhibition), (Segev, 1999). In addition, when mitral and tufted cells activate a granule cell strongly enough to emit an action potential, it propagates through the dendritic tree, causing widespread lateral inhibition (global inhibition), (Egger et al., 2003). A critical role of the dendrodendritic lateral inhibition of mitral cells by granule cells is to enhance contrast between the activity of mitral cells transmitting information about different odour stimuli (odour discrimination). In addition, changes in the efficacy of the dendrodendritic reciprocal excitatory-inhibitory synapses between mitral cells and granule cells mediates odour memory (Shepherd & Greer, 1998).

As it was seen, the olfactory bulb is a complex system that is made up of a large number of neurons and interconnections, which play different roles in the odour coding. In this section, the most important characteristics of the olfactory bulb have been enumerated. This information should lay the basis for later chapters, where an implementation of a simplified model of the olfactory bulb is presented.

Chapter 3

The programmable construction kit

3.1 Introduction

Numerical simulation of large scale networks of spiking neurons and real-time neuromorphic system implementation require distributed computing (Morrison, Mehring, Geisel, Aertsen, & Diesmann, 2005). Existing general purpose microprocessors, although extremely versatile, rely largely on serial processing of data, which severely limits their computational throughput. This serial dependence comes about through centralized arithmetic resources (such as ALU or FPU) which are restricted to one or a small number of concurrent operations. This class of numerical simulation problem, due to its inherent parallelism, is challenging for single-core processor architectures, rendering real-time operation impossible

for all but the simplest of neural systems. The fact that cluster computing approaches are so successful in speeding up neuronal simulations demonstrates this serial bottleneck in computation. Clearly then, single-core microprocessor based neural simulators offer flexibility but are limited by serial processing constraints.

Fully customized hardware (such as analog VLSI), on the other hand, potentially offers high computational power at the expense of flexibility and design iteration times. Consequently there is a need for a rapid prototyping platform for neuronal models which is extremely fast with similar flexibility to general purpose microprocessors. Field-programmable hardware (in the forms of FPGA gate or FPAA analog arrays) is an ideal technology to fulfil these requirements, since devices are fast (up to 1 GHz. clock speeds), can be reprogrammed in milliseconds, and offer vast numbers of individual circuit elements which are inherently parallel in nature and may be configured arbitrarily.

Programmable logic promises to deliver computational speeds approaching that of custom silicon solutions whilst providing a flexible substrate for numerical simulation. Delivering on this promise, however, requires that field-programmable neuronal element circuit designs exploit the inherent parallelism of both the problem domain and target technology. Without this fine-grained parallelism this approach cannot compete in terms of processing performance with single-core microprocessors, in the form of pipelined and RISC architectures optimized for serial computation. Hence, to achieve the necessary performance in programmable logic

requires deploying robust, extremely low-complexity neuron element designs which are inherently self-contained (i.e. no shared resources) and operate independently and in parallel. Furthermore, to achieve efficient operation one should consider only single clock cycle iteration solutions (i.e. one clock cycle equals one numerical iteration) without sacrificing numerical performance. Multi-cycle architectures of neuronal models have been previously discussed (Graas, Brown, & Lee, 2004). Single-cycle architectures have independently been investigated by (Weinstein & Lee, 2006).

FPGAs are digital integrated circuits (IC), which internally contain configurable blocks of logic, as well as programmable inter-block connections (Xilinx, 2002). Such devices can be configured in an arbitrary fashion to perform a variety of signal and data processing tasks. As a first step in the implementation, designs must satisfy specific criteria to guarantee a functional circuit, which is free from logical errors. Generally designs are specified in a hardware description language (HDL), such as VHDL or Verilog, although schematic level entry is also possible. The HDL program must then be synthesized, which implies a process of minimization and optimization, which ends in the conversion of the sequential coded description into a collection of parallel registers (memory storage) and Boolean relationships. The gate-level functions obtained from this synthesis process, are then mapped onto the physical layer of the device, which means assigning the logical design to available chip resources, depending upon the chosen target de-

vice. From this process a map file is created, which defines the placing of the logic onto the physical device, as well as the routing of the signals between logic elements (so-called place and route). Finally a "bitstream" is created, which is a file containing the information to internally configure the FPGA device (see (Xilinx, 2003), and (Maxfield, 2004)). Design tools to aid the FPGA synthesis process are developing rapidly.

Here we present a set of reduced complexity programmable logic designs for exponential decay and alpha/beta-function synapse with spike time dependent plasticity (STDP) learning, as well as integrate-and-fire soma complete with axonal delays. Together these designs form a neuronal modelling kit, simulating all the major components commonly used in neuronal modelling of large-scale networks. The designs are of sufficiently low complexity to be realizable in massive numbers on a single FPGA device through multiplexing, yet feature single clock cycle numerical iteration.

We begin by making mathematical comparisons between forward-Euler (FE) and exact integration (EI) numerical iteration schemes in the case of linear ODE solvers. We show that this comparison leads to a surprisingly simple solution for implementing neuronal elements with exact numerical properties. By simulating and evaluating these designs, we demonstrate FPGAs as a viable technology for large-scale spiking neuron model implementation. The designs are finally tested against numerical and analytical results, verifying exact integration behaviour.

3.2 Numerical considerations

Neuronal dynamics are commonly modelled in digital hardware using numerical methods for solving ODEs. The simplest scheme for numerical simulation of dynamical system behaviour is the FE approach. For an initial value problem (IVP) of the form

$$\dot{y}(t) = f(y, t), \qquad y(0) = y_0, \tag{3.1}$$

a first order (linear) approximation to its solution is given by the FE approximation (Lambert, 1973)

$$\tilde{y}_{k+1} = \tilde{y}_k + \Delta f(y_k, t_k), \tag{3.2}$$

which is an iteration scheme that begins from an initial value (y_0), where k is an integer defining the iteration number ($k = 0, 1, \cdots$), and Δ is the fixed step size, in part determining the accuracy of the approximation. In general, this numerical integration scheme has a truncation error of order $O(\Delta^2)$. More sophisticated iteration schemes can be used that reduce the single step error (such as Runge-Kutta), but these require greater computational effort and hence more complex implementations.

In this context, considering an homogeneous first-order ODE of the form

$$\dot{y}(t) = ay(t), \qquad y(0) = y_0, \tag{3.3}$$

we can approximate its solution by applying the FE method as follows

$$\tilde{y}_{k+1} = \tilde{y}_k(1 + \Delta a), \qquad \tilde{y}(0) = y_0. \tag{3.4}$$

As an alternative, there is an exact way to perform digital simulation of general linear time invariant systems, which is described by (Rotter & Diesmann, 1999). In order to obtain an EI solution of equation 3.3, we make use of this method, yielding the following expression

$$y_{k+1} = e^{\Delta a} y_k, \qquad y(0) = y_0. \tag{3.5}$$

In general, both methods will yield different values. However, in order to find a relation between the FE and the EI method for the linear ODE case, we make use of the parameter a, which determines the time constant of the system as the relational parameter. Let us now define $\tilde{a}$ and a as the factors determining the time constants for the FE and EI solutions, respectively. If both iteration schemes begin from the same initial value y_0, then clearly they will give identical results if the following condition is met

$$1 + \Delta\tilde{a} = e^{\Delta a}. \tag{3.6}$$

To satisfy this condition, we must first solve for $\tilde{a}$ and then substitute this value into equation 3.4 instead of a. Hence for first order linear time invariant dynamical

systems, such as we consider here, the FE solution is simply a time-scaled version of the exact solution, which can be corrected by adopting the $\tilde{a}$ parameter in equation 3.4. In the following circuit implementations we will exploit this fact to derive extremely low complexity circuit designs capable of implementing an EI of common neuronal modeling components.

3.3 Neuron model

We first consider the two main neuronal elements – a synapse model which reproduces postsynaptic dendritic current dynamics resulting from a presynaptic action potential, and a soma model which integrates these currents over time to generate a membrane potential. We describe the implementation of both models in turn, providing the numerical details upon which they are based, as well as their optimized programmable logic circuit implementations.

3.3.1 Synapse model

3.3.1.1 Exponential decay synapse model

One of the most common methods to model dendritic currents generated by a synapse in response to a spike train, is through an exponential decay over multiple spike inputs occurring at times $(t_1, t_2, \ldots, t_j, \ldots t_l)$ to give the dendritic current

$$I(t) = w \sum_{j=1}^{l} H(t - t_j) e^{-\frac{(t-t_j)}{\tau_e}}, \tag{3.7}$$

where $H(\bullet)$ is the Heaviside function, w is the synaptic efficacy (weight) which determines the current increment in response to the arrival of each presynaptic action potential and τ_e the time constant of the exponential decay, resulting from the arrival of each action potential.

The above equation is the solution to the first order ODE of the form

$$\dot{I}(t) = w \sum_{j=1}^{l} \delta(t - t_j) - \frac{1}{\tau_e} I(t). \tag{3.8}$$

Which can be approximated using the forward-Euler scheme for $a = -\frac{1}{\tau_e}$ as

$$I_{k+1} = w\delta_{k+1,j} + I_k(1 - \frac{\Delta}{\tau_e}). \tag{3.9}$$

This numerical scheme may be implemented directly in programmable logic by keeping a running accumulation of I over time by adding the current value to itself and subtracting a fraction of I_k at each time step. When a time step occurs in which a spike is received, the constant factor w must also be added to the accumulated value. This scheme makes for a very simple architecture with the exception of the multiplication involved in the fractioning process, which in its most general form is expensive to implement in programmable logic.

The resulting register transfer level (RTL) description of the synapse which can be directly implemented in programmable logic is shown in Figure 3.1a, as derived from the FE iteration scheme given in equation 3.1a. The implementation assumes that within a single clock cycle (identical to the step time Δ) only a single

action potential may be received at the input. This is reasonable if we assume that every synapse is connected to a single presynaptic cell, which typically has an absolute refractory period far exceeding a single time step. $n-$bit integer arithmetic may be used without loss of precision as long as we scale the circuit weight input w_B according to $w_B = k_I w$, by choosing k_I such that the bit count output of the circuit, B, extends across the integer number line $\{0, 1, 2, \ldots, 2^{n-1}\}$. In this case the dendritic current can be recovered from the circuit output via $I(t) = B/k_I$. The real-time response of this circuit to a single action potential shown in Figure 3.1b is an exponential decay, with starting value equal to the weight of the synapse as shown in Figure 3.1c. The simulation proceeds at least 3 orders of magnitude faster than biological time, requiring a dimensionless speed up factor k_t to translate between biological time constants and those achieved by the FPGA. The speed up factors k_t are calculated based on a biological time constant for the synapse of 5 ms for Figures 3.1 and 3.2, and a biological time constant for the soma of 20 ms for Figures 3.3, 3.4 and 3.7.

Using the same arguments as previously, it is clear that the FE scheme describing the synaptic dynamics is equivalent to the EI solution as long as the following corrected time constant is substituted for τ_e in equation 3.9

$$\tilde{\tau}_e = \frac{\Delta}{1 - e^{-\frac{\Delta}{\tau_e}}}. \tag{3.10}$$

The behavior of this circuit to the regular spike train shown in Figure 3.1d is

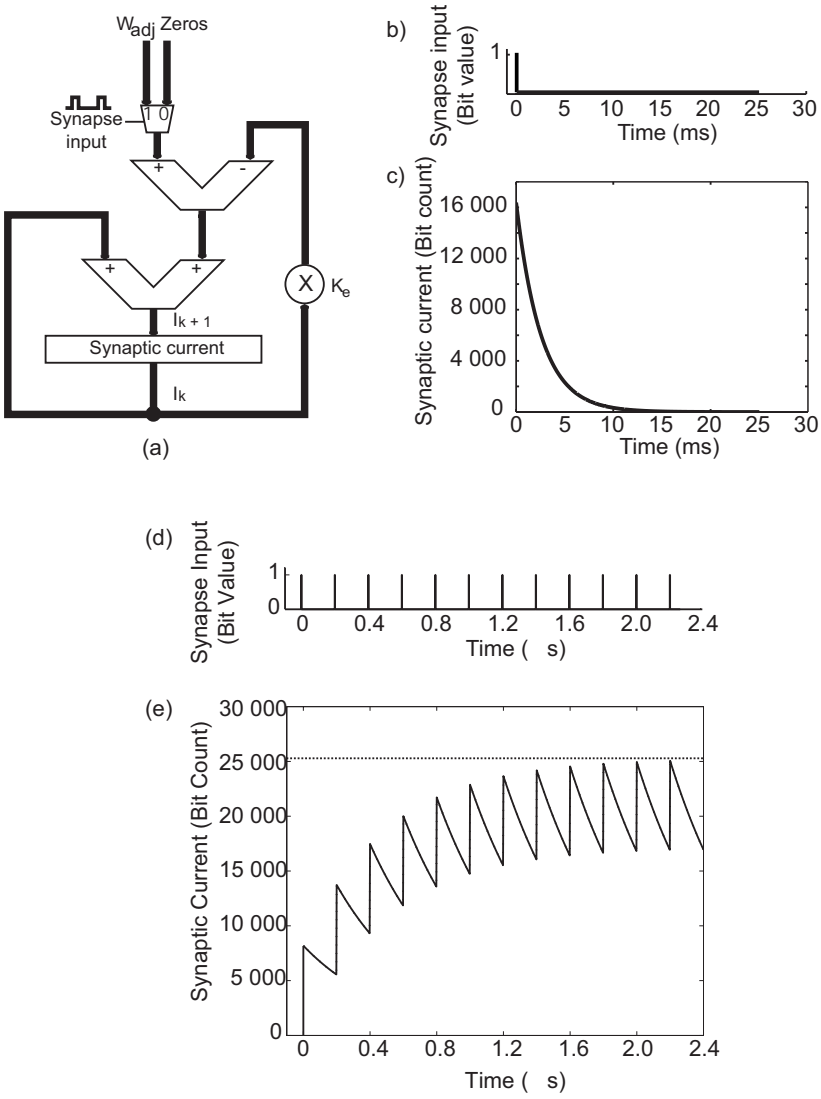

Figure 3.1: Exponential decay synapse implementation. (A) RTL description of the synapse architecture. Spiking synaptic input is represented by 0-1 logic levels, which controls the addition of weight value at each clock cycle. Thick solid lines represent $m-$bit digital buses (representing unsigned integers), thin solid line represents an individual control line. (B) A single spike event at time $t = 0$ occurs at the input of the synapse. (C) An exponential decay is generated in the circuit as response to the input. For a synapse with a current increment of 50 pA, the bit count output, B, can be converted to synaptic current using $I(t) = B/k_I$, where $k_I = 3.28 \times 10^{14}$ counts A^{-1}. (D) Spiking input at a regular firing frequency, $f_{sp} = 5\,\mathrm{MHz}$., used to test the synapse implementation. (E) Real-time synapse response to this regular spiking input for FPGA synapse implementation. The theoretical asymptotic value of peak synaptic current is shown by the upper dashed line. The clock frequency was set to $f_{clk} = 100$ MHz giving a step time, $\Delta = 10\,\mathrm{ns}$, and a speed up factor $k_t = 1953$ resulting in time constants, $\tilde{\tau}_e = 2.56\,\mu\mathrm{s}$ and weight $w = 16384$ for (C) and $w = 8192$ for (E).

shown in Figure 3.1e. The limiting value of peak synaptic current is compared to the asymptotic value (dotted line), which in the case of a regular spiking input at fixed frequency, f_{sp}, can be shown to be

$$I_{peak} = \frac{w}{1 - e^{-\frac{1}{f_{sp}\tilde{\tau}_e}}}. \tag{3.11}$$

The asymptotic peak response of the circuit is found to be within one LSB of the theoretical value, I_{peak}.

3.3.1.2 Alpha and Beta function synapse models

Alpha and beta functions are also popular physical models for synaptic dynamics (Jack, Noble, & Tsien, 1975); (Gerstner & Kistler, 2002a); (Tuckwell, 1988). The dendritic current generated by an alpha function synapse responding to multiple spike inputs occurring at times $(t_1, t_2, \ldots, t_j, \ldots t_l)$ is described by

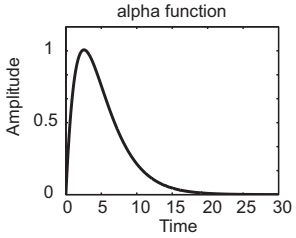

$$I(t) = \frac{w}{\tau_\alpha} \sum_{j=1}^{l} H(t - t_j)(t - t_j) e^{-\frac{t-t_j}{\tau_\alpha}}, \tag{3.12}$$

where w is again the efficacy of the synapse and τ_α is the characteristic time constant for the synapse.

In a beta function model, current in a postsynaptic dendrite generated in

response to multiple presynaptic spikes occurring at times $(t_1, t_2, \ldots, t_j, \ldots t_l)$ is described by

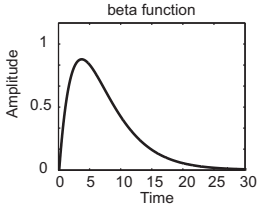

$$I(t) = w\beta \sum_{j=1}^{l} H(t - t_j)(e^{-\frac{t-t_j}{\tau_{\beta_1}}} - e^{-\frac{t-t_j}{\tau_{\beta_2}}}), \tag{3.13}$$

where τ_{β_1} and τ_{β_2}, now determine the time constant of the synapse, and β is a parameter adjusted to produce a (dimensionless) beta function with unit amplitude.

Rotter and Diesmann (1999) show how a matrix exponential can be used to describe the exact solution to greater than first-order linear ODEs (see Appendix A), such as alpha and beta function dynamics. Due to their second-order dynamics, the matrix exponential for either the alpha (equation A.2) or beta function (equation A.3), consist of two exponential decay terms in the diagonal, and a third off-diagonal term. This fact provides us with a simple method for implementing either function by deploying in cascade two exponential decay elements detailed in section 3.3.1.1.

There is, however, a non-zero off diagonal term in both matrices, which acts as a scaling function that must ordinarily be applied when coupling both exponential decay elements. We see that this matrix element is in fact a constant factor, and so can be implemented by means of a multiplier in this circuit. Yet, to keep the

design as simple as possible, this constant factor may be directly applied to the weight of the synapse instead. Adjusting the synaptic weight in this way does not change the dynamics of the function, but eliminates the necessity of multipliers between exponential decay elements, resulting in a simpler circuit. Thus, the resulting adjusted weight for the alpha function is

$$w_{adj} = \Delta e^{-\frac{\Delta}{\tau_\alpha}} w, \tag{3.14}$$

whereas, for the beta function it is

$$w_{adj} = \frac{w\tau_{\beta_1}\tau_{\beta_2}}{\tau_{\beta_1} - \tau_{\beta_2}}(e^{-\frac{\Delta}{\tau_{\beta_1}}} - e^{-\frac{\Delta}{\tau_{\beta_2}}}). \tag{3.15}$$

The schematic for this class of synapse is shown in Figure 3.2a. In this case, action potentials, acting as input, are received at the first exponential decay element whilst the output from the second element follow alpha/beta function dynamics. The parameter ρ, shown, will be proved to be an important parameter when the circuit is used in combination with a soma circuit to reproduce the membrane potential of a neuron, but is not relevant for isolated synapses and can then be set to zero. Figure 3.2c shows an alpha function generated by this circuit as a response to a single input spike applied at time $t = 0$ (Figure 3.2b). Note that we have again adjusted each time constant according to equation 3.10 to guarantee an EI solution.

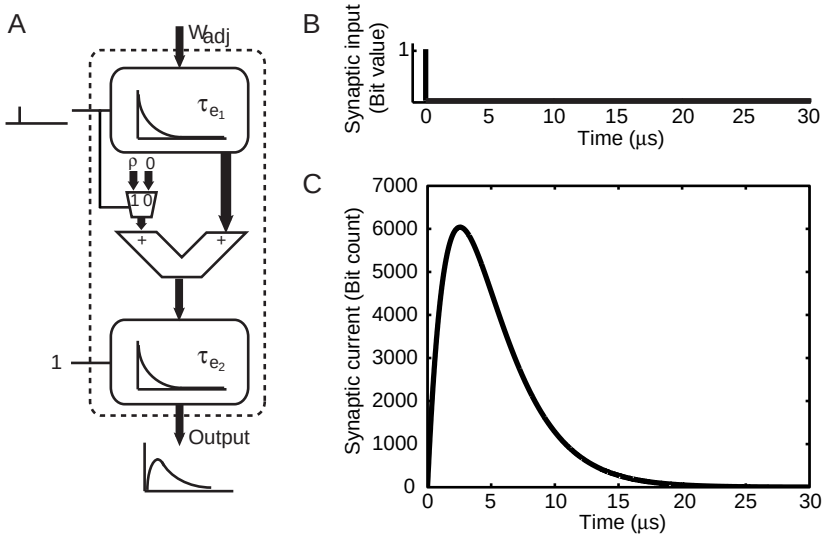

Figure 3.2: Alpha/beta function synapse implementation. (A) Block diagram of the implementation of an alpha/beta function generator implemented by connecting in cascade two exponential decay synapses. When $\tau_{e_1} = \tau_{e_2}$, the function generated is an alpha function, otherwise, it is a beta function. Each time an action potential arrives at the synapse, both the adjusted weight and the value of ρ are added to the circuit. The parameter ρ is only used when the alpha/beta function is fitted to a soma circuit to produce a combined neuron model, in such cases, the value of ρ is determined using equations 3.18 and 3.19. When simply performing isolated alpha function synapses ρ has no effect in the circuit, therefore set $\rho = 0$ and no value of ρ will be added during spikes, whereas w_{adj} is determined by equations 3.14 or 3.15 depending on the type of synapse. (B) A single spike event at time $t = 0$ occurs at the input of the synapse. (C) An alpha function is generated as real-time response to the input. A 32−bit representation was used in the circuit with parameters clock frequency $f_{clk} = 100$ MHz., step time, $\Delta = 10$ ns, $k_t = 1953$, $\tilde{\tau}_\alpha = 2.56\,\mu$s, $\rho = 0$ and adjusted weight $w_{adj} = 64$.

3.3.2 Soma model

The popular integrate-and-fire model which receives synaptic input of the form $I(t)$ has a membrane potential, $V(t)$, the dynamics of which are described in between generated action potentials by

$$\dot{V}(t) = -\frac{V(t)}{\tau_m} + \frac{I(t)}{C_m}, \tag{3.16}$$

where the membrane capacitance, C_m, is a constant and τ_m is the characteristic time constant for the cell. Once $V(t)$ reaches a fixed threshold potential, V_{th}, say at time t', $V(t')^- = V_{th}$, the soma then resets to the after-hyperpolarization potential, $V(t')^+ = V_{ahp}$, and a spike is generated by the soma and integration of the current input continues. Again, using the FE approach the solution of equation 3.16 may be approximated as

$$V_{k+1} = V_k(1 - \frac{\Delta}{\tau_m}) + \frac{\Delta}{C_m} I_k, \tag{3.17}$$

resulting in a similar implementation to that of the exponential decay synapse, except that the dendritic input is added at each time step. In the next section, we show how, again, EI can be implemented within the FE scheme if the dynamics of I is appropriately taken into account.

The RTL description for the soma implementation, complete with spike generating mechanism is shown in Figure 3.3a. A comparator is used to detect threshold

crossings, which gates a single flip-flop producing a $0 \rightarrow 1 \rightarrow 0$ transition on the axon output lasting one clock cycle. If required, a fixed input bias may be added at each time step in order to determine the resting potential of the cell. Similar to before, the bit count held in the soma potential register, B, is a linearly scaled representation of the soma potential, such that $V(t) = B/k_V$. The soma model responding to two current pulses of different magnitudes (shown in Figure 3.3b) is shown in Figure 3.3c.

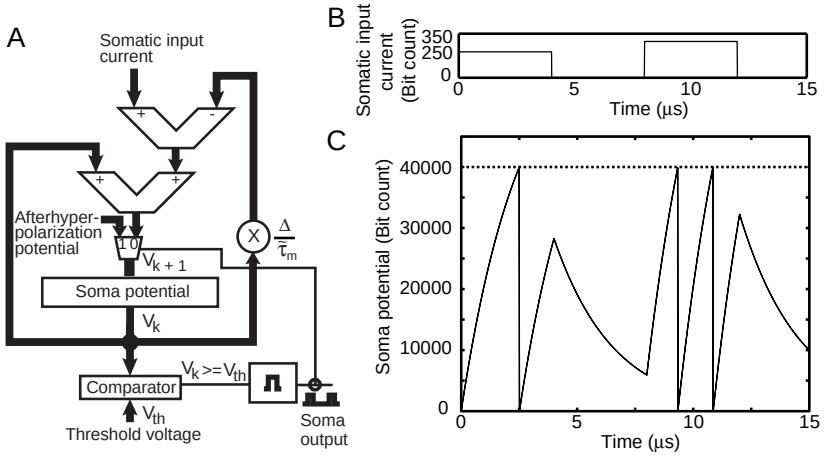

Figure 3.3: Integrate-and-fire soma implementation. (A) RTL description of soma architecture. Somatic input current, $I(t)$, after-hyperpolarization (reset) potential, V_{ahp}, and the threshold potential, V_{th} are each represented by an $p-$bit signed integer (thick solid lines). A fire event (spike) is represented by a $0 \rightarrow 1$ transition on the soma output line lasting a single clock cycle. (B) Somatic current pulses (see Rotter & Diesmann, 1999, sect. 3.2.3 for the appropriate EI coefficient) of $I = 250$ and 350 bit count respectively lasting and separated by 4 μs were used to test the soma implementation. (C) Real-time soma response to the current input for the FPGA implementation with a speed up factor $k_t = 7813$. For a soma with a threshold of 20 mV above resting potential, the soma potential bit count, B, can be converted to soma potential $V(t) = B/k_V$, where $k_V = 2 \times 10^6$ counts V^{-1}. A $32-$bit representation was used with parameters clock frequency $f_{clk} = 100$ MHz., step time, $\Delta = 10$ ns, resulting in $\tilde{\tau}_m = 2.56\,\mu$s, and $V_{th} = 40000$ which is indicated by the horizontal dashed line.

3.3.3 Combined neuron model

We have now developed programmable logic circuits that implement EI solutions for all the main neuronal modelling components described by equations 3.7, 3.12, 3.13 and 3.16. These synapse and soma circuits must next be combined in such a way as to obtain an EI solution for the complete neuron model. This process is not immediate, since unfortunately combining individual elements with EI performance does not guarantee EI system performance when coupled together. Thus, some important considerations must be taken into account before connecting these components.

First we use the matrix exponential of the combined system given by (Diesmann, Gewaltig, Rotter, & Aertsen, 2001), as in equation B.1. In this case the matrix exponential describes the state space representation of a combined neuron comprising synapse and soma. We see from this representation that a simple cascade connection of these components will not suffice, since there exist non-vanishing off-diagonal elements which act as constant factors between stages, again requiring the use of multipliers.

In order to optimize the combined neuron model for the case of alpha-function synapse and soma, we apply a linear transformation (Appendix B), which permits the direct cascade of synapse and soma elements without need of coupling factors. An important consequence of this transformation, however, is the necessity to again adjust the synaptic weight and also apply a constant addition factor (ρ) in

between stages according to,

$$w_{adj} = \frac{\tau_\alpha \tau_m \Delta e^{-\frac{\Delta}{\tau_\alpha}}(e^{-\frac{\Delta}{\tau_\alpha}} - e^{-\frac{\Delta}{\tau_m}})}{C(\tau_\alpha - \tau_m)} w, \tag{3.18}$$

and

$$\rho = \frac{\tau_\alpha \tau_m((\tau_\alpha - \tau_m)\Delta e^{-\frac{\Delta}{\tau_\alpha}} - \tau_\alpha \tau_m(e^{-\frac{\Delta}{\tau_\alpha}} - e^{-\frac{\Delta}{\tau_m}}))}{C(\tau_\alpha - \tau_m)^2} w. \tag{3.19}$$

These parameters may again be calculated off line to avoid the necessity of multipliers in the circuit, yielding the far simplified combined neuron circuit shown in Figure 3.4a.

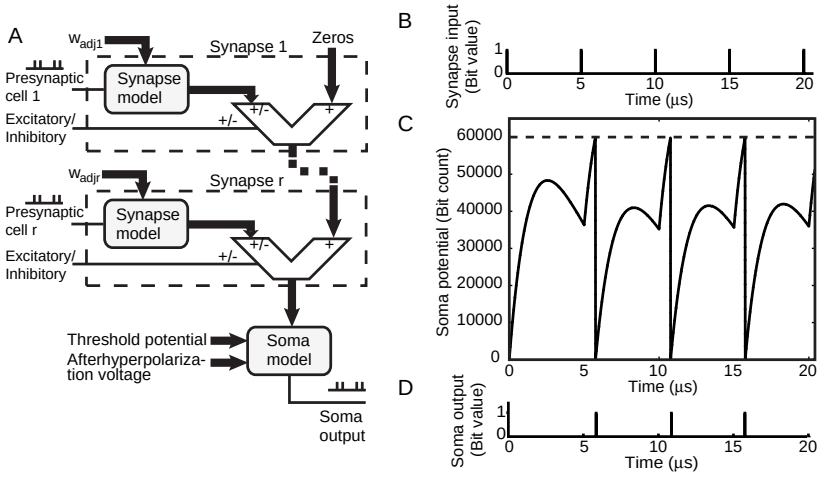

Figure 3.4: Combined neuron implementation. (A) RTL description of the combined neuron architecture. Spiking input is represented by 0-1 logic levels received at r synapses. Weights, w_i, for synapses ($i = 1, \ldots, r$), the after-hyperpolarization (reset) potential, V_{ahp}, and the threshold potential, V_{th} are represented by $m-$bit unsigned integers (thick solid lines). (B) Spiking input at a regular firing frequency, $f_{sp} = 200\,\text{kHz}$, used to test the combined neuron implementation (only one synapse input ($i = r = 1$) was considered). (C) Real-time soma response to the synapse input for the FPGA combined neuron implementation. (D) Spikes generated by the combined neuron model in response to the spiking input defined in (B). A $32-$bit representation was used for both circuits with clock frequency $f_{clk} = 100\,\text{MHz}$, step time, $\Delta = 10\,\text{ns}$ and $k_t = 7813$. For the synapse, time constant of $\tilde{\tau}_e = 2.56\,\mu\text{s}$ and adjusted weight $w_{adj} \approx 0.61681$; for the soma, $\tilde{\tau}_m = 2.56\,\mu\text{s}$, $C = 12$ pF and $V_{th} = 60000$ which is again indicated by the horizontal dashed line.

Using similar arguments for the exponential decay synapse and soma case (Appendix C) we can again find an adjusted weight which results in combined EI performance

$$w_{adj} = \frac{w\tau_e\tau_m}{C(\tau_e - \tau_m)}(e^{-\frac{\Delta}{\tau_e}} - e^{-\frac{\Delta}{\tau_m}}). \tag{3.20}$$

Now that we have determined the conditions required to perform an exact integration for each case, synapse and soma may now be combined to form a self-contained, single clock cycle operation, spiking neuron implementation. Figure 3.4a shows a generalized multi synapse scheme for a single neuron. The neuron comprises r synapses, which receive spikes from different presynaptic cells, generating dendritic currents which are summed in a single clock cycle and integrated to produce the membrane potential of the soma. In general a greater number of bits will be need to be deployed at the soma as compared to the synapse, since integration of the input occurs at each time step (not just after spike arrival) and multiple synapse inputs may be summed. In order to minimize the total number of bits required in the soma, we can limit the maximum and minimum weights in the synapses to avoid overloading the soma, which as we will see is also a desirable characteristic for the learning algorithm we will consider later.

In order to demonstrate the EI performance of the combined designs, we tested an exponential decay type synapse and soma. Input spikes were applied to the combined neuron model as seen in Figure 3.4b which gave rise to the resulting membrane potential shown in Figure 3.4c. We see that in this case the membrane

potential crosses the threshold (V_{th}) three times, generating the same number of spikes (Figure 3.4d).

3.3.4 Axonal Delays

Axonal delays play an important role in the dynamics of spiking neuron network models (Crook, Ermentrout, Vanier, & Bower, 1997) and are simple to implement in this design. In general, axonal delays will not be constant across all cells of the network. Instead, each axon should have associated with it a particular delay (Figure 3.5a).

When a spike occurs at a soma output, this should not be delivered instantly to the target synapse. Rather, the action potential must be presented in some $n\Delta$ time steps after the spike occurred. In this design, axonal delays are implemented using a ring buffer (Figure 3.5b). The spike history (up to time $n\Delta$) is stored in the ring buffer from each soma and at each time step the nth element is transmitted to the target synapse, while the current state of the soma is written to the buffer. Ring buffers have the advantage that spike history data is automatically overwritten as it becomes redundant.

3.3.5 Learning by STDP

There are many Hebbian (correlation) based plasticity mechanisms which can be used for learning purposes in spiking neuron models (Abbott & Nelson, 2000); (Gutig et al., 2003). One of the most common of these is spike timing dependent

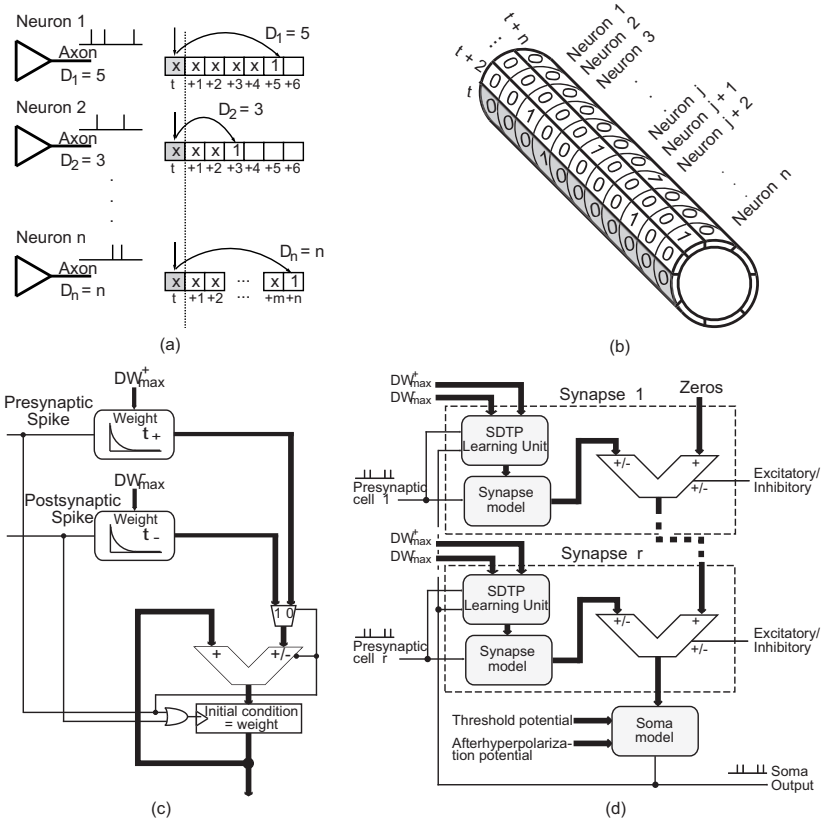

Figure 3.5: Axonal delay and STDP learning implementation. (A) Each axon is programmed to have an specific delay (defined by D_n for the $n-$axon), which is implemented using a ring buffer. (B) Action potentials are read from the ring buffer at time t, the synapses from other neurons receive the delayed spikes according with the programmed delay for each neuron. (C) RTL design of the STDP learning unit. Superpositions of exponential decays with height equal to the amount of weight modification (ΔW^+ to increment or ΔW^- to decrement) are generated, the order of presynaptic and postsynaptic fire times defines both the amount and the sign of the weight modification. (D) Neuron model with STDP learning. The STDP unit receives presynaptic spikes arriving at a specific synapse as well as the action potentials generated by its respective soma. The adjusted weight is fed to the synapse every time a presynaptic or postsynaptic spike takes place.

plasticity (STDP) proposed by (Song et al., 2000). This plasticity mechanism relies on the difference in presynaptic and postsynaptic spike times to adjust the strength of excitatory synapses.

As an example of how plasticity mechanisms may be conveniently combined with the neuronal element designs for on-chip learning in real-time we have implemented STDP with some synapses. Figure 3.5c shows the RTL design of the STDP unit, which contains two exponential decay elements reused from the synapse designs. The exponential decay unit situated in the upper section of the diagram receives presynaptic spiking input, in the same way as the synapse itself. Each time a spike is received at this exponential decay unit a value equal to the maximum amount of change of the synapse strength (ΔW^+) is added to its output, while during latency periods this value decays exponentially according to equation 3.7. Once a spike is generated in the postsynaptic neuron, the strength of the synapse is increased by the current value output by this exponential decay unit. The second exponential decay unit behaves in the opposite way. That is, the second element has as input postsynaptic action potentials that add to the current value an amount equal to the maximum possible change of synapse weakening (ΔW^-). When a presynaptic action potential is received, the current value of this exponential decay unit is subtracted from the weight of the synapse. In this way synapses compete to control the postsynaptic spike timing of the neuron. Figure 3.5d shows the implementation of the STDP unit in the generalized neuron

model.

The weight of the synapse is limited to the range $[0, W_{max}]$. A requirement for stable synaptic modification requires that $\Delta W^+ < \Delta W^- < W_{max}$ and experimental results suggest that $\Delta W^-/\Delta W^+ = 1.05$ (Song, Miller & Abbott, 2000). The maximum weight W_{max} should be chosen so as not to overload the soma.

3.4 Results

RTL designs for each neuronal component were implemented in VHDL and executed on a PCI-based FPGA development board (model ADM-XRC-II Pro, manufactured by Alpha Data Systems, UK), which hosts a Xilinx Virtex II Pro device (product code XC2VP100-5). Numerical results were tested against the equivalent exact numerical solution as calculated on a standard PC with Intel Pentium IV running at a clock speed of 3.06 GHz with 1 GB of external memory, programmed in C++. All responses shown in Figures 3.1, 3.2 and 3.3 (b, c) were compared against their corresponding EI solution and the differences plotted in Figure 3.6 (left). In all cases the errors show a random behaviour about zero, which suggests that the difference is due to round-off as a result of the finite length number representation. This conclusion is confirmed by the histograms of the error (Figure 3.6, right) which show that in all cases the distributions closely resemble the shape of the uniform probability density function, which is the expected behaviour generated by a round-off process (Barnes, Tran, & Leung, 1985).

With increasing time the response error becomes more regular as the output of the circuits approaches zero, since the time derivative becomes very small (itself an exponential decay). In the case of the alpha-function synapse (Figure 3.6b.), although we see a random uniform distribution about zero of $\pm$ 0.5 bits for each of the two stages, when combined the two errors may accumulate in the positive direction leading to an error greater than $\pm$ 0.5 bits for a single neuron. However the total error will never exceed $\pm$ 1 bit and is not systematic, since the asymptotic behaviour is toward zero.

An additional experiment was carried out using a combined neuron model comprising an alpha function synapse and a soma, which was excited by a single spike at time ($t = 0$). The membrane potential was again compared against the numerical solution given by the EI method. The error between the circuit implementation and the EI solution shows the same behaviour as in the preceding case, namely a uniform distribution due to the round-off process (Figure 3.6d).

To further test the numerical performance and robustness of these designs, a combined neuron simultaneously integrating signals from five exponential decay synapses driven by Poisson processes (Figure 3.7a) was implemented. The total resulting synaptic current is shown in Figure 3.7b. The difference between the membrane potential obtained by the EI scheme, and the value generated by the circuit (Figure 3.7c), again shows a random behaviour about zero, ruling out any systematic error in the circuit behaviour (Figure 3.7d). In this case, a total of 308

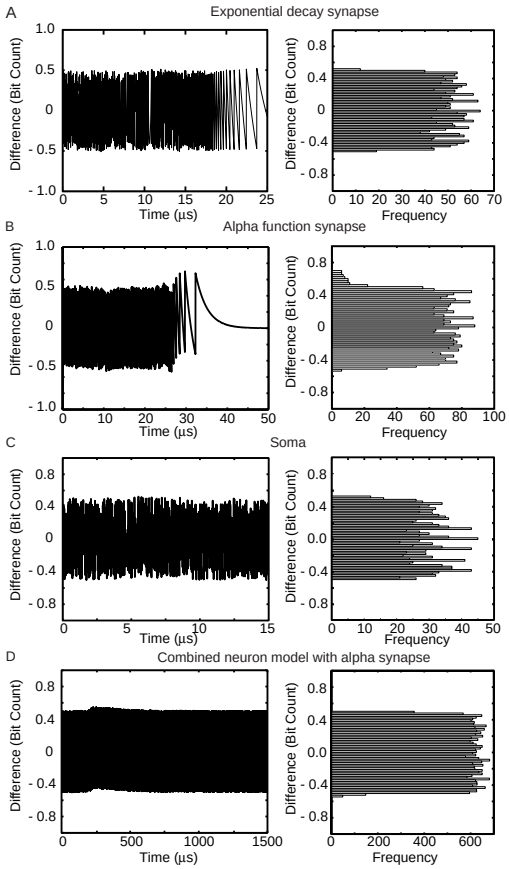

Figure 3.6: Differences between the numerical solution and the circuit responses. Difference over time (left) and histograms of their corresponding error distribution (right) for (A) exponential decay synapse response, (B) the alpha function synapse response, (C) the soma response and (D) combined neuron model made up of alpha function synapse and integrate-and-fire model. The error corresponds to those responses shown in Figures 3.1-3.3 except for the combined neuron model whose response comes from a single spike at ($t = 0$). The parameters of the three first circuits are the same than the ones specified for each response, while for the combined model the parameters are: $\tilde{\tau}_\alpha = 25.6$ μs, $\tilde{\tau}_m = 4.096$ ms, $C = 250$ pF, adjusted weight $w_{adj} \approx 0.5089$ and $\rho \approx 0.2553$. All errors show the same characteristics: a random behaviour about zero and a uniformly distributed probability density function. The clock frequency was set to $f_{clk} = 100$ MHz giving a time step of $\Delta = 10$ ns. Numerical solutions were carried out in C++ using long double precision, using an 80 bits representation with 64 bits for the mantissa and 14 for the exponent.

action potentials were generated by the circuits (Figure 3.7e), exactly the same number of spikes which were obtained through the EI scheme. Critically, there were no differences in firing times for both the circuit and the numerical solution – all spikes were time coincident within a single clock cycle (Figure 3.7f). This confirms that for the purposes of simulation of integrate-and-fire neuron and exponential decay based synapse dynamics this circuit produces EI performance under realistic simulation conditions, only limited by the restricted bit length of the representation, which is the case for any digital neuronal model implementation.

3.5 Conclusion

Designs for leaky integrate-and-fire soma and exponential/alpha/beta function synapses with STDP learning and axonal delays are presented in this thesis which are suitable for implementation in programmable logic. Together these designs provide a neuronal modelling construction kit of the most popular elements which can be deployed in arbitrary configurations for hyper real-time implementation. This programmable logic construction kit supports the building of large and complex architectures of spiking neuron networks by means of an efficient communication and multiplexing scheme of the neuronal elements. The circuits proposed here have the advantage that they work in parallel rather than depending upon serial computation, being capable of simulating neuronal models in hyper real-time.

The implementation we present is restricted to the class of integrate-and-

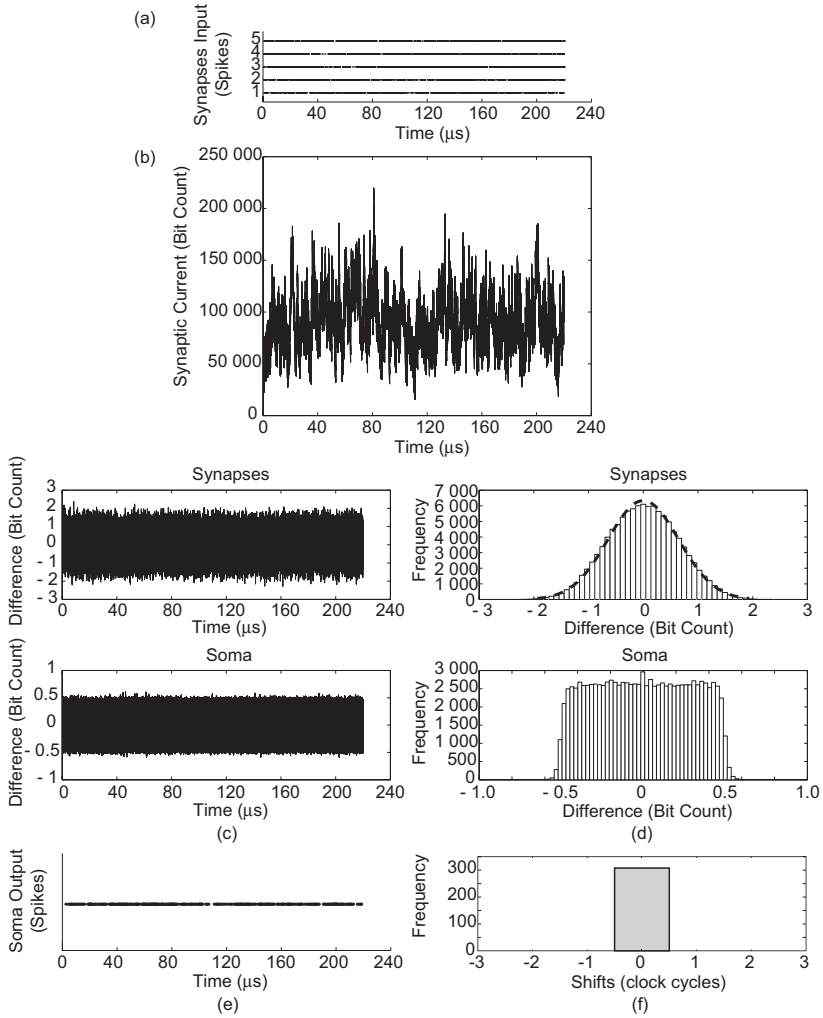

Figure 3.7: Numerical error for the combined neuron. (A) Random spikes trains applied at the input of each synapse. (B) Total synaptic current generated by the circuit. (C) The error between the exact integration numerical implementation and the circuit response for the membrane potential again shows a random behaviour about zero. (D) Histogram of the error distribution, which uniform distribution corroborates the round-off effects as the only cause of the error. (E) Over 300 spikes were generated by the soma. (F) Spike-timing for both the exact integration numerical implementation and circuit response. All spikes from the circuit were exactly coincident with the spike times given by the numerical solution. A $m-$bit representation was used with parameters $\tilde{\tau}_{e_1} = 5.12\,\mu$s, $\tilde{\tau}_{e_2} = 2.56\,\mu$s, $\tilde{\tau}_{e_3} = 1.28\,\mu$s, $\tilde{\tau}_{e_4} = 0.64\,\mu$s, $\tilde{\tau}_{e_5} = 1.28\,\mu$s, adjusted weights $w_{adj_1} \approx 0.077026$, $w_{adj_2} \approx 0.077101$, $w_{adj_3} \approx 0.077253$, $w_{adj_4} \approx 0.077558$ and $w_{adj_5} \approx 0.077253$. Whereas $\tilde{\tau}_m = 2.56\,\mu$s, for the soma, Capacitance $C = 12$ pF, threshold potential, $V_{th} = 65000$. The clock frequency was set to $f_{clk} = 100$ MHz, giving a step time, $\Delta = 10$ ns and a speed up factor, $k_t = 7813$. Numerical solutions were carried out in C++ using long double precision using an 80 bits representation with 64 bits out of them for the mantissa and 14 for the exponent.

fire models where synapses are described by time dependent currents. However, with conductance based synapses only the differential equation for the membrane potential is no longer linear time-invariant. Future work will need to explore whether an implementation with exact integration (EI) for the conductances and an approximate method for the membrane equation (e.g. FE as described in section 2) can effectively be combined.

The circuit designs have been demonstrated to perform exact integration in a single clock cycle and are also self-contained (no shared resources). The advantage of single clock cycle operation is that designs may operate faster than biological time scales (milliseconds); depending on their complexity and the extent of optimization, processing speeds may be able to approach the clock frequency of the FPGA. This hyper real-time operation provides us with the opportunity of multiplexing the physical neuron architecture to achieve far greater neuron numbers. This is made possible since only digital spike events need to be communicated between neurons, thereby simplifying connectivity circuitry. Thus, programmable logic offers neuronal simulation speeds approaching those of fully custom silicon solutions, but not at the expense of flexibility, design times, or network capacity, since once the design process outlined in Section 1 is complete, large-scale models may be downloaded and adapted in milliseconds.

Most importantly, by using fully parallel single clock cycle implementations this neuronal modelling approach leverages the impressive advances in pro-

grammable logic, in terms of clock speeds and device capacities, specialized DSP components, cost, and ongoing development of advanced design tools. FPGA capabilities and operating speeds are currently under exponential growth. Over the past ten years capacity has increased more than 200-fold with every indication that Moores law will continue for these devices some way into the future (Alfke & Hitesh, 2005). This should ensure the possibility for growth of neuronal modelling capability that is commensurate with advances in programmable logic.

We can estimate the total neuronal capacity of any given FPGA device by calculating the amount of resources each neuronal element would require. FPGA resources are measured in terms of slices, each of which contains the fundamental digital elements required to implement arbitrary combinational logic functions (Xilinx, 2002). Thus, the number of slices required per neuron element limits the total physical numbers implementable on a single device. Using a 16 bit representation for the synapse and a 32 bits representation for the soma requires a total of 70 slices for the (exponential decay) synapse circuit and 90 slices for the soma. Current FPGA devices exceed 50,000 slices. Therefore, it is possible to configure, for instance, over 500 physical synapses without STDP (or 250 with STDP) and 100 physical somas, running in parallel with single clock cycle iteration.

Such an arrangement would be ideal in the case of small/medium network designs for which we require hyper real-time operation, in order to understand or optimize its performance in different portions of its parameter space. Over

100,000 prototypes of the same network could be simulated in the time taken for one iteration of the biological network it represents. Hence, programmable logic provides a powerful technology for understanding and optimizing small/medium spiking neuronal models.

Synapses with a common target soma often have similar time constants in the brain. We can exploit this fact to make further gains in total synapse numbers by using only one physical synapse and convolving the incoming spikes of many virtual synapses. This is mathematically equivalent to implementing large numbers of separate synapses with identical time constants. In this way, a very large degree of synaptic convergence can be achieved, which is particularly relevant to cortical models.

In order to test the comparative speed performance of the FPGA implementation with a single PC we run parallel trials of the olfactory bulb model (Figure 3.8) on both PC and FPGA. The identical network was coded in C using the same set of equations as implemented by the hardware, compiled using GNU gcc and executed on an Intel Pentium IV 3.06 GHz with 1 GB RAM. The PC performed 10,000 numerical iterations of the network in 0.76 s without disk access. Due to single clock cycle numerical iteration, the FPGA performed the same number of steps on-chip in 303.03 μs, giving a speed up factor of *ca.* 2,500. This provides a speed-up factor of 3-4 orders of magnitude which may be further optimized either by improving the placement and routing of the logic of the design implementa-

tion, or by employing a faster FPGA (for instance, Virtex IV devices offer faster internal speeds and shorter propagation delays). In further experiments, we were able to increase the clock frequency up to 50 MHz. In both cases, about 55% of the FPGA resources were utilized.

We may also choose to exploit this hyper real-time operation to increase network sizes through the use of a multiplexing scheme. In this case we create virtual exponential decay units by storing and replacing the current state at each numerical step and optionally the associated parameters such as weight, after-hyperpolarization potential, threshold potential and/or time constant. This requires storage either on or off chip, which depending upon the access time will determine the communication overhead associated with applying a multiplexing scheme.

FPGAs have on-chip RAM block storage which has parallel access single clock cycle operation, which minimizes this overhead (Xilinx XC2VP125 device has 556 such blocks which may be variously configured). In principle, for this Xilinx device we can use 556, 1024 $\times$ 18-bit buffers to create between $10^5 - 10^6$ virtual exponential decay elements operating in biological time (18-bit precision). However, in practice there are two issues that must be addressed when using FPGAs to build large-scale neuronal models that exploit such multiplexed architectures. Firstly, at each numerical step we must store, update and replace the state of each element. This imposes a time overhead, which is at least one additional clock cycle

per numerical iteration step to move the data to and from on-chip memory. This reduces the total number of virtual elements that can be operated in biological time. Secondly, we must consider connectivity between neurons, which imposes constraints on the scale of architectures that can be deployed on a single device.

Cortical models represent a particular challenge due to highly convergent synaptic input, which is often thousands of synapses targeting each neuron. Since most cortical models adopt only one or two time constants for these convergent synapses, arriving input spikes may be convolved through only one virtual synapse for each time constant, leading to a massive reduction in resource usage. Such scaling issues represent an important focus of future research for implementing FPGA neuronal models to achieve cortical model scales in real-time.

Chapter 4

The olfactory bulb model

After reviewing the theoretical foundations of the neuron and giving a brief description of the most popular neuron models, a digital model of the neuron based on the Integrate and Fire model was designed. It was proved that such a model was able to generate exact calculations of the IF model, resulting in the construction of exact neuronal networks.

We also went through the basis of the olfactory bulb, in which we analysed the most important type of cells which comprises the olfactory bulb. Connections among elements as well as how each cell interact with each other were also reviewed. Therefore, with all these elements we are in a position to implement a biologically inspired model of the olfactory bulb. In other words, knowing the elements of the olfactory bulb and their connections, and having the construction kit for neuronal modelling on FPGA, we have all the elements to come up with a simplified version of the olfactory bulb.

In the last chapter, we have presented a construction kit for neuronal modelling on FPGA, which was able to perform at hyper real-time. One of the most important advantages of implementing circuits on FPGAs is that applications can run in parallel, which allows the circuits to process more information per clock cycle. Thus, we are in a position to implement a biologically inspired neuronal network which would run much faster than its biological counterpart. As previously mentioned, an important goal in this research, is to implement a simplified model of the olfactory bulb. Such a model has to keep the characteristics of detection and classification of the biological olfactory bulb. This simplified model was based on the olfactory systems of the vertebrates and it was described in (Pearce et al., 2005).

Figure 4.1 an schematic of the simplified model of the olfactory bulb is presented. At the input of the olfactory bulb there are 75 olfactory receptor neurons (ORNs), which express 25 different types of odours. The ORNs are represented in the schematic as light triangles receiving input from the sensors (shown by irregular polygons). ORNs expressing the same type of odorant converge into a single glomerulus (ellipses) where they make excitatory synapses (light circles) with the mitral/tufted cells (M/T) shown as dark triangles in the schematic. The inhibitory dendrodendritic connections of the granule cells onto the M/T cells are represented by feedback loops coming out from the axon of the M/T cells toward every other M/T cell via an inhibitory synapse (dark circles). This connection

effectively represents the lateral inhibition interaction between the granule cells onto the M/T cells. Finally, the output of the M/T cells project to the lateral olfactory tract (LOT), where the decoding is carried out.

4.1 Implementation

This model comprised 100 integrate-and-fire somas and 675 exponential decay synapses describing two classes of neuron in the mammalian olfactory bulb (Figure 4.1a). M/T neuron outputs in the vertebrate olfactory system are under tight regulation through lateral inhibition, mediated by dendrodendritic interaction. This interaction effects complex synchronous firing behaviour across the bulb output that is stimulus specific, reminiscent of that observed in electro-physiological studies (Friedrich & Laurent, 2001), (Friedrich, Habermann, & Laurent, 2004) and demonstrated in this model (Figure 4.1b, c). Due to the similarity of synapse time constants in this model it was possible to implement the design on a single Virtex II Pro device (Xilinx) running at a very conservative clock speed of 33 MHz.

In order to test the comparative numerical performance of the FPGA implementation with PC technology, we tested it against its software equivalent. For this purpose, the same network was coded in C++ using the same set of equations as implemented by the hardware, compiled using GNU gcc and executed on an Intel Pentium IV 3.06 GHz with 1 GB RAM. As before, the error between the

circuit and the software implementation is within a single bit and uniformly distributed (Figure 4.1d). Spike timing analysis reveals that no incorrect translation occurs between the FPGA and PC based solutions.

The olfactory bulb shown here is a simplified model of its biological counterpart. Among the simplifications applied to the circuit, one that stands out is the omission of the dendrodendritic connections between M/T cells and periglomerular cells. Nonetheless, this model effectively keeps the most relevant behaviour of the olfactory bulb such as detection, classification and memory. The inhibitory connections of the granule cells play a critical role for learning and detection (Shepherd & Greer, 1998), hence feedback loops coming out from the axon of the M/T cells toward every other M/T cell via inhibitory synapses were added to the circuit.

4.1.1 Initial results

The olfactory bulb circuit, as shown in the Figure 4.1a was implemented on the FPGA. For computational simplicity and to reflect biological diversity, the initial synaptic weights were randomly selected. In addition, for testing purposes and to show the olfactory bulb response to a simulated constant concentration exposure, random constant inputs were applied to each input of the olfactory bulb. The time constants for the implemented circuit were chosen according to (Rotter & Diesmann, 1999), where $\tau_E \approx 4\,\text{ms}$, $\tau_I \approx 16\,\text{ms}$, and $\tau_m \approx 10\,\text{ms}$. The Figure 4.2 shows the spike response from all the 25 M/T cells. At this stage, no learning

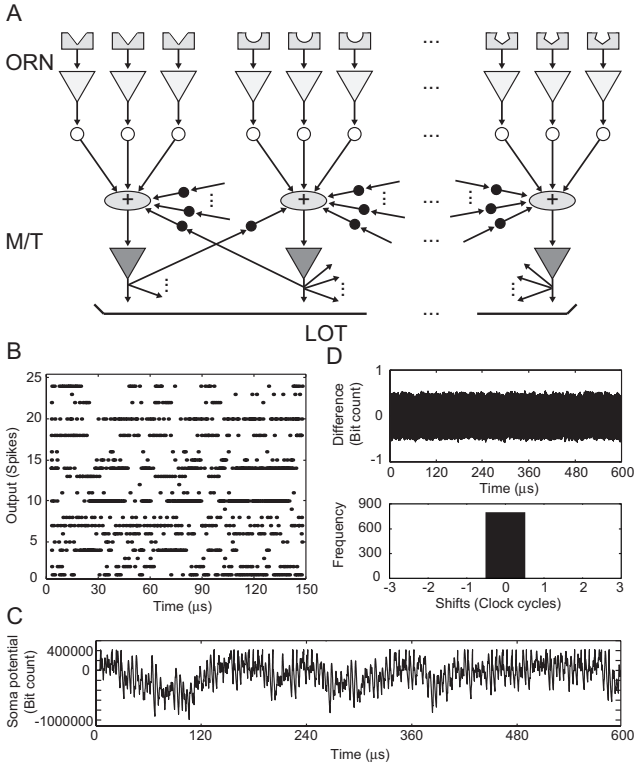

Figure 4.1: Simplified olfactory bulb neuronal model implementation comprising 100 somas and 675 exponential decay synapses. (A) Schematic of the olfactory bulb architecture. 25 mitral/tufted (M/T) cells, represented by integrate-and-fire elements provide the main olfactory bulb output (corresponding to the lateral olfactory tract). These cells are reciprocally connected via exponential decay synapses, which mediate lateral inhibition in the model representing inhibitory coupling between M/T cells in vertebrates (open circles: excitatory synapse, closed circles: inhibitory synapse). Excitatory input to the model is provided by olfactory receptor neurons (ORNs) driven by population coded receptor input shown by irregular polygons. Synaptic input from identical ORNs are summed to represent receptor input convergence at a single glomerulus (ellipse). (after Pearce, *et al.*, 2005). (B) Firing behaviour of all 25 M/T cells in the network over time. (C) Membrane potential of a randomly selected M/T cell. (D) The error between the exact integration numerical implementation and the circuit response for the membrane potential and spike timing analysis. A 32−bit representation was used with parameters $\tilde{\tau}_{e_E} \approx 2.1$ ms for the excitatory synapses, and $\tilde{\tau}_{e_I} \approx 17.1$ ms for the inhibitory synapses. The adjusted weights for the excitatory synapses were fixed to $w_{adj_E} = 256.8$, whereas the inhibitory weights w_{adj_I} were randomly chosen in a range between 1.5 and 32 inclusive. The time constants of both the ORN and mitral cells were set to $\tilde{\tau}_m \approx 10.2$ ms, with a Capacitance $C = 250$ pF, and threshold potential, $V_{th} = 432640$ where $k_V = 21.6 \times 10^6$ counts V^{-1}. For the ORNs, constant values randomly selected in a range between 4240 and 6400, were used to represent a constant concentration of an odour stimulus. The clock frequency was set to $f_{clk} = 33$ MHz, giving a step time, $\Delta \approx 30.3$ ns and a speed up factor, $k_t = 3300$. Numerical solutions were carried out in C++ using long double precision using an 80 bits representation with 64 bits out of them for the mantissa and 14 for the exponent.

algorithm was applied to the system, so the output only reflects the response of the untrained olfactory bulb system.

Figure 4.2 shows three different spatio-temporal relations between pairs of cells. Neurons 10 and 14 are clearly locked in a particular identity-temporal relation. A similar situation exists with neurons 18 and 24, whose spatio-temporal relation is different from the early mentioned pair of neurons; and cells 4 and 13 also show a spatio-temporal relation although to a lesser extent. The rest of the cells either do not show any relation at all, or they simply seem to spike in a random fashion.

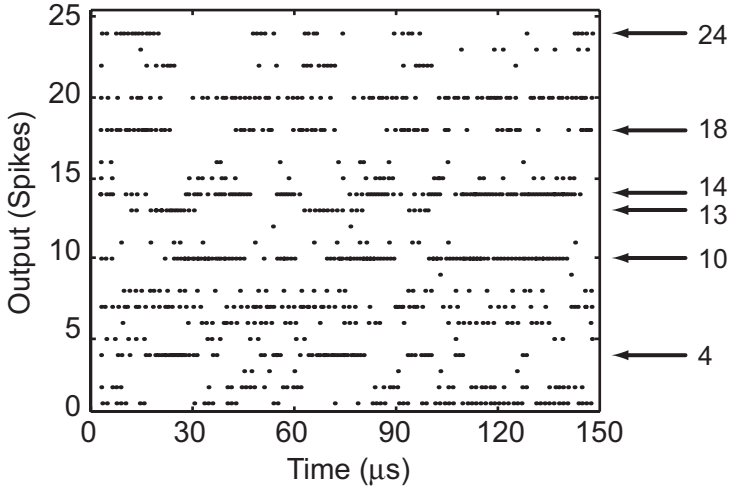

Figure 4.2: Olfactory bulb response

4.2 The Hebbian learning algorithm

For training the olfactory bulb, the Hebbian learning algorithm, which uses a rate-based Hebbian rule was performed for the circuit. As the name implies, the

learning algorithm will train the network in such a way that the output of a particular odour (which is being applied to the input of the olfactory bulb) serves as a base for the calculation of the new weights of the olfactory bulb. The new weights should increase the activity of some neurons (M/T cells) while inhibiting the activity of others. The calculation of the new weights under the Hebbian learning algorithm is based on the firing rates of each mitral cell.

As mentioned earlier, the Hebbian learning rule employed in the olfactory bulb, uses the firing rates of both the postsynaptic cell and the presynaptic cell to calculate the amount of change of the inhibitory synaptic weights. In terms of the olfactory bulb, the firing rate of a M/T cell is considered as the postsynaptic activity, but at the same time, as this M/T cell is connected to every other M/T cell by inhibitory synapses, this same firing rate plays the role of the presynaptic activity. The synaptic change is obtained by the equation (Gerstner & Kistler, 2002a):

$$\frac{d}{dx}w_{ij} = c \cdot v_i \cdot v_j, \tag{4.1}$$

where v_i and v_j are the firing rates of the postsynaptic and presynaptic cells respectively (M/T cells), c is a parameter which in order to adhere to the Hebbian learning rule has to satisfy $c > 0$.

4.2.1 The indicator function

The indicator function will let us know when the olfactory bulb has reached a particular state, which should be only reached under some specific conditions i.e. in the presence of a target odour. The equation for the indicator function is given by

$$f = \sum \alpha_i \cdot v_i, \tag{4.2}$$

where v_i is the firing rate of the M/T cell i and α_i is a firing rate, which is compared to the olfactory bulb response. The responses from the M/T cells show a firing rate related to the input of the olfactory bulb, i.e. the applied odour. During the training process, the firing rates from M/T cells are recorded and used to train the olfactory bulb according to equation (4.1). After the training of the olfactory bulb and in the presence of the same odour, it is expected that the output of the circuit tends to approach the firing rates given by the α's. Therefore, apart from using the recorded firing rates for training the system, we also use them as the matching firing rates. The indicator function thus will reach a maximum when the current firing rate of the M/T cells resembles the matching firing rate.

4.3 Olfactory bulb system integration

For the experiments, an FPGA PCI card (model ADM-XP manufactured by Alpha-Data, UK and containing a Virtex II pro FPGA device, Xilinx Inc., USA)

was used together with a host PC (see Fig. 4.3). Communication to/from the PC is performed by a host program written in C++, which controls the initial model parameters (such as weights) and FPGA sensory input in real-time. Fig. 5 shows an overall schematic of the olfactory bulb implementation. Excitatory weights, inhibitory weights and sensory inputs are stored on the PC and sent to the FPGA, where they are latched in individual registers (for excitatory and inhibitory synapses as well as ORN input). Since the PCI is a 32-bits, these values must be sent sequentially and then appropriately distributed on-chip. To achieve this incoming values are first stored in an internal memory RAM (BRAM) on the device. Then applying a multiplexing scheme, each value is sent to its respective register and access is subsequently controlled by a decoder, which enables only one register at a time.

4.3.1 Odor representation

We tested the neuromorphic implementation by applying inputs to the OB circuit and recording the spiking responses as well as the indicator functions corresponding to learnt odours. Figure 4.4 shows the responses of the OB to the application of a constant and arbitrary input pattern (which we term Odour A), simulating the receptor response to a fixed concentration of a certain odour. The top row of figures show the responses of the untrained network, which may be contrasted with the same responses in the bottom row after the application of the Hebbian learning algorithm to lateral inhibitory weights in the network.

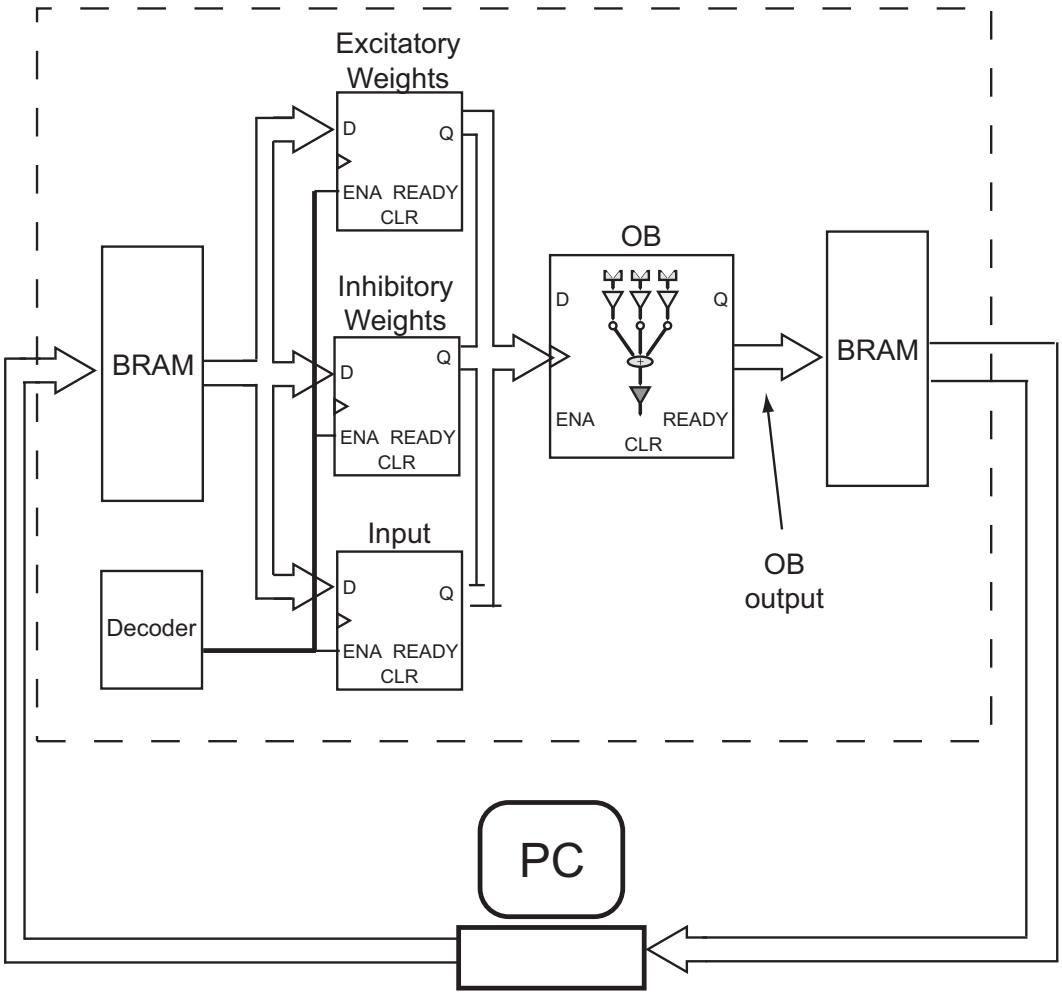

Figure 4.3: System architecture for a neuromorphic FPGA olfactory bulb implementation. BRAM memory blocks are used both at the input and at the output to support data transfer between FPGA and PC. In the initial stage, the BRAM stores and distributes the excitatory and inhibitory weights as well as the input to the internal registers of the olfactory bulb (OB) unit, enclosed in the dashed box. Odour identification and classification is carried out by the OB circuit. The resulting spike response is sent to a PC where the Hebbian learning algorithm is computed. Responses are finally stored and manipulated on a PC.

Figures 4.4a and 4.4d show the membrane potential of one particular M/T (#6) cell within the network. Before training, this particular cell showed largely periodic spiking behaviour, whereas after training increased inhibition from other M/T cells forces its own dynamics to be exclusively subthreshold. Note that the network dynamics are periodic and largely synchronized due to lateral inhibition, which is also present in the the biological system as indicated by the presence of oscillations.

Figures 4.4b and 4.4e show the spiking responses of the entire network to an arbitrary odour input pattern both before and after learning. The same indicator function calculated for the trained and untrained network (Fig. 4.4c and f, respectively) demonstrates a very large increase after training (50:1) demonstrating that the learnt odour stimulus is able to invoke a stored attractor in the state space of the OB model which may be exploited for classification.

4.3.2 Odour classification

In order to demonstrate the classification properties of the OB model, the same network was subjected to a second arbitrary but constant input pattern (which we term Odour B), representing the receptor response to a distinct odour at the input.

Hebbian learning was then applied again to further adapt the lateral weights, this time to the new input pattern. After training, each odour (Odour A and Odour B) was presented sequentially and the corresponding indicator functions

for both learnt odours calculated over time (see Figure 4.5). We see that the corresponding indicator function for the learnt odour is high after a short time, whereas the other indicator function is low. When we present the second odour the situation is the opposite, indicating that the network is able to store two attractors corresponding to the two odours and we can read these out to classify the odours accordingly.

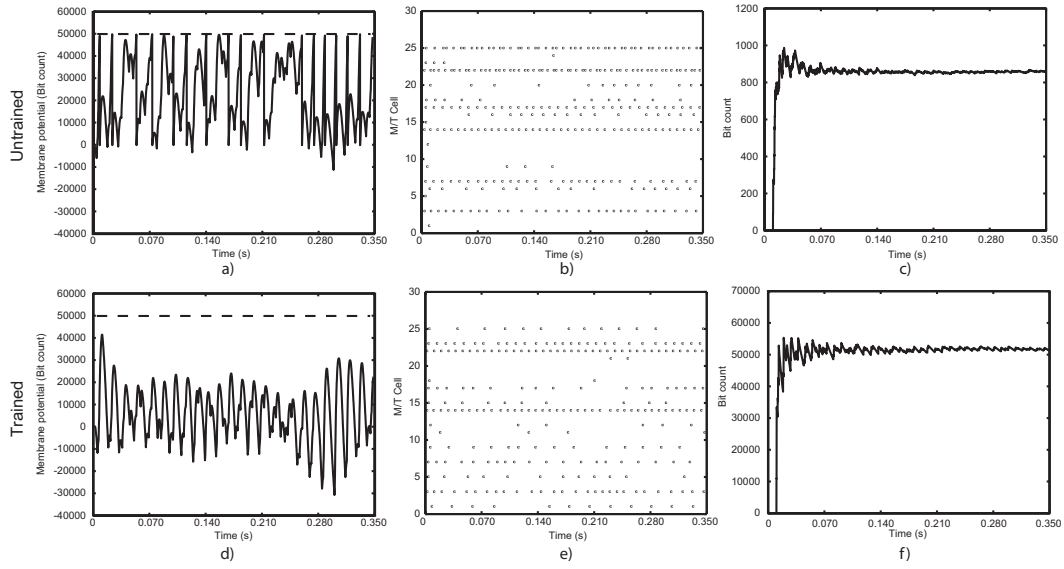

Figure 4.4: Neuronal responses and indicator functions to an arbitrary odour input pattern 'Odour A' before and after learning in the OB model. Comparison between the untrained network (upper graphs) and the trained network (lower graphs). Fig: a) and d). Membrane potential of a randomly selected M/T cell (#6). Fig b) and e): spike response for the 25 M/T cell population at the output of the circuit. Fig c) and f) Indicator function of the circuit in response to the same stimulus, Odour A, before and after training showing a large increase in magnitude. The time constant parameters we have used for the OB model are equivalent to the biological values: $\tau_E = 4$ ms (excitatory synapses), $\tau_I = 16$ ms (inhibitory synapses), $\tau_m = 10$ ms (ORNs and M/T cells), at a sampling frequency $fs = 10$ kHz.

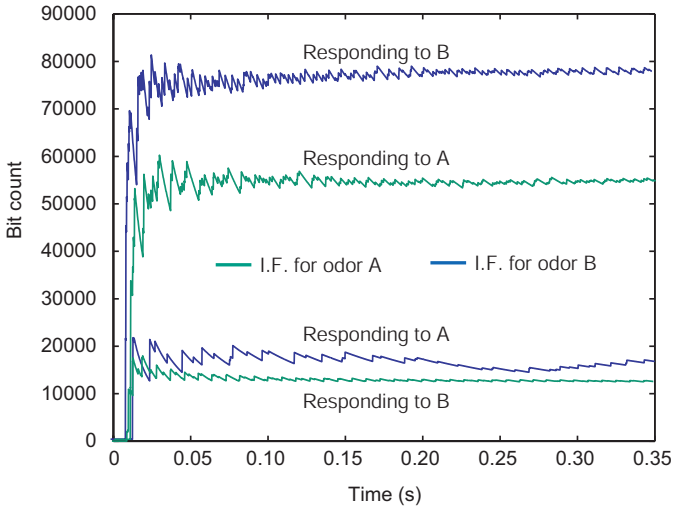

Figure 4.5: Indicator functions for the odour classification task. The same network is trained to 2 odours, A and B from which indicator functions (I.F.) are constructed. Shown is the indicator function response for both A and B when odour A and B are presented. In each case the indicator function for the learnt odour is far higher than that for the distracting odour. The time constant parameters we have used for the OB model are equivalent to the biological values: $\tau_E = 4$ ms (excitatory synapses), $\tau_I = 16$ ms (inhibitory synapses), $\tau_m = 10$ ms (ORNs and M/T cells), at a sampling frequency $fs = 10$ kHz.

4.3.3 Learning capabilities

In order to find out how many odours can be stored in the olfactory bulb, the model was trained for several odours and their characteristics were analysed. Initially, the olfactory bulb was trained for 5 odours, a principal component analysis was carried out to obtain the characteristics of the trajectories for each odor. In addition, an ANOVA test was performed to define whether the mean value among the first principal component from all odours were different. That is, we want to reject the following hypothesis:

$$H_0 : \mu_1 = \mu_2 = \cdots = \mu_n \tag{4.3}$$

Total of odours	F-value	p-value
5	20007.5	0
6	11887.1	0
7	29194.3	0
8	2811.5	0

Table 4.1: ANOVA test results for the comparison among mean values from each principal component from each odours. The olfactory bulb trained for 5, 6, 7 and 8 odours and the mean value of each first principal component was compared by an ANOVA test. In all cases, the null hypothesis was rejected in favour of the alternative hypothesis.

in favour of

$$H_a : \mu_i \neq \mu_j, \tag{4.4}$$

where $i \neq j$ and for at least two means being different.

Figure 4.6(g) shows the principal component analysis for the olfactory bulb trained for 5, 6, 7, and 8 different odours. As it can be seen, as more odours are added to the olfactory bulb, higher are the probabilities of the trajectories to overlap in the space of the principal components. However, to effectively asses the differences among mean values for each odour, the following table shows the results from the ANOVA test conducted for the model trained for 5, 6, 7 and 8 odours.

Given the results obtained by the ANOVA test, and since all null hypothesis were rejected in all experiments, the next step is conduct multiple comparisons to identify those means whose value are different. The multiple comparisons were carried out using Tukey's procedure. Figure 4.6(g) also show the results yielded by the multiple comparison analysis. For 5 and 6 odours, all mean values were different, which means that the olfactory bulb should be able to effectively identify

among these odours. However, for 7 odours, the mean value for the odour 3 turned out to be the same as the random odour (background noise), which could result in misidentification of the random odour as the odour 3 or conversely, a lack of detection of the odour 3 by regarding it as a random odour. Even worse, for 8 odours, the Tukey's procedure reveals that the mean value of odour 8 and the random odour are the same; and the mean values of odours 3 and 4 cannot be rejected that they are different. Therefore, the learning capabilities of the olfactory bulb are then constrained to about 5 to 6 odours at most.

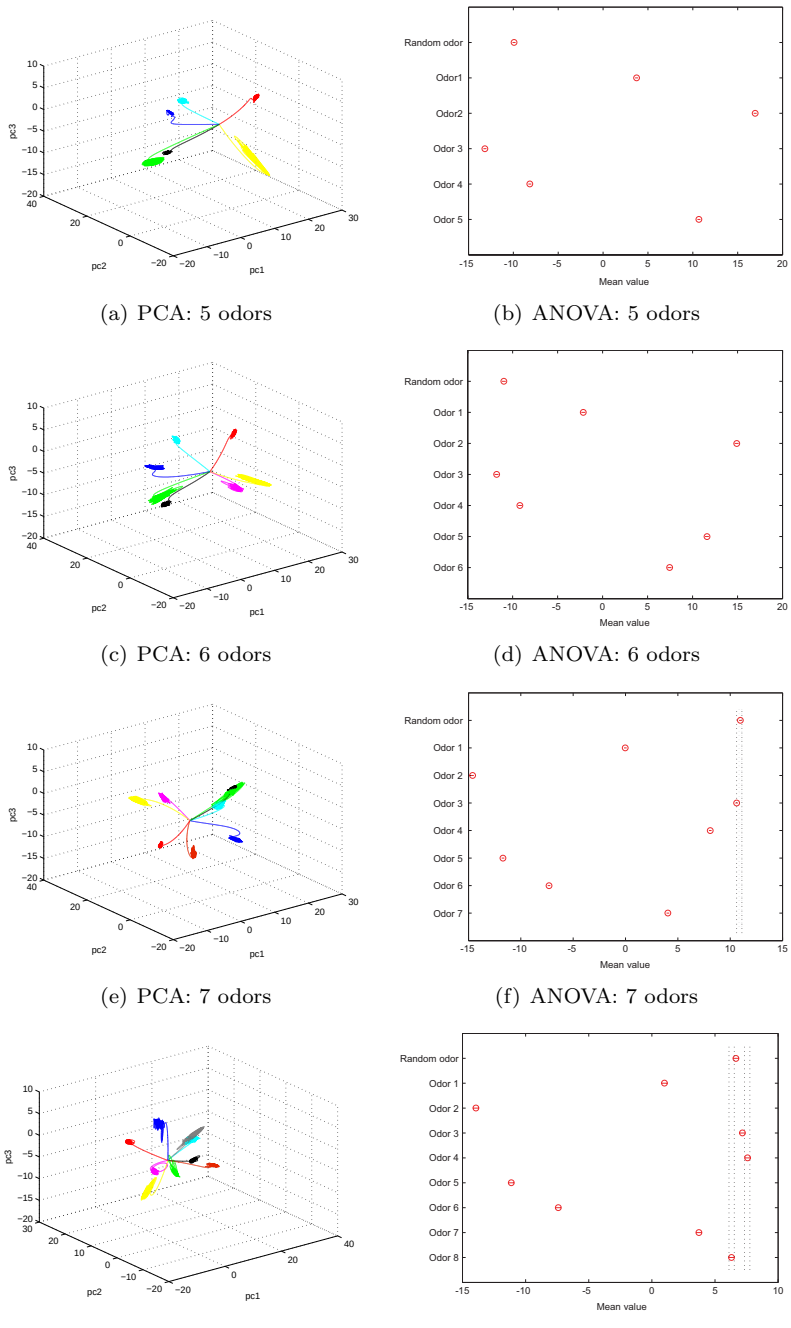

(a) PCA: 5 odors (b) ANOVA: 5 odors

(c) PCA: 6 odors (d) ANOVA: 6 odors

(e) PCA: 7 odors (f) ANOVA: 7 odors

(g) PCA: 8 odors (h) ANOVA: 8 odors

Figure 4.6: Learning capabilities of the olfactory bulb trained to 5, 6, 7 and 8 odours.

Chapter 5

Identification and segmentation of real data

5.1 Introduction

Having tested the construction kit for neuronal modelling by means of implementing the olfactory bulb, it is now necessary to validate the olfactory bulb model using real data. For this, we resort to an interesting experiment carried out by researchers at the laboratory of Chemistry at Tufts University, in the USA. Part of their experiment consisted in collecting odour information obtained by means of specialized sensors called 'fluorescent microbeads'.

Sensor responses reflect changes in fluorescence intensity and wavelength shifts that occur as vapours are presented to the sensor array. Many parameters (e.g. vapour diffusion through the polymer layer, polymer type, surface-vapour inter-

Type of bead	Number of beads in the array
af	3
alltech	1
chirex	7
chirexpta	42
lunaphenhex	11
lunapte	12
phenoscn	3
prop	9
scxptb	383
scxptc	227
scxptf	166
sel	4
tbap	1

Table 5.1: Types of beads embedded in the microbead sensors array.

actions, pulse time, and pulse regime) contribute to the optical response resulting in unique chemical signatures for a particular vapour-sensor combination.

Fluorescent microbead sensor arrays were developed in the laboratory of chemistry of Tufts University. These are made up of thousands of fluorescent sensors which detect changes in fluorescence intensity due to the presence of a vapour. Different vapours cause different responses from the sensor array, a characteristic which should allow the identification of a variety of pure vapours as well as compounds (Bencic-Nagale & Walt, 2005). It is therefore the response from these microbead arrays that is of particular interest to us as it contains valuable odour information under different conditions (i.e. responses to pure or mixed vapours under different backgrounds and concentrations). Here, we apply such responses from several experiments to the olfactory bulb circuit to demonstrate the identification, classification and segmentation capabilities of the model.

5.2 Data collection

A CCD system was coupled to an optical fibre and used to record changes in the fluorescence due to the presence of a vapour. The CCD device was able to measure changes in the intensity caused by the vapour by passing an excitation light through the optical fibre. The resulting responses from the microbead sensors array were captured in a 30 frames movie (where the first five frames correspond to the baseline, about 20 subsequent frames to the vapour pulse while the remaining frames were obtained after the pulse was withdrawn (Bencic-Nagale, Sternfeld, & Walt, 2006)). The microbead sensors array used in the experiment consisted of 869 beads of 13 different types (see Table 5.1).

The collected data set consisted of a total of 7 pure odours (see Table 5.2), which shall be used later in the identification, classification and segmentation experiments. In order to collect sufficient data for these experiments, each pure odour was exposed to the sensor array 10 times. In addition, mixtures (compounds) of these seven odours were also obtained and processed by the bead sensors so their corresponding responses could be recorded. As will be shown later, these data prove to be valuable for demonstrating the identification, classification and segmentation capabilities of the olfactory bulb. These compounds were obtained by mixing all possible pairs of pure odours in the same proportion. Similarly, all possible combinations of three odours were mixed in the same proportion to get different compounds. This process was repeated for mixtures of 4,

vapour key	Description
A	Toluene
B	Methyl Salicylate
C	Ethanol
D	Heptane
E	P-Cymene
F	Cyclohexanone
G	Chloroform

Table 5.2: vapours used in the laboratory of chemistry in the Tufts University for segmentation tasks.

5, 6 and 7 odours. Unlike pure odours, which were scheduled for 10 times each in the experiment, mixtures were scheduled to be processed by the sensors for five times only.

It is well known that the different elements of a measuring system such as the one described here suffer changes over the time. These changes can be caused by several factors (which are sometimes out of the control of the experimenter). Among some of the most common examples, we can mention:

- Natural changes on the sensitivity of the sensors due to the prolonged use and the length of the experiment.
- Changes in the sensitivity of the recording components.
- Changes in the intensity of the sources of the system (for instance, the intensity of the lights used to stimulate the sensors may also add noise to the response).

Therefore, an additional neutral substance (bleach) was systematically scheduled to be processed several times during the entire experiment as a 'control run'

Date	Time	Run number
14/12/05	2:13 PM	1 - 101
15/12/05	8:11 AM	102 -203
15/12/05	2:49 PM	204 - 305
19/12/05	10:00 AM	306 -406
19/12/05	1:30 PM	407 - 508
19/12/05	5:09 PM	509 - 610
20/12/05	11:00 AM	610 - 711
20/12/05	3:30 PM	712 - 817

Table 5.3: Schedule of all the runs of the entire experiment performed in the laboratory of chemistry in the Tufts University for segmentation tasks.

to quantify the extent of change in the sensors' response as a consequence of the above factors. As the total experiment (which consisted of 817 runs), was carried out over several days, control runs were scheduled each day prior to and after the scheduled odours trials. Additional control runs were scheduled every seventh run to gain more detailed information on the changes on the recording system. All the pure odours and all compounds were randomly scheduled for this experiment prior to the start of the experiment, only control runs were scheduled as previously described. Appendix D shows the odours and compounds associated with each run.

5.3 Quantifying changes in the responses

As previously explained, control runs were run at the beginning and at the end of each daily recording sessions. They were intended to quantify the deviations among responses, so that differences due to changes in the sensitivity of the sensors can be detected. The inactivity period to which the sensors were subjected at the

end of each day may be an additional cause of change in the response as it might allow the different elements of the system to recover from a long period of activity. Besides, as the lifespan of the sensors is limited because of the photo bleaching of the dyes attached to the microbeads, a special filter (called ND filter) has to be changed at some point during the experiment (Bencic-Nagale & Walt, 2005), which accounts for some change in the response of the sensors. The new filter could also be responsible for changes in the intensity of the excitation light and thus in the responses.

As already mentioned, in addition to the first and last control runs (which mark the beginning and end of the experiment for each day), control runs were inserted after six consecutive trials. Figure 5.1 shows the evolution of the control responses over the time. The first trial corresponds to the response at the bottom of the plot; successive runs show an upward tendency in the baseline of the response.

In Figure 5.1 the response is shown by frames of which a total of 30 were obtained for each run. As the figure suggests, the stimulus is applied from the fifth frame (however it only seems clear that the stimulus is indeed present from the seventh frame) to about the twenty third frame.

Figure 5.1 shows that the response varies among trials as the baseline seems to move upward from trial to trial. This could primarily be caused by the change in the sensors as the experiment progresses. First, it is necessary to quantify the

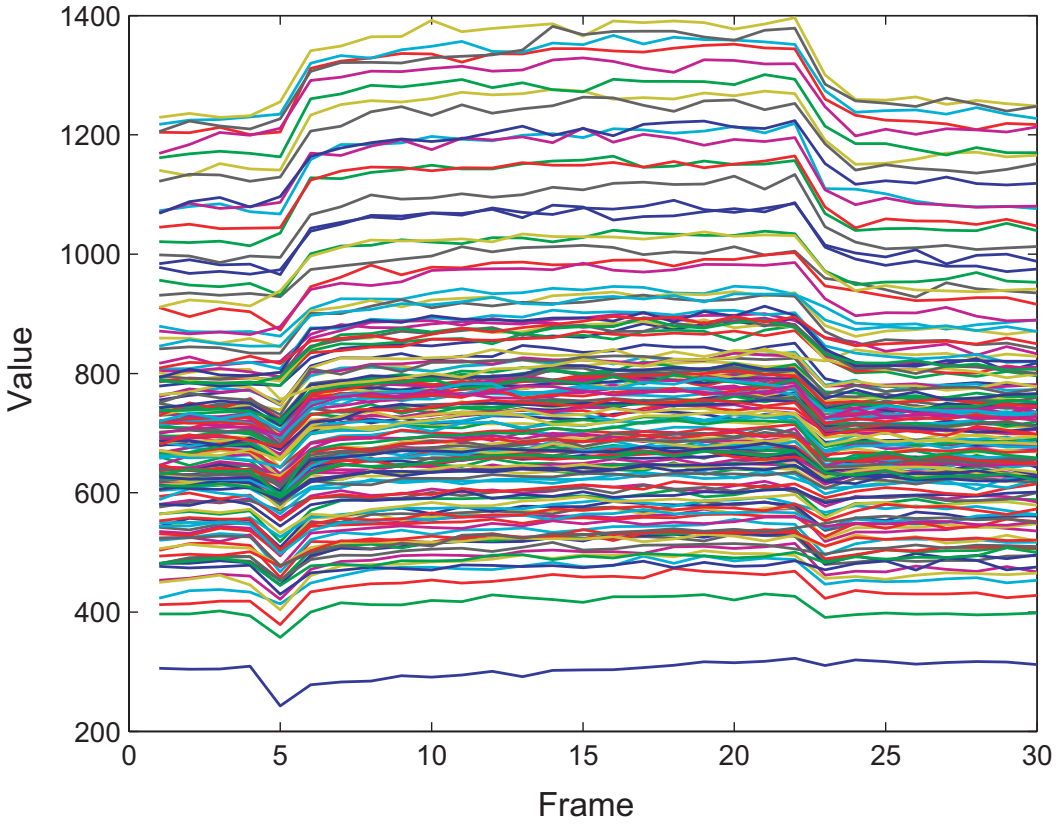

Figure 5.1: Response of the control experiments over the time. A total of 147 control runs were carried out along the experiment. Control runs can identify possible deviations in the response of the beads over the time due to the natural change in sensitivity of the sensors by the use. Each individual response is recorded over 30 frames. Control runs use a neutral substance as a mean to obtain a baseline reading. The first control run corresponds to the response shown at the bottom of the plot. As the experiment progresses, the response drifts away from the baseline. Control runs show a growing tendency in the response.

variation of the sensors responses from trial to trial (for the entire data collection). For this, data per control run were first sorted by bead type. Then data from each type of bead were added together and averaged to obtain a unique or characteristic response for that bead type. The ratio of change in response before and during the stimulus can then be calculated using the equation

$$r_n = \frac{(x_a - x_b)}{x_b} \tag{5.1}$$

where x_a is the mean response for bead during the application of the stimulus (from frame 7 to frame 21) and x_b is the mean response prior to the application of the stimulus (from frame 1 to frame 4). Figure 5.2 shows the change of this ratio over the experiment for each type of bead. Most of the type of beads show an initial decaying tendency, followed by some discontinuities (due to some recovery of the sensors) after which, the decaying tendency is present again. The tendency only reverses to a growing trend after the discontinuity located near run 600.

Figure 5.3 displays a view of the control responses of the bead type 'scxptb'. Of particular interest are the ratios in the vicinity of points 300 and 600, which show an important discrepancy from the last run. As previously explained, this behaviour was expected due to the resting time between runs (refer to the schedule for the experiments shown in Table 5.3). The schedule clearly explains the jump in the response at the point 306, due to a longer resting period of 3 days between runs. For the point 611, although the experiments were resumed the following

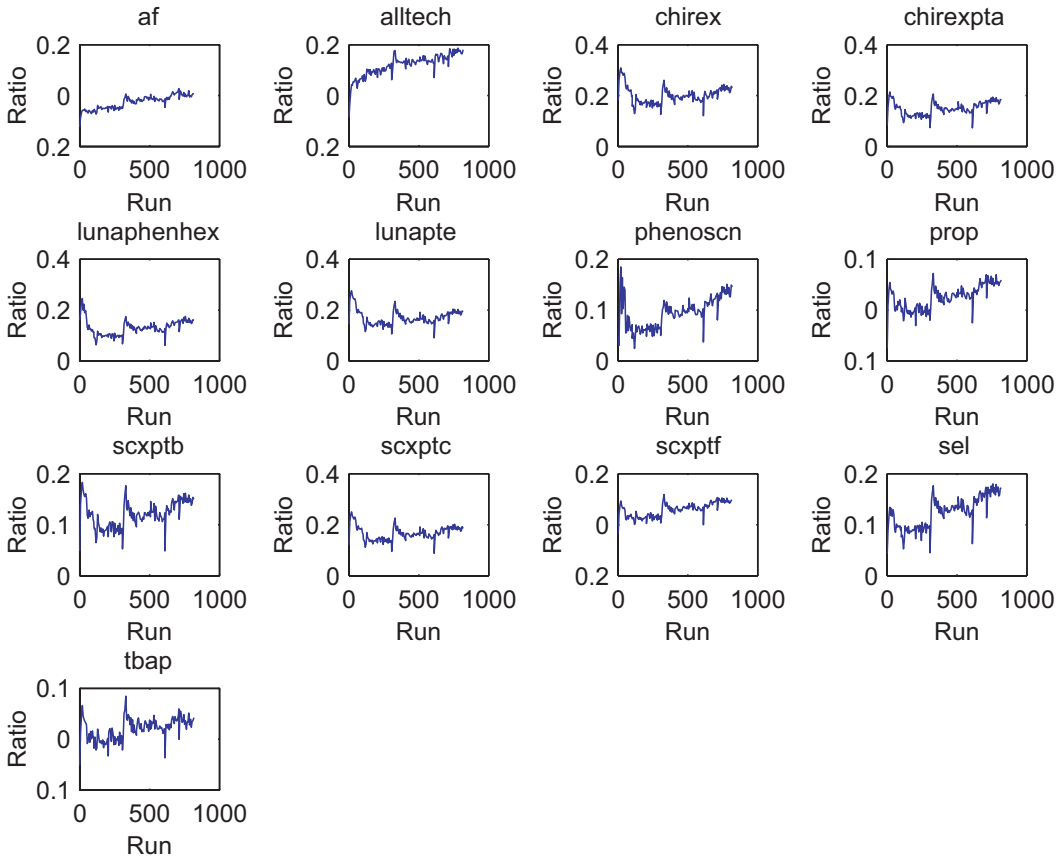

Figure 5.2: Variation in the sensors response over the time. The changes in sensitivity of the sensors over the time are calculated using equation 5.1. Changes were calculated by type of bead and shown above. Most of the type of beads show an initial decaying tendency, followed by some discontinuities (due to some recovery of the sensors) after which, the decaying tendency is present again. The tendency only reverses to a growing trend after the discontinuity located near run 600.

date, the jump in response is explained by the ND filter (used to attenuate the excitation light), which was changed for a new one. This change of filter was needed to compensate for sensor photo-bleaching.

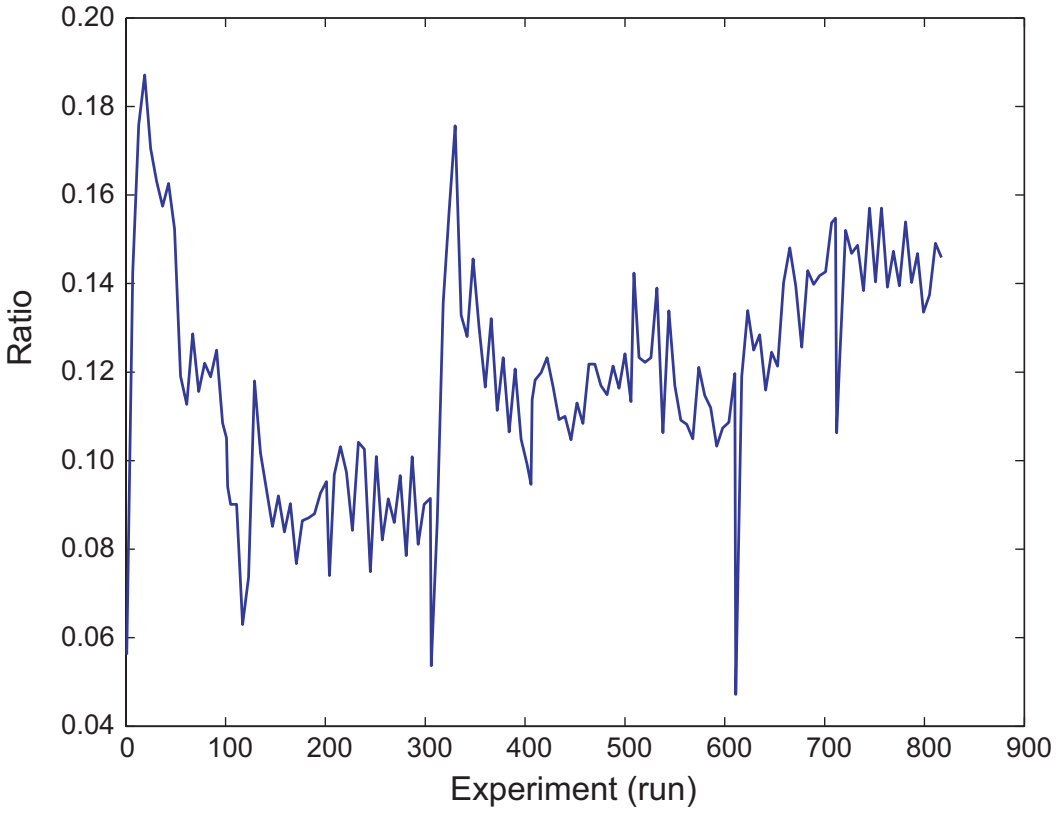

Figure 5.3: Variation in the sensors response for the type of bead 'scxptb' over the time. The changes on the sensitivity of the sensors over the time are calculated by the equation 5.1. Changes were calculated by type of bead and shown above. This type of bead show a typical behaviour among the beads, with an initial decaying tendency, followed by some discontinuities (due to some recovery of the sensors) after which, the decaying tendency is present again. Only after the discontinuity located near the run 600, the tendency reverses to a growing trend.

Figure 5.3 shows a decaying tendency on the sensor response, which continues up to experiment 305. After the recovery caused by the resting period, the response continues decaying up to the point 610, in which the filter replacement

occurs. However after the new filter is used, the response shows a growing tendency until the end of the experiment. This pattern repeats for most of the bead types ('chirex', 'chirexpta', 'lunaphenhex', 'lunapte', 'phenoscn', 'prop', 'sxcptc', 'scxptf', 'sel' and 'tbap'). Although the pattern is similar for most types of beads, the scales are different. Types 'af' and 'alltech' unlike most types of beads, show a continuous growing tendency.

5.4 Analysis of the odour information

A closer inspection on the experimental responses of individual odours, for all ten experiments per odour are shown in Figures 5.4 and 5.5. Sensors presented a strong response to the odours Ethanol, Cyclohexanone, and Chloroform, whereas Toluene, Methyl Salicylate, Heptane and P-Cymene, seem to contain less information. However, as shown later, they contain buried odour information which may be useful for detection purposes.

The mean response per bead type is calculated using the formula:

$$\bar{x}_{i,j} = \frac{1}{n} \sum x_{i,j} \tag{5.2}$$

where $\bar{x}_{i,j}$ is the average response of odour i and bead type j, n is the total number of trials (10 for pure odours and 5 for compounds), and $x_{i,j}$ is the individual response per experiment for odour i and bead type j. Additionally, it is of practical importance to calculate the standard deviation of all responses. For this, we used

the equation:

$$\sigma_{i,j} = \frac{1}{n-1} \sum (\bar{x}_{i,j} - x_{i,j})^2, \tag{5.3}$$

where $\sigma_{i,j}$ is the standard deviation of odour i and bead type j.

Figures 5.6 to 5.8 show radar plots for all pure odours and some selected mixtures. As can be seen, all responses have different characteristics for the mean and standard deviation, which makes them susceptible to be tagged as different odours.

Figures 5.6 to 5.8 show the mean response and the values below and above one standard deviation by bead type for all pure odours (Figure 5.6 and Figure 5.7) and for selected mixtures (Figure 5.8). The control data shows higher values than odours for the mean and standard deviation by bead type. The bead of type 'af' has a lower value for the control data than the rest of the bead types for the same control data. Ethanol, Cyclohexanone and Chloroform show a more varied mean response by type of bead. These responses also show higher standard deviations. The sensor response for Ethanol has the highest variability in the type of bead 'alltech', 'af' and 'scxptf'. Cyclohexanone data has more variability in the beads of type 'phenoscn', 'lunaphenhex' and 'scxptf'. Finally, Chloroform shows higher variability in beads of type 'phenoscn' 'alltech' and 'scxptf'.

On the other hand, Toluene, Methyl Salicylate, Heptane and P-cymene show a somewhat similar behaviour, which might complicate the identification of these pure odours by the olfactory bulb.

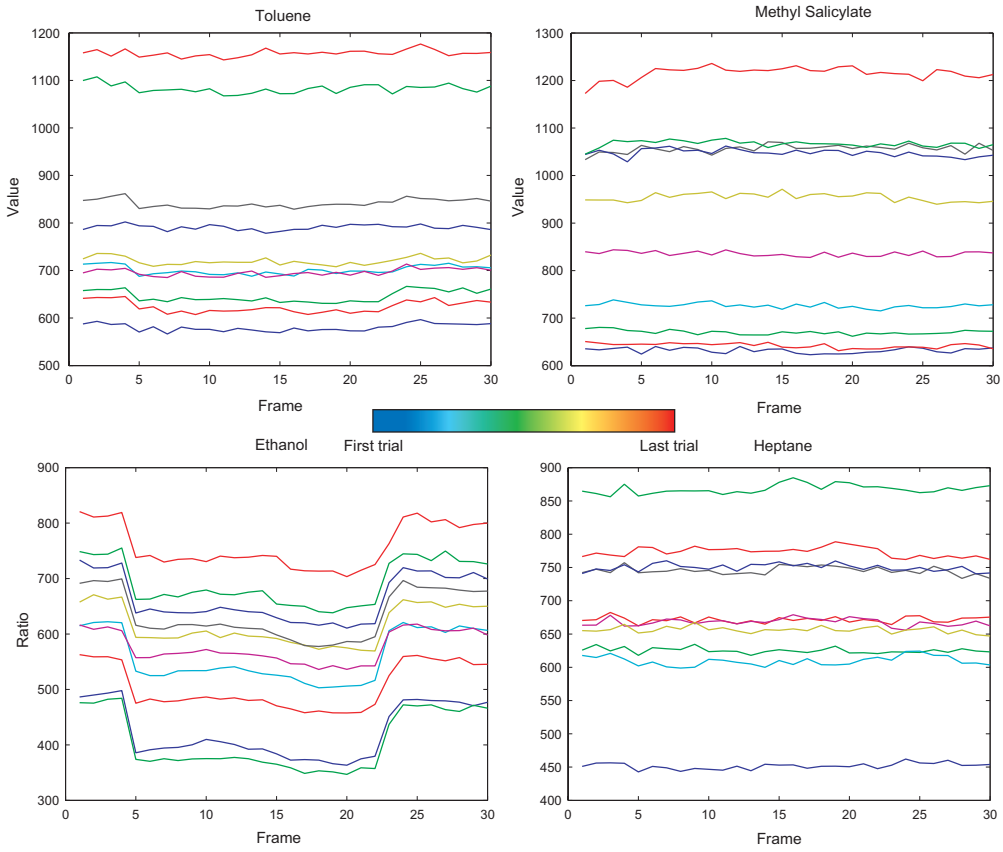

Figure 5.4: Response of the experiments to Toluene, Salicylate, Ethanol and Heptane, over time. A total of 670 odour runs were carried out. Having 7 pure odours (table 5.2), there were 10 runs per odour, whereas all possible combinations of mixtures for two, three, four, five, six and seven odours were carried out 5 times each combination. A random selection of the order of the trials was obtained. Odour runs consist of recording the intensity of a light by the sensors (beads), which respond with a change in the readings every time an odour is applied. The first trial for each odour corresponds to a dark blue line, whereas the last trial is indicated by the red solid line, intermediate runs take a colour between the blue-red range. The odour stimulus is applied by the fifth frame and remains until the 23th frame.

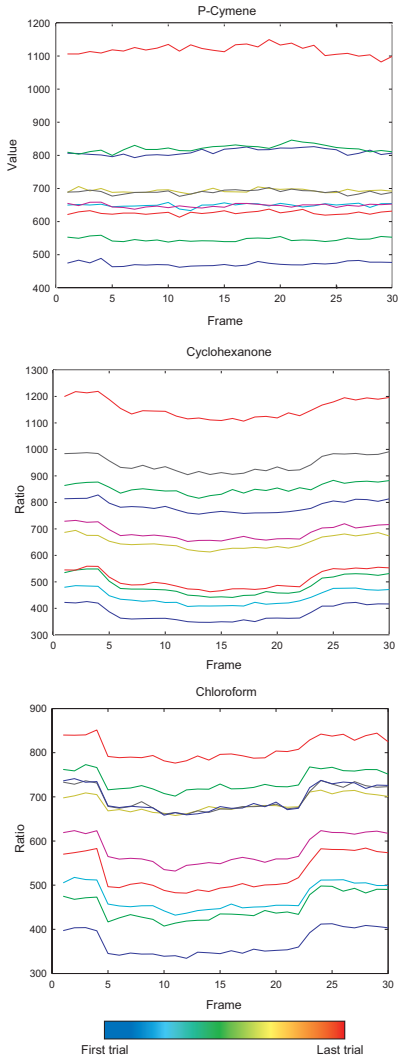

Figure 5.5: Response of the experiments to P-Cymene, Cyclohexanone and Chloroform, over time, obtained in an identical fashion to Figure 5.4.

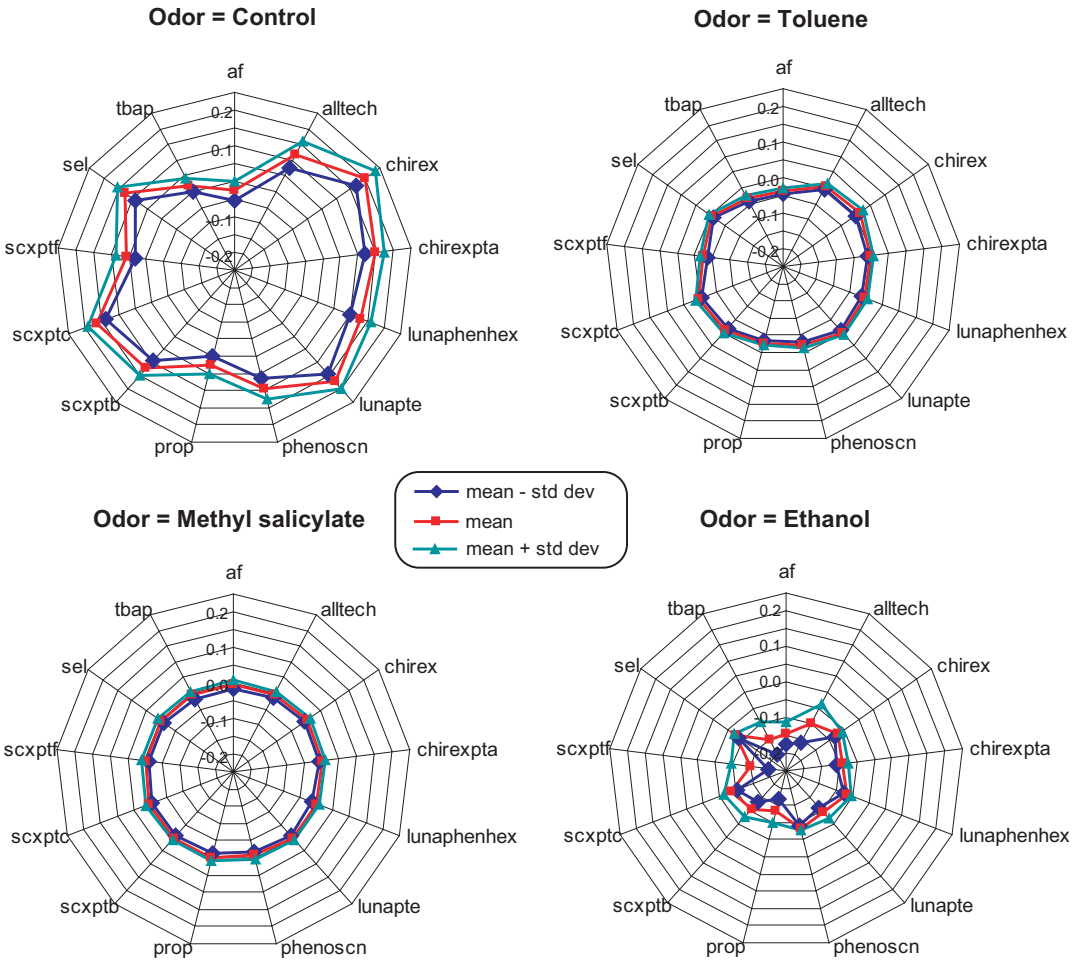

Figure 5.6: Radar plots of the mean response by type of bead for the odour responses (Toluene, Salicylate and Ethanol). The radar plots show the mean value for each odour by type of bead, as well as the value of the mean plus and minus the standard deviation. As the plots suggest, the mean values and the standard deviations are different for each odour, indicating that they have different characteristic from each other.

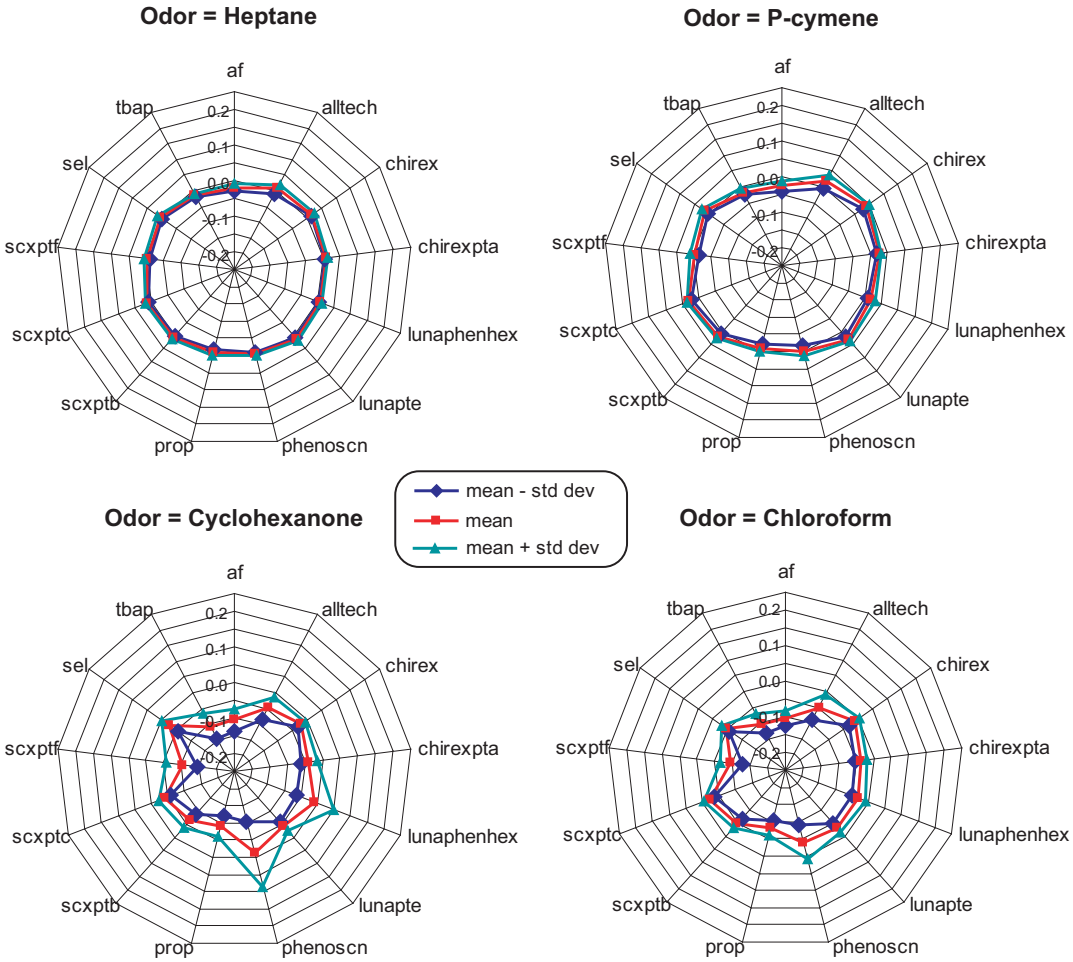

Figure 5.7: Radar plots of the mean response by type of bead for for the odour responses (Heptane, P-Cymene, Cyclohexanone and Chloroform) as in Figure 5.6.

Therefore, Ethanol, Cyclohexanone and Chloroform seem to contain the most useful information for identification purposes, since these odours show the most unique characteristics among all the odours, whereas the rest of the pure odours might be misidentified due to the similarity between mean values.

A different situation occurs for mixtures of Toluene with other pure odours. The selected compounds (containing Toluene) show very unique response characteristics. For instance, Toluene + Methyl Salicylate + Ethanol + Heptane has high standard deviations for all mean values by type of bead, whereas if we add P-cymene to the previous mixture, the overall response by type of bead is increased, but the standard deviation is reduced. In the same way, the compound containing all of the pure odours shows mean responses with a high degree of variability for each type of bead. The highest standard deviation is obtained in the type of bead 'chirexpta'. Yet when the Chloroform is not present, the standard deviation with the highest value is found in the bead type 'phenoscn'.

As is evident in figures 5.6 to 5.8, all pure odours and the selected compounds have different characteristics. Therefore, it is reasonable to expect positive identifications by the olfactory bulb model.

5.5 Identification and categorization test

Having analysed the characteristics of the odour information data obtained in the laboratory of Chemistry in Tufts University, we are now in a position to test the

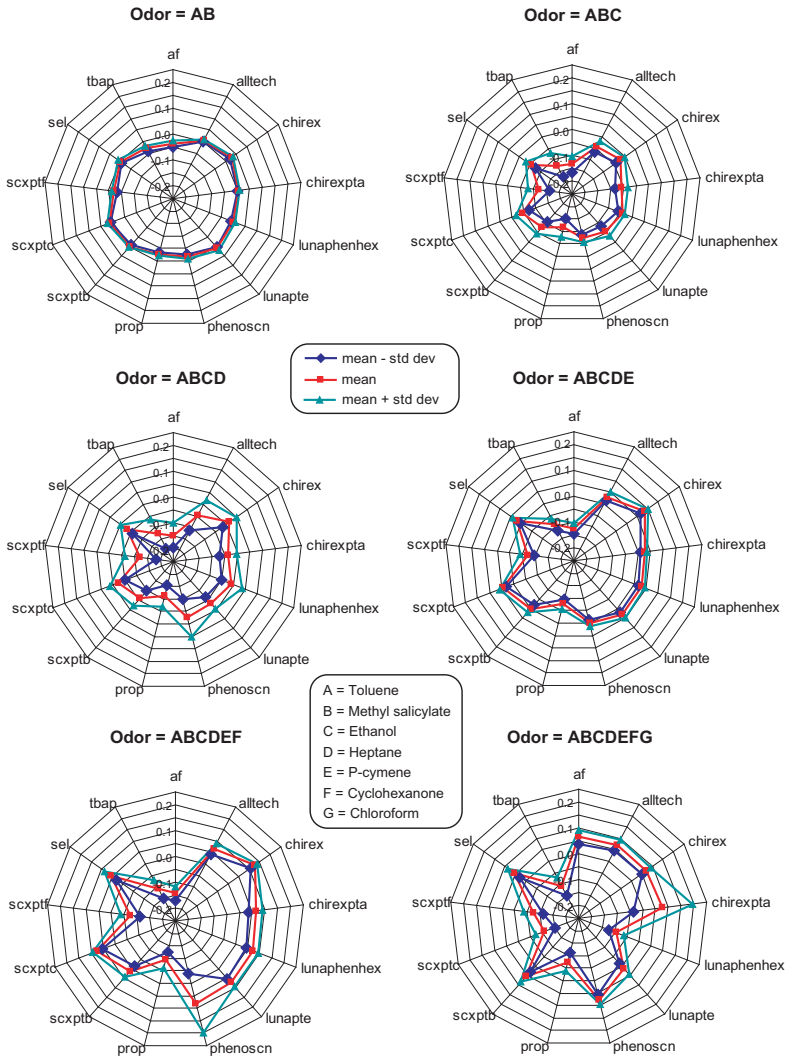

Figure 5.8: Radar plots of the mean response by type of bead for the selected mixtures. The radar plots show the mean value for some mixtures and by type of bead, as in Figure 5.6.

olfactory bulb model using real data.

From the analysis of the responses recorded with the fluorescent microbead sensors array, we assume that based on the particular characteristics of each odour, it should be possible for the olfactory bulb to identify each odour without any preprocessing. The next part of this section presents two different experiments using the data previously discussed.

The first experiment deals with the identification problem. The olfactory bulb will be trained for a particular odour (for instance Toluene) and then different data from the same odour will be fed to the model. Responses form several runs will be compared, to determine whether or not the olfactory bulb was successful at detecting the runs containing the target odour.

The second experiment will tackle a classification task. The model will be trained for several odours simultaneously. Multiple runs of distinct odours will show whether or not the olfactory bulb could effectively distinguish to what odour each run belongs.

If these experiments are successful our model would be confirmed as a plausible neuronal model of the olfactory bulb.

5.5.1 Identification

As discussed earlier, the data set obtained from the fluorescent microbead sensors array system contains information of single odours as well as mixtures of two or more types. Hence, the main concern is to prove that the olfactory bulb will be

able to identify trials containing the target odour.

All responses from the microbead sensor array were processed in the following fashion:

1. The ratio for each bead type was obtained according to equation 5.1.

2. Prior to being fed to the model, the data were processed by the following equation:

$$r_n^{'} = \frac{K}{1 + e^{-\frac{r_n - a}{b}}} + c, \tag{5.4}$$

where $r_n^{'}$ is the ratio of change of the signal for the type of bead designated by n, r_n was obtained by the equation 5.1; $K = 500$, $a = 0$, $b = 0.01$, and $c = 500$.

Equation 5.4 is a sigmoid function (Figure 5.9) which spreads or compresses the data, limiting them to the range between 500 and 1000, the range in which the olfactory bulb should be operating (more on this in chapter 6). Each run of the data set was reduced to information from 13 different types of bead.

The olfactory bulb consists of 75 olfactory receptor neurons (ORN) at the input. Groups of three ORNs converge to a single glomerulus. Each glomerulus expresses the same type of odorant (Friedrich, 2006) and altogether, there are 25 glomeruli in the olfactory bulb model.

In order to fit the odour information from the 13 different types of beads of the microbead sensors array into the 25 separate glomeruli of the olfactory bulb, the information from one type of bead is sent to two different glomeruli. This

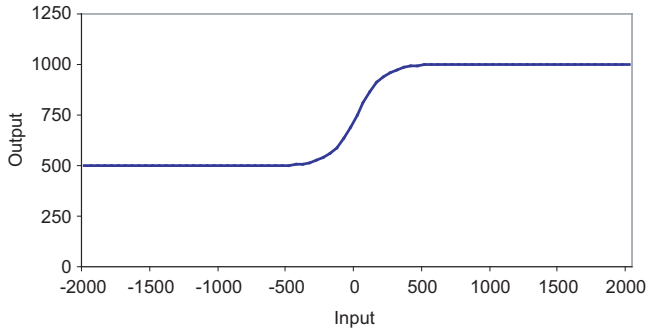

Figure 5.9: Sigmoid function used for fitting data to the input of the olfactory bulb. The parameters of this sigmoid function are: $K = 500$, $a = 0$, $b = 0.01$, and $c = 500$, limiting the data to the range of 500 to 1000.

is however not unproblematic since an extra glomerulus is then needed to fit the data into the olfactory bulb. As adding an extra glomerulus to the olfactory bulb could result in changes to the model, it is preferable not to duplicate the data of one type of bead but rather to send that particular type of bead to just one glomerulus. Since the bead type 'tbap' is embedded only once in the array, it has been (arbitrarily) decided to choose this bead as the one to be connected to a single glomerulus.

The same parameters of the olfactory bulb used in a previous experiment (see Chapter 4) will be adopted. Hence, the time constant for the excitatory synapses is set to $\tau_E \approx 4\,\text{ms}$, for the inhibitory synapses to $\tau_I \approx 16\,\text{ms}$, and for all types of somas (ORNs and mitral cells), $\tau_m \approx 10\,\text{ms}$.

To configure the olfactory bulb, the initial state of the weights of the model were randomly chosen within a range of 96 to 192 for the inhibitory synapses and

within a range of 1000 to 1400 for the excitatory synapses. These ranges were selected by trial and error in order to allow most of the neurons to show some spiking activity.

The identification experiment was carried out in two stages. First the response of the untrained model to one odour was obtained, followed by the response from the trained model. A comparison of the responses before and after training then allows to observe the effect of the training on the olfactory bulb. At the end of the experiment, we should be able to determine whether the olfactory bulb is effectively detecting these cases where the target odour is present.

5.5.1.1 Experiment using Toluene as the target odour

For this first experiment, odours containing Toluene will be used to determine if the olfactory bulb is correctly identifying whenever Toluene is present. As mentioned in the section 5.2 of this chapter, a total of 10 runs were performed for pure odours by the microbead sensors array system. In order to keep the characteristics of the responses for all 10 trials, the average value from all the 10 runs is used as the target odour, which would represent the average response of the sensors array to Toluene.

Figure 5.10a shows that the untrained model produces very little activity at the output. Mitral cells 2, 3, 10, 15, 16 and 23 responded to the stimulus of Toluene applied at the input of the olfactory bulb. A cross-correlation analysis found synchrony among cells 2, 3, 15 and 16. Figure 5.11 show larger peaks on

the cross-correlation plots for those cells. In the same way, mitral cells 10 and 23 obtained a high cross-correlation value, indicating synchrony between them.

In the second stage of the experiment, the olfactory bulb was trained using the Hebbian algorithm (see Chapter 4 for more details). The average response of Toluene was used as the target odour. A total of 100 training iterations were carried out before the model was considered trained. Figure 5.10b shows the response of the trained olfactory bulb to the same input used for the untrained model. The response of the trained circuit shows a different behaviour than the untrained response. More spiking activity is elicited at the output of the model. Figure 5.12 shows the cross-correlation among the cells with more activity. As in the untrained response, the same synchronized cells are present here. Additionally, cells 1, 14 and 19 also present some synchrony. It is important to emphasize that this synchrony is based on much more spiking activity than the untrained response. Therefore, the learning algorithm modified the synaptic weights of the cells originally responding to the Toluene (in the untrained model), resulting in an enhanced response to this odour.

After training the olfactory bulb for the target odour (Toluene), we test the model by first feeding odours in which Toluene is present and odours in which it is not, and then comparing the outputs.

The principal component analysis shown in Figure 5.13 summarizes the experimental results. Figure 5.13a shows the response for two runs containing Toluene:

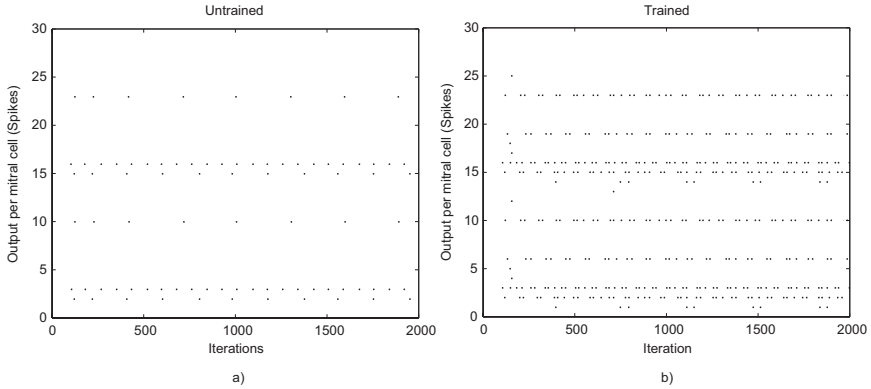

Figure 5.10: Spiking response of the olfactory bulb to a pure concentration of Toluene. a) Spiking response of the untrained model. The response shows very little spiking activity limited to cells 2, 3, 10, 15, 16 & 23. b) Spiking response of the trained model. Unlike the untrained response, more spiking activity is obtained by the trained model. Cells 1, 14 and 19 now also show spiking activity.

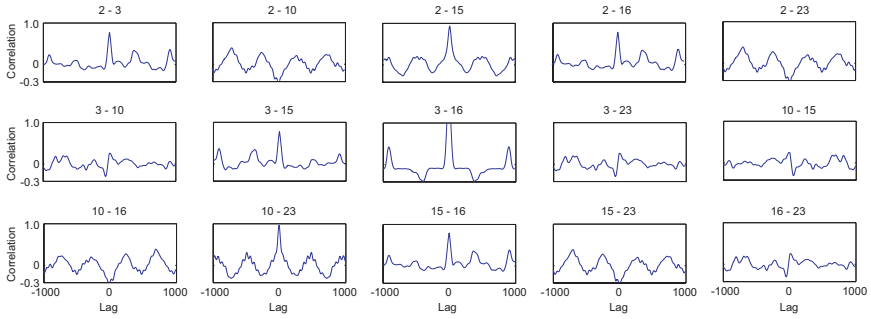

Figure 5.11: Cross-correlation analysis of the spiking response of the untrained model to a pure concentration of Toluene. The cross-correlation analysis shows some synchrony among some cells (cells involved are indicated above each plot). Cells with a stronger cross-correlation among them are: 2, 3, 15 and 16; and 10 - 23. Others cells show an oscillatory behaviour, such as cells 2 -10, 2 - 23, 10 - 16 and 15 - 23.

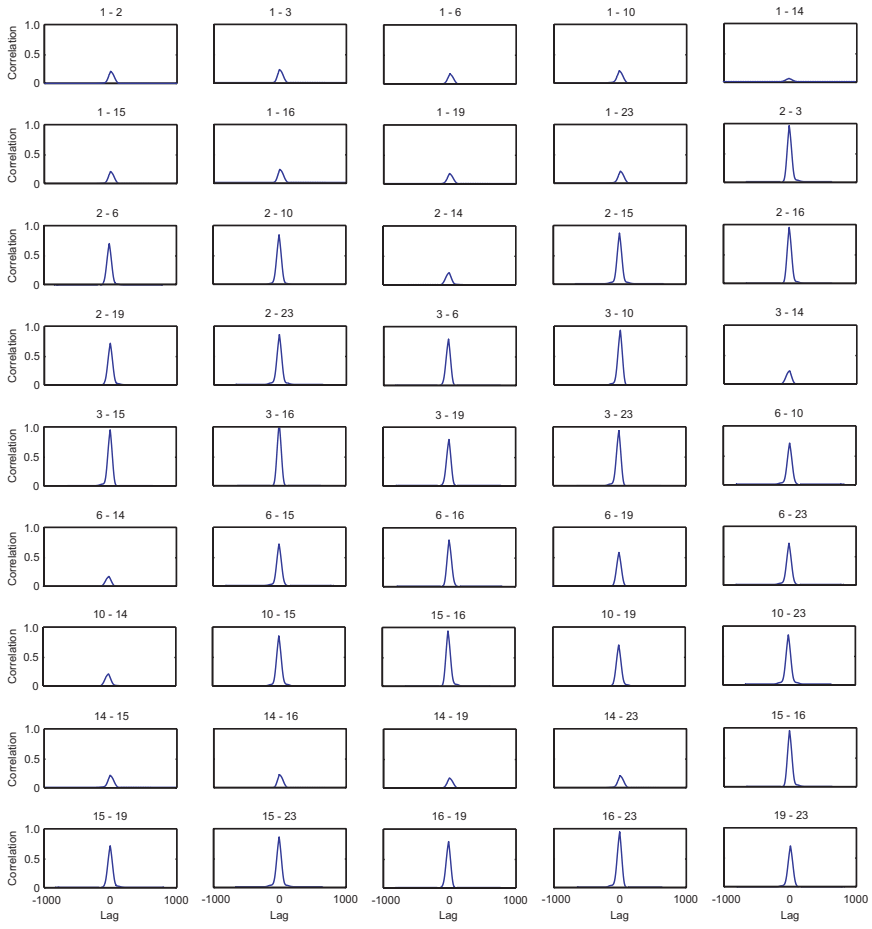

Figure 5.12: Cross-correlation analysis of the spiking response of the trained model to a pure concentration of Toluene. The cross-correlation analysis show strong synchrony among some cells (cells involved are indicated above each plot). Cells with a stronger cross-correlation among them are: 2, 3, 6, 10, 15, 16, 19 and 23; Cells 1 and 14 show a weaker cross-correlation.

the response belongs to the averaged runs from Toluene (black) and the response of the olfactory bulb to the first run containing pure Toluene (blue). As can be seen, they both follow similar trajectories. Figure 5.13b is the same experiment, but with an added second run of pure Toluene. Again all three responses follow similar trajectories. We then added a random input not containing Toluene to the experiment. Figure 5.13c shows that the trajectories of the runs containing Toluene tend to follow similar paths, whereas the random input clearly follows a different trajectory.

In order to determine the identification capabilities of the olfactory bulb, a linear discriminant analysis was performed using the fifth run containing Toluene and the random odour to train the discriminant algorithm. The response produced by the third run of Toluene was used as the odour to be classified. A total of 50000 data points were classified, from which 49729 points were adequately classified as Toluene while 271 points were misclassified as random odour, resulting in a success rate of 99.46%. Figure 5.13d shows the resulting classification of the data points for this experiment. A magnified view depicts (in black) the points which were wrongly classified as the random odour, which occurred for the first data points of the Toluene response. This experiment proves that the olfactory bulb could successfully identify when the target odour was present. Trajectories for runs containing the target odour follow similar paths yielding positive classifications by the linear discrminant analysis.

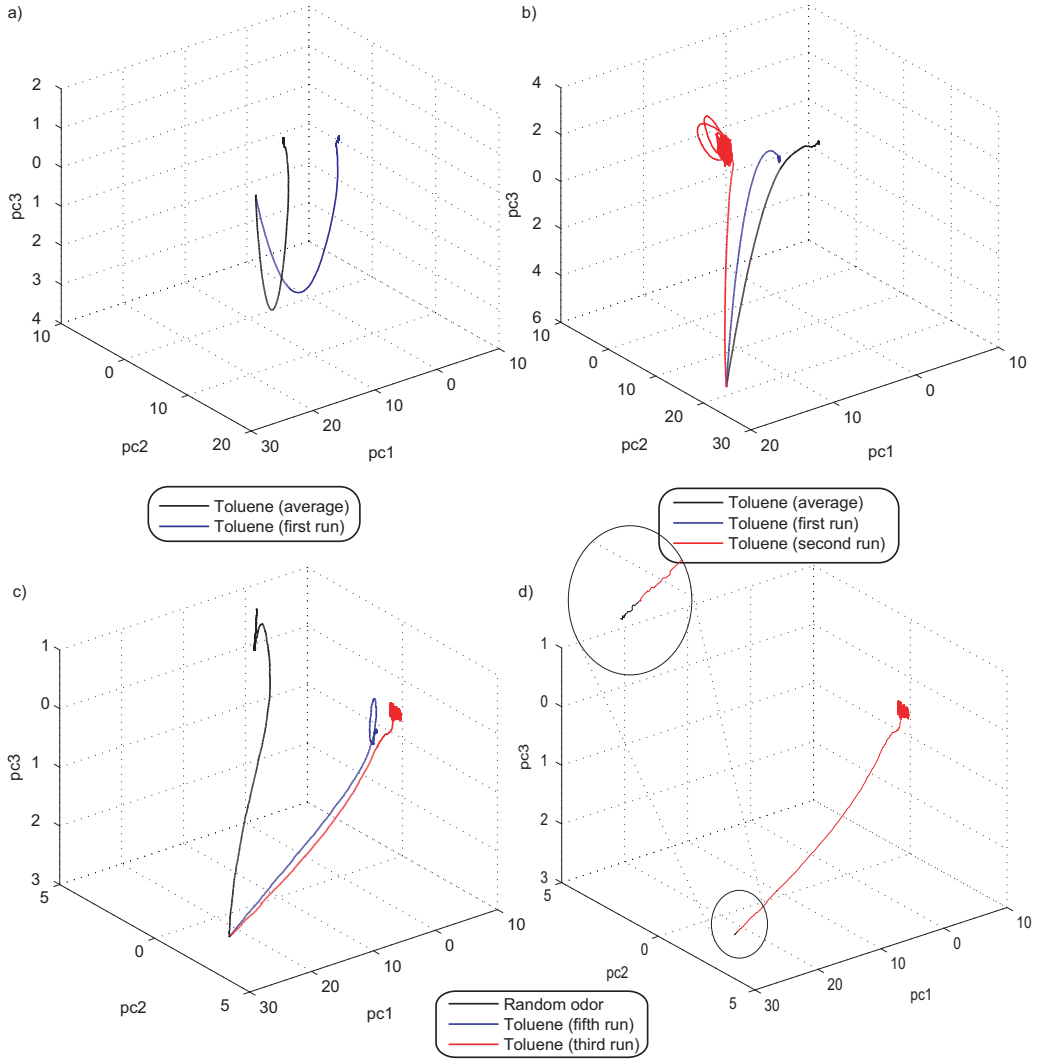

Figure 5.13: Principal component analysis for the olfactory bulb response to a pure concentration of Toluene. The olfactory bulb was trained for Toluene using the averaged input of all 10 responses from the beads to a pure concentration of Toluene as training input. a) PCA of the response of the olfactory bulb to the training input (black) and the first trial of Toluene (blue). Both trajectories follow similar paths. b) PCA of the response of the olfactory bulb to the training input (black) and the first and second trials of Toluene (blue and red respectively). All trajectories follow similar paths. c) PCA of the response of the olfactory bulb to the fifth (blue) and third (red) trials of Toluene plus a random input (black). Toluene trajectories follow similar paths, whereas the random input follows a path with a different direction. d) Plot of the response of the model to the second run of Toluene after the linear discriminant analysis was performed. A magnification view of the start of the trajectory is also shown. Dots in black represent data misclassified as the random odour, whereas dots in red are the correctly classified dots as the trained odour.

A final identification experiment consist in testing all 10 trials containing pure concentrations of Toluene to verify how well the olfactory bulb could identify the presence of the target odour in each trial. As previously described, the olfactory bulb is trained to detect Toluene by using the average response of all 10 trials containing pure concentrations of Toluene, after which the linear discriminant analysis algorithm is used to determine which data points from each run belong to Toluene and and which to a different odour.

Figure 5.5.1.14a show the principal components of the response from the olfactory bulb to the average data of Toluene (blue trajectory). For comparison purposes the black trajectory corresponds to the response evoked by a different odour. Responses from each individual trial containing pure concentrations of Toluene are shown in green. these trajectories will be classified by means of the linear discriminant analysis algorithm.

Figure 5.5.1.14b shows the result of the classification obtained by the LDA algorithm. As can be seen, 8 out of 10 trajectories were clearly identified as Toluene. However, two responses failed to be classified as the target odour, being misclassified as the different odour instead. In other words, 79.7% of the data points (398,672 out of 500,000) were correctly identified. The success rate of nearly 80% suggests that the olfactory bulb is a reliable model for identification purposes.

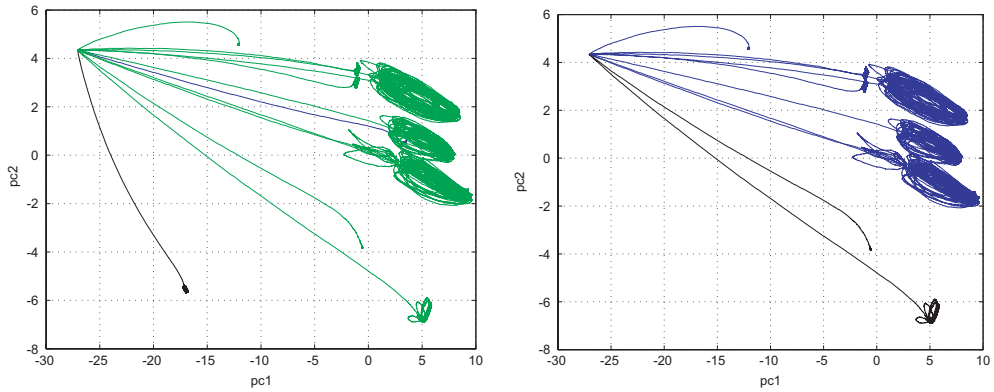

(a) Toluene: all trials response.

(b) Toluene: Linear discriminant analysis.

Figure 5.14: Toluene identification by LDA. a) Olfactory bulb response to each individual trial of Toluene. The model was trained using the average response of Toluene (blue line) and individual trials were used to test the response of the OB (green lines). Additionally a random odour was added to the experiment (black lines). b) Categorization of Toluene trials by means of linear discriminant analysis. Data classified as Toluene are shown in blue, whereas data identified as the random odour are shown in black. A total of half a million data points were categorized as either odour. About 80% of the points were correctly identified as Toluene, which correspond to 8 out of 10 odours were successfully categorized, the remaining data points were misclassified as the random odour.

5.5.1.2 An exhaustive identification experiment

In order to fully test the identification capabilities of the model, from the entire data set one vapour is selected as the target odour whereas the rest of vapours will serve as distractors in the identification task. First, the olfactory bulb is trained to detect the Toluene as the target odour. Trials of pure Toluene are used for this purpose. Trials of pure odours different to Toluene, plus compounds containing mixtures of the various vapours (except for Toluene), will help complete the identification experiment. It is expected that concentrations of pure Toluene be effectively detected by the olfactory bulb, whereas the remaining odours be ignored by the model, that is, a good separation between vapours containing and

not containing the target odour.

Figure 5.15 shows the principal components of the response for the untrained model. As can be seen, Toluene responses (blue) overlap with the responses elicited by non-target odours. Prior the training, responses from vapours containing or not the target odour are treated in the same way by the olfactory bulb, therefore no distinctions can be made between odours.

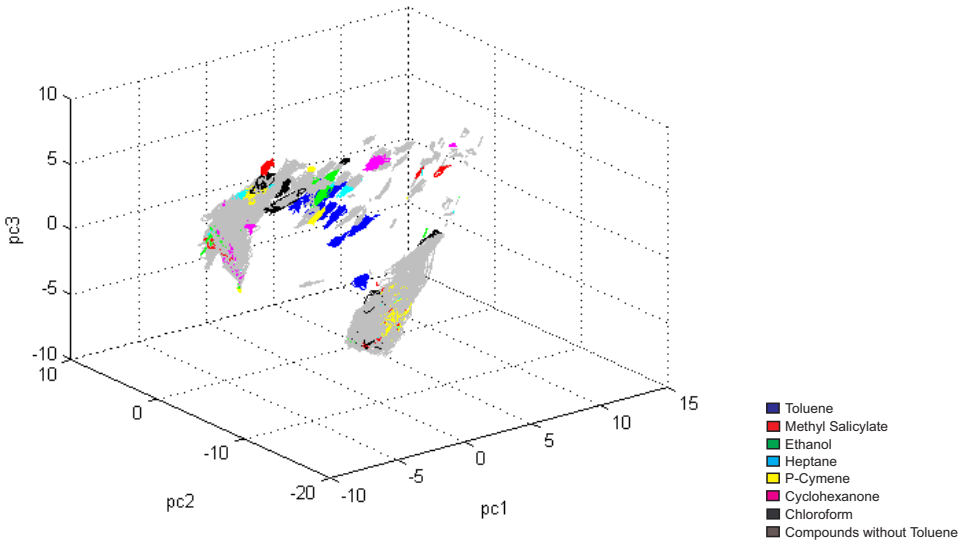

Figure 5.15: Principal component analysis of the response of the untrained olfactory bulb for all pure odours and compounds. Responses from vapours of pure Toluene are mixed with the responses evoked by other odours, covering a wide area in the three-dimensional space.

On the other hand, Figure 5.16 shows the response of the olfactory bulb after the model was trained for Toluene. As can be seen, the learning algorithm modified the responses of the model, by concentrating the Toluene responses in some area and by setting apart responses belonging to different odours. However, separation is not perfect and some responses from Toluene vapours and non-Toluene vapours

are found in the vicinity of each other.

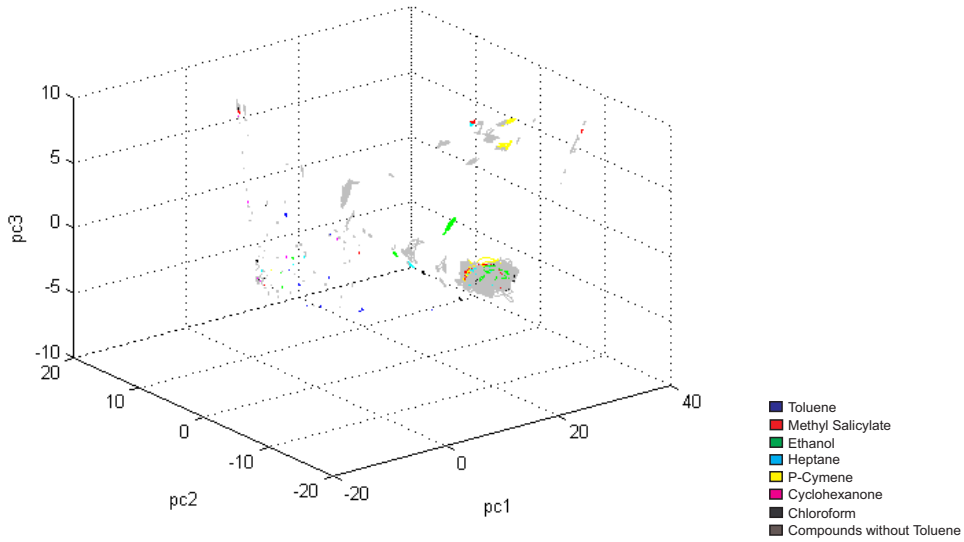

Figure 5.16: Principal component analysis of the response of the trained olfactory bulb for all pure odours and compounds. Responses from vapours of pure Toluene are concentrated in an area around the centre of the principal components space. Most of the responses evoked by other odours are set apart of the Toluene responses, however, some responses remain in the vicinity of the responses from the target odour.

Additionally, a Multivariate analysis of variance (MANOVA) test is conducted to determine whether or not there are differences between the Toluene responses and the non-toluene responses. The MANOVA test is a statistical method used for evaluating group differences across two or more dependent variables based on one or more independent variables. For this test, odours were separated in three groups:

1. Pure odours containing Toluene.

2. Pure odours different than Toluene.

3. Compounds not containing toluene.

In this MANOVA test, responses from all trials grouped as above described are compared. The null hypothesis is

$$Ho : \mu_1 = \mu_2 = \mu_3, \tag{5.5}$$

where μ_1, μ_2, μ_3 are the population means for the groups 1, 2 and 3, respectively. The statistic used here for testing the validity of the null hypothesis is the Wilk's Lambda statistic (Λ), which is given by the following equation,

$$\Lambda = \frac{|\mathbf{W}|}{|\mathbf{B} + \mathbf{W}|}, \tag{5.6}$$

where $\mathbf{W}$ is the within-group sum of squares and cross-product matrix, and $\mathbf{B}$ is the between-group sum of squares and cross-product matrix.

The MANOVA test was carried out for these three groups prior and after the training. The results are summarized in Table 5.4. As the table suggests, both prior and after the training, the three groups are perfectly differentiable. This results from the spreading of the data for each group, yielding population means for each group which are certainly different. Therefore, in order to effectively measure the identification capabilities of the olfactory bulb additional tests are necessary.

Another way to test the identification capabilities of the model is by means of a linear discriminant analysis. Linear discriminant analysis is a statistical method used to find the linear combination of characteristics which best separate

Untrained		Trained	
P-value	Wilks-Lambda	P-value	Wilks-Lambda
0.000	0.9518	0.000	0.9762
0.003	0.9467	0.000	0.9955

Table 5.4: P-value and Wilks-Lambda test statistics for the MANOVA test after the training of the model (identification).

Data points correctly identified as Toluene		
Before training	After training	Difference
54.5%	65.8%	11.3%

Table 5.5: Percentage of data correctly (and incorrectly) classified as the target odour before and after training the model by the linear discriminant function (identification).

two or more groups of data. Linear discriminant analysis uses training data to estimate the parameters of discriminant functions of the predictor variables. The discriminant functions define regions in predictor space between classes, finally the functions discriminate new data among the classes based on the predictor data. For this analysis, random samples from the different groups were selected to form the training set. The remaining data from the responses are categorized by the algorithm in one of the three groups.

Prior the training process, the linear discriminant algorithm correctly classified 54.5% of the data points within their corresponding group (see Table 5.5). However, after the training, the algorithm correctly classified 65.8% of the data points. An increase of about 11% of the data points correctly categorized compared to the same test prior the training.

As a final test, a cluster analysis of the data was carried out. Data were grouped in clusters by applying the k-means method and using the squared Euclidean distance. K-means is an iterative algorithm which solves a clustering prob-

lem. The algorithm starts by placing k centroids (one for each cluster). Next, each point is associated to the nearest centroid. Now, k new centroids are re-calculated for each cluster resulting from the initial association. With the new centroids, new clusters are obtained by associating all points to the nearest new centroid. This process is repeated until centroids do not change location. The goal is to minimize the following equation:

$$J = \sum_{j=1}^{k} \sum_{i=1}^{n} \left\| x_i - \theta_j \right\|^2, \tag{5.7}$$

where $\left\| x_i - \theta_j \right\|^2$ is the distance between a data point x_i and the centroid θ_j.

The iterative process can be summarized as follow:

1. Randomly place k centroid into the space defined by the data points.
2. Assign each data point to the nearest centroid.
3. Recalculate the position of the k centroids.
4. Repeat steps 2 and 3 until centroids do not change location.

Data points from responses obtained by the olfactory bulb prior and after the model was trained are used in this algorithm (k-means). It is expected that the algorithm will cluster data points of responses from similar odours, that is, data points from responses obtained by pure Toluene should be clustered in a single group. Data points from responses elicited by different odours should be grouped in different clusters.

Data points correctly classified as Toluene		Data points wrongly classified as Toluene	
Before training	After training	Before training	After training
49.5%	88.8%	3.9%	12.0%

Table 5.6: Percentage of data correctly (and incorrectly) clustered as the target odour before and after training the model (identification).

For this experiment, a total of 8 groups were defined for the entire set of responses, expecting data to be grouped by odours. Figure 5.17 shows how the responses from the trained model were clustered by the k-means algorithm. The results of the cluster analysis before and after training the model are summarized in table 5.6. As can be seen, there is an increase in the percentage of data which was correctly clustered as the target odour (Toluene) as a consequence of the the training process. Initially, 49.5% of the data points from responses of pure Toluene were correctly classified, however, after training the model, 88.8% of the data points were correctly classified as Toluene.

On the other hand, there was also an increase in the cases of data points from responses generated by odours other than Toluene, which were wrongly classified as Toluene. Data points clustered as Toluene, when in fact they belong to a different category increased from 3.9% to 12.0% as an undesirable consequence of the training.

Based on the results, the learning algorithm has a positive effect on the olfactory bulb, by increasing the probability of the model to detect a target odour. However, it also increases the probability of obtaining false positive detections.

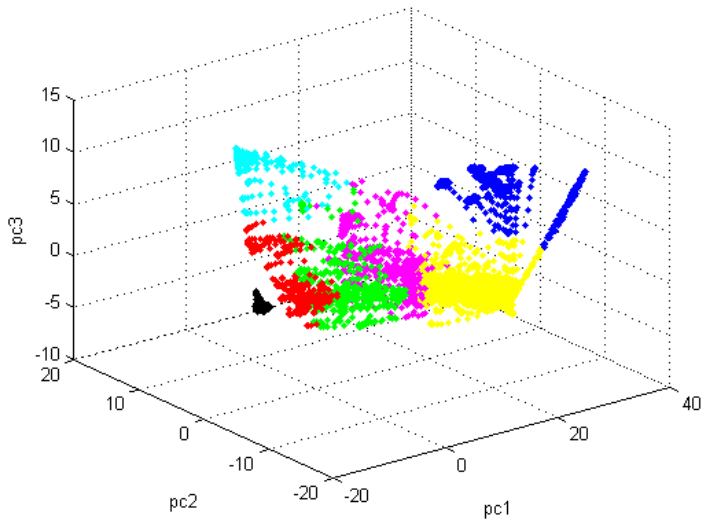

Figure 5.17: Cluster analysis of the data from all pure odours plus non-Toluene mixtures. The cluster analysis was carried out using k-means. The squared Euclidian distance was used by the clustering algorithm. A total of 8 groups were defined for the total data set. Colours separate differnt groups.

5.5.2 Classification

The second experiment was designed to prove that the olfactory bulb circuit can classify odours. For this experiment, 3 odours (Ethanol, Cyclohexanone and Chloroform) were used. As in the previous experiment, the runs for each odour were averaged to obtain the characteristic sensor response for each odour.

Unlike the identification problem in which one odour was used, we have to train the network to detect 3 different odours. The training process is therefore carried out as follows: the first odour is applied to the circuit and its response used as a base for the Hebbian learning algorithm. The learning algorithm should change the synaptic inhibitory weights (based on the firing rates of the mitral cells in response to the input) according to the equation 2.19. This process is carried

out for the second odour (Cyclohexanone) and the third one (Chloroform), giving rise to new inhibitory weights after each odour is applied. This process starting from the first odour (Ethanol) to the third odour (Chloroform) is repeated until 100 training runs have been completed, at which the point the olfactory bulb is considered trained.

Figure 5.18a shows the principal component analysis for the responses for all 3 odours from the trained olfactory bulb. Each odour follows a trajectory that tends to a different location in the space of the principal components. All trajectories also show the tendency to reach an attractor, which in this case corresponds to a limit cycle for each odour.

So far, we have shown that the responses of the olfactory bulb to different odours follow different directions and tend to an attractor for each odour. The next step is to verify whether inputs containing information from the same odours will behave in similar manner. For this task, different mixtures containing the target odours (Ethanol, Cyclohexanone and Chloroform) will be applied to the circuit. In addition, a random input (which makes the function of an independent odour) will also be applied. Figure 5.18b shows the PCA of this experiment. It clearly indicates that trials containing the same type of odour tend to follow similar trajectories. Different odours follow trajectories with more distance between them.

To verify whether the olfactory bulb is categorizing odours, a linear discriminant analysis was performed. For this aim, one response out of each odour was

used to train the algorithm. In addition, the random odour was also used for training purposes. Figure 5.18c graphically represents the results obtained by the discriminant analysis. The test odours were categorized by the LDA algorithm, and coloured by resulting odour. As it can be seen, misclassification of the data points occurred for the first points of each response, and data points were classified as the random odour (black segments).

The remaining data points were correctly classified as the right odour, with only a short segment of Ethanol being misclassified as Cyclohexanone. Nonetheless, the rest of the data points were clearly identified as Ethanol. A total of 50000 per run should be classified as Ethanol, Cyclohexanone, Chloroform or random odour, yielding a total of 450000 data points for all 9 different trials. 98.87% of all points were successfully categorized in their respective odour, while only 5096 points were wrongly assigned to a different odour. These results demonstrate that the olfactory bulb can effectively categorize different odours.

5.5.3 Segmentation

So far, it has been shown that the olfactory bulb model can in most cases identify a trained odour, hence illustrating its utility in practical situations. As a further step in the verification of the olfactory bulb, it is desirable to verify whether the model could be able to detect a target odour when it is buried within some background odour information (noise), i.e. an odour compound made up of Toluene plus a different substance which plays the role of noisy information.

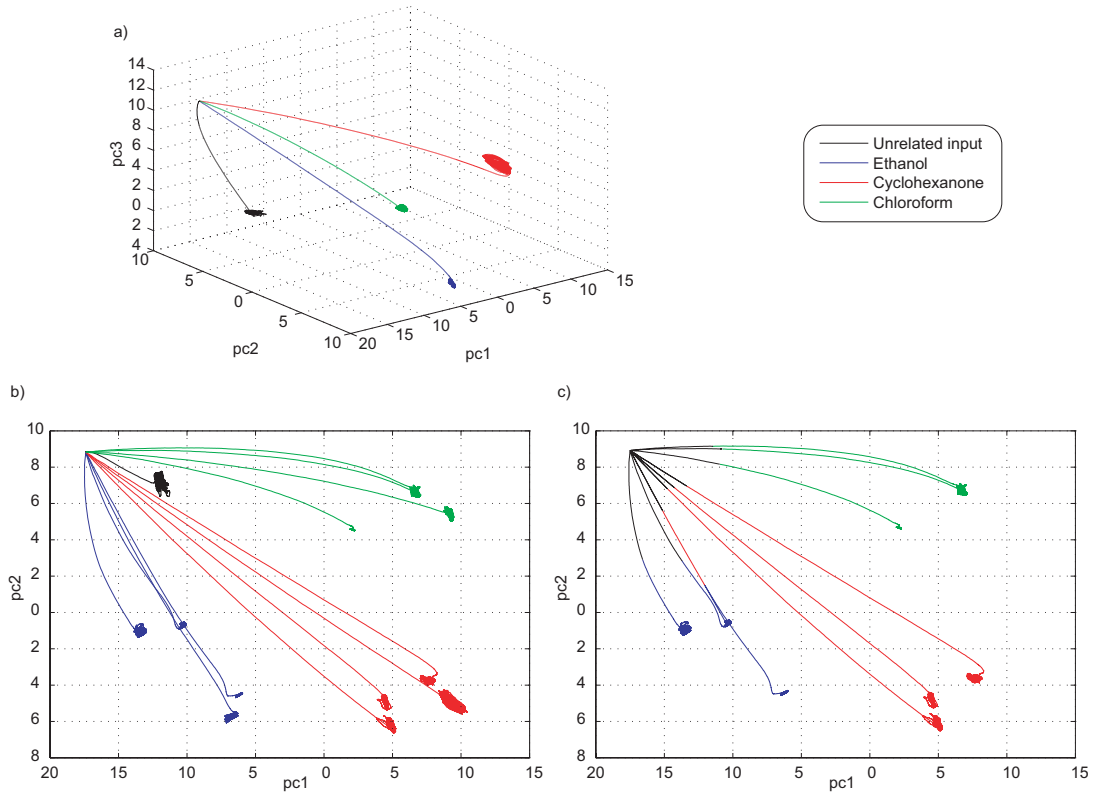

Figure 5.18: Principal component analysis for the olfactory bulb response to pure concentrations of Ethanol, Cyclohexanone and Chloroform. The olfactory bulb was trained for Ethanol, Cyclohexanone and Chloroform using as training inputs the averaged inputs of all 10 responses from the beads to pure concentrations of those substances. a) PCA of the trained response of the olfactory bulb to to pure concentrations of Ethanol (blue), Cyclohexanone (red) and Chloroform (green). Each trajectory follow a different direction. An additional input of an unrelated input was added (black), no training was carried out for this last input. b) PCA of the trained response of the olfactory bulb to to pure concentrations of Ethanol (blue), Cyclohexanone (red) and Chloroform (green). Four different trials for each concentration were used in this experiment. Trajectories from the same odour follow the same direction, the unrelated input follows a different path. As trajectories belonging to the same odour have similar directions between them, but different directions to other odours, the olfactory bulb proves to be an efficient model to perform classification tasks for odours. c) Plot of the response of the model to a subset of the inputs shown in b) after the linear discriminant analysis was performed. At the start of the trajectories, misclassified data are represented in black, which is regarded as the misclassification of the LDA as the random odour.

Compound	Total data points	Correct	Wrong	success (%)
Toluene + Ethanol	250000	250000	0	100.0
Toluene + Chloroform	250000	205004	44996	82.0
Toluene + Heptane	250000	200222	49778	80.0
Toluene + Cyclohexanone	250000	148951	101049	59.6
Toluene + P-Cymene	250000	148714	101286	59.5
Toluene + Methyl Salicylate	250000	70662	179338	28.3

Table 5.7: Compounds containing Toluene used for the segmentation task. Compounds are sorted by percentage of success given by the linear discriminant analysis.

For this part of the experiment, the olfactory bulb was first trained to identify Toluene as the target odour. As in previous phases of the experiment, a total of 100 training iterations were carried out before considering the system fully trained. For the segmentation task, compounds containing Toluene plus an additional odour will be used to verify whether the model is able to positively identify if the target odour (Toluene) is present in the compound.

After the olfactory bulb has been trained for Toluene, the compounds described in Table 5.7 will be fed to the model. Let us recall that the entire data set consists of 5 different trials for each compound; thus for this experiment, all compounds consisting of two substances (one being Toluene) will be used. The response of the trained model to these compounds yielded the following results:

Figures 5.19 and 5.20 (left), show the principal component analysis of the response of the olfactory bulb to Toluene (blue trajectory) and a random odour different to Toluene (black trajectory). In addition, the trajectories of the responses of the model to the 5 trials of the compounds are shown in green.

Figures 5.19 and 5.20 (right), also show the classification obtained by the linear discriminant analysis carried out to the outputs of each trial. The linear

discriminant analysis used the response from the pure toluene trial and the response of the different odour as a basis for the classification task. Compounds were either classified as Toluene or as the different odour. Data points classified as Toluene are shown in blue, whereas the other data points are shown in black.

As suggested by the Figures 5.19 and 5.20, the compound made up of Toluene + Ethanol was successfully identified as trials containing the target odour in all 5 runs. Compounds Toluene + Heptane and Toluene + Chloroform were successful in 4 out of 5 trials each. With a lower percentage of success, compounds Toluene + P-Cymene and Toluene + Cyclohexanone were correctly classified in 3 out of 5 trials. Finally, the model failed to effectively detect Toluene in the compound with Methyl Salicylate. Results are summarized in Table 5.7

5.5.3.1 An exhaustive segmentation experiment

A more exhaustive segmentation experiment is presented here. For this experiment, first the olfactory bulb is trained to detect a target odour (Toluene), remaining pure odours and compounds made of concentrations of the remaining pure odours will serve as distractors. Compounds containing Toluene will also be used in this experiment. The purpose is to verify if the olfactory bulb (which was initially trained to detect Toluene) can positively detect the presence of the target odour (Toluene) in compounds containing Toluene.

Figure 5.21 shows the principal components of the response for the untrained model. As can be seen, Toluene responses (blue) overlap with the rest of responses. In the same way, compounds containing a certain concentration of Toluene (orange) are also spread out in the principal components space. Remaining responses confound with the vapours containing Toluene.

Figure 5.22 shows the response of the olfactory bulb after training. As can be seen, the responses belonging to pure Toluene after the training are concentrated in an area around the central area of the pc1-pc2 plane. Similarly, some compounds containing the target odour (Toluene) fall within this area, however, some of these compounds fall far away of this area.

Additionally, a MANOVA test was conducted to determine whether or not there are differences between the responses evoked by vapours containing pure concentrations of Toluene, vapours of different odours, compounds containing con-

Untrained		Trained	
P-value	Wilks-Lambda	P-value	Wilks-Lambda
0.000	0.9699	0.000	0.9816
0.003	0.9911	0.030	0.9984
0.529	0.9999	0.528	0.9999

Table 5.8: P-value and Wilks-Lambda test statistics for the MANOVA test prior the training of the model (segmentation).

centrations of Toluene and compounds without Toluene at all. For this purpose, odours were separated in four groups:

1. Pure odours containing Toluene.

2. Compounds containing come concentration of Toluene.

3. Pure odours different than Toluene.

4. Compounds not containing toluene.

The MANOVA test was carried out for these four groups of responses for both prior and after the training. The results obtained by the MANOVA test are summarized in Table 5.8. Results prior and after the training process show similar behaviour. The third p-values indicates that there are separated groups which in fact belong to the same group. In order to identify what groups are more similar, a dendrogram plot of the group means after the multivariate analysis of variance is obtained. Figure 5.23 shows the dendrogram of the groups before the model is trained. As the figure suggests, groups of compounds (regardless of the presence of Toluene) are more similar between them.

On the other hand, Figure 5.24 shows the dendrogram of the groups after the

model was trained. As can be seen, after the training, the groups of pure vapours (both Toluene and non-Toluene) seem to be more similar between them than before the training. Groups of compounds are also very similar between them. The results obtained by MANOVA are not conclusive, therefore, additional tests are necessary.

An alternative way to test the identification capabilities of the model is by means of a linear discriminant analysis. Linear discriminant analysis is a statistical method used to find the linear combination of characteristics which best separate two or more groups of data. For this analysis, random samples from the groups 1, 3 and 4 (Pure Toluene, Non-Toluene pure odours and non-Toluene compounds respectively) were selected to form the training set. The remaining data from the responses (group of Toluene compounds inclusive) should be categorized by the algorithm into one of these three groups. Ideally, the discriminant function should also classify compounds containing Toluene within the group of pure Toluene.

Prior the training process, the linear discriminant algorithm correctly classified 41.8% of the Toluene data points within their corresponding group (Toluene). After the training, the algorithm correctly classified 61.4% of the data points (see Table 5.9). An increase of about 20% of the data points correctly categorized compared to the same test prior the training. The learning algorithm has a positive effect on the olfactory bulb, by increasing the probability of correct detection.

As a final test, a cluster analysis on the responses from the olfactory bulb was

Data points correctly identified as Toluene		
Before training	After training	Difference
41.8%	61.4%	19.6%

Table 5.9: Percentage of data correctly classified as the target odour before and after training the model by the linear discriminant function (segmentation).

Pure Toluene points correctly identified		Toluene compounds points correctly identified	
Before training	After training	Before training	After training
19.7%	49.3%	6.9%	48.0%

Table 5.10: Percentage of data correctly clustered as the target odour before and after training the model (segmentation).

carried out. Data points (from each individual response) were grouped in clusters by applying the k-means method and using the squared Euclidean distance. A total of 9 groups were defined for the entire set of responses, expecting data to be grouped by odours. Figure 5.24 shows the clusters obtained from the responses from the olfactory bulb after the training process was carried out. The results of the cluster analysis before and after the training are summarized in table 5.10.

As can be seen, the training increased the likelihood (percentage) of data points to be classified in their right cluster, since before training, about 20% of data points belonging to pure Toluene were clustered in the group of 'Toluene', however, after the training, this percentage rose to about 50%. In the same way, data points belonging to a compound containing Toluene, about 7% were initially clustered within the 'Toluene group', however, after the training process, about 50% of these data points were correctly classified within the 'Toluene group'.

5.5.4 Comparison with other pattern recognition methods

In order to set a benchmark for the performance of the olfactory bulb in comparison with other pattern recognition methods, the results from the identification and segmentation experiments obtained by the olfactory bulb are compared with results obtained using two different pattern recognition methods. The selected methods for this aim are:

1. Support Vector Machine.

2. Multilayer Perceptron.

5.5.4.1 Support Vector Machine

A Support Vector Machine (SVM) is a set of statistical tools used for classification and regression (Vapnik, 1995). Defining the input data as two different sets of vectors in an n-dimensional space, a Support Vector Machine solves a quadratic optimization problem which leads to a separating hyperplane in that space (Joachims, 1999). The SVM^{light} software implementation of Support Vector Machines (Joachims, 1999) was employed for the identification and segmentation problems.

For the identification problem, the same set of inputs utilized by the olfactory bulb are used. A random sample of 35 trials out of the total trials used in the identification experiment (see Section 5.5.1.2 within this chapter) are selected to train the SVM. Inputs containing Toluene were tagged as '+1', whereas inputs

	OB model - LDA	OB model - cluster	SVM	Multilayer Perceptron
Identification	65.8%	88.8%	94.7%	36.4%
Segmentation	61.4%	47.9%	47.5%	29.6%

Table 5.11: Percentage of data correctly classified by the OB (LDA and cluster analysis), Support Vector Machine and Multilayer Perceptron for the identification and segmentation experiments.

not containing Toluene were tagged as '-1'. The rest of the trials were used to test the classification capabilities of the method. Initially, the SVM was trained using the set of training inputs. After the training, the remaining inputs were used to test how many trials the SVM could correctly identify as Toluene, and how many trials were correctly identified as non-toluene input.

The same procedure was carried out for the classification task, were a random sample of 50 trials out of the total trials used in the classification experiment (see Section 5.5.3.1 within this chapter) were selected to train the SVM.

The results are summarized in Table 5.11. As can be seen, the SVM was superior in the identification task to the olfactory bulb model, since 94.7% of the inputs were correctly classified by the SVM in comparison with 88.8% of the data points correctly classified by the olfactory bulb using the cluster analysis. However, in the segmentation task, the olfactory bulb model (by means of the linear discriminant function) was able to outperform the Support Vector Machine.

5.5.4.2 Multilayer Perceptron

A Multilayer Perceptron (MLP) is an artificial neural network (ANN) model which maps a set of inputs onto a set of outputs by means of an activation function. A Multilayer Perceptron consists of an input layer, two or more hidden layers

and an output layer. For this experiment, the MLP consists of 2 hidden layers. Every neuron which makes up the MLP contains an activation function, which either turns on or turns off the neuron, that is, the activation function determines whether or not the neuron fires. Typically the activation function is a sigmoid function. For this experiment, the activation function is an hyperbolic tangent defined by the following equation:

$$y(u_j) = \tanh(u_j), \tag{5.8}$$

where $y(u_j)$ is the output of the network whose values can be either +1 or -1, and u_j is the weighted sum of the input synapses.

For this experiment, the software for artificial neural networks NeuralLab version 3.1 was used. An input layer consisting of 75 inputs plus a first and second hidden layer made up of 300 neurons each layer was constructed. The output layer consisting of a single neuron would fire if the odour at the input is the target odour, otherwise, the neuron should remain silent.

For the identification problem, the same set of inputs utilized by the olfactory bulb are used. A random sample of 35 trials out of the total trials used in the identification experiment (see Section 5.5.1.2 within this chapter) are selected to train the MLP. Inputs containing Toluene were tagged as '+1', whereas inputs not containing Toluene were tagged as '-1'. The rest of the trials were used to test the identification capabilities of the ANN. Initially, the MLP was trained using

the set of training inputs. After the training, the remaining inputs were used to test how many trials the MLP could correctly identify as Toluene, and how many trials were correctly identified as non-toluene input.

The same procedure was carried out for the classification task, were a random sample of 50 trials out of the total trials used in the classification experiment (see Section 5.5.3.1 within this chapter) were selected to train the MLP.

The results are summarized in Table 5.11. As the table suggests, the olfactory bulb model showed a better performance than the MLP for the identification and segmentation task. The best performance for the MLP was in the case of the identification task, where 36.4% of the inputs were correctly classified. In contrast, the olfactory bulb emplying the linear discriminant function obtained 65.8% of the data points correctly classified, in addition, the cluster analysis of the responses from the olfactory bulb model could correctly classify 88.8% of the data points.

5.5.5 Conclusions

Classification and identification of odours could be difficult tasks to deal with, yet the olfactory bulb circuit has proven to be a good choice when dealing with these problems. More interestingly, we have shown that using real data (which was collected in Tufts University, USA), the olfactory bulb model showed very promising results.

The olfactory bulb was tested for three different tasks, i.e. identification, classification and segmentation. For the identification task, the olfactory bulb

was able to identify in most cases the presence of toluene, even when background noise was present (see Figure 5.14). The statistical analysis proved that the effects of the learning algorithm helped the model to increase the likelihood of correctly identifying the presence of a target odour.

For testing the classification capabilities of the olfactory bulb model, the model was trained for three different odours. Again, the results showed that the olfactory bulb model could effectively perform the classification task for the three odours, obtaining a high rate of success for all odours. All three odours were correctly classified by the model.

As for the segmentation experiment, the olfactory bulb was trained to detect the presence of a target odour. The model was exposed to odours not containing the target odour as well as to odours containing different concentrations of the target odour. This experiment turned out to be more challenging for the olfactory bulb, however, the model showed promising results.

Finally, based on the results, the olfactory bulb model showed a rich variety of dynamics. Such responses should still convey important information. However, the study of the dinamics of the model are left for future experiments.

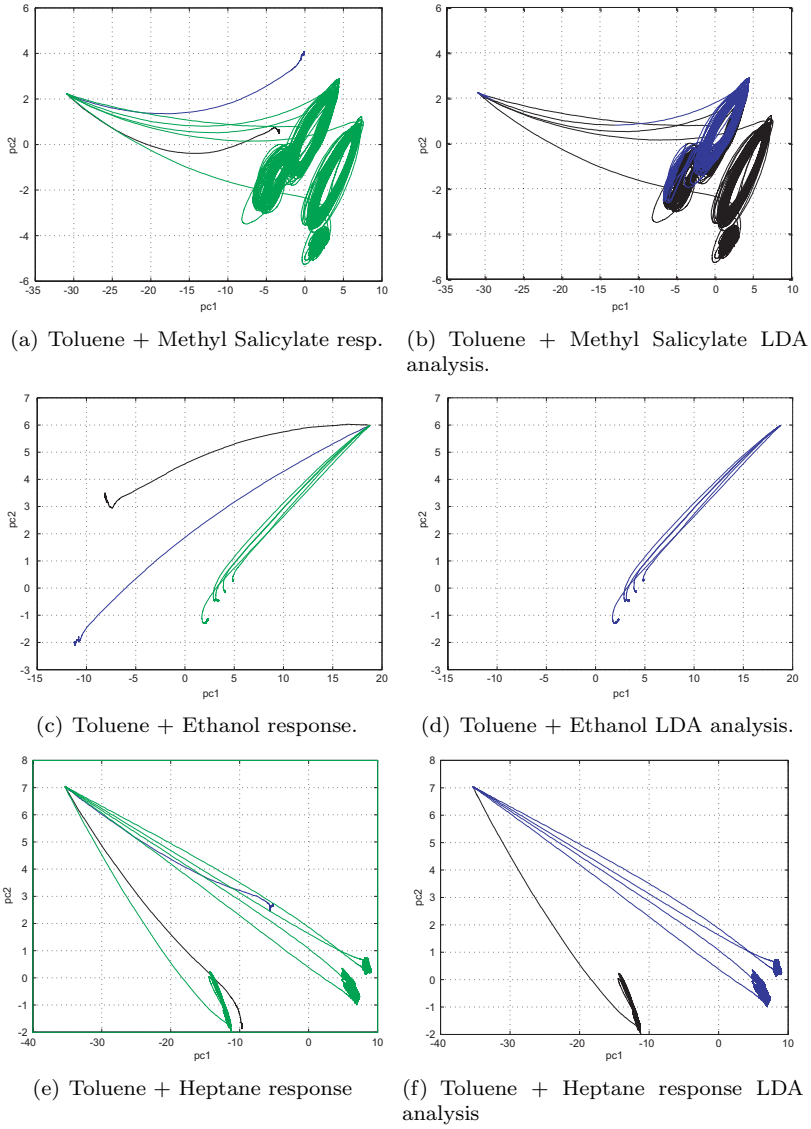

(a) Toluene + Methyl Salicylate resp.

(b) Toluene + Methyl Salicylate LDA analysis.

(c) Toluene + Ethanol response.

(d) Toluene + Ethanol LDA analysis.

(e) Toluene + Heptane response

(f) Toluene + Heptane response LDA analysis

Figure 5.19: Segmentation capabilities of the olfactory bulb. a), c) and e) Principal component of the response of the olfactory bulb to odour compounds, all containing Toluene plus Methyl Salicylate (5.19(a)), Ethanol (5.19(c)) and Heptane (5.19(e)). The model was trained for Toluene, whose response is shown in blue, whereas testing compounds are all shown in green lines. A random odour was added to the experiment (black line). b), d) and f) Linear discriminant analysis of the compounds using the trained response of Toluene as basis of the supervised learning algorithm. Data points were re-drawn according to the resulting classification of the data points from the linear discriminant algorithm, i.e. data points in blue correspond to points classified as Toluene, whereas data points in black were considered as the random odour by the discriminant algorithm.

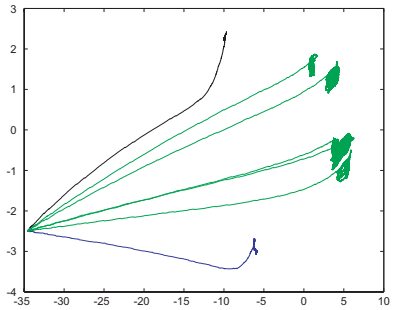

(a) Toluene + P-Cymene response.

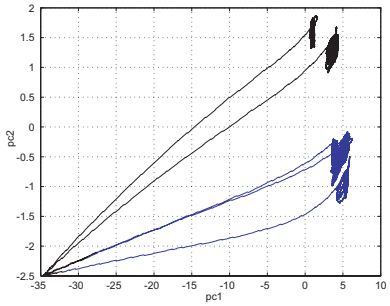

(b) Toluene + P-Cymene LDA analysis.

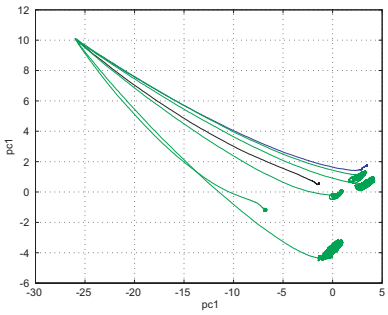

(c) Toluene + Cyclohexanone response.

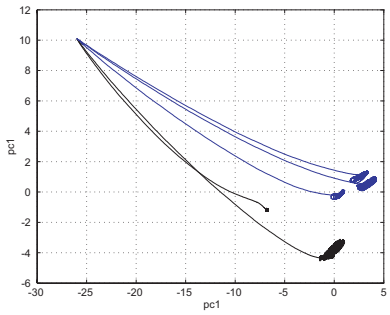

(d) Toluene + Cyclohexanone LDA analysis.

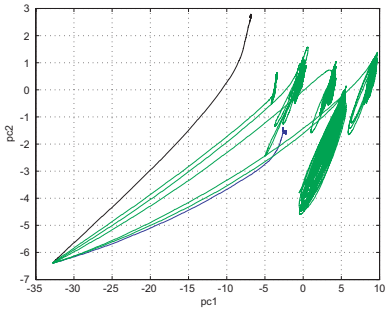

(e) Toluene + Chloroform response.

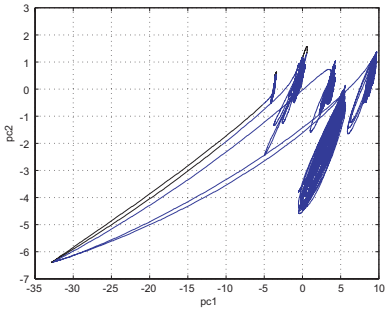

(f) Toluene + Chloroform LDA analysis.

Figure 5.20: Segmentation capabilities of the olfactory bulb. a), c) and e) Principal component of the response of the olfactory bulb to odour compounds, all containing Toluene plus P-Cymene 5.20(a), Cyclohexanone 5.20(c) and Chloroform 5.20(e). The model was trained for Toluene, whose response is shown in blue, whereas testing compounds are all shown in green lines. A random odour was added to the experiment (black line). b), d) and f) Linear discriminant analysis of the compounds using the trained response of Toluene as basis of the supervised learning algorithm. Data points were re-drawn according to the resulting classification of the data points from the linear discriminant algorithm, i.e. data points in blue correspond to points classified as Toluene, whereas data points in black were considered as the random odour by the discriminant algorithm.

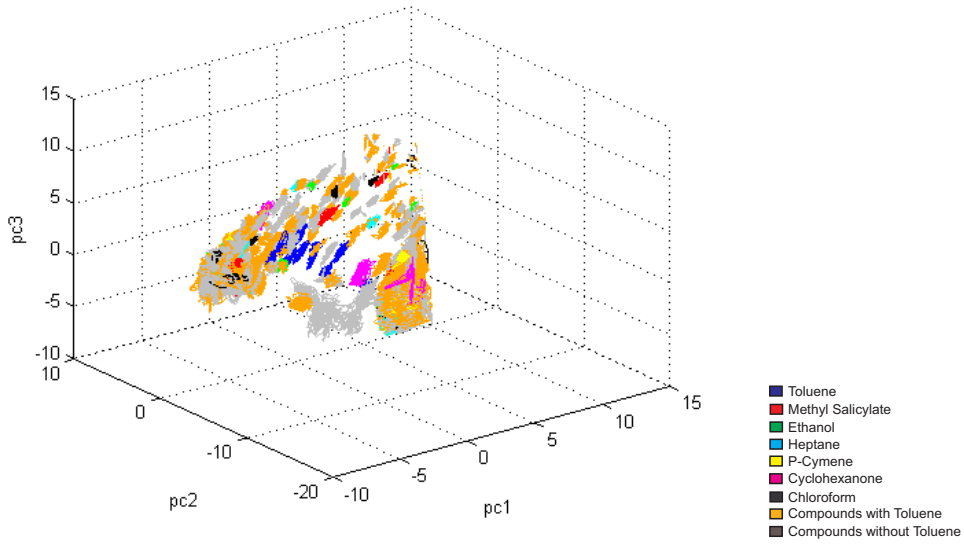

Figure 5.21: Principal component analysis of the untrained olfactory bulb for all pure odours and compounds. Responses from vapours of pure Toluene are mixed with the responses evoked by other odours, covering a wide area in the three-dimensional space.

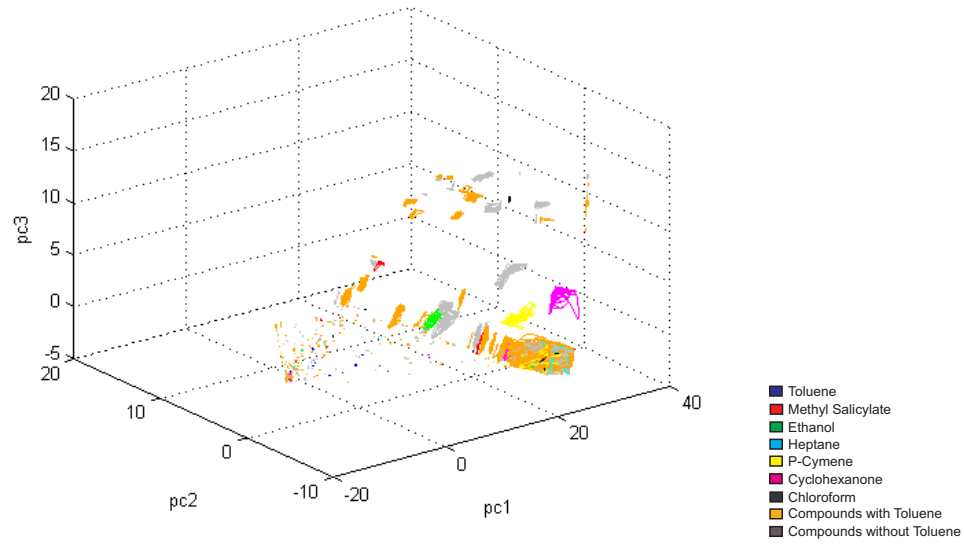

Figure 5.22: Principal component analysis of the trained olfactory bulb for all pure odours and compounds. Responses from vapours of pure Toluene are concentrated in an area surrounded by the dotted circle. Within this area, compounds containing concentrations of Toluene are also located, although, some responses from these compounds fall far away of this area. Similarly, responses evoked by other odours are set apart of the Toluene responses, however, some responses still remain in the vicinity of the responses from the target odour.

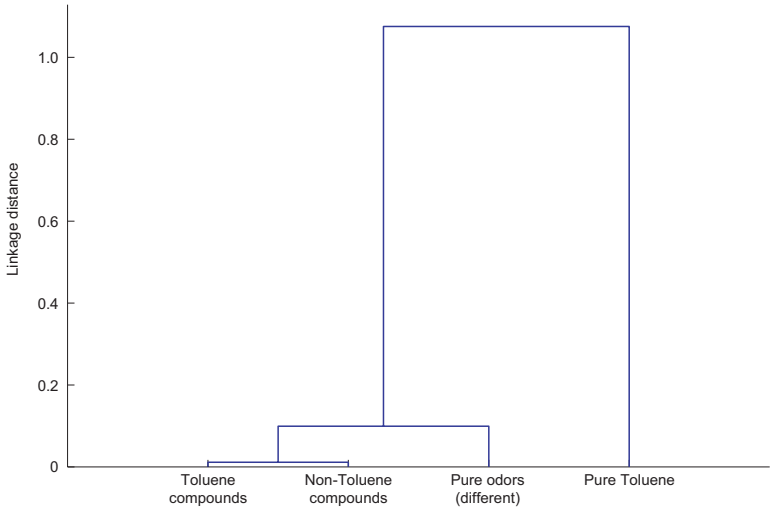

Figure 5.23: Dendrogram plot of the group means after MANOVA for the untrained olfactory bulb. The distances between groups of compounds (regardless of the presence of Toluene) indicate that these groups are very similar.

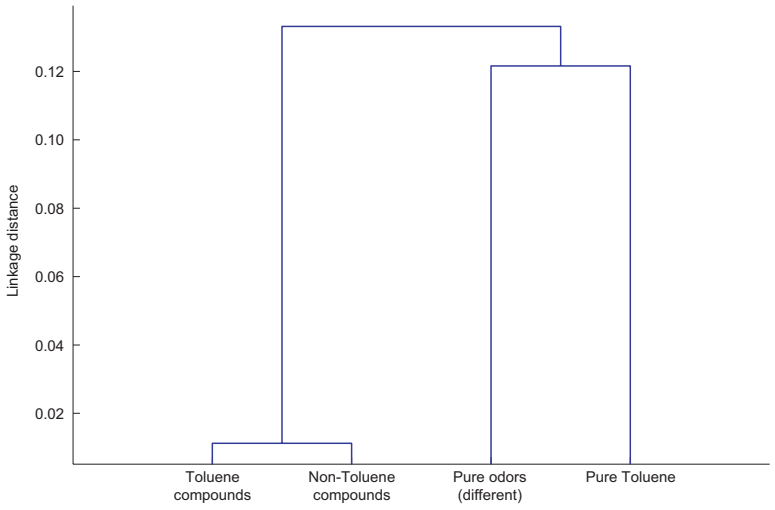

Figure 5.24: Dendrogram plot of the group means after MANOVA for the trained olfactory bulb. The distances between groups of compounds (regardless of the presence of Toluene) indicate that these groups are very similar. Unlike the dendrogram for the untrained case, pure odours seem to be more similar between them, than before the training process was applied.

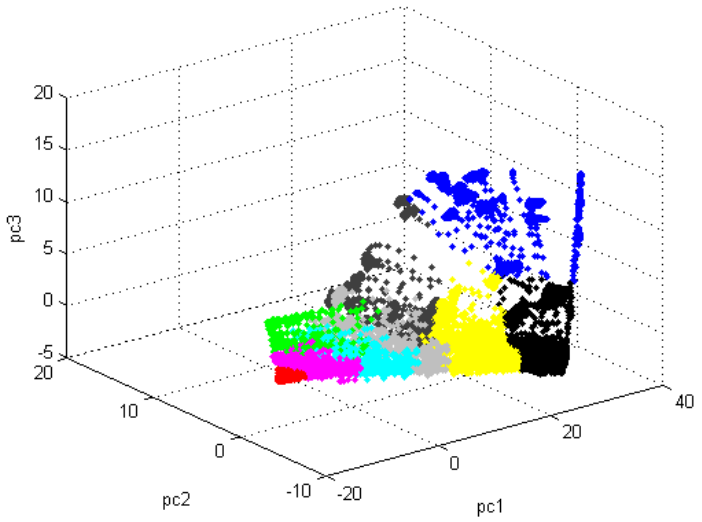

Figure 5.25: Cluster analysis of the data from all pure odours plus all mixtures. The cluster analysis was carried out using k-means in Matlab. The squared Euclidean distance was used by the clustering algorithm. A total of 9 groups were defined for the total data set. Colours are used to separate groups.

Chapter 6

Comprehensive behavioural analysis of neuronal networks

The experiment presented here was designed to demonstrate the most important feature of the construction kit for neuronal networks: the possibility of a massive parametric analysis of neuronal models. We will show that by exploiting the inherent capabilities of the FPGA to run digital circuitry in parallel, an implemented mid-scale neuronal network can be used for a comprehensive behavioural analysis.

6.1 Setting up the model

The experiments consist in doing a full inspection of the effects that variations in the inputs as well as in inhibitory weights have on the model's response. For this

aim, five different odours were randomly selected using the techniques previously explained in chapter 4. From now, these inputs form the target odours. The olfactory bulb will be trained for the target odours, and the responses around the trained parameters (target odours and inhibitory weights) analysed.

Initially, the olfactory bulb is untrained and therefore the untrained response of the model is obtained. Figure 6.1 shows the output of the olfactory bulb for all five odours under untrained conditions. As can be seen, the trajectories for each odour follow different directions in the PC space. Interestingly, the fifth odour (yellow line) shows a much longer trajectory than the others. This is caused by the higher spiking frequency yielded by the fifth odour, showing an increased responsiveness of the olfactory bulb to this odour.

Next, the learning algorithm is applied to the model as follows: the first odour is presented to the olfactory bulb and the response is used to train the network to this odour using a Hebbian learning algorithm as in Chapter 2. This process (the training) modifies the inhibitory weights of the model according to the activity of each mitral cell.

The second odour is then applied to the model and the response is used to train the circuit to this new input. The learning algorithm takes the output for the second odour and based on the activity elicited by each mitral cell, the new inhibitory weights are calculated, reeplacing the old values. Therefore, the learning algorithm is an iterative process in which weights are continously adjusted. The

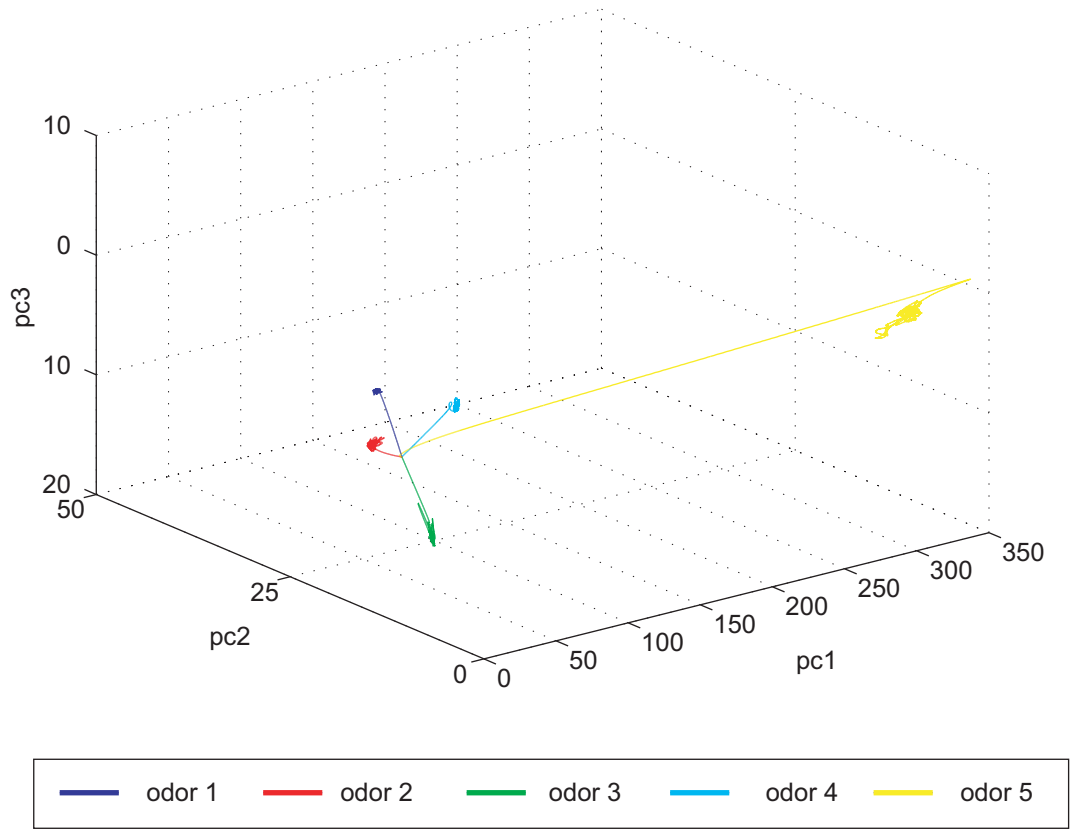

Figure 6.1: Principal component analysis for the untrained olfactory bulb. A total of 5 different odours were used in this experiment, each one represented by a different colour. The time constants of both the ORN and mitral cells were set to $\tilde{\tau}_m \approx 10$ ms, with a threshold potential, $V_{th} = 50000$. The time constants of the excitatory synapses were set to $\tilde{\tau}_E \approx 4$ ms, whereas for the inhibitory synapses the time constants were set to $\tilde{\tau}_I \approx 16$ ms. For the ORNs, constant values randomly selected in a range between 500 and 1000, were used to represent a constant concentration of each odour stimulus. The total running time in terms of biological values is equivalent to 5 seconds at a sampling frequency of $f_{smp} = 10$ kHz, although the clock frequency was set to $f_{clk} = 10$ MHz thus each run lasted for 5 ms of the FPGA processing time.

weights now reflect the effects of training for the first two odours. This process is then repeated for odours three, four and five.

Every time the learning process is applied to a different odour, the inhibitory weights change according to the activity evoked by that odour The learning is reinforced by repeating the Hebbian learning algorithm sequentially from the first to the fifth odour for 100 training iterations. Once the training has been completed, the inhibitory weights are fixed for the remainder of the experiment.

The trained response of the olfactory bulb for all five odours is then obtained. Figure 6.2 shows the principal component analysis of the trained network for all 5 odours. As the plot suggests, in contrast with the untrained response, the trajectories for each odour (besides quickly tending towards an attractor in the form of a limit cycle) indicate a similar response of the olfactory bulb to each odour. In conclusion, the training optimizes the response of the olfactory bulb, making it more sensitive to the presence of the target odours, which directs the response towards a characteristic limit cycle.

6.2 Comprehensive analysis of the olfactory bulb response by scanning the input

The most powerful characteristic of the construction kit for neuronal modelling on a FPGA, is the capability to run networks at a much higher speed, making the massive parametric analysis of neuronal networks feasible. In other words, the

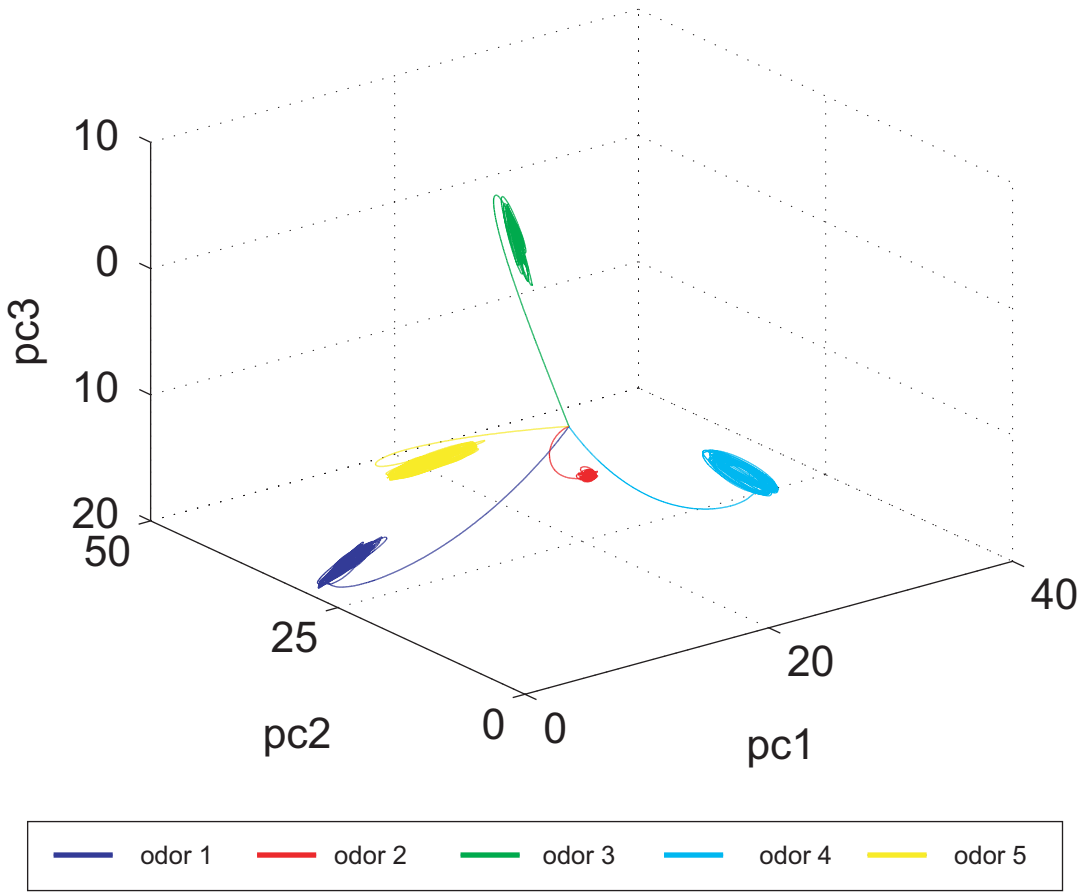

Figure 6.2: Principal component analysis for the trained olfactory bulb. A total of 5 different odours were used in this experiment, each one represented by a different colour.

model can be run repeatedly under many different conditions to determine the impact of a given parameter (such as input or synaptic weights).

To demonstrate this, the following experiment was designed: The experiment employs the olfactory bulb circuit described in the previous section, which is already trained for 5 odours and its purpose is to determine the effect of a changing input on the trained model. The network already responds to five different odours, which are represented by five distinct sets of values, corresponding to the output delivered by the sensors to the olfactory bulb.

While investigating the effects of the input on the trained network, we are mainly interested in input values close to the target (trained) odours which cause the circuit to produce (or deviate from) the characteristic response of the model to the trained odour. As these input values are not known, the task consists in feeding the olfactory bulb with all possible input values. Their respective responses will help us detect those critical input values which produce a turning point in the response.

The ideal experiment should run the olfactory bulb with all possible combinations of values for the 75 values which make up the input. The limiting range of values for the input is within 500 and 1000 inclusive (as explained in earlier chapters). A complete analysis of the effects of the input should scan the entire range of values for each one of the 75 values of the input with a step size of 1, since 1 is the lowest value that can be represented in integer digital logic (used

to represent the input of the network). However, the total number of possible combinations under these conditions comes to 501^{75} combinations, well beyond our current processing means. Even when the step size is increased to 50 (which might compromise the extent of detail of the qualitative analysis) the total number of combinations is in the order of 11^{75}. Assuming an unrealistic processing speed of 1 million combinations per second, the experiment would then take over 4^{64} years to complete.

A better (and a more realistic approach) is to select a reasonable large number of combinations which allow the analysis of the effects of the inputs on the trained network. We therefore selected the inputs by subtracting (or adding) a percentage of the difference between the lowest (or highest) possible value of the input and the value of the trained odour, yielding values from below to above the trained odour without exceeding the limit of the allowed range for the inputs. Mathematically, the new inputs are obtained from the following equations:

$$X_i = x_i + (x_i - L)p \tag{6.1}$$

$$X_i = x_i + (U - x_i)p \tag{6.2}$$

where X_i is the new value for input i, while x_i is the initial value based on the trained odour, and p is a value between -1 and 1, with a step size of 0.2, denoting the percentage of change between the lower limit of the range (L) and the trained value (x_i), or between the upper limit of the range (U) and the trained value

(x_i). For this experiment we set $L = 500$ and $U = 1000$. A total of 99 input combinations were obtained per odour, starting with $p = .98$ and increasing p by a step size of 0.02. 495 runs were needed to scan all 5 odours of this experiment.

The evolution of the behaviour of the olfactory bulb for all combinations of inputs is shown in Appendix E. In this section, only plots displaying noticeable behaviour are shown. As can be seen, inputs in the vicinity of the trained odour (Figures 6.3 to 6.5) tend to reach the characteristic limit cycle of the trained responses at a much faster speed (Figure 6.4). As the input becomes less similar to the trained input, the limit cycle trajectories start to decline (Figures 6.6 and 6.7) passing a point where the trajectories do not reach any attractor (Figures 6.8 and 6.9), and finally show a chaotic behaviour (Figures 6.10 and 6.11).

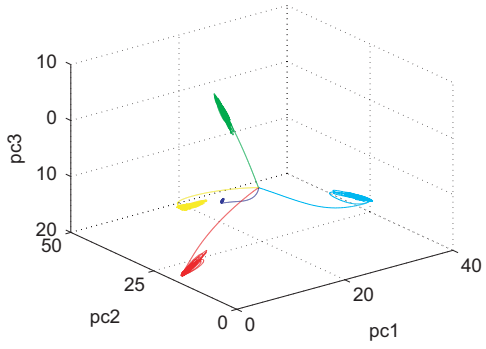

Figure 6.3: PCA for the trained olfactory bulb for an input of -20% from its trained value.

The trajectories of the principal component analysis thus show a chaotic behaviour if the input is distant from the trained odour. As this distance decreases, the trajectories begin to take different directions. At a certain turning point in the vicinity of the trained odour, the trajectories start to tend towards an attractor

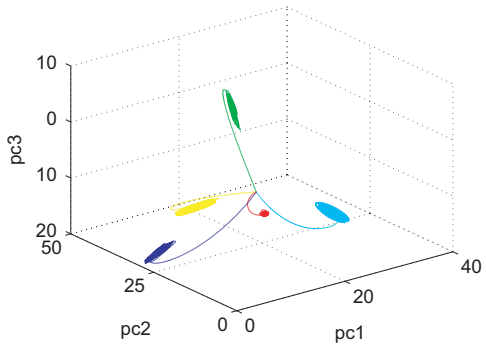

Figure 6.4: PCA for the trained olfactory bulb for an input of 0% from its trained value.

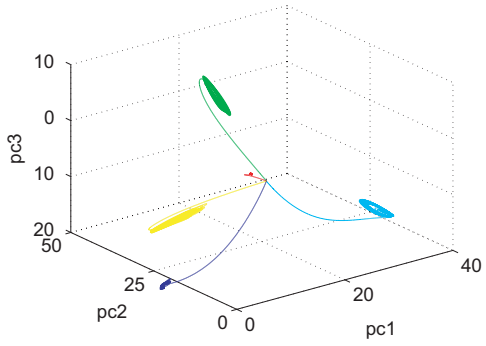

Figure 6.5: PCA for the trained olfactory bulb for an input of +20% from its trained value.

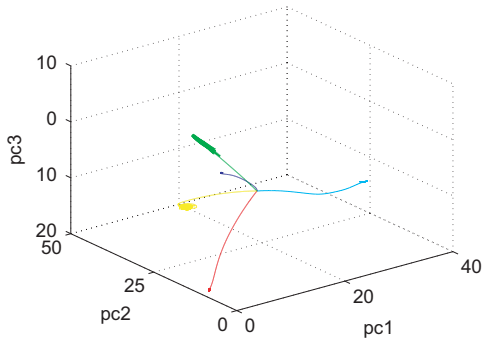

Figure 6.6: PCA for the trained olfactory bulb for an input of -30% from its trained value.

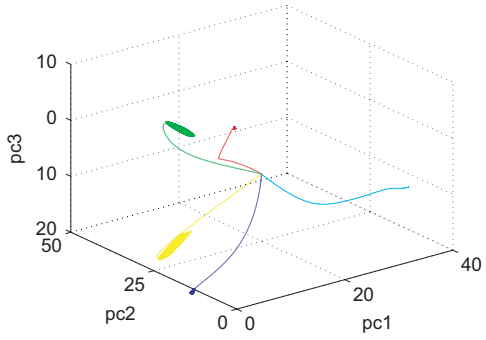

Figure 6.7: PCA for the trained olfactory bulb for an input of +30% from its trained value.

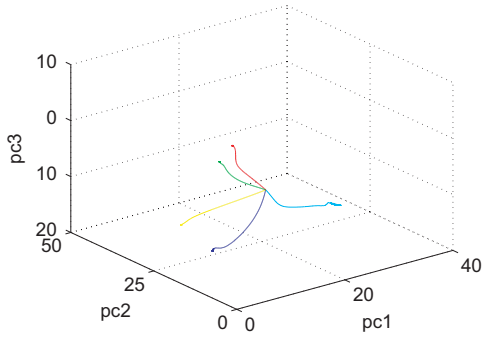

Figure 6.8: PCA for the trained olfactory bulb for an input of -50% from its trained value.

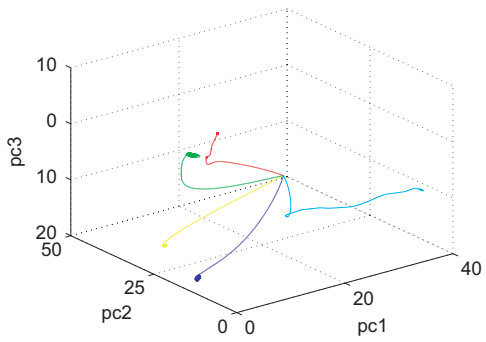

Figure 6.9: PCA for the trained olfactory bulb for an input of +50% from its trained value.

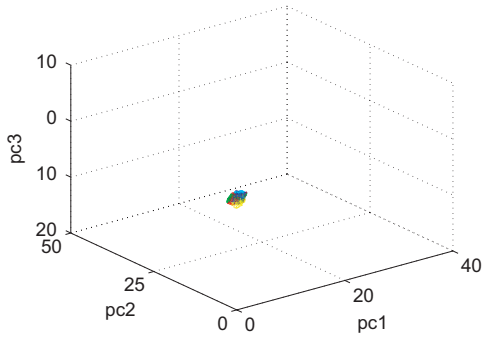

Figure 6.10: PCA for the trained olfactory bulb for an input of -98% from its trained value.

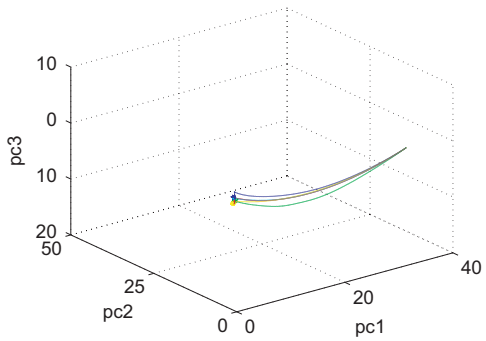

Figure 6.11: PCA for the trained olfactory bulb for an input of +98% from its trained value.

in the form of a limit cycle. As the input becomes closer to the trained odour, the trajectories of the principal component analysis tend to become increasingly similar to the trajectories of the trained odour.

There is therefore a range of inputs similar, but not identical to the trained odours for which the response of the circuit can be considered similar to the target response. We have thus shown that the olfactory bulb is robust against some levels of noise.

6.2.1 Discriminant analysis

The discriminant function analysis is a method used to classify observations into predefined classes. For this experiment, a linear discriminant analysis to determine if odours could be effectively categorized into their right class was carried out as follows: Responses from five different odours for which the olfactory bulb was trained to detect, were obtained and used to train discriminant algorithm. These inputs form the training set for the linear discriminant algorithm. Responses from all different inputs used for the previous experiment were then used as a test set. Figure 6.12 shows the result of this experiment. As it suggests, input values close to the values for which the olfactory bulb was trained were correctly classified in most cases. Inputs whose values differ in greater extent to the target odours show a percentage of success of about 40% and below.

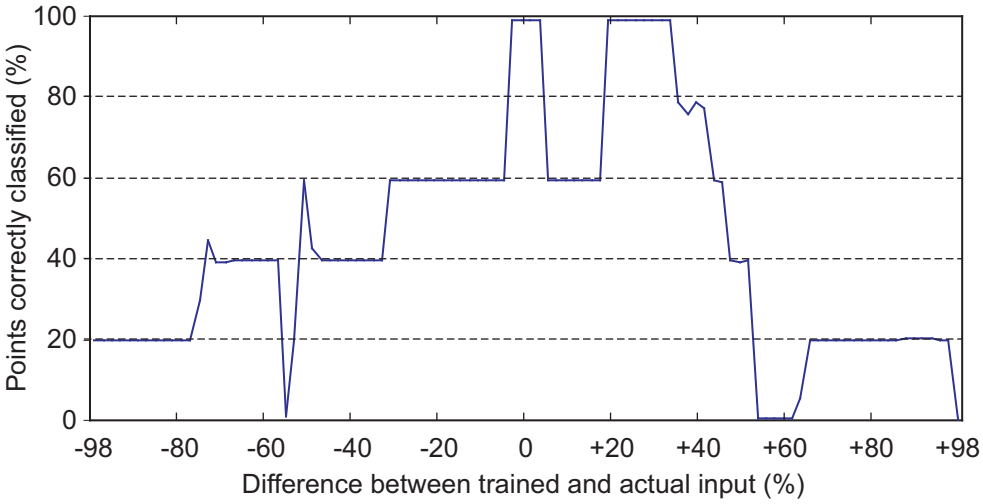

Figure 6.12: Linear discriminant analysis results for the comprehensive inputs analysis experiment. The percentage of successfully classified point for each different input show that input values in the vicinity of the odours generate responses more likely to be detected as the response evoked by the right odour.

6.2.2 Spatio-temporal relation between the trained odour and other responses.

A spatio-temporal analysis of the responses should provide insights into the similarities and differences between the several responses of the olfactory bulb. Although we are mainly concerned with inputs similar to the trained odours, it is nonetheless interesting to investigate how the spatio-temporal relations change as the inputs become increasingly different to the target odours for which the olfactory bulb was trained.

In order to detect synchrony between responses, we first focus on the cross-correlation analysis of the first principal component obtained by the responses from the 5 odours that are part of this experiment, before analysing the spatio-

temporal relations among individual mitral cells from each response. The cross-correlation analysis was carried out starting with an input with values close to the lower limit range of the valid inputs, and growing towards the upper limit of the valid input range. Figure 6.13 clearly displays how the cross-correlation changes with the input. To avoid redundancy, figure 6.13 only shows selected plots of cross-correlation. It can be seen that, as the input gets closer to the target odours, the similarity between responses increases. Conversely, as the distance between actual and trained inputs increases, the responses become more different. Hence, signals are more alike in the vicinity of the target odours (i.e. inputs within about 5% of the target odours) and signals differ more for values farther away of the target odours.

This behaviour is also observed in individual mitral cells. The evolution of the cross-correlation between the responses from the same mitral cell to each different odour are shown in the Appendix G. It is not until the inputs are within about 20% of the target inputs, that similarities among responses from mitral cells start to become apparent. Again, as inputs approach the similarity increases and shows some synchrony among responses. Stronger synchrony is obtained in the vicinity of $\pm 10\%$. Outside the $\pm 20\%$ range, responses show no similarity at all. This pattern is consistent across odours, as suggested by the evolution of the spatio-temporal relations depicted on the plots for each individual odour in Appendix G.. For instance, Figure 6.14 shows the autocorrelation plots for each M/T cell.

As the figure suggests, an oscillatory behaviour can be seen among the model response and their lagged and lead values of the autocorrelation. This oscillations indicate periodic spiking, which is supported by the presence of limit cycles, as previously observed in the principal component analysis (Figure 6.4). Therefore, the presence of the target odour causes the olfactory bulb response to fall into an attractor (limit cycle). Moreover, this behaviour is also observed for input values similar to the target odour, which indicates that the olfactory bulb model is robust to noise (see Appendix G).

6.3 Comprehensive analysis of the olfactory bulb response by scanning the inhibitory weights

Here, we present a second experiment exploiting the advantages of our construction kit for neuronal modelling over other approaches. Specifically, we carried out a major exploration of the effects of the inhibitory weights on the behaviour of a trained model. Since the inhibitory weights are subject to changes in the learning algorithm used in this experiments, an analysis of the effects that the inhibitory weights have on the response of the circuit will provide a better understanding of the dynamics of the model.

Initially, the inhibitory weights for a new experiment are randomly selected within a range of 0 to 192 inclusive. As already stated, this range was empirically obtained by observing the response of the olfactory bulb to a constant input while

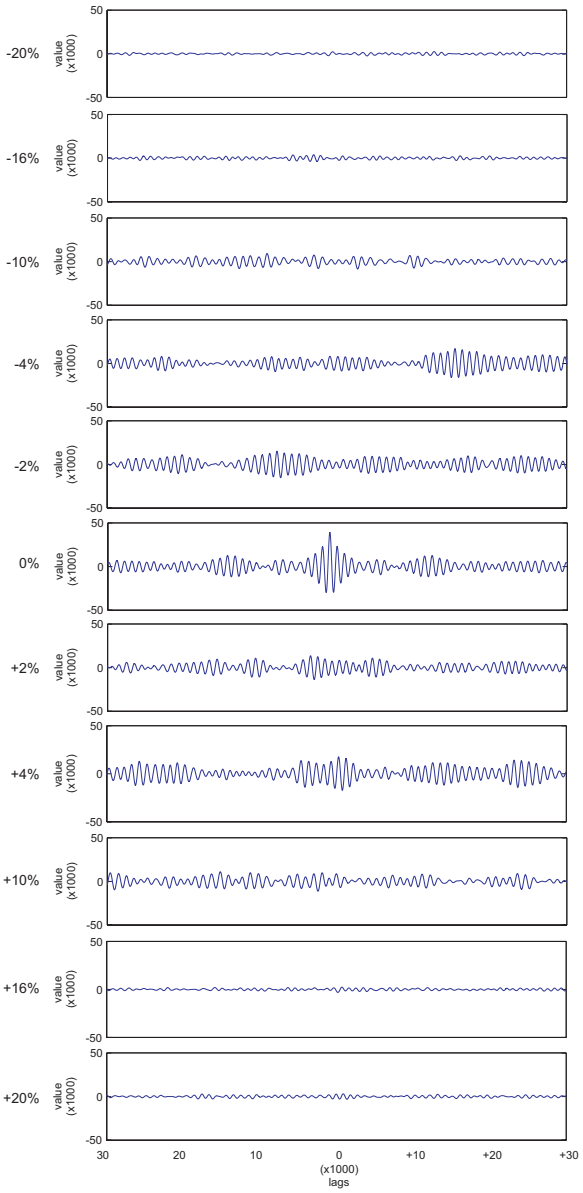

Figure 6.13: Cross-correlation analysis of the principal component obtained by sweeping the input. Plots correspond to the trained input ± 20% of the difference between the target input and the lower/upper limit of the input range. The time constants of both the ORN and mitral cells were set to $\tilde{\tau}_m \approx 10$ ms, with a threshold potential, $V_{th} = 50000$. The time constants of the excitatory synapses were set to $\tilde{\tau}_E \approx 4$ ms, whereas for the inhibitory synapses the time constants were set to $\tilde{\tau}_I \approx 16$ ms. For the ORNs, constant values randomly selected in a range between 500 and 1000, were used to represent a constant concentration of each odour stimulus. The total running time in terms of biological values is equivalent to 5 seconds at a sampling frequency of $f_{smp} = 10$ kHz. Although the clock frequency was set to $f_{clk} = 10$ MHz thus each run lasted for 5 ms of the FPGA processing time.

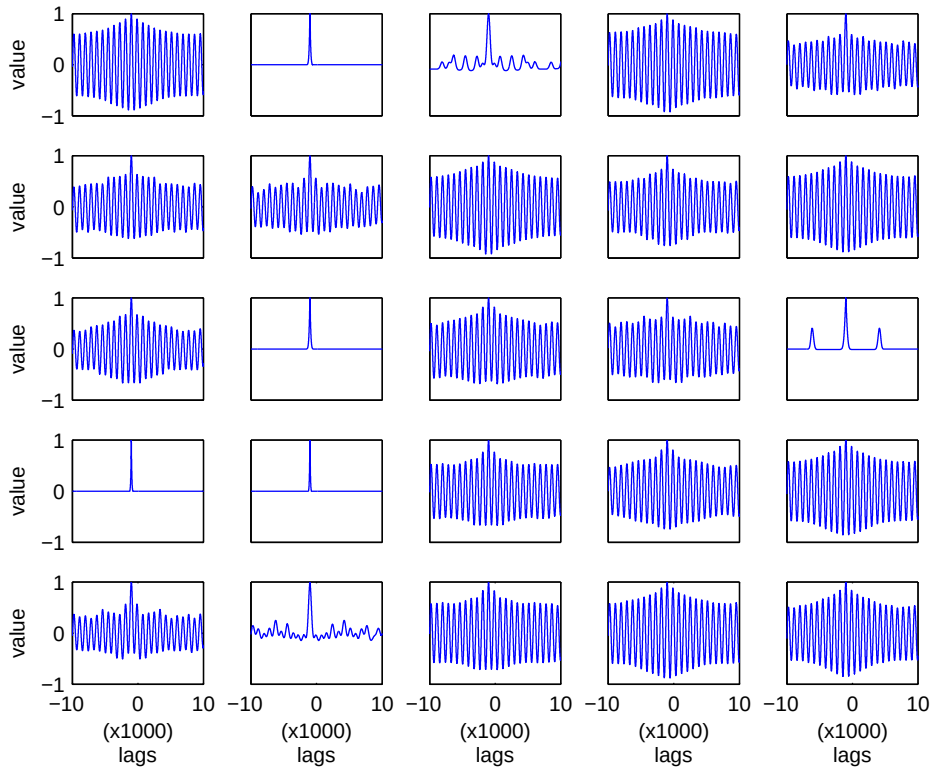

Figure 6.14: Cross-correlation analysis for odour 4: trained input vs. 0% difference input. The Cross-correlation analysis was carried out between the response of the olfactory bulb of the trained input and the input minus a percentage of the difference between input value and the limit range for the input. Plots are sorted from left to right and from up to down, starting from the cross-corelation between for the first mitral cell (the first column and first row) up to the 25th mitral cell in the last column at the bottom. Plots with zero response result from Mitral cells which remain silent for this particular input. The time constants of both the ORN and mitral cells were set to $\tilde{\tau}_m \approx 10$ ms, with a threshold potential, $V_{th} = 50000$. The time constants of the excitatory synapses were set to $\tilde{\tau}_E \approx 4$ ms, whereas for the inhibitory synapses the time constants were set to $\tilde{\tau}_I \approx 16$ ms. For the ORNs, constant values randomly selected in a range between 500 and 1000, were used to represent a constant concentration of each odor stimulus. The total running time in terms of biological values is equivalent to 5 seconds at a sampling frequency of $f_{smp} = 10$ kHz. Although the clock frequency was set to $f_{clk} = 10$ MHz thus each run lasted for 5 ms of the FPGA processing time.

varying the inhibitory weights. It was noted that for inhibitory weights within this range (0 to 192), responses from the olfactory bulb showed a more varied as well as more balanced behaviour. The learning algorithm modifies the weights based on the firing rates of each presynaptic and postsynaptic cell (Maass & Bishop, 1999), making the response of the network more sensitive to the trained input. It is therefore in the trained weights where the odour identification occurs. In order to fully investigate the qualitative effects of the inhibitory weights on the trained network, all the possible combinations of inhibitory weights should be applied to the olfactory bulb.

Ideally, all possible combinations of inhibitory weights with a step size of one should be analysed. However, as the model consists of 600 inhibitory synapses, a total description of the inhibitory weights is impossible as it would be necessary to process 197^{600} possible combinations.

It is simpler yet still effective to use the same approach as previously (see subsection 6.2 within this chapter). Combinations of inhibitory weights were selected by subtracting (or adding) a percentage of the difference between the lowest (or highest) possible value of the inhibitory weight and the value of the trained odour, producing values from below to above the trained inhibitory weights without exceeding the limit of the allowed range for the inputs. With this reasonably large number of combinations of inhibitory weights, an effective analysis of the effects of the inhibitory weights on the trained network is possible. The procedure used

to obtain the inhibitory weights utilized for this experiment is described by the following equations:

$$W_i = w_i + (w_i - L_w)p, \tag{6.3}$$

$$W_i = w_i + (U_w - w_i)p, \tag{6.4}$$

where W_i is the value for the new inhibitory weight, while w_i is the initial trained inhibitory weight, and p is a value between -1 and 1 denoting the percentage of change between the lower limit of the range for the inhibitory weights (L_w) and the current value of the trained weight (w_i), or between the upper limit of the range (U_w) and the trained weight (w_i). For this experiment, we set $L_w = 0$ and $U_w = 192$. A total of 99 combinations of inhibitory weights were obtained per odour, starting from $p = .98$ and increasing p by a step size of 0.02, 495 runs were needed to scan all 5 odours in this experiment.

The combinations of inhibitory weights which were selected by equations 6.3 and 6.4 give rise to the evolution of the behaviour of the olfactory bulb that is shown in Appendix F. For the sake of clarity, only figures which deliver important information are also shown in this section. From figures 6.15 to 6.17, it can be seen that inhibitory weights whose values are in the vicinity of the valued of the trained weights tend to reach the characteristic limit cycle obtained by the trained weights (Figure 6.16) at a much faster speed than other combinations. For the rest of the combinations, the limit cycle trajectories start to decline (Figures 6.18

and 6.19), until they reach a point in which the trajectories not longer tend to a stable attractor (Figures 6.20 and 6.21).

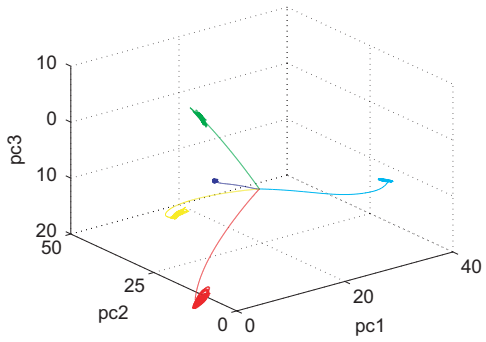

Figure 6.15: PCA for the trained olfactory bulb for an input of -10% from its trained value.

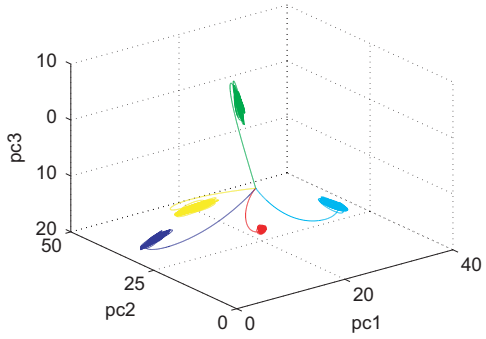

Figure 6.16: PCA for the trained olfactory bulb for an input of 0% from its trained value.

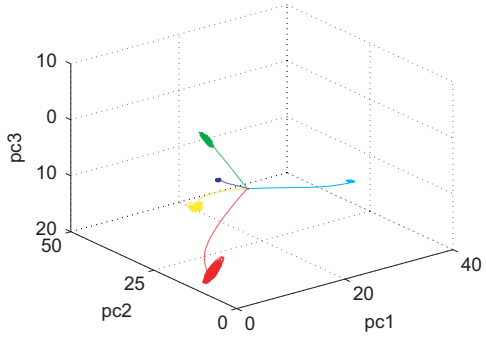

Figure 6.17: PCA for the trained olfactory bulb for an input of +20% from its trained value.

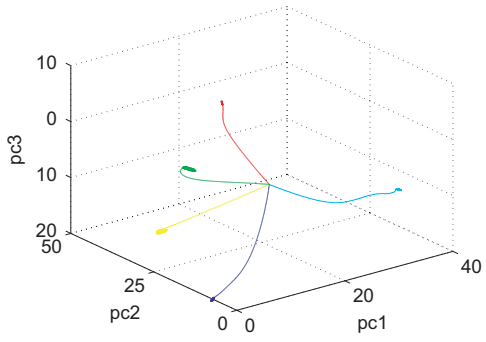

Figure 6.18: PCA for the trained olfactory bulb for an input of -20% from its trained value.

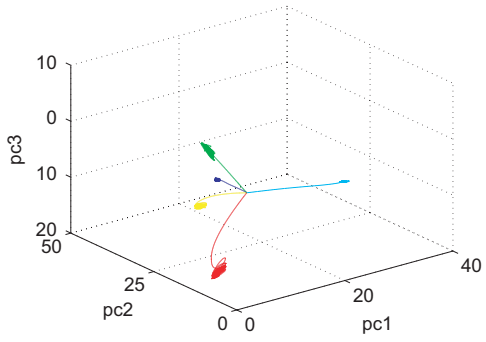

Figure 6.19: PCA for the trained olfactory bulb for an input of +30% from its trained value.

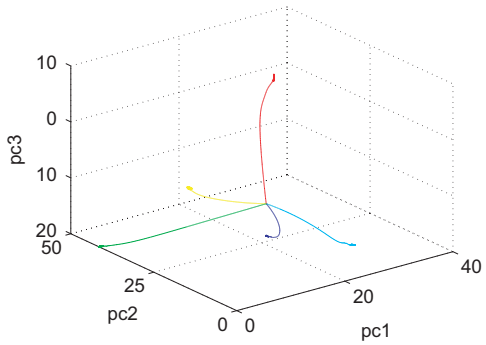

Figure 6.20: PCA for the trained olfactory bulb for an input of -30% from its trained value.

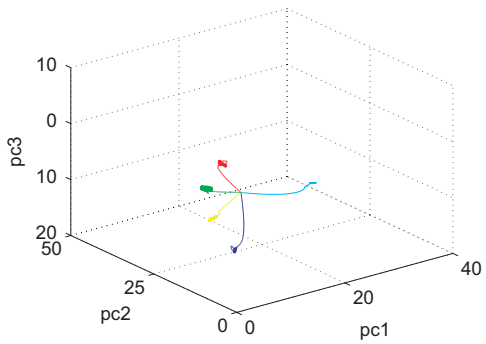

Figure 6.21: PCA for the trained olfactory bulb for an input of +60% from its trained value.

Therefore, for values of inhibitory weights that are distant from the trained weights, the trajectories of the principal component analysis do not reach an attractor, although they do take different directions. However, as the inhibitory weights get closer to the trained weights, the responses reach a turning point at which the trajectories start to form a limit cycle attractor. The closer the input to the trained odour, the more alike the trajectories of the principal component analysis are to the trajectories of the trained weights. Conversely, the more distant the values of the weights from the trained weights, the more dissimilar the response to the trained response. There is thus a range for the inhibitory weights close to the trained values within which the circuit can successfully identify target odours.

6.3.1 Discriminant analysis

A linear discriminant analysis was carried out in the same fashion as in the previous section. Figure 6.22 shows the result of this experiment. As can be seen, a perfect success rate is only obtained when weights are equal to the trained weights,

indicating that the olfactory bulb is more sensitive to changes in the weights than in the inputs. Trials with weights in the vicinity of the trained weights obtained a percentage of success of about 60%, whereas inhibitory weights very different to the trained weights ony showed a percentage of success about 40% and below.

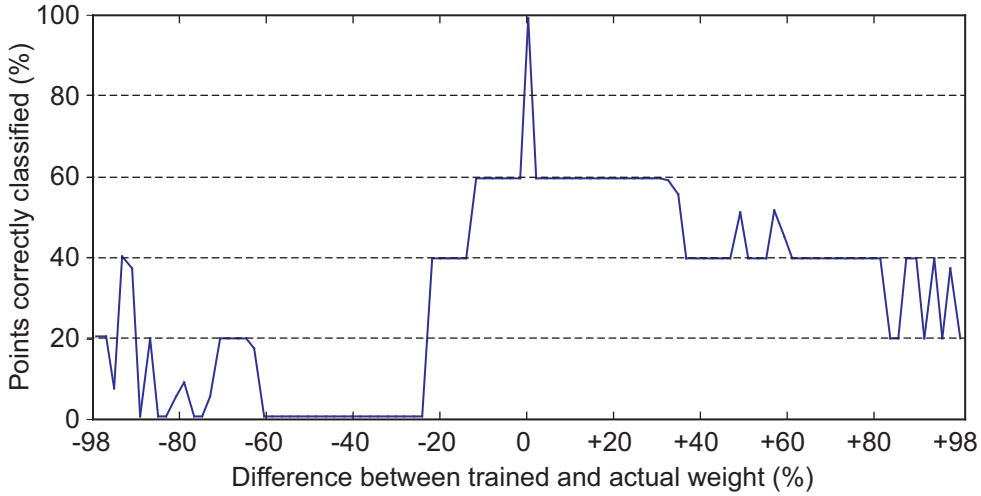

Figure 6.22: Linear discriminant analysis results for the comprehensive weight analysis experiment. The percentage of successfully classified point for each different inhibitory weight, show that weight values in the vicinity of the trained weights generate responses which are more likely to be detected as the response evoked by the right set of training weights.

6.3.2 Spatio-temporal relation between responses.

A spatio-temporal analysis of the responses will provide insights into the similarities and differences between the several responses of the olfactory bulb. Although we are mainly concerned with inhibitory weights similar the trained weights, it is nonetheless interesting to investigate how the spatio-temporal relations change as the weights become increasingly different to the inhibitory weights for which the

olfactory bulb was trained.

Before analysing the spatio-temporal relations among individual mitral cells from each response, we first focus on a cross-correlation analysis of the first principal component obtained by the responses from the 5 odours which are part of this experiment. The cross-correlation analysis was carried out starting from an input with values closer to the lower limit range of the valid inhibitory weights, and growing towards the upper limit of the valid weight range. Figure 6.23 clearly displays how the cross-correlation changes as the weights change. To avoid redundancy, Figure 6.23 only shows selected plots of cross-correlation, which depict the behaviour of the cross-correlation among inhibitory weights. As the figure suggests, as the weight values gets closer to the trained weights, the similarity of the responses increases. Conversely, as the distance between actual and trained weights increases, the responses become more different. Hence, signals are more alike in the vicinity of the inhibitory weight values (i.e. weights within 5% of the trained weights) and differ for values farther away of the trained weights.

This behaviour is also observed in individual mitral cells. The evolution of the cross-correlation between the responses from the same Mitral cell to each different odour are shown in the Appendix H. It is not until the weights are within about 20% of the trained values, that similarities among responses from Mitral cells start to become apparent. Again, as weights approach the trained value the similarities increases and shows some synchrony among responses. Stronger synchrony is

obtained in the vicinity of the ±10%. Outside the ±20% range, responses show very little if any similarity. This pattern is consistent across odours, as suggested by the evolution of the spatio-temporal relations depicted on the plots for each individual odour in Appendix H. For instance, Figure 6.24 shows the autocorrelation plots for each M/T cell. As the figure suggests, an oscillatory behaviour can be seen among the model response and their lagged and lead values of the autocorrelation. This oscillations indicate periodic spiking, which is supported by the presence of limit cycles, as previously observed in the principal component analysis (Figure 6.16). Therefore, as shown by Figure 6.24 and Figure 6.16, the main effect of the learning algorithm on the olfactory bulb model consists in creating attractor points (limit cycles) for each learnt odour, in such a way that in the presence of a learnt odour, the olfactory bulb generates oscillations around an attractor point. This behaviour remains for weight values around the trained values (see Appendix H).

6.4 Conclusions

The construction kit for neuronal models and the applications that have been presented in this document clearly illustrate some of the most important characteristics of the FPGA technology when used to model neuronal networks. Perhaps the most important characteristic of the FPGA is the capability to implement digital neuronal networks running in parallel. This allows all the elements of a mid-size

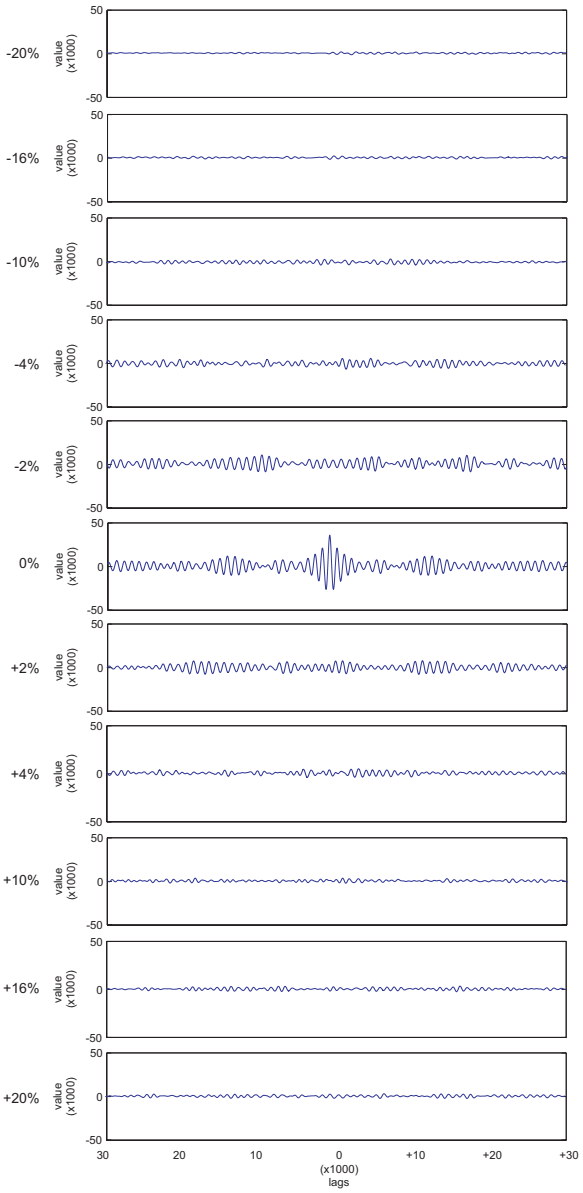

Figure 6.23: Cross-correlation analysis of the principal component obtained by sweeping the inhibitory weights. Plots correspond to the trained weight ± 20% of the difference between the trained weight value and the lower/upper limit of the weight range. The time constants of both the ORN and mitral cells were set to $\tilde{\tau}_m \approx 10$ ms, with a threshold potential, $V_{th} = 50000$. The time constants of the excitatory synapses were set to $\tilde{\tau}_E \approx 4$ ms, whereas for the inhibitory synapses the time constants were set to $\tilde{\tau}_I \approx 16$ ms. For the ORNs, constant values randomly selected in a range between 500 and 1000, were used to represent a constant concentration of each odour stimulus. The total running time in terms of biological values is equivalent to 5 seconds at a sampling frequency of $f_{smp} = 10$ kHz. Although the clock frequency was set to $f_{clk} = 10$ MHz thus each run lasted for 5 ms of the FPGA processing time.

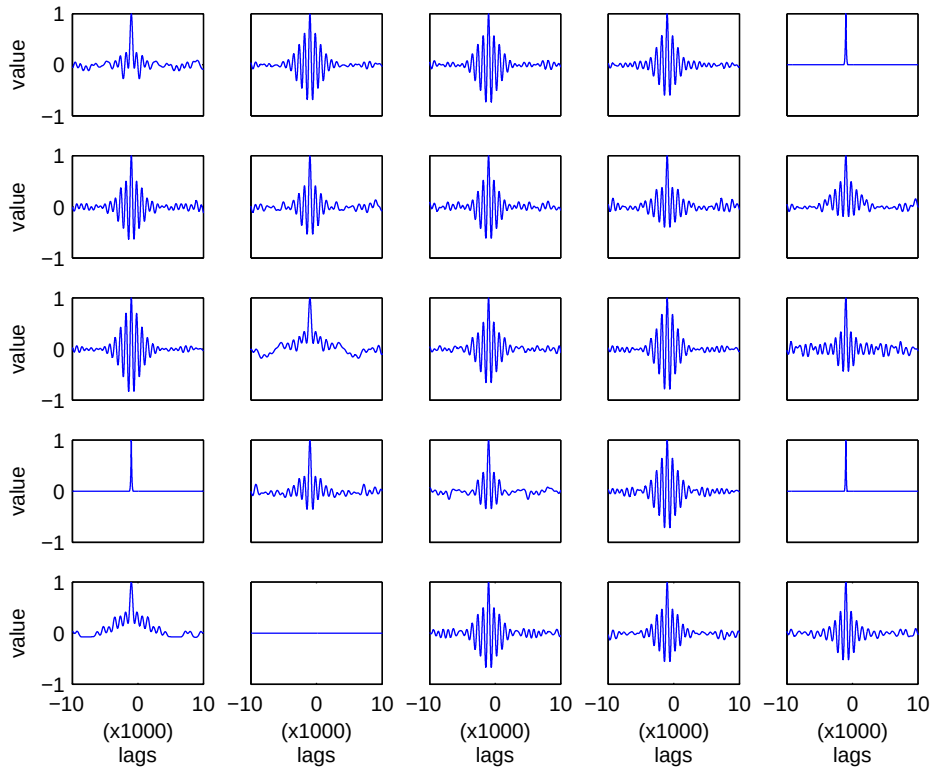

Figure 6.24: Cross-correlation analysis for odour 3: trained weights vs. 0% difference weights. The Cross-correlation analysis was carried out between the response of the olfactory bulb of the trained weights and the weights minus a percentage of the difference between weight values and the limit range for the weights. Plots are sorted from left to right and from up to down, starting from the cross-corelation between for the first mitral cell (the first column and first row) up to the 25th mitral cell in the last column at the bottom. Plots with zero response result from Mitral cells which remain silent for these particular weight values. The time constants of both the ORN and mitral cells were set to $\tilde{\tau}_m \approx 10$ ms, with a threshold potential, $V_{th} = 50000$. The time constants of the excitatory synapses were set to $\tilde{\tau}_E \approx 4$ ms, whereas for the inhibitory synapses the time constants were set to $\tilde{\tau}_I \approx 16$ ms. For the ORNs, constant values randomly selected in a range between 500 and 1000, were used to represent a constant concentration of each odor stimulus. The total running time in terms of biological values is equivalent to 5 seconds at a sampling frequency of $f_{smp} = 10$ kHz. Although the clock frequency was set to $f_{clk} = 10$ MHz thus each run lasted for 5 ms of the FPGA processing time.

neuronal network to run at each clock cycle. Thus, unlike serial processors only one clock cycle is needed to obtain the output of the network.

A serious disadvantage of most of the technologies used for neuronal modelling (including the one presented in this document) is that they have to rely on slow storage devices such as hard drives to store the huge amounts of information which can be generated while analysing neuronal networks. This is unfortunately unavoidable at the moment of writing this document, and unless something extraordinary happens soon, it will take a long time before a fast storing technology becomes available to replace the existing devices.

The experiments shown in this chapter illustrate how we can take advantage of parallel processing. A massive analysis of the behaviour of the olfactory bulb was carried out by means of hundreds of runs for the model. The total time consumed by each experiment was about 2.5 seconds of processing time of the FPGA. Therefore, for comprehensive analysis of neuronal networks, the FPGA technology is a good option as it combines high processing speed with reliability. The construction kit presented in this document is therefore a very important tool for this type of tasks.

Chapter 7

Conclusions

7.1 Conclusions

Neural networks have a growing number of applications in a large number of fields. For example, in medicine, neural networks are now used in cardiopulmonary diagnostics (Suki et al., 2003). There is also increasing research in modelling parts of the human body by means of neural netwoks (Guo-Dong & Wei-Yan, 2008). In finance, neural networks are used to make predictions of the stock market (Walczak, 2001) and banks use them to determine whether or not a loan should be granted (Witkowska, 1999). Another important field in which neural networks are also used is neuromorphic engineering, which deals with the design of biologically inspired electronic circuits which reproduce the behaviour of biological nervous systems. In this thesis, we have presented an interesting neuromorphic application based on the mammalian olfactory bulb, using a novel construction

kit for neuronal modelling in hyper real-time.

In chapter 3 we have detailed the design of our construction kit for neuronal networks. We have also shown that exact calculations of the dynamics of the Integrate and Fire model, as well as that the dynamics of the synapse can be obtained through mathematical adjustments. We have presented circuits capable of reproducing synaptic currents in the form of exponential decay, alpha and beta functions. The steps required to obtain an exact calculation of the neuronal response were detailed in this same chapter. Thus, the construction kit offers a wide variety of basic elements which allows exact modelling of neuronal networks with the advantage of running at hyper real-time but without the cost of large demands of hardware.

Although there are physical limits and hardware restrictions to what is possible to implement, we have shown that there are simplification tricks that can be used to overcome this. This has made possible to implement moderately large neuronal networks. If larger neuronal networks are needed, a multiplexing scheme, a multi-FPGA configuration or even a combination of them can be considered.

In order to prove the versatility and utility of the construction kit, a biologically inspired model of the olfactory bulb was implemented using several neuronal elements that form part of the kit. A total of 675 synapses and 100 somas were needed for the model. The output of the circuit consisted of 25 somas, mimicking the mitral cells in the olfactory bulb of mammals. Each mitral cell had

inhibitory connections to every other mitral cell, resulting in a total of 600 inhibitory synaptic connections. Although all synaptic currents were modelled by exponential decays, time constants were different for excitatory synapses (4 ms) and inhibitory connections (16 ms).

The results shown in chapter 5 indicate that even at low concentrations, the olfactory bulb could differentiate a target odour (from which the circuit was previously trained) from a random input, corresponding to a different odour. In the same experiment, the results showed that the olfactory bulb, was able to effectively differentiate between odours, i.e. the model was able to perform segmentation correctly in most cases. Hence, identification and segmentation tasks were successfully tested with this experiment.

The same olfactory bulb was utilized to demonstrate a determinant characteristic of the neuron model presented in this thesis: hyper real-time performance, which gives the model an important advantage over other ways to construct neuronal networks. This powerful characteristic allows comprehensive behavioural analysis by means of massive parametric scanning as shown in chapter 6.

In conclusion, the aim of the work presented here was to develop a reliable alternative for neuronal modelling which besides offering versatility and flexibility, would be able to offer advantages unavailable in alternative approaches. The construction kit presented here definitely delivers on this goal.

7.2 Recommendations for further work

A different approach which could also give us a more in-depth insight on the dynamics of the responses from the olfactory bulb model, is a nonlinear time series analysis. As we have already verified the existence of limit cycles in the response of the model, further characteristics of the output, may be explored by analysing the properties of such limit cycles. Such properties could be helpful in characterizing responses elicited by the presence of target odours. However, as the analysis of such dynamics is very broad, this step is left for future work.

In addition, the results presented in this thesis also show that the field of applications of the construction kit is very promising. A very interesting area in which the proposed kit would be extremely useful is the field of image processing, in which heavy data processing tasks need to be performed in real-time (Alippi, Casagrande, Scotti, & Piuri, 2000). For example, real-time face recognition in an airport could help enhance security by obtaining instant detection of known suspects (Chandrasekaran, 2005). Given the hyper real-time characteristics shown by the construction kit presented in this thesis, the kit seems to be a natural choice for such processing tasks.

References

Abbott, L. F., & Nelson, S. B. (2000). Synaptic plasticity: Taming the beast. *Nature Neuroscience*, *3*(Supplement), 1178-1183.

Alfke, P., & Hitesh, P. (2005). *Achieving breakthrough performance with virtex-4, the worlds fastest fpga.*

Alippi, C., Casagrande, E., Scotti, F., & Piuri, V. (2000). Composite real-time image processing for railways track profile measurement. *IEEE Transactions on Instrumentation and Measurement*, *49*(3), 559-564.

Alocilja, E. C., Ritchie, N. L., & Grooms, D. L. (2003). Protocol development using an electronic nose for differentiating e. coli strains. *IEEE Sensors Journal*, *3*(6), 801-805.

Andonie, R., Chronopoulos, A. T., Grosu, D., & Galmeanu, H. (2005). An efficient concurrent implementation of a neural network algorithm. *Concurrency and Computation: Practice and Experience*, *18*(12), 1559-1573.

Awapara, J., Landua, A. J., Fuerst, R., & Seale, B. (1950). Free gamma-aminobutyric acid in brain. *J. Biol. Chem.*(182), 35-39.

Balzera, W., Takahashia, M., Ohtaa, J., & Kyuma, K. (1991). Weight quantization in boltzmann machines. *Neural Networks*, *4*(3), 405-409.

Banks, M. I., Haberly, L. B., & Jackson, M. B. (1996). Layer-specific properties of the transient k current (i-a) in piriform cortex. *Journal of Neuroscience*, *16*(12), 3862-3876. (88)

Barnes, C. W., Tran, B. N., & Leung, S. H. (1985). On the statistics of fixed-point roundoff error. *IEEE Trans. Acoustic, Speech, and Signal Proc.*, *33*(3), 595-606.

Belluscio, L., Lodovichi, C., Feinstein, P., Mombaerts, P., & Katz, L. C. (2002). Odorant receptors instruct functional circuitry in the mouse olfactory bulb. *Nature*, *419*(6904), 296-300.

Bencic-Nagale, S., Sternfeld, T., & Walt, D. R. (2006). Microbead chemical switches: An approach to detection of reactive organophosphate chemical warfare agent vapors. *Journal American Chemical Society*, *128*(15), 5041-5048.

Bencic-Nagale, S., & Walt, D. R. (2005). Extending the longevity of fluorescence-based sensor arrays using adaptive exposure. *Analytical Chemistry*, *77*(19), 6155-6162.

Bernard, C., Ge, Y. C., Stockley, E., Willis, J. B., & Wheal, H. V. (1994). Synaptic integration of nmda and non-nmda receptors in large neuronal network models solved by means of differential equations. *Biological Cybernetics*, *70*(3), 267-273.

Cang, J. H., & Isaacson, J. S. (2003). In vivo whole-cell recording of odor-evoked synaptic transmission in the rat olfactory bulb. *Journal of Neuroscience*, *23*(10), 4108-4116.

Chandrasekaran, R. (2005). Security assurance using face recognition; detection system based on neural networks. *IEEE ICNNB '05 International Conference on Neural Networks and Brain, 2005*, *2*(1), nil9-1106.

Constanti, A., & Sim, J. A. (1987). Calcium-dependent potassium conductance in guinea-pig olfactory cortex neurons invitro. *Journal of Physiology-London*, *387*, 173-194. (59)

Crill, W. E. (1996). Persistent sodium current in mammalian central neurons. *Annual Review of Physiology*, *58*, 349-362. (77)

Crook, S. M., Ermentrout, G. B., Vanier, M. C., & Bower, J. M. (1997). The role of axonal delay in the synchronization of networks of coupled cortical oscillators. *Journal of Computational Neuroscience*, *4*(2), 161-172.

Dayan, P., & Abbott, L. F. (2001). *Theoretical neuroscience: Computational and mathematical modeling of neural systems* (1st. ed.). Cambridge, MA.: The MIT Press.

Dayhoff, J. E. (1990). *Neural network architectures. an introduction* (3rd. ed.). New York, NY. USA.: Van Nostrand Reinhold.

Destexhe, A. (1997). Conductance-based integrate-and-fire models. *Neural Computation*, *9*(3),

503-514. (22)

Diesmann, M., Gewaltig, M., Rotter, S., & Aertsen, A. (2001). State space analysis of synchronous spiking in cortical neural networks. *Neurocomputing*, *38-40*, 565-571.

Edmods, B., Gibb, A. J., & Colquhoun, D. (1995). Mechanisms of activation of glutamate receptors and the time course of excitatory synaptic currents. *Annual Review Physiol.*(57), 495-519.

Egger, V., Svoboda, K., & Mainen, Z. F. (2003). Mechanisms of lateral inhibition in the olfactory bulb: Efficiency and modulation of spike-evoked calcium influx into granule cells. *Journal of Neuroscience*, *23*(20), 7551-7558.

Feng, J. F., & Brown, D. (2004). Decoding input signals in time domain - a model approach. *Journal of Computational Neuroscience*, *16*(3), 237-249. (22)

Filosa, J. A., & Putnam, R. W. (2003). Multiple targets of chemosensitive signaling in locus coeruleus neurons: role of k+ and ca2+ channels. *American Journal of Physiology-Cell Physiology*, *284*(1), C145-C155. (67)

Frerking, M., Malenka, R. C., & Nicoll, R. A. (1998). Synaptic activation of kainate receptors on hippocampal interneurons. *Nature Neuroscience*, *1*(6), 479-486. (42)

Friedrich, R. W. (2006). Mechanisms of odor discrimination: neurophysiological and behavioral approaches. *Trends in Neurosciences*, *29*(1), 40-47.

Friedrich, R. W., Habermann, C. J., & Laurent, G. (2004). Multiplexing using synchrony in the zebrafish olfactory bulb. *Nature Neuroscience*, *7*, 862-871.

Friedrich, R. W., & Laurent, G. (2001). Dynamic optimization of odor representations by slow temporal patterning of mitral cell activity. *Science*, *291*(5505), 889-894.

Gabbiani, F., Midtgaard, J., & Knopfel, T. (1994). Synaptic integration in a model of cerebellar granule cells. *Journal of Neurophysiology*, *72*(2), 999-1009. (68)

Gerstner, W., & Kistler, W. (2002b). *Spiking neuron models.* Cambridge: Cambridge University

Press.

Gerstner, W., & Kistler, W. M. (2002a). Mathematical formulations of hebbian learning. *Biological Cybernetics*, *87*(5-6), 404-415.

Gibson, J. R., & Connors, B. W. (2003). Neocortex: Chemical and electrical synapses. In M. A. Arbib (Ed.), *The handbook of brain theory and neural networks* (2nd. ed., p. 725-729). Cambridge, Massachusetts. USA: The MIT Press.

Graas, E. L., Brown, E. A., & Lee, R. H. (2004). An fpga-based approach to high-speed simulation of conductance-based neuron models. *Neuroinformatics*, *2*(4), 417-436.

Graham, L. J., & Kado, R. T. (2003). Biophysical mosaic of the neuron. In M. A. Arbib (Ed.), *The handbook of brain theory and neural networks* (2nd. ed., p. 170-175). Cambridge, Massachusetts. USA: The MIT Press.

Guo-Dong, L., & Wei-Yan, D. (2008). Human body feature curve generating method based on neural network for 3d human body modelling. *Image and Signal Processing, 2008. CISP*, *2*(27), 758-762.

Gutig, R., Aharonov, R., Rotter, S., & Sompolinsky, H. (2003). Learning input correlations through nonlinear temporally asymmetric hebbian plasticity. *Journal of Neuroscience*, *23*(9), 3697-3714. (38)

Hansel, D., Mato, G., Meunier, C., & Neltner, L. (1998). On numerical simulations of integrate-and-fire neural networks. *Neural Computation*, *10*(2), 467-483. (13)

Hebb, D. O. (1949). *The organization of behavior: a neuropsychological theory.* New York: Wiley.

Hille, B. (2001). *Ionic channels of excitable membranes* (3rd. ed.). Sunderland, MA. USA.: Sinauer Associates Inc.

Hodgkin, A. L., & Huxley, A. F. (1952a). The components of membrane conductance in the giant axon of loligo. *Journal of Physiology*, *4*(116), 473-496.

Hodgkin, A. L., & Huxley, A. F. (1952b). Currents carried by sodium and potassium ions through the membrane of the giant axon of loligo. *Journal of Physiology*, *4*(116), 449-472.

Hodgkin, A. L., & Huxley, A. F. (1952c). The dual effect of membrane potential on sodium conductance in the giant axon of loligo. *Journal of Physiology*, *4*(116), 497-506.

Hodgkin, A. L., & Huxley, A. F. (1952d). A quantitative description of membrane current and its application to conduction and excitation in nerve. *Journal of Physiology*, *4*(117), 500-544.

Huguenard, J. R. (1996). Low-threshold calcium currents in central nervous system neurons. *Annual Review of Physiology*, *58*, 329-348. (111)

Isaacson, J. S., & Strowbridge, B. W. (1998). Olfactory reciprocal synapses: Dendritic signaling in the cns. *Neuron*, *20*(4), 749-761.

Jack, J. J. B., Noble, D., & Tsien, R. W. (1975). *Electric current flow in excitable cells* (1st. ed.). London: Oxford University Press.

Jahr, C. E., & Stevens, C. F. (1990a). A quantitative description of nmda receptor-channel kinetic-behavior. *Journal of Neuroscience*, *10*(6), 1830-1837.

Jahr, C. E., & Stevens, C. F. (1990b). Voltage dependence of nmda-activated macroscopic conductances predicted by single-channel kinetics. *Journal of Neuroscience*, *10*(9), 3178-3182.

Joachims, T. (1999). Olfactory bulb. In B. Schlkopf, C. Burges, & A. Smola (Eds.), *dvances in kernel methods - support vector learning* (1st. ed.). MIT-Press.

Kammermeier, P. J., & Jones, S. W. (1997). High-voltage-activated calcium currents in neurons acutely isolated from the ventrobasal nucleus of the rat thalamus. *Journal of Neurophysiology*, *77*(1), 465-475. (58)

Kandel, E. R., Schwartz, J. H., & Jessel, T. M. (2000). *Principles of neural science* (4th. ed.). New York: McGraw-Hill.

Kazuki, J., Yoshihiro, M., & Sei, M. (1990). Construction of a large-scale neural network: Simulation of handwritten japanese character recognition on ncube. *Concurrency: Practice and Experience*, *2*(2), 79-107.

Kemp, J. A., & McKernan, R. M. (2002). Nmda receptor pathways as drug targets. *Nature Neuroscience*, *5*, 1039-1042. (37 Suppl. S)

King, T. L., Horine, F. M., Daly, K. C., & Smith, B. H. (2004). Explosives detection with hard-wired moths. *IEEE Transactions on Instrumentation and Measurement*, *53*(4), 1113-1118.

Kish, L. B., Li, Y. F., Solis, J. L., Marlow, W. H., Vajtai, R., Granqvist, C. G., et al. (2005). Detecting harmful gases using fluctuation-enhanced sensing with taguchi sensors. *IEEE Sensors Journal*, *5*(4), 671-676.

Koch, C., Mo, C., & Softky, W. (2003). Single cell models. In M. A. Arbib (Ed.), *The handbook of brain theory and neural networks* (2nd. ed., p. 349-353). Cambridge, Massachusetts. USA: The MIT Press.

Kosaka, T., & Kosaka, K. (2004). Neuronal gap junctions between intraglomerular mitral/tufted cell dendrites in the mouse main olfactory bulb. *Neuroscience Research*, *49*(4), 373-378.

Kuenzi, F. M., & Dale, N. (1998). The pharmacology and roles of two k+ channels in motor pattern generation in the xenopus embryo. *Journal of Neuroscience*, *18*(4), 1602-1612. (50)

Levitan, I. B., & Kaczmarek, L. K. (1997). *The neuron. cell and molecular biology* (2nd. ed.). New York, NY. USA.: Oxford University Press.

Lorenzon, N. M., & Foehring, R. C. (1995). Characterization of pharmacologically identified voltage-gated calcium-channel currents in acutely isolated rat neocortical neurons .1. adult neurons. *Journal of Neurophysiology*, *73*(4), 1430-1442. (54)

Lozano, J., Santos, J. P., Aleixandre, M., Sayago, I., Gutierrez, J., & Horrillo, M. C. (2006). Identification of typical wine aromas by means of an electronic nose. *IEEE Sensors Journal*,

6(1), 173-178.

Maass, W., & Bishop, C. M. (Eds.). (1999). *Pulsed neural networks* (1st. ed.). Cambridge, Massachusetts. USA: The MIT Press.

Martinez-Pinna, J., Davies, P. J., & McLachlan, E. M. (2000). Diversity of channels involved in ca2+ activation of k+ channels during the prolonged ahp in guinea-pig sympathetic neurons. *Journal of Neurophysiology*, *84*(3), 1346-1354. (61)

Maxfield, C. (2004). *The design warriors guide to fpgas* (1st. ed.). Burlington, MA. USA.: Newnes.

McCormick, D. (1998). Olfactory bulb. In G. M. Shepherd (Ed.), *The synaptic organization of the brain.* (4th. ed., p. 37-75). Oxford : Oxford University Press.

Mizrahi, A., & Katz, L. C. (2003). Dendritic stability in the adult olfactory bulb. *Nature Neuroscience*, *6*(11), 1201-1207.

Mori, K., Nagao, H., & Yoshihara, Y. (1999). The olfactory bulb: Coding and processing of odor molecule information. *Science*, *286*(5440), 711-715.

Morrison, A., Mehring, C., Geisel, T., Aertsen, A., & Diesmann, M. (2005). Advancing the boundaries of high-connectivity network simulation with distributed computing. *Neural Computation*, *17*(8), 1776-1801.

Mott, D. D., Xie, C. W., Wilson, W. A., Swartzwelder, H. S., & Lewis, D. V. (1993). Gaba(b) autoreceptors mediate activity-dependent disinhibition and enhance signal transmission in the dentate gyrus. *Journal of Neurophysiology*, *69*(3), 674-691. (84)

Nabet, B., Darling, R. B., & Pinter, R. B. (1992). Implementation of front-end processor neural networks. *Neural Networks*, *5*(6), 891-902.

Nakamura, S., Sawai, H., & Sugiyama, M. (1992). Speaker-independent phoneme recognition using large-scale neural networks. *ICASSP-92 IEEE International Conference on Acoustics, Speech, and Signal Processing, 1992.*, *1*, 409-412.

Nicoll, R. A., Frerking, M., & Schmitz, D. (2000). Ampa receptors jump the synaptic cleft. *Nature Neuroscience*, *3*(6), 527-529. (15)

Pardo, M., & Sberveglieri, G. (2002). Coffee analysis with an electronic nose. *IEEE Transactions on Instrumentation and Measurement*, *51*(6), 1334-1339.

Pearce, T. C., Fulvi-Mari, C., Covington, J. A., Tan, F. S., Gardner, J. W., Koickal, T. J., et al. (2005). Silicon-based neuromorphic implementation of the olfactory pathway. In *2005 2nd internatinoal ieee/embs conference on neural engineering* (p. 307-312).

Pearce, T. C., Gardner, J. W., Friel, S., Bartlett, P. N., & Blair, N. (1993). Electronic nose for monitoring the flavor of beers. *Analyst*, *118*(4), 371-377.

Perez-Reyes, E. (2003). Molecular physiology of low-voltage-activated t-type calcium channels. *Physiological Reviews*, *83*(1), 117-161. (463)

Rodriguez-Mendez, M. L., Arrieta, A. A., Parra, V., Bernal, A., Vegas, A., Villanueva, S., et al. (2004). Fusion of three sensory modalities for the multimodal characterization of red wines. *IEEE Sensors Journal*, *4*(3), 348-354.

Rossum, M. C. W. van, Bi, G. Q., & Turrigiano, G. G. (2000). Stable hebbian learning from spike timing-dependent plasticity. *Journal of Neuroscience*, *20*(23), 88128821.

Rotter, S., & Diesmann, M. (1999). Exact digital simulation of time-invariant linear systems with applications to neuronal modeling. *Biological Cybernetics*, *81*(5-6), 381-402.

Schoppa, N. E., & Urban, N. N. (2003). Dendritic processing within olfactory bulb circuits. *Trends in Neurosciences*, *26*(9), 501-506.

Segev, I. (1999). Taming time in the olfactory bulb. *Nature Neuroscience*, *2*(12), 1041-1043. (15)

Shepherd, G. M., & Greer, C. A. (1998). Olfactory bulb. In G. M. Shepherd (Ed.), *The synaptic organization of the brain.* (4th. ed.). New York, NY. USA: Oxford : Oxford University Press.

Silver, R. A., Traynelis, S. F., & Cullcandy, S. G. (1992). Rapid-time-course miniature and evoked excitatory currents at cerebellar synapses insitu. *Nature*, *355*(6356), 163-166. (32)

Siwei, L., & Zhen, H. (1998). Large scale neural networks and its application on recognition of chinese character. *ICSP 98. IEEE Fourth International Conference on Signal Processing Proceedings, 1998.*, *1*, 1273-1276.

Smith, T. C., & Jahr, C. E. (2002). Self-inhibition of olfactory bulb neurons. *Nature Neuroscience*, *5*(8), 760-766.

Song, S., & Abbott, L. F. (2001). Cortical development and remapping through spike timing-dependent plasticity. *Neuron*, *32*(2), 339-350. (45)

Song, S., Miller, K. D., & Abbott, L. F. (2000). Competitive hebbian learning through spike-timing-dependent synaptic plasticity. *Nature Neuroscience*, *3*(9), 919-926. (50)

Soto-Trevino, C., Thoroughman, K. A., Marder, E., & Abbott, L. F. (2001). Activity-dependent modification of inhibitory synapses in models of rhythmic neural networks. *Nature Neuroscience*, *4*(3), 297-303. (38)

Spruston, N., & Kath, W. L. (2004). Dendritic arithmetic. *Nature Neuroscience*, *7*(6), 567-569. (15)

Stevens, C. F., & Zhu, Y. (2003). Synaptic transmission. In M. A. Arbib (Ed.), *The handbook of brain theory and neural networks* (2nd. ed., p. 1134-1136). Cambridge, Massachusetts. USA: The MIT Press.

Suki, B., Alencar, A. M., Frey, U., Ivanov, P. C., Buldyrev, S. V., Majumdar, A., et al. (2003). Fluctuations, noise and scaling in the cardio-pulmonary system. *Fluctuation and Noise Letters*, *3*(1), R1-R25.

Talley, E. M., Cribbs, L. L., Lee, J. H., Daud, A., Perez-Reyes, E., & Bayliss, D. A. (1999). Differential distribution of three members of a gene family encoding low voltage-activated (t-type) calcium channels. *Journal of Neuroscience*, *19*(6), 1895-1911. (67)

Tan, A. Y. Y., Zhang, L. I., Merzenich, M. M., & Schreiner, C. E. (2003). Tone-evoked excitatory and inhibitory synaptic conductances of primary auditory cortex neurons. *J. Neurophysiol.*(92), 630-643.

Tuckwell, H. (1988). *Introduction to theoretical neurobiology* (1st. ed.). New York, NY. USA.: Cambridge University Press.

Uchida, N., Takahashi, Y. K., Tanifuji, M., & Mori, K. (2000). Odor maps in the mammalian olfactory bulb: domain organization and odorant structural features. *Nature Neuroscience*, *3*(10), 1035-1043.

Usrey, W. M. (2002). Ampa autoreceptors fill the gap in olfactory temporal coding. *Nature Neuroscience*, *5*(11), 1108-1109.

Vapnik, V. N. (1995). *The nature of statistical learning theory* (1st. ed.). Springer.

Walczak, S. (2001). An empirical analysis of data requirements for financial forecasting with neural networks. *Journal of Management Information Systems*, *17*(4), 203-222.

Weinstein, R. K., & Lee, R. H. (2006). Architecture for high-performance fpga implementations of neural models. *Journal of Neural Engineering*, *1*(3), 21-34.

Wijekoon, J. H. B., & Dudek, P. (2008). Compact silicon neuron circuit with spiking and bursting behaviour. *Neural Networks*, *21*(2-3), 524-534.

Witkowska, D. (1999). Applying artificial neural networks to bank-decision simulations. *International Advances in Economic Research*, *5*(3), 350-368.

Xilinx. (2002). *Virtex-ii pro: Platform fpga handbook.*

Xilinx. (2003, March 17, 2005). *Development system reference guide.*

Appendices

A. Alpha and beta functions matrices exponentials

The general solution of the exact integration (EI) scheme (Rotter & Diesmann, 1999) for an *nth* order system of linear time invariant ODEs is described by

$$\mathbf{y}_{k+1} = e^{\mathbf{A}\Delta}\mathbf{y}_k, \qquad \mathbf{y}(0) = \mathbf{y}_0, \tag{A.1}$$

where $e^{\mathbf{A}\Delta}$ is the matrix exponential of the system. The diagonal elements of this matrix describe the step dynamics for each of the exponential decay stages to be used as part of the solution, which can be cascaded to simulate the *nth* order system. However to maintain an exact solution the remaining off-diagonal elements must be applied as coupling factors between the cascaded stages.

A.1 Matrix exponential of the alpha function synapse.

$$\mathbf{P}_\alpha = e^{\mathbf{A}\Delta} = \begin{bmatrix} e^{-\frac{\Delta}{\tau_\alpha}} & 0 \\ \Delta e^{-\frac{\Delta}{\tau_\alpha}} & e^{-\frac{\Delta}{\tau_\alpha}} \end{bmatrix}. \tag{A.2}$$

A.2 Matrix exponential of the beta function synapse.

$$\mathbf{P}_\beta = e^{\mathbf{A}\Delta} = \begin{bmatrix} e^{-\frac{\Delta}{\tau_{\beta_1}}} & 0 \\ \frac{\tau_{\beta_1}\tau_{\beta_2}(e^{-\frac{\Delta}{\tau_{\beta_1}}} - e^{-\frac{\Delta}{\tau_{\beta_2}}})}{\tau_{\beta_1} - \tau_{\beta_2}} & e^{-\frac{\Delta}{\tau_{\beta_2}}} \end{bmatrix}. \tag{A.3}$$

B. Matrix exponential of the combined neuron model based on alpha function synapse

B.1 Matrix exponential of the combined neuron model based on alpha function synapse.

$$\mathbf{P}_m = e^{\mathbf{A}\Delta} = \begin{bmatrix} e^{-\frac{\Delta}{\tau_\alpha}} & 0 & 0 \\ \Delta e^{-\frac{\Delta}{\tau_\alpha}} & e^{-\frac{\Delta}{\tau_\alpha}} & 0 \\ \frac{\tau_\alpha\tau_m((\tau_\alpha-\tau_m)\Delta e^{-\frac{\Delta}{\tau_\alpha}}-\tau_\alpha\tau_m(e^{-\frac{\Delta}{\tau_\alpha}}-e^{-\frac{\Delta}{\tau_m}}))}{C(\tau_\alpha-\tau_m)^2} & \frac{\tau_\alpha\tau_m(e^{-\frac{\Delta}{\tau_\alpha}}-e^{-\frac{\Delta}{\tau_m}})}{C(\tau_\alpha-\tau_m)} & e^{-\frac{\Delta}{\tau_m}} \end{bmatrix}. \tag{B.1}$$

B.2 Linear transformation of the matrix exponential of the combined neuron model based on alpha function synapse.

Here we describe a linear transformation which may be applied to the matrix exponential in order to simplify the combined neuron circuit. The goal of this transformation is to reduce the hardware required to implement the combined neuron model by removing the requirement for multipliers.

First of all, for the sake of the simplicity, let us rewrite the matrix exponential ($\mathbf{P}_m = e^{\mathbf{A}\Delta}$) in a more general form as

$$\mathbf{P}_m = \begin{bmatrix} \alpha & 0 & 0 \\ r & \beta & 0 \\ q & p & \gamma \end{bmatrix}, \tag{B.2}$$

where α, β, and γ define the three exponential decay circuits connected in cascade and p, q, and r are constant coupling factors, which call for the use of multipliers. We would like to express the matrix exponential in the form

$$\begin{bmatrix} \alpha & 0 & 0 \\ 1 & \beta & 0 \\ 0 & 1 & \gamma \end{bmatrix}, \tag{B.3}$$

which means that the resulting combined neuron model circuit will be made up of three exponential decay elements connected in cascade, but crucially, with no multiplication factors coupling them. The best way to achieve this form without altering the dynamics is by applying a linear transformation. We must find a linear transformation that when applied to the matrix exponential, such as equation B.1, yields a transformed matrix exponential of the form shown in equation B.3. The following transformation matrix fulfils this requirement

$$\mathbf{Q} = \begin{bmatrix} b & 0 & 0 \\ f & c & 0 \\ 0 & 0 & d \end{bmatrix}. \tag{B.4}$$

Thus, we must now find the values of b, c, d, and f which transform equation B.1 into the form of equation B.3.

Applying this transformation matrix to the general solution (equation A.1) gives,

$$\mathbf{y} = \mathbf{Q}\mathbf{z}, \tag{B.5}$$

which gives rise to the linear transformation of equation A.1 given by,

$$\mathbf{z}_{k+1} = \mathbf{Q}^{-1}\mathbf{P}_m\mathbf{Q} \cdot \mathbf{z}_k, \qquad \mathbf{z}(0) = \mathbf{z}_0, \tag{B.6}$$

where

$$\mathbf{Q}^{-1}\mathbf{P}_m\mathbf{Q} = \begin{bmatrix} \alpha & 0 & 0 \\ (-\frac{f}{bc}\alpha + \frac{1}{c}r)b + \frac{f}{c}\beta & \beta & 0 \\ \frac{b}{d}q + \frac{f}{d}p & \frac{c}{d}p & \gamma \end{bmatrix}. \tag{B.7}$$

As was already mentioned, in order to keep simplicity in the circuit, the transformed matrix exponential should be in the form of equation B.3. The following conditions ensure that this is accomplished

$$\begin{aligned} -f\alpha + br + f\beta &= c, \\ bq + fp &= 0, \\ cp &= d. \end{aligned} \tag{B.8}$$

To maintain the dynamic of the membrane potential it is required that $d = 1$.

Now we can easily solve for b, c, and f, which results in

$$b = \frac{-1}{(\beta - \alpha)q - pr}, \tag{B.9}$$

$$c = \frac{1}{p}, \tag{B.10}$$

$$d = 1, \tag{B.11}$$

$$f = \frac{q}{p((\beta - \alpha)q - pr)}. \tag{B.12}$$

In turn, the transformed initial conditions for a single presynaptic action potential should then be

$$\mathbf{z}(0) = \begin{bmatrix} \frac{1}{b}\frac{we}{\tau_\alpha} \\ -\frac{f}{bc}\frac{we}{\tau_\alpha} \\ 0 \end{bmatrix}. \tag{B.13}$$

In the context of the combined circuit, the first and second row of the equation B.13 correspond to the initial conditions of the exponential decay units (in the same order), which produces the alpha function synapse (See Figure 2a). The first row requires us to adjust the synaptic weight according to

$$w_{adj} = \frac{1}{b}\frac{we}{\tau_\alpha}, \tag{B.14}$$

where b is defined in equation B.9, and w is the synaptic weight.

In turn, the second row gives the initial condition that must be applied to the second exponential decay unit of the alpha function synapse, which is carried out by making

$$\rho = -\frac{f}{bc}\frac{we}{\tau_\alpha}, \tag{B.15}$$

where b, c and f are defined in equations B.9 to B.12. It is important to point out that ρ must be non-zero in combined neuron models based on alpha/beta function synapses, otherwise $\rho = 0$ and can be neglected. Furthermore, since equation A.1 describes the dynamics of the combined neuron model in between spikes, both w_{adj} and ρ should be added every time an action potential is received at the synapse (see Figure 3.2a).

Finally, the soma model requires initial conditions set to zero. Meeting this conditions will guarantee an EI of a leaky integrate-and-fire model receiving dendritic currents modelled by alpha functions.

C. Exponential decay synapse based combined neuron model matrix exponential

C.1 Matrix exponential of the combined neuron model based on exponential decay synapse.

$$\begin{bmatrix} e^{-\frac{\Delta}{\tau_e}} & 0 \\ \frac{\tau_e\tau_m(e^{-\frac{\Delta}{\tau_e}}-e^{-\frac{\Delta}{\tau_m}})}{C(\tau_e-\tau_m)} & e^{-\frac{\Delta}{\tau_m}} \end{bmatrix}. \tag{C.1}$$

Trial	Vapour	Trial	Vapour	Trial	Vapour	Trial	Vapour	Trial	Vapour
001	control	021	dfg	041	cdg	061	control	081	abdg
002	cdeg	022	cde	042	abcd	062	de	082	abcdfg
003	adef	023	abcdeg	043	control	063	abef	083	aef
004	adfg	024	acdg	044	ceg	064	abcdf	084	g
005	adg	025	control	045	abcefg	065	bdeg	085	control
006	de	026	e	046	abdfg	066	abcdfg	086	abf
007	control	027	cf	047	acef	067	control	087	be
008	abcef	028	abf	048	bcf	068	befg	088	bce
009	g	029	d	049	control	069	abdfg	089	befg
010	bcefg	030	abcdg	050	cf	070	f	090	aceg
011	f	031	control	051	bcdef	071	adef	091	control
012	df	032	ef	052	c	072	abdefg	092	bdg
013	control	033	abcef	053	g	073	control	093	bg
014	bdefg	034	abdg	054	bdefg	074	bcdg	094	bcd
015	acdfg	035	abcefg	055	control	075	abefg	095	f
016	bcdef	036	bcdeg	056	bcde	076	cdf	096	ade
017	bc	037	control	057	c	077	cdeg	097	control
018	cd	038	abce	058	bde	078	abcf	098	de
019	control	039	abcg	059	bcdef	079	control	099	cdefg
020	bf	040	adf	060	abcefg	080	e	100	bdg

Table D.1: Description of the vapours used for trials 1 to 100.

D List of vapors (odors) used by trial number

Trial	Vapour	Trial	Vapour	Trial	Vapour	Trial	Vapour	Trial	Vapour
101	control	121	abcdfg	141	control	161	cdfg	181	abdf
102	control	122	df	142	abdeg	162	abcefg	182	abcdeg
103	ce	123	control	143	beg	163	acfg	183	control
104	bcdeg	124	def	144	acfg	164	af	184	ade
105	control	125	cefg	145	bef	165	control	185	abd
106	g	126	acef	146	bf	166	bf	186	bcef
107	abcdg	127	afg	147	control	167	abef	187	aceg
108	eg	128	cde	148	bcdef	168	abcf	188	bde
109	dfg	129	control	149	abceg	169	a	189	control
110	acdg	130	cfg	150	ae	170	ab	190	abc
111	control	131	abef	151	cdef	171	control	191	acg
112	cef	132	acg	152	bdef	172	abefg	192	acdeg
113	aeg	133	cfg	153	control	173	def	193	abcfg
114	aef	134	acdg	154	bf	174	bfg	194	aeg
115	adg	135	control	155	df	175	ac	195	control
116	adef	136	bcde	156	c	176	adf	196	g
117	control	137	cef	157	adefg	177	control	197	afg
118	ad	138	abcde	158	df	178	acf	198	acd
119	f	139	abdg	159	control	179	acdf	199	adeg
120	aeg	140	bcefg	160	acdef	180	abeg	200	abcdef

Table D.2: Description of the vapours used for trials 101 to 200.

Trial	Vapour	Trial	Vapour	Trial	Vapour	Trial	Vapour	Trial	Vapour
201	control	221	control	241	cdg	261	cdfg	281	control
202	e	222	cg	242	b	262	aefg	282	abcd
203	control	223	abcf	243	abdfg	263	control	283	bcdefg
204	control	224	bdf	244	fg	264	bef	284	cef
205	abdefg	225	aef	245	control	265	cdef	285	acdef
206	abcdf	226	aef	246	e	266	abcdg	286	dg
207	ade	227	control	247	abcdefg	267	ac	287	control
208	abce	228	ace	248	bdfg	268	ab	288	bfg
209	control	229	af	249	bdeg	269	control	289	a
210	abd	230	ce	250	abceg	270	acefg	290	cdefg
211	afg	231	abeg	251	control	271	adfg	291	bdf
212	d	232	cg	252	dg	272	df	292	abfg
213	cdefg	233	control	253	a	273	abde	293	control
214	acdg	234	abdefg	254	bcfg	274	cdeg	294	cf
215	control	235	beg	255	bcf	275	control	295	cdg
216	bdeg	236	acdfg	256	aefg	276	ace	296	abef
217	bcdf	237	efg	257	control	277	bdfg	297	acd
218	be	238	fg	258	d	278	efg	298	bcd
219	c	239	control	259	abeg	279	abd	299	control
220	acg	240	bdf	260	defg	280	e	300	bcg

Table D.3: Description of the vapours used for trials 201 to 300.

Trial	Vapour	Trial	Vapour	Trial	Vapour	Trial	Vapour	Trial	Vapour
301	abcd	321	acdeg	341	eg	361	aefg	381	cdefg
302	abceg	322	af	342	control	362	acfg	382	bdf
303	bc	323	ef	343	defg	363	befg	383	ae
304	ade	324	control	344	afg	364	g	384	control
305	control	325	adeg	345	abg	365	bcfg	385	cfg
306	control	326	adg	346	bcg	366	control	386	af
307	acdefg	327	g	347	aceg	367	f	387	adf
308	bd	328	acdf	348	control	368	a	388	acf
309	bce	329	cdfg	349	bdg	369	adg	389	abcdeg
310	d	330	control	350	be	370	abdeg	390	control
311	adeg	331	adefg	351	cdf	371	abdef	391	abceg
312	control	332	deg	352	bcdg	372	control	392	acdef
313	abcdg	333	bdefg	353	bc	373	bdef	393	abc
314	acde	334	abdef	354	control	374	abfg	394	acf
315	abdf	335	bceg	355	bfg	375	g	395	bdefg
316	cfg	336	control	356	ac	376	abcde	396	control
317	abcdef	337	def	357	abg	377	ac	397	ce
318	control	338	fg	358	abdfg	378	control	398	bcf
319	bcef	339	bg	359	acde	379	acdg	399	acde
320	efg	340	cd	360	control	380	adefg	400	beg

Table D.4: Description of the vapours used for trials 301 to 400.

Trial	Vapour	Trial	Vapour	Trial	Vapour	Trial	Vapour	Trial	Vapour
401	ag	421	cdef	441	abde	461	d	481	bcdf
402	control	422	control	442	ceg	462	adef	482	control
403	e	423	abdefg	443	abcdefg	463	b	483	abcf
404	abcde	424	bcdfg	444	adefg	464	control	484	abefg
405	abd	425	b	445	e	465	abde	485	c
406	control	426	abef	446	control	466	abefg	486	adfg
407	control	427	bdfg	447	abefg	467	bcdefg	487	cde
408	ef	428	control	448	beg	468	cdg	488	control
409	abcdefg	429	bef	449	bcefg	469	ab	489	cdfg
410	control	430	bef	450	bde	470	control	490	def
411	abc	431	f	451	adfg	471	abc	491	abdef
412	acdeg	432	d	452	control	472	bce	492	adefg
413	eg	433	efg	453	abdefg	473	acdf	493	de
414	cdeg	434	control	454	abcef	474	c	494	control
415	ad	435	bcefg	455	ace	475	bg	495	abcef
416	control	436	eg	456	abe	476	control	496	abe
417	cfg	437	bg	457	beg	477	cdg	497	c
418	cf	438	bdefg	458	control	478	cg	498	cd
419	bdfg	439	cg	459	abcfg	479	bdfg	499	acd
420	aeg	440	control	460	bf	480	abcdefg	500	control

Table D.5: Description of the vapours used for trials 401 to 500.

Trial	Vapour	Trial	Vapour	Trial	Vapour	Trial	Vapour	Trial	Vapour
501	abdeg	521	abfg	541	acdfg	561	abf	581	abcg
502	aef	522	c	542	g	562	control	582	efg
503	bcdefg	523	cefg	543	cefg	563	abdf	583	aceg
504	ace	524	bef	544	control	564	acefg	584	abe
505	bdg	525	acfg	545	abe	565	bcdeg	585	bce
506	control	526	control	546	ae	566	befg	586	control
507	abde	527	abdef	547	bcde	567	bcf	587	bd
508	control	528	b	548	abcdef	568	control	588	abdeg
509	control	529	acd	549	bcd	569	ceg	589	bde
510	abg	530	acef	550	control	570	ag	590	abce
511	bdf	531	acdfg	551	bdeg	571	bcdfg	591	abdf
512	abcfg	532	control	552	cg	572	abde	592	control
513	bg	533	bcdg	553	cdefg	573	bcdeg	593	bd
514	control	534	abcef	554	bcde	574	control	594	adg
515	adfg	535	fg	555	d	575	abcdef	595	abcdeg
516	bceg	536	abce	556	control	576	abcf	596	ab
517	a	537	d	557	acdefg	577	bcefg	597	a
518	bcdefg	538	control	558	bcg	578	bfg	598	control
519	bc	539	dg	559	acdefg	579	adf	599	abcde
520	control	540	acg	560	abcdfg	580	control	600	acefg

Table D.6: Description of the vapours used for trials 501 to 600.

Trial	Vapour	Trial	Vapour	Trial	Vapour	Trial	Vapour	Trial	Vapour
601	afg	621	cef	641	control	661	bcdfg	681	bcdfg
602	c	622	abfg	642	be	662	ag	682	bfg
603	ef	623	control	643	g	663	f	683	control
604	control	624	deg	644	bcd	664	e	684	acd
605	cdfg	625	abcdef	645	ceg	665	control	685	a
606	bce	626	f	646	dg	666	cef	686	dfg
607	cdeg	627	abg	647	control	667	acdf	687	abdg
608	ef	628	bdg	648	ce	668	bcdf	688	ag
609	adeg	629	control	649	abeg	669	acdeg	689	control
610	control	630	abceg	650	ac	670	af	690	acef
611	control	631	bcdg	651	def	671	control	691	dfg
612	deg	632	abcdf	652	abg	672	abdef	692	abcd
613	abcdeg	633	de	653	control	673	abcde	693	abcdg
614	bcef	634	bcd	654	b	674	bcef	694	abfg
615	cde	635	control	655	bcde	675	d	695	control
616	acefg	636	acf	656	cdf	676	bd	696	defg
617	control	637	d	657	abdf	677	control	697	abf
618	acdfg	638	eg	658	aceg	678	acdef	698	acdeg
619	abcfg	639	ab	659	control	679	abd	699	cdef
620	deg	640	a	660	cdf	680	ag	700	e

Table D.7: Description of the vapours used for trials 601 to 700.

Trial	Vapour	Trial	Vapour	Trial	Vapour	Trial	Vapour	Trial	Vapour
701	control	721	control	741	abcefg	761	ae	781	control
702	c	722	bceg	742	ae	762	e	782	bcfg
703	abdfg	723	f	743	adf	763	control	783	cd
704	dg	724	aeg	744	cdef	764	a	784	acg
705	acdefg	725	abcdf	745	control	765	abf	785	abcfg
706	bcdeg	726	bcfg	746	ce	766	abeg	786	a
707	control	727	control	747	bcdf	767	abcg	787	control
708	acdf	728	fg	748	adef	768	acefg	788	cdefg
709	bcdef	729	abdeg	749	deg	769	control	789	be
710	cd	730	acfg	750	abdg	770	abe	790	bcdefg
711	control	731	defg	751	control	771	cefg	791	bde
712	control	732	b	752	b	772	bceg	792	dfg
713	bceg	733	control	753	b	773	aefg	793	control
714	abc	734	cefg	754	abcg	774	bcdf	794	bdef
715	control	735	ceg	755	acdef	775	control	795	acdefg
716	bcef	736	bcdfg	756	aefg	776	bdef	796	bcfg
717	acde	737	abcd	757	control	777	ade	797	bdef
718	bc	738	acf	758	cde	778	cf	798	ace
719	bdeg	739	control	759	befg	779	bcg	799	control
720	acef	740	adeg	760	ad	780	b	800	cdf

Table D.8: Description of the vapours used for trials 701 to 800.

Trial	Vapour	Trial	Vapour	Trial	Vapour	Trial	Vapour	Trial	Vapour
801	ad	805	control	809	abcdefg	812	f	815	abcdf
802	bd	806	bcf	810	abcdfg	813	b	816	abcg
803	bcg	807	acde	811	control	814	ad	817	control
804	bcdg	808	abce						

Table D.9: Description of the vapours used for trials 801 to 817.

E. Evolution of the PCA over the progressive scanning of the inputs.

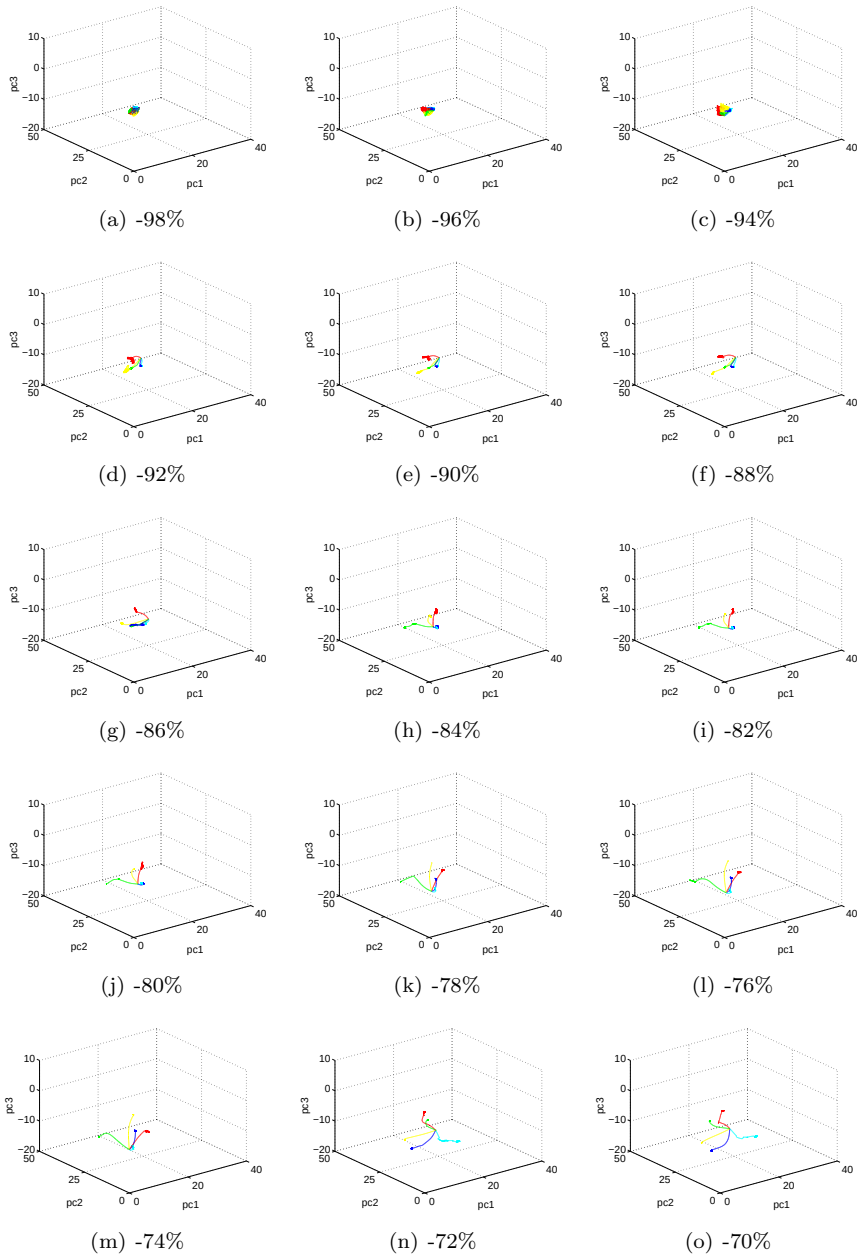

(a) -98% (b) -96% (c) -94%

(d) -92% (e) -90% (f) -88%

(g) -86% (h) -84% (i) -82%

(j) -80% (k) -78% (l) -76%

(m) -74% (n) -72% (o) -70%

Figure D.1: Evolution of the PCA over the progressive scanning of the inputs. Inputs varying from -98% to -70%.

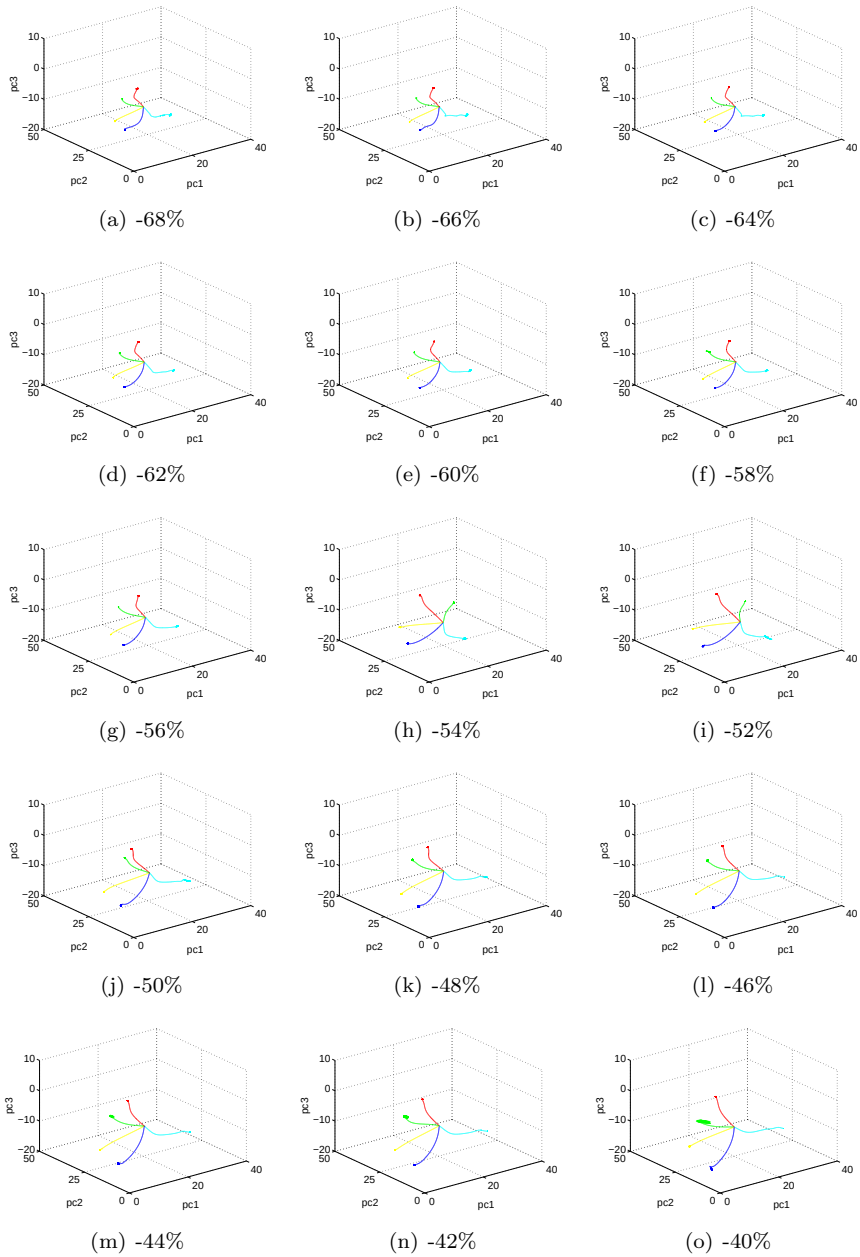

(a) -68% (b) -66% (c) -64%

(d) -62% (e) -60% (f) -58%

(g) -56% (h) -54% (i) -52%

(j) -50% (k) -48% (l) -46%

(m) -44% (n) -42% (o) -40%

Figure D.2: Evolution of the PCA over the progressive scanning of the inputs. Inputs varying from -68% to -40%.

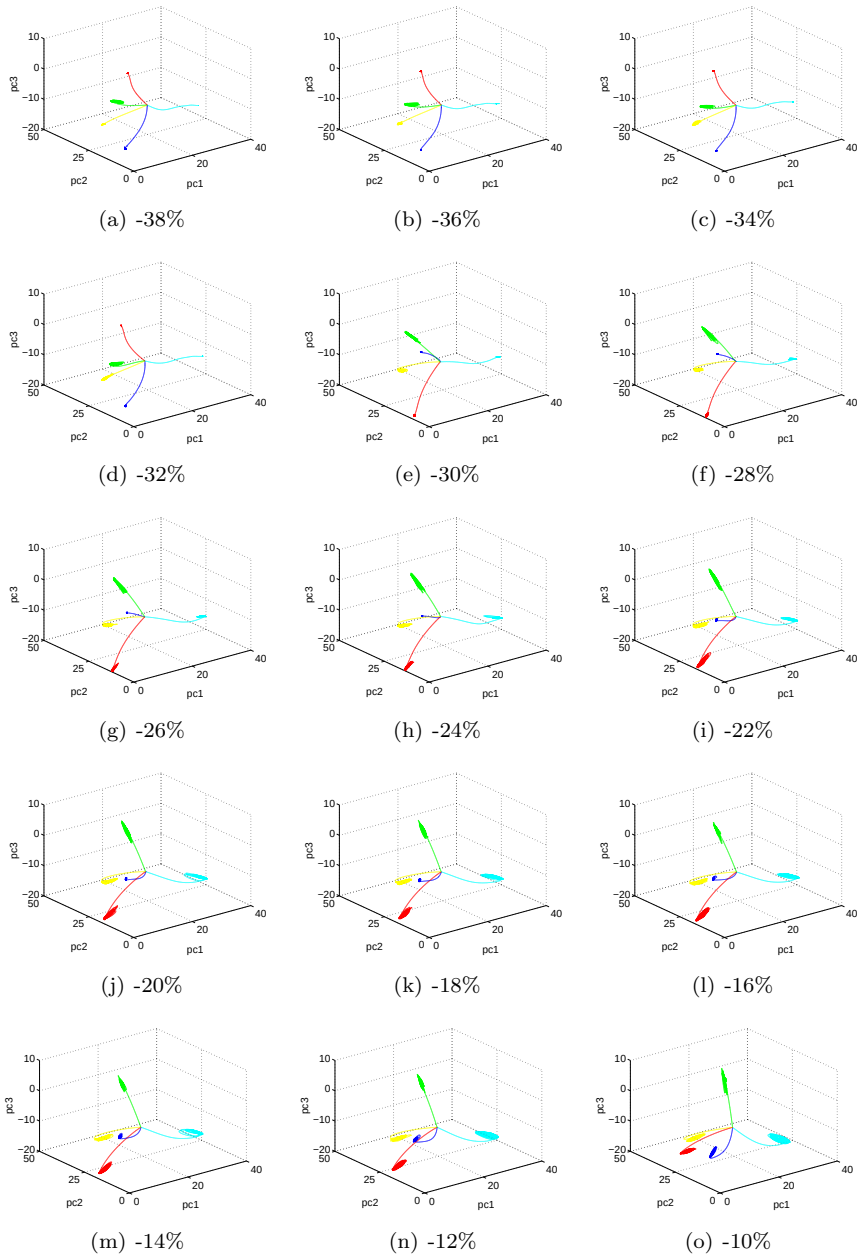

(a) -38% (b) -36% (c) -34%

(d) -32% (e) -30% (f) -28%

(g) -26% (h) -24% (i) -22%

(j) -20% (k) -18% (l) -16%

(m) -14% (n) -12% (o) -10%

Figure D.3: Evolution of the PCA over the progressive scanning of the inputs. Inputs varying from -38% to -10%.

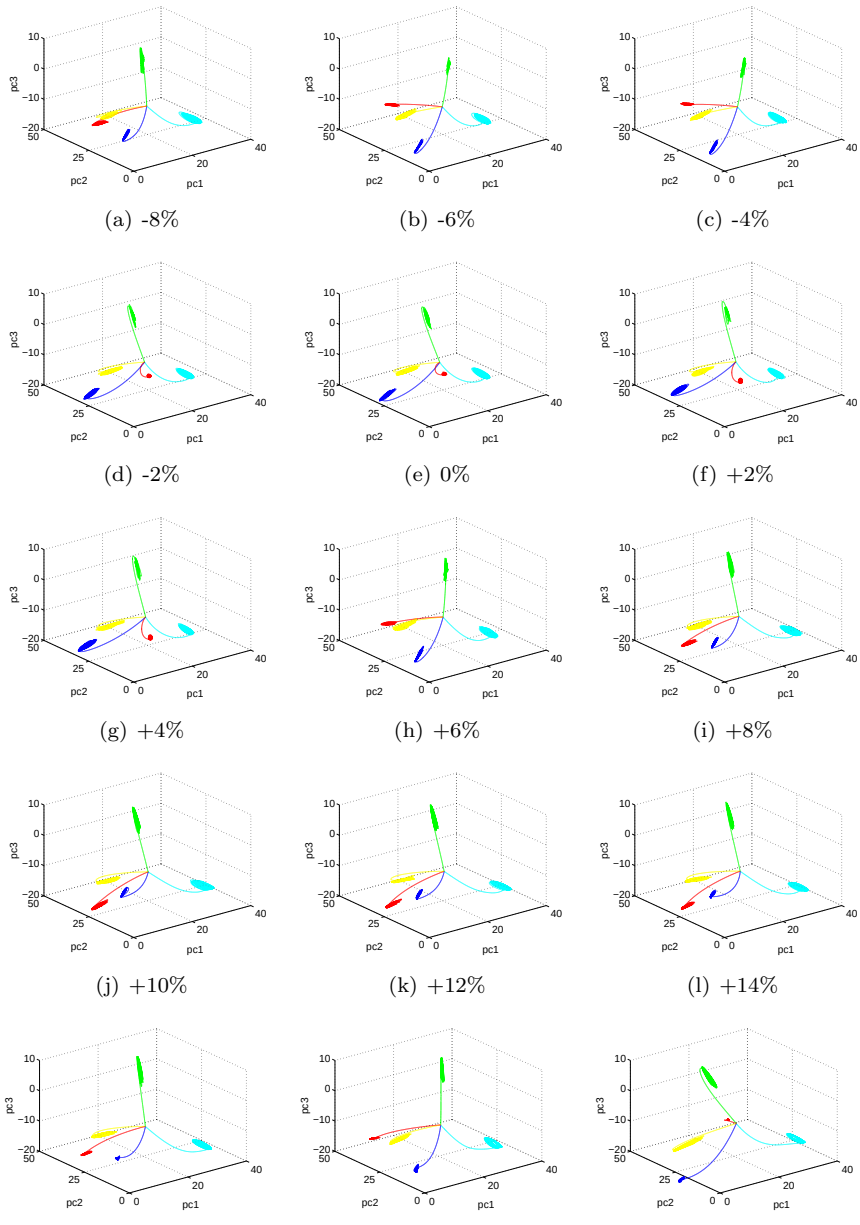

(a) -8% (b) -6% (c) -4%

(d) -2% (e) 0% (f) +2%

(g) +4% (h) +6% (i) +8%

(j) +10% (k) +12% (l) +14%

(m) +16% (n) +18% (o) +20%

Figure D.4: Evolution of the PCA over the progressive scanning of the inputs. Inputs varying from -8% to $+20\%$.

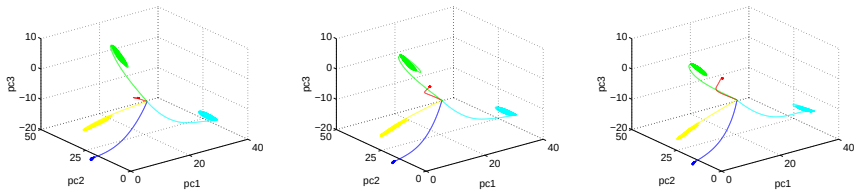

(a) +22%

(b) +24%

(c) +26%

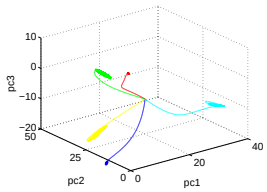

(d) +28%

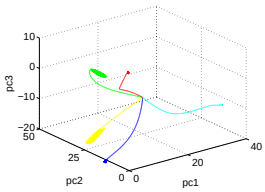

(e) +30%

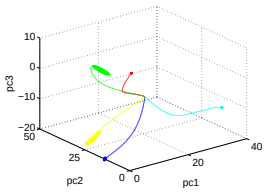

(f) +32%

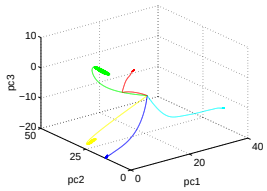

(g) +34%

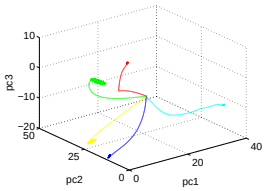

(h) +36%

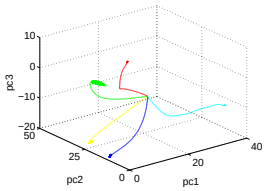

(i) +38%

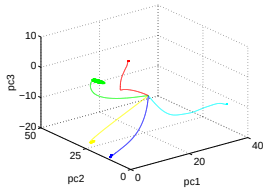

(j) +40%

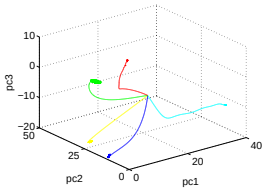

(k) +42%

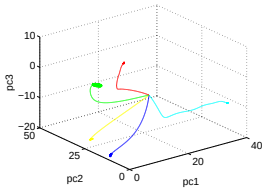

(l) +44%

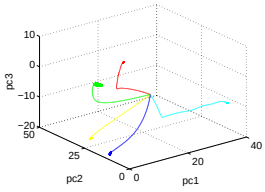

(m) +46%

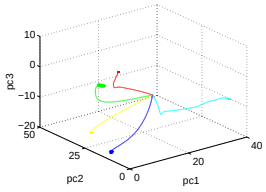

(n) +48%

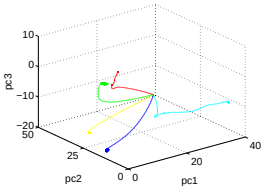

(o) +50%

Figure D.5: Evolution of the PCA over the progressive scanning of the inputs. Inputs varying from +22% to +50%.

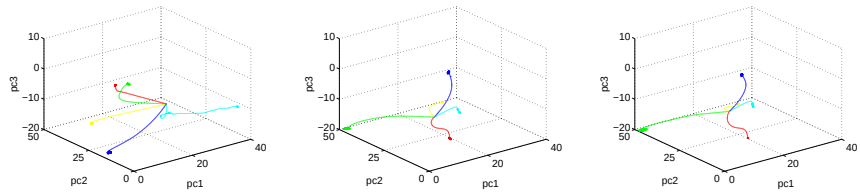

(a) +52%

(b) +54%

(c) +56%

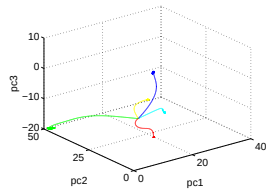

(d) +58%

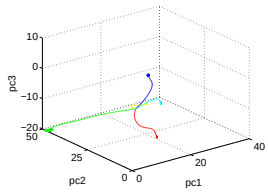

(e) +60%

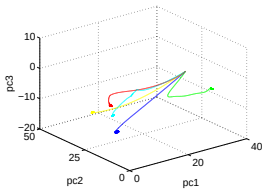

(f) +62%

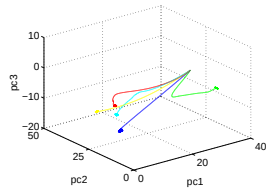

(g) +64%

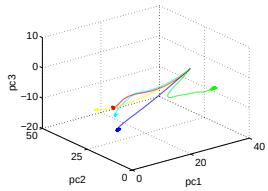

(h) +66%

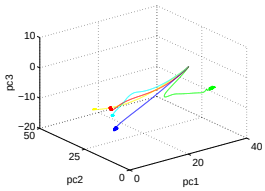

(i) +68%

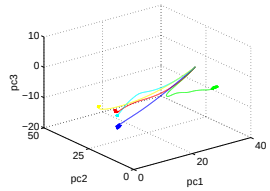

(j) +70%

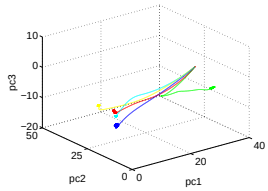

(k) +72%

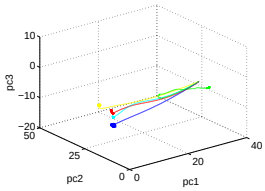

(l) +74%

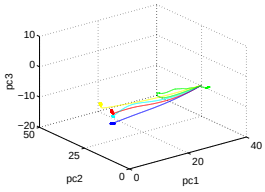

(m) +76%

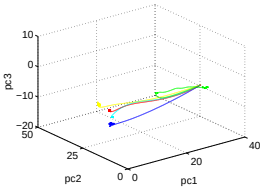

(n) +78%

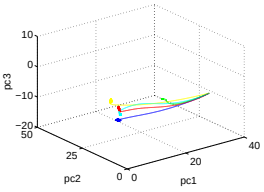

(o) +80%

Figure D.6: Evolution of the PCA over the progressive scanning of the inputs. Inputs varying from +52% to +80%.

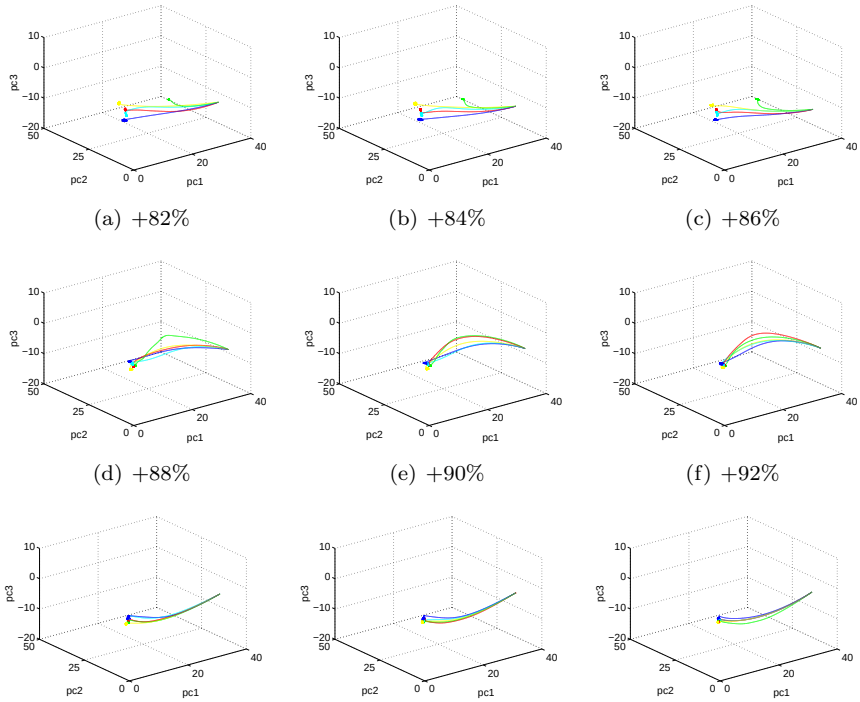

(a) +82% (b) +84% (c) +86%

(d) +88% (e) +90% (f) +92%

(g) +94% (h) +96% (i) +98%

Figure D.7: Evolution of the PCA over the progressive scanning of the inputs. A total of 99 different inputs were obtained to scan the model response to each input. All inputs were calculated by the equation 6.1, hence a percentage of the difference between the trained odor and the lower/upper limit of the allowed values for the inputs is subtracted/added to the trained odor thus obtaining a new input. A PCA analysis of each response was carried out and shown in Figures E. to E.. Inputs varying from -98% to $+98\%$ difference between the trained odor and the limit for the inputs with a progression of 2% between inputs were obtained. The PCA plots were fitted in different figures to allow a more detailed view of each subplot. A total of 5 different odors were used in this experiment, each one represented by a different color in the following fashion: odor 1 in blue, odor 2 in red, odor 3 in green, odor 4 in light blue and odor 5 in yellow. The time constants of both the ORN and mitral cells were set to $\tilde{\tau}_m \approx 10$ ms, with a threshold potential, $V_{th} = 50000$. The time constants of the excitatory synapses were set to $\tilde{\tau}_E \approx 4$ ms, whereas for the inhibitory synapses the time constants were set to $\tilde{\tau}_I \approx 16$ ms. For the ORNs, constant values randomly selected in a range between 500 and 1000, were used to represent a constant concentration of each odor stimulus. The total running time in terms of biological values is equivalent to 5 seconds at a sampling frequency of $f_{smp} = 10$ kHz, although the clock frequency was set to $f_{clk} = 10$ MHz thus each run lasted for 5 ms of the FPGA processing time.

F. Evolution of the PCA over the progressive scanning of the inhibitory weights.

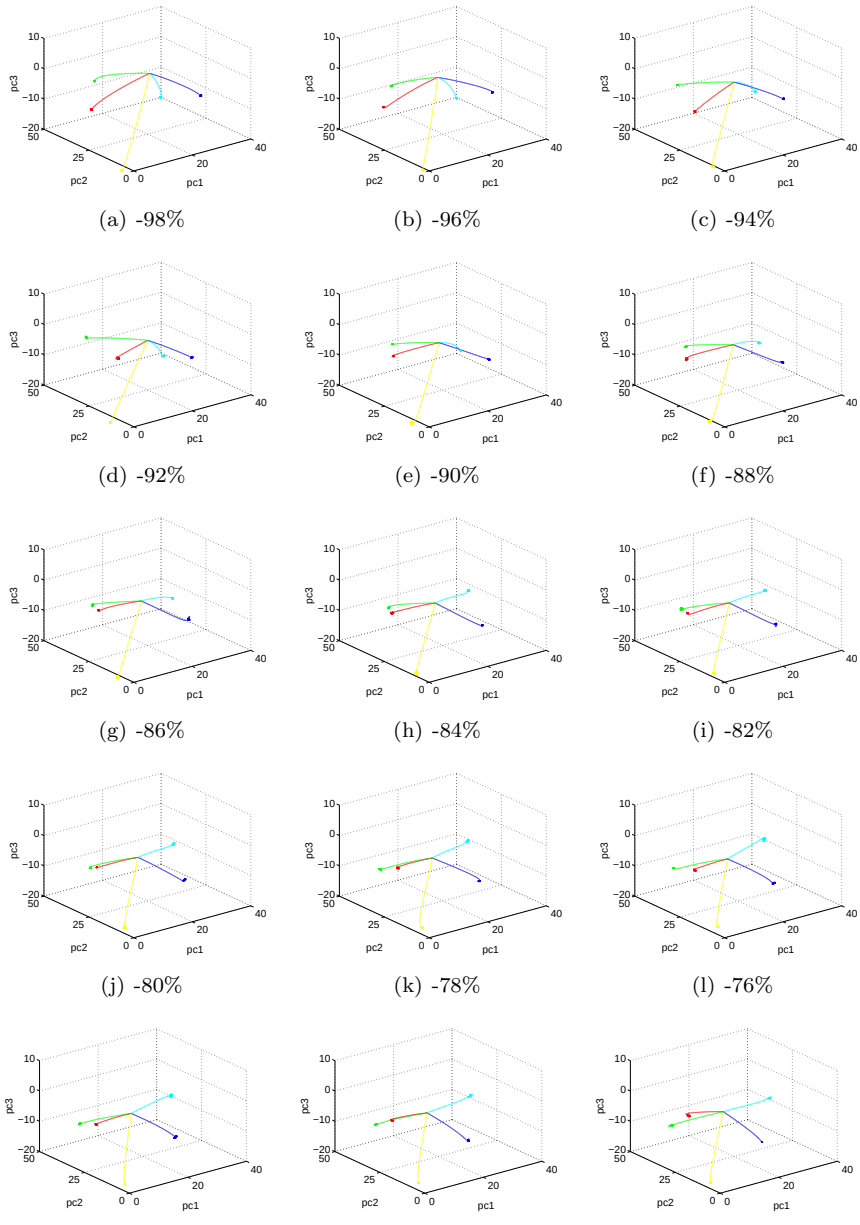

(a) -98% (b) -96% (c) -94%

(d) -92% (e) -90% (f) -88%

(g) -86% (h) -84% (i) -82%

(j) -80% (k) -78% (l) -76%

(m) -74% (n) -72% (o) -70%

Figure F.1: Evolution of the PCA over the progressive scanning of the weights. Weights varying from -98% to -64%.

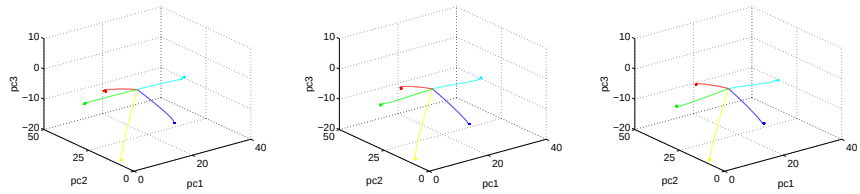

(a) -68%

(b) -66%

(c) -64%

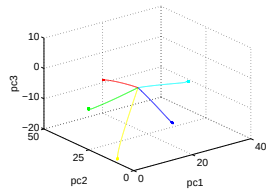

(d) -62%

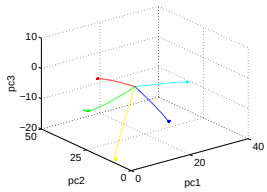

(e) -60%

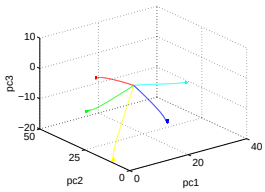

(f) -58%

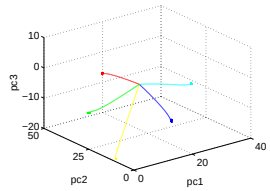

(g) -56%

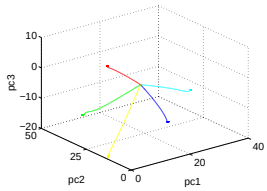

(h) -54%

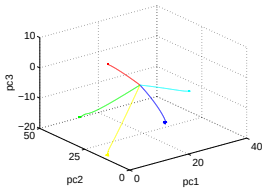

(i) -52%

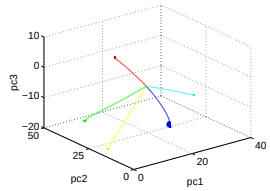

(j) -50%

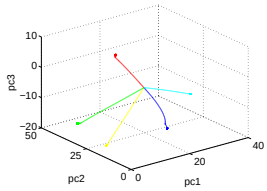

(k) -48%

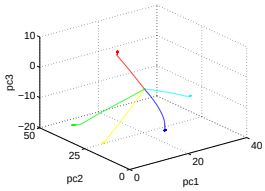

(l) -46%

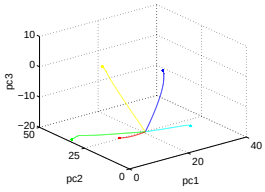

(m) -44%

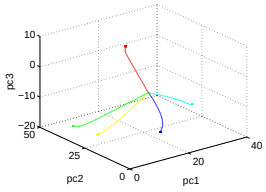

(n) -42%

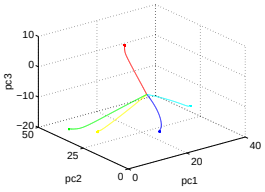

(o) -40%

Figure F.2: Evolution of the PCA over the progressive scanning of the weights. Weights varying from -62% to -28%.

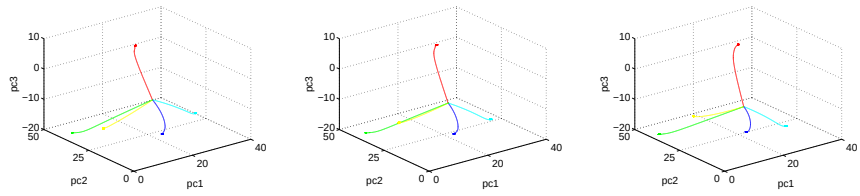

(a) -38%

(b) -36%

(c) -34%

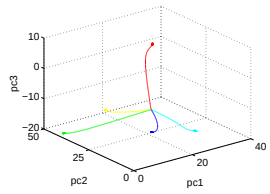

(d) -32%

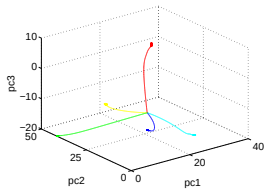

(e) -30%

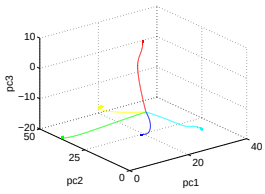

(f) -28%

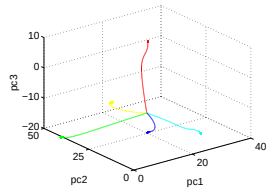

(g) -26%

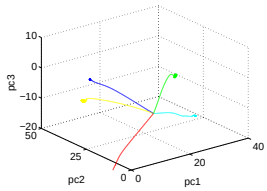

(h) -24%

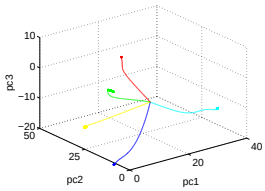

(i) -22%

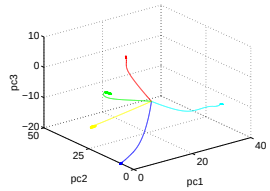

(j) -20%

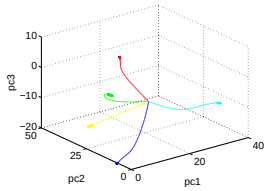

(k) -18%

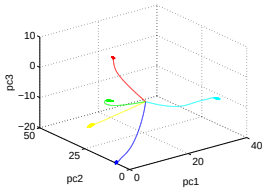

(l) -16%

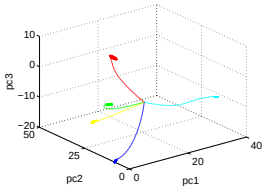

(m) -14%

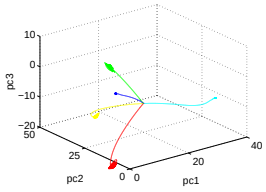

(n) -12%

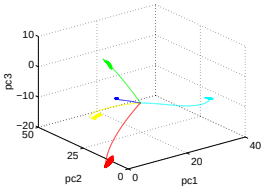

(o) -10%

Figure F.3: Evolution of the PCA over the progressive scanning of the weights. Weights varying from -26% to $+8\%$.

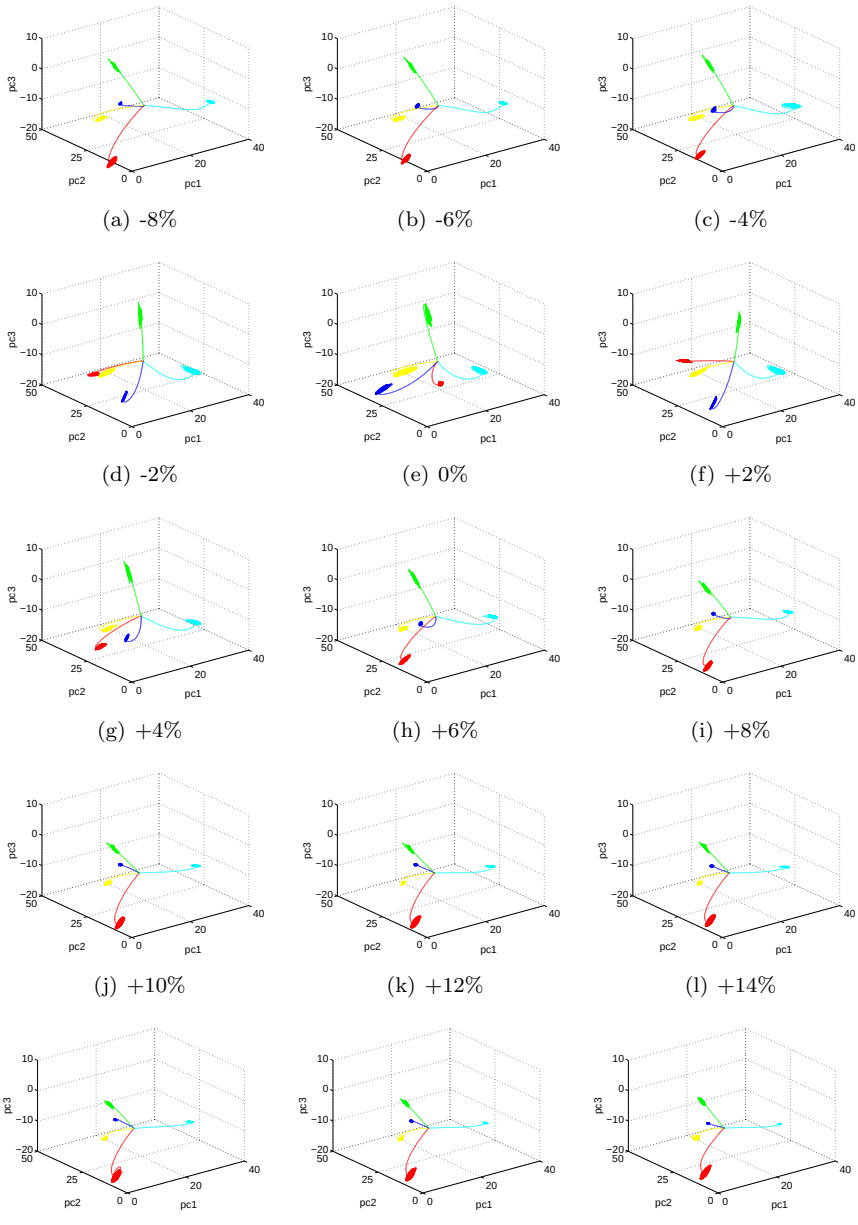

(a) -8% (b) -6% (c) -4%

(d) -2% (e) 0% (f) +2%

(g) +4% (h) +6% (i) +8%

(j) +10% (k) +12% (l) +14%

(m) +16% (n) +18% (o) +20%

Figure F.4: Evolution of the PCA over the progressive scanning of the weights. Weights varying from +10% to +44%.

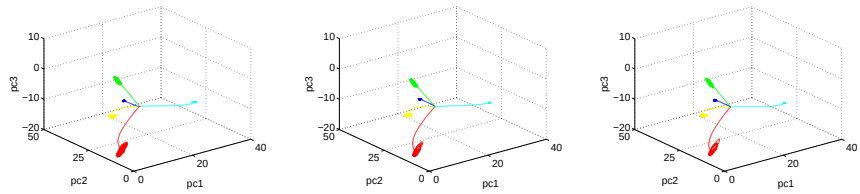

(a) +22%

(b) +24%

(c) +26%

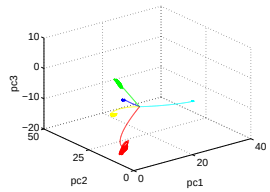

(d) +28%

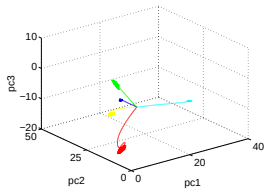

(e) +30%

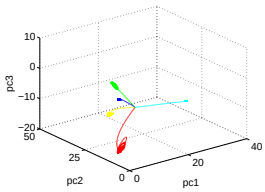

(f) +32%

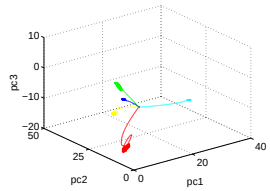

(g) +34%

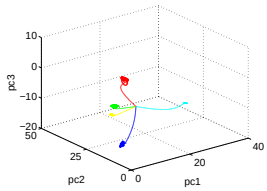

(h) +36%

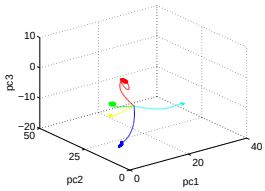

(i) +38%

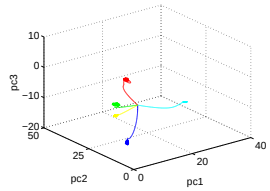

(j) +40%

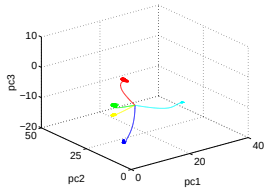

(k) +42%

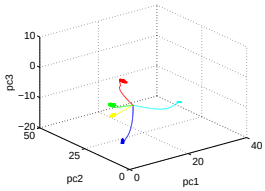

(l) +44%

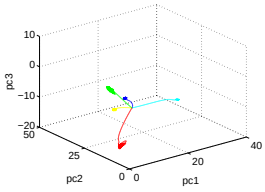

(m) +46%

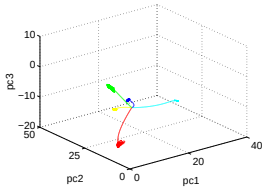

(n) +48%

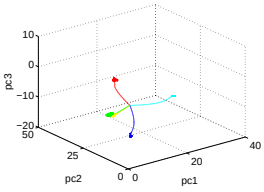

(o) +50%

Figure F.5: Evolution of the PCA over the progressive scanning of the weights. Weights varying from +46% to +80%.

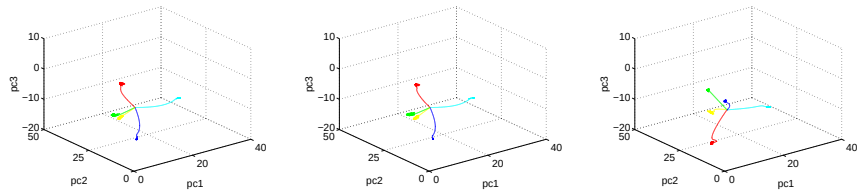

(a) +52%

(b) +54%

(c) +56%

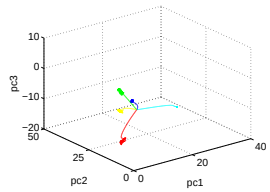

(d) +58%

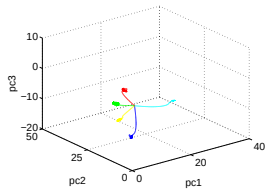

(e) +60%

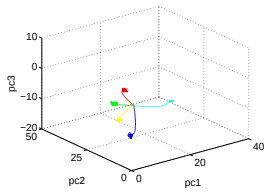

(f) +62%

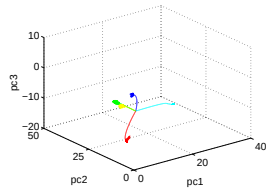

(g) +64%

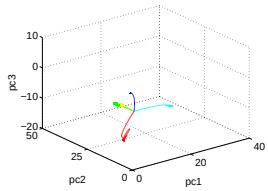

(h) +66%

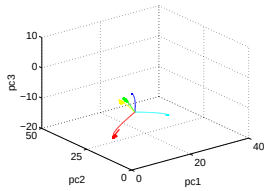

(i) +68%

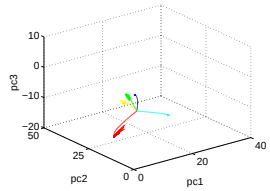

(j) +70%

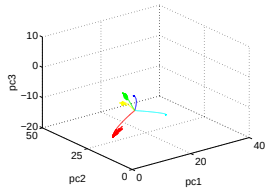

(k) +72%

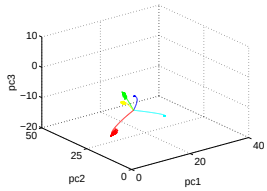

(l) +74%

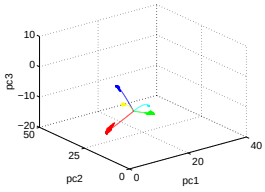

(m) +76%

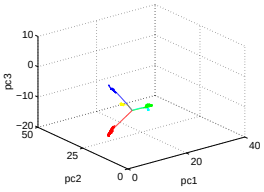

(n) +78%

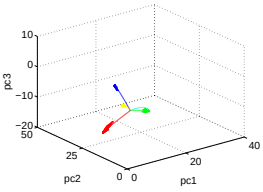

(o) +80%

Figure F.6: Evolution of the PCA over the progressive scanning of the weights. Weights varying from +46% to +80%.

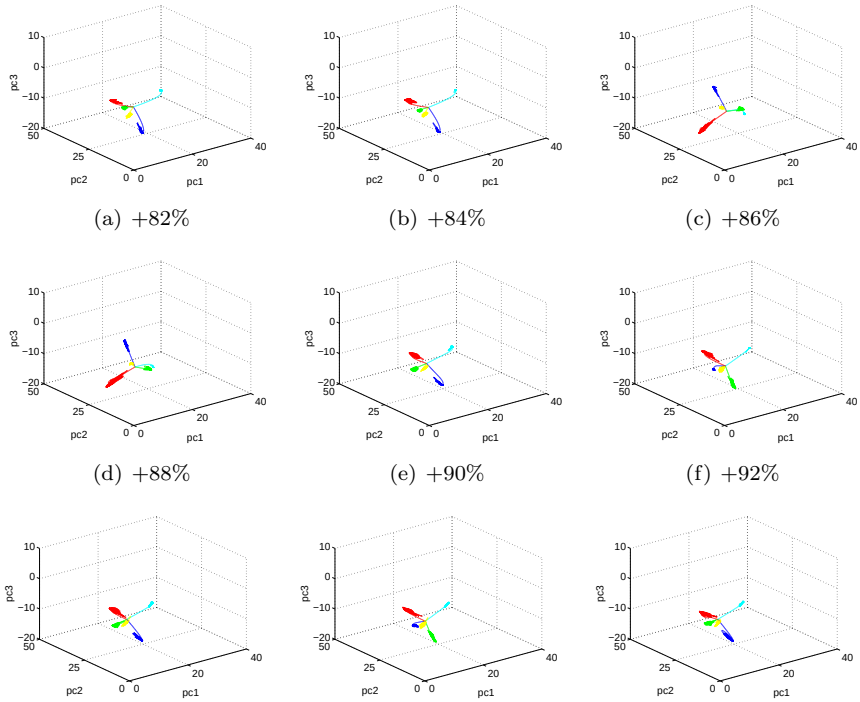

(a) +82% (b) +84% (c) +86%

(d) +88% (e) +90% (f) +92%

(g) +94% (h) +96% (i) +98%

Figure F.7: Evolution of the PCA over the progressive scanning of the inhibitory weights. A total of 99 different sets of inhibitory weights were obtained to scan the model response to each odor. All weights were calculated by the equation 6.3, hence a percentage of the difference between the trained weight and the lower/upper limit of the allowed values for the inhibitory weights is subtracted/added to the trained odor thus obtaining a new set of weights. A PCA analysis of each response was carried out and shown in Figures F. to F.. Inputs varying from -98% to $+98\%$ difference between the trained weight and the limit value of the weights with a progression of 2% between inhibitory weights were obtained. The PCA plots were fitted in different figures to allow a more detailed view of each subplot. A total of 5 different odors were used in this experiment, each one represented by a different color in the following fashion: odor 1 in blue, odor 2 in red, odor 3 in green, odor 4 in light blue and odor 5 in yellow. The time constants of both the ORN and mitral cells were set to $\tilde{\tau}_m \approx 10$ ms, with a threshold potential, $V_{th} = 50000$. The time constants of the excitatory synapses were set to $\tilde{\tau}_E \approx 4$ ms, whereas for the inhibitory synapses the time constants were set to $\tilde{\tau}_I \approx 16$ ms. For the ORNs, constant values randomly selected in a range between 500 and 1000, were used to represent a constant concentration of each odor stimulus. The total running time in terms of biological values is equivalent to 5 seconds at a sampling frequency of $f_{smp} = 10$ kHz, although the clock frequency was set to $f_{clk} = 10$ MHz thus each run lasted for 5 ms of the FPGA processing time.

G. Evolution of the Cross-correlation over the progressive scanning of the inputs.

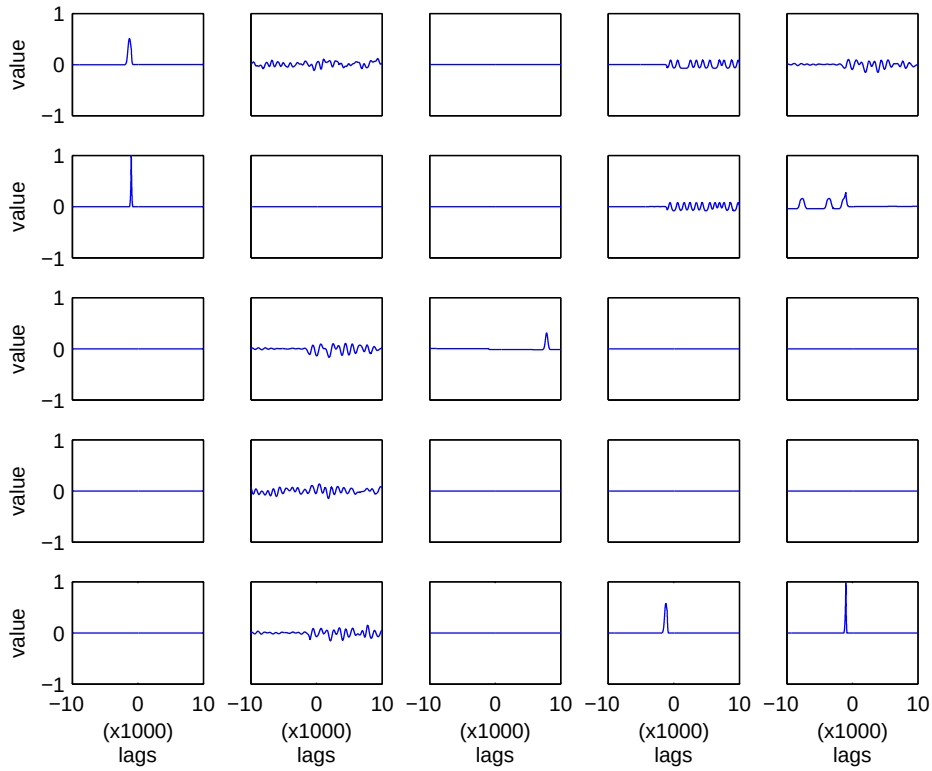

Figure G.1: Cross-correlation analysis for odour 1: trained input vs. -80% difference input. The Cross-correlation analysis was carried out between the response of the olfactory bulb of the trained input and the input minus a percentage of the difference between input value and the limit range for the input. Plots are sorted from left to right and from up to down, starting from the cross-corelation between for the first mitral cell (the first column and first row) up to the 25th mitral cell in the last column at the bottom. Plots with zero response result from Mitral cells which remain silent for this particular input. The time constants of both the ORN and mitral cells were set to $\tilde{\tau}_m \approx 10$ ms, with a threshold potential, $V_{th} = 50000$. The time constants of the excitatory synapses were set to $\tilde{\tau}_E \approx 4$ ms, whereas for the inhibitory synapses the time constants were set to $\tilde{\tau}_I \approx 16$ ms. For the ORNs, constant values randomly selected in a range between 500 and 1000, were used to represent a constant concentration of each odor stimulus. The total running time in terms of biological values is equivalent to 5 seconds at a sampling frequency of $f_{smp} = 10$ KHz. Although the clock frequency was set to $f_{clk} = 10$ MHz thus each run lasted for 5 ms of the FPGA processing time.

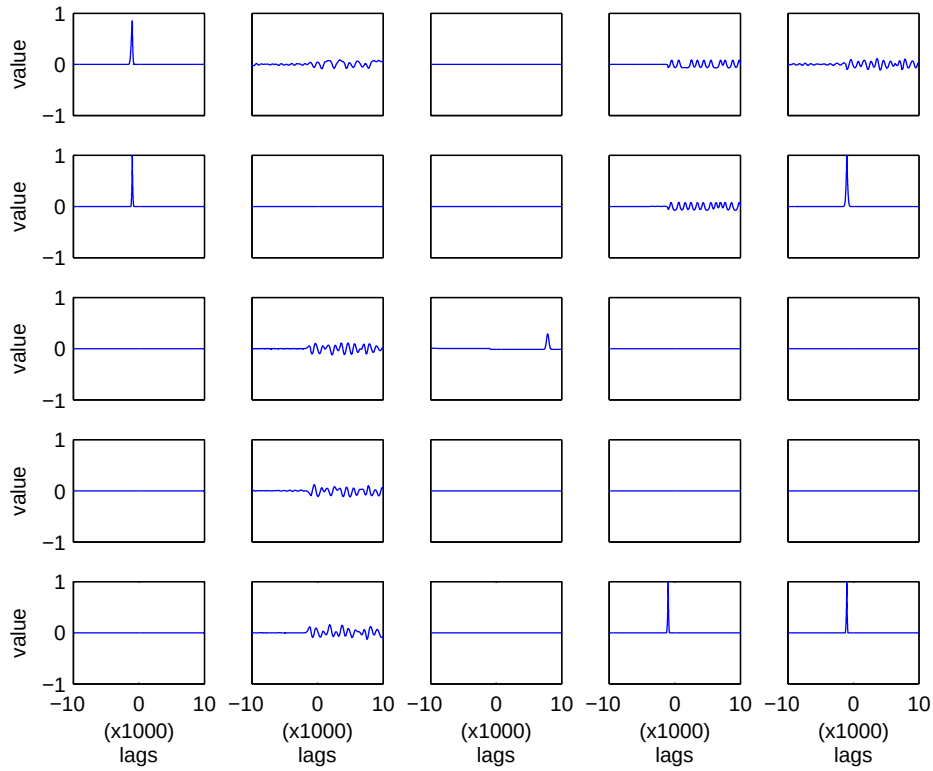

Figure G.2: Cross-correlation analysis for odour 1: trained input vs. -60% difference input. The Cross-correlation analysis was carried out between the response of the olfactory bulb of the trained input and the input minus a percentage of the difference between input value and the limit range for the input. Plots are sorted from left to right and from up to down, starting from the cross-corelation between for the first mitral cell (the first column and first row) up to the 25th mitral cell in the last column at the bottom. Plots with zero response result from Mitral cells which remain silent for this particular input. The time constants of both the ORN and mitral cells were set to $\tilde{\tau}_m \approx 10$ ms, with a threshold potential, $V_{th} = 50000$. The time constants of the excitatory synapses were set to $\tilde{\tau}_E \approx 4$ ms, whereas for the inhibitory synapses the time constants were set to $\tilde{\tau}_I \approx 16$ ms. For the ORNs, constant values randomly selected in a range between 500 and 1000, were used to represent a constant concentration of each odor stimulus. The total running time in terms of biological values is equivalent to 5 seconds at a sampling frequency of $f_{smp} = 10$ KHz. Although the clock frequency was set to $f_{clk} = 10$ MHz thus each run lasted for 5 ms of the FPGA processing time.

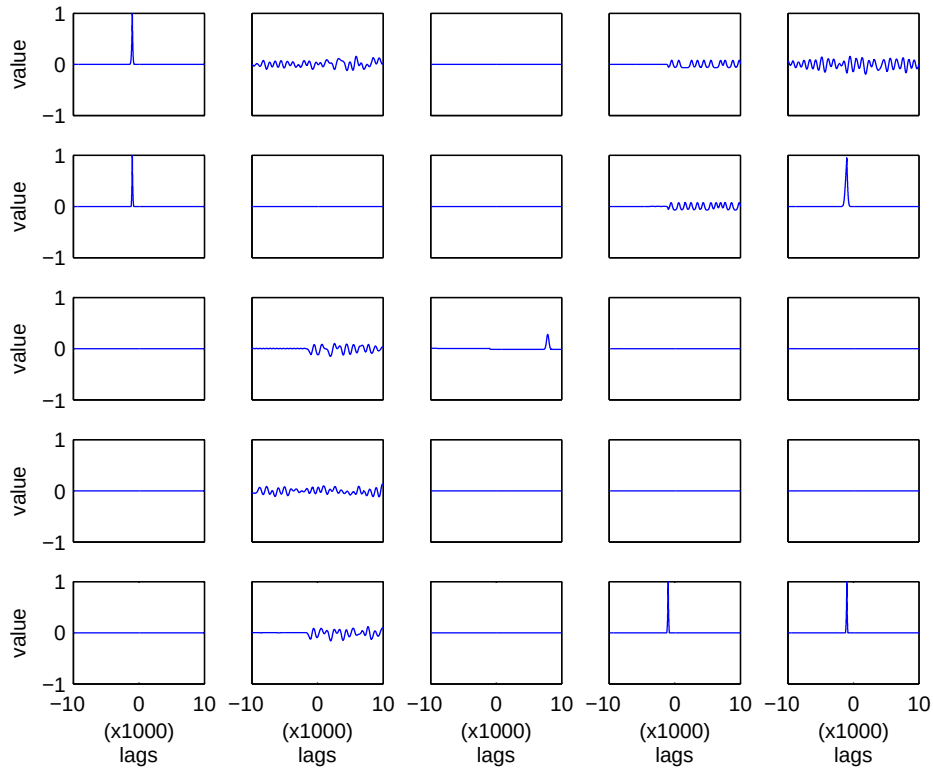

Figure G.3: Cross-correlation analysis for odour 1: trained input vs. -40% difference input. The Cross-correlation analysis was carried out between the response of the olfactory bulb of the trained input and the input minus a percentage of the difference between input value and the limit range for the input. Plots are sorted from left to right and from up to down, starting from the cross-corelation between for the first mitral cell (the first column and first row) up to the 25th mitral cell in the last column at the bottom. Plots with zero response result from Mitral cells which remain silent for this particular input. The time constants of both the ORN and mitral cells were set to $\tilde{\tau}_m \approx 10$ ms, with a threshold potential, $V_{th} = 50000$. The time constants of the excitatory synapses were set to $\tilde{\tau}_E \approx 4$ ms, whereas for the inhibitory synapses the time constants were set to $\tilde{\tau}_I \approx 16$ ms. For the ORNs, constant values randomly selected in a range between 500 and 1000, were used to represent a constant concentration of each odor stimulus. The total running time in terms of biological values is equivalent to 5 seconds at a sampling frequency of $f_{smp} = 10$ KHz. Although the clock frequency was set to $f_{clk} = 10$ MHz thus each run lasted for 5 ms of the FPGA processing time.

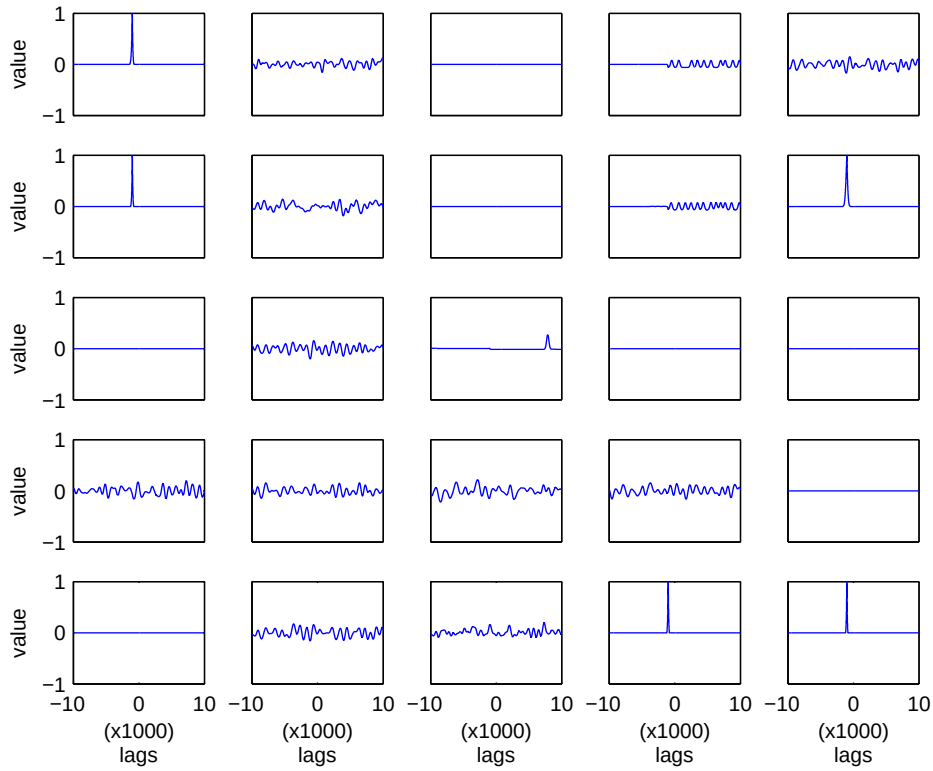

Figure G.4: Cross-correlation analysis for odour 1: trained input vs. -20% difference input. The Cross-correlation analysis was carried out between the response of the olfactory bulb of the trained input and the input minus a percentage of the difference between input value and the limit range for the input. Plots are sorted from left to right and from up to down, starting from the cross-corelation between for the first mitral cell (the first column and first row) up to the 25th mitral cell in the last column at the bottom. Plots with zero response result from Mitral cells which remain silent for this particular input. The time constants of both the ORN and mitral cells were set to $\tilde{\tau}_m \approx 10$ ms, with a threshold potential, $V_{th} = 50000$. The time constants of the excitatory synapses were set to $\tilde{\tau}_E \approx 4$ ms, whereas for the inhibitory synapses the time constants were set to $\tilde{\tau}_I \approx 16$ ms. For the ORNs, constant values randomly selected in a range between 500 and 1000, were used to represent a constant concentration of each odor stimulus. The total running time in terms of biological values is equivalent to 5 seconds at a sampling frequency of $f_{smp} = 10$ KHz. Although the clock frequency was set to $f_{clk} = 10$ MHz thus each run lasted for 5 ms of the FPGA processing time.

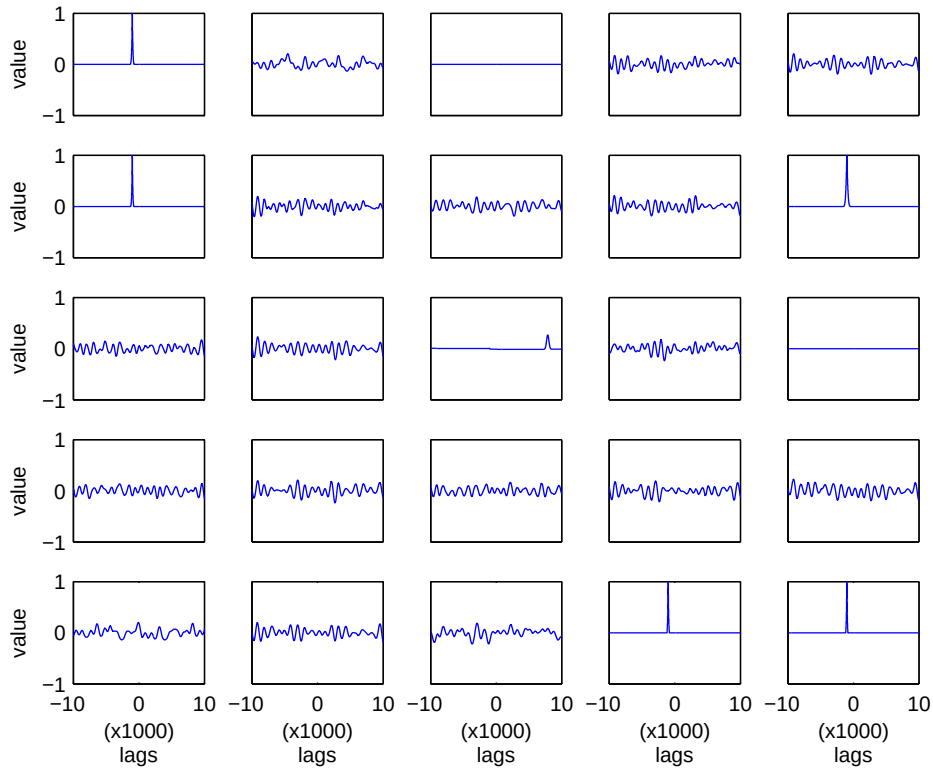

Figure G.5: Cross-correlation analysis for odour 1: trained input vs. -10% difference input. The Cross-correlation analysis was carried out between the response of the olfactory bulb of the trained input and the input minus a percentage of the difference between input value and the limit range for the input. Plots are sorted from left to right and from up to down, starting from the cross-corelation between for the first mitral cell (the first column and first row) up to the 25th mitral cell in the last column at the bottom. Plots with zero response result from Mitral cells which remain silent for this particular input. The time constants of both the ORN and mitral cells were set to $\tilde{\tau}_m \approx 10$ ms, with a threshold potential, $V_{th} = 50000$. The time constants of the excitatory synapses were set to $\tilde{\tau}_E \approx 4$ ms, whereas for the inhibitory synapses the time constants were set to $\tilde{\tau}_I \approx 16$ ms. For the ORNs, constant values randomly selected in a range between 500 and 1000, were used to represent a constant concentration of each odor stimulus. The total running time in terms of biological values is equivalent to 5 seconds at a sampling frequency of $f_{smp} = 10$ KHz. Although the clock frequency was set to $f_{clk} = 10$ MHz thus each run lasted for 5 ms of the FPGA processing time.

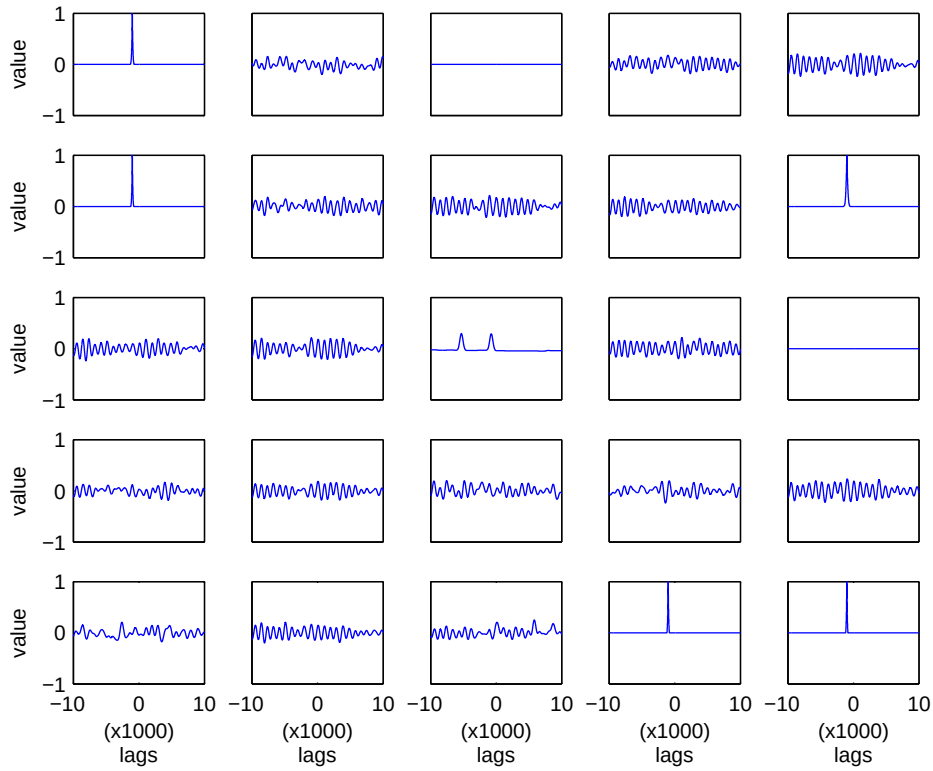

Figure G.6: Cross-correlation analysis for odour 1: trained input vs. -4% difference input. The Cross-correlation analysis was carried out between the response of the olfactory bulb of the trained input and the input minus a percentage of the difference between input value and the limit range for the input. Plots are sorted from left to right and from up to down, starting from the cross-corelation between for the first mitral cell (the first column and first row) up to the 25th mitral cell in the last column at the bottom. Plots with zero response result from Mitral cells which remain silent for this particular input. The time constants of both the ORN and mitral cells were set to $\tilde{\tau}_m \approx 10$ ms, with a threshold potential, $V_{th} = 50000$. The time constants of the excitatory synapses were set to $\tilde{\tau}_E \approx 4$ ms, whereas for the inhibitory synapses the time constants were set to $\tilde{\tau}_I \approx 16$ ms. For the ORNs, constant values randomly selected in a range between 500 and 1000, were used to represent a constant concentration of each odor stimulus. The total running time in terms of biological values is equivalent to 5 seconds at a sampling frequency of $f_{smp} = 10$ KHz. Although the clock frequency was set to $f_{clk} = 10$ MHz thus each run lasted for 5 ms of the FPGA processing time.

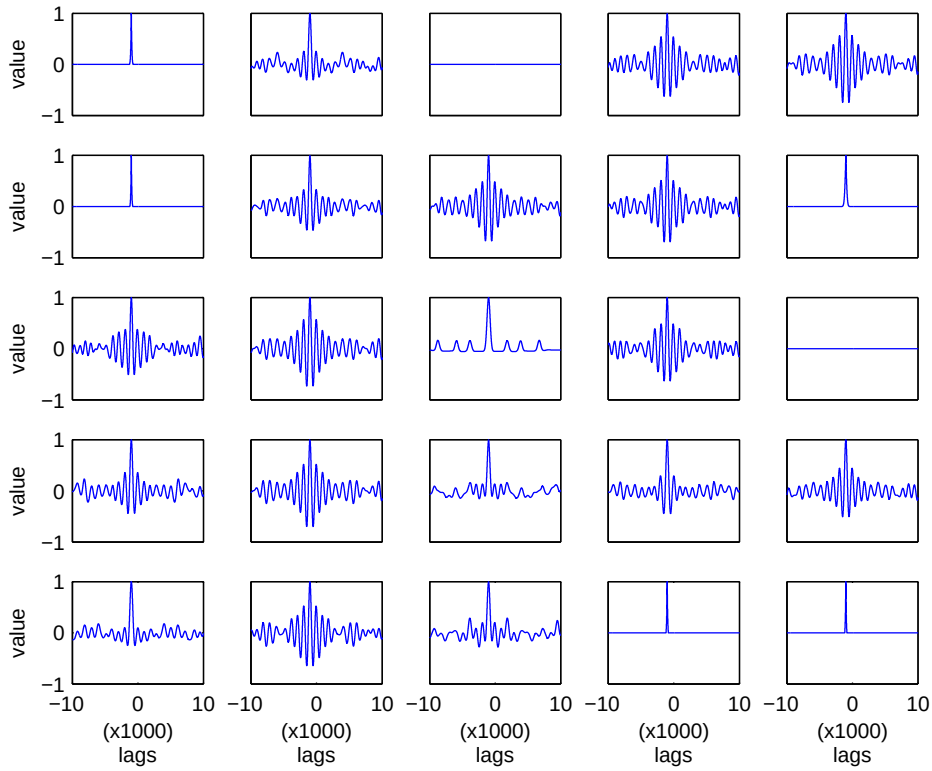

Figure G.7: Cross-correlation analysis for odour 1: trained input vs. 0% difference input. The Cross-correlation analysis was carried out between the response of the olfactory bulb of the trained input and the input minus a percentage of the difference between input value and the limit range for the input. Plots are sorted from left to right and from up to down, starting from the cross-corelation between for the first mitral cell (the first column and first row) up to the 25th mitral cell in the last column at the bottom. Plots with zero response result from Mitral cells which remain silent for this particular input. The time constants of both the ORN and mitral cells were set to $\tilde{\tau}_m \approx 10$ ms, with a threshold potential, $V_{th} = 50000$. The time constants of the excitatory synapses were set to $\tilde{\tau}_E \approx 4$ ms, whereas for the inhibitory synapses the time constants were set to $\tilde{\tau}_I \approx 16$ ms. For the ORNs, constant values randomly selected in a range between 500 and 1000, were used to represent a constant concentration of each odor stimulus. The total running time in terms of biological values is equivalent to 5 seconds at a sampling frequency of $f_{smp} = 10$ KHz. Although the clock frequency was set to $f_{clk} = 10$ MHz thus each run lasted for 5 ms of the FPGA processing time.

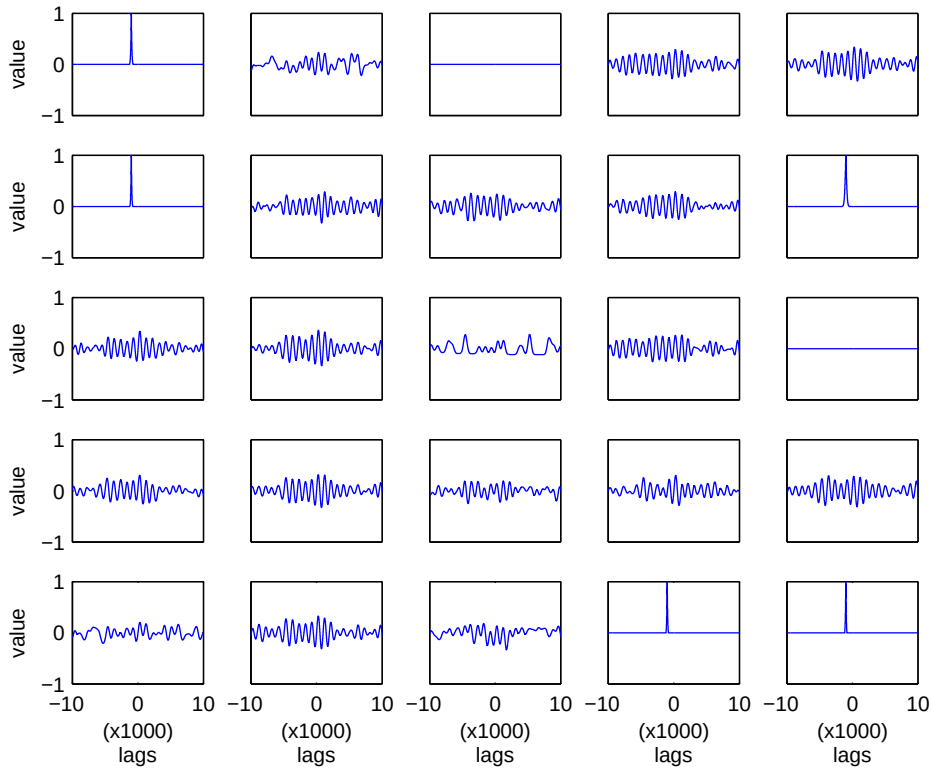

Figure G.8: Cross-correlation analysis for odour 1: trained input vs. +4% difference input. The Cross-correlation analysis was carried out between the response of the olfactory bulb of the trained input and the input minus a percentage of the difference between input value and the limit range for the input. Plots are sorted from left to right and from up to down, starting from the cross-corelation between for the first mitral cell (the first column and first row) up to the 25th mitral cell in the last column at the bottom. Plots with zero response result from Mitral cells which remain silent for this particular input. The time constants of both the ORN and mitral cells were set to $\tilde{\tau}_m \approx 10$ ms, with a threshold potential, $V_{th} = 50000$. The time constants of the excitatory synapses were set to $\tilde{\tau}_E \approx 4$ ms, whereas for the inhibitory synapses the time constants were set to $\tilde{\tau}_I \approx 16$ ms. For the ORNs, constant values randomly selected in a range between 500 and 1000, were used to represent a constant concentration of each odor stimulus. The total running time in terms of biological values is equivalent to 5 seconds at a sampling frequency of $f_{smp} = 10$ KHz. Although the clock frequency was set to $f_{clk} = 10$ MHz thus each run lasted for 5 ms of the FPGA processing time.

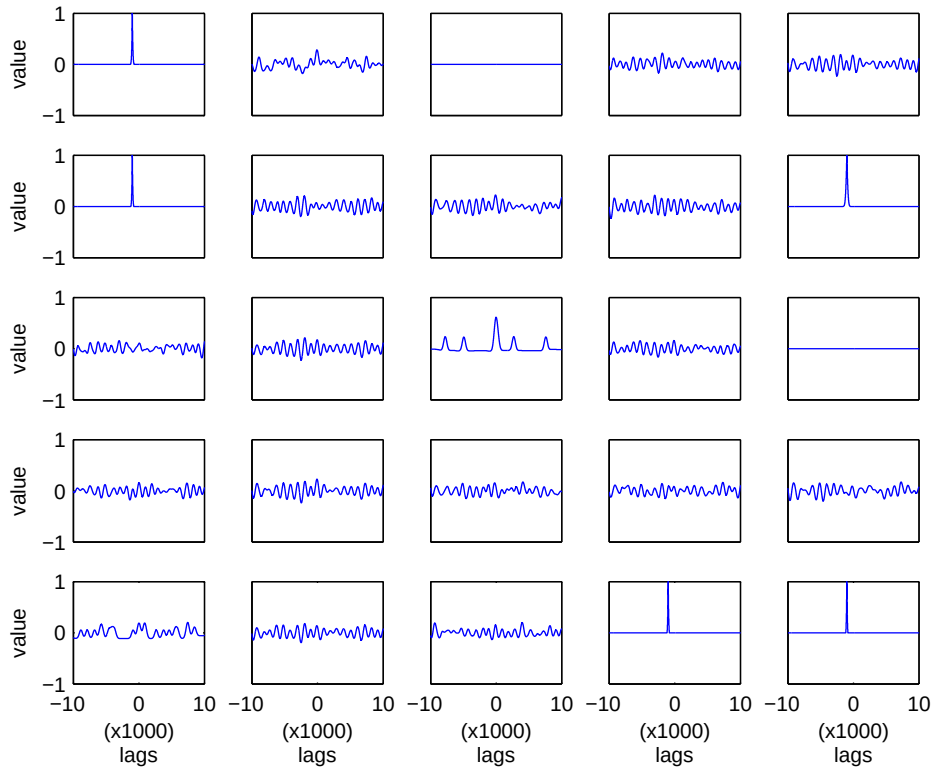

Figure G.9: Cross-correlation analysis for odour 1: trained input vs. +10% difference input. The Cross-correlation analysis was carried out between the response of the olfactory bulb of the trained input and the input minus a percentage of the difference between input value and the limit range for the input. Plots are sorted from left to right and from up to down, starting from the cross-corelation between for the first mitral cell (the first column and first row) up to the 25th mitral cell in the last column at the bottom. Plots with zero response result from Mitral cells which remain silent for this particular input. The time constants of both the ORN and mitral cells were set to $\tilde{\tau}_m \approx 10$ ms, with a threshold potential, $V_{th} = 50000$. The time constants of the excitatory synapses were set to $\tilde{\tau}_E \approx 4$ ms, whereas for the inhibitory synapses the time constants were set to $\tilde{\tau}_I \approx 16$ ms. For the ORNs, constant values randomly selected in a range between 500 and 1000, were used to represent a constant concentration of each odor stimulus. The total running time in terms of biological values is equivalent to 5 seconds at a sampling frequency of $f_{smp} = 10$ KHz. Although the clock frequency was set to $f_{clk} = 10$ MHz thus each run lasted for 5 ms of the FPGA processing time.

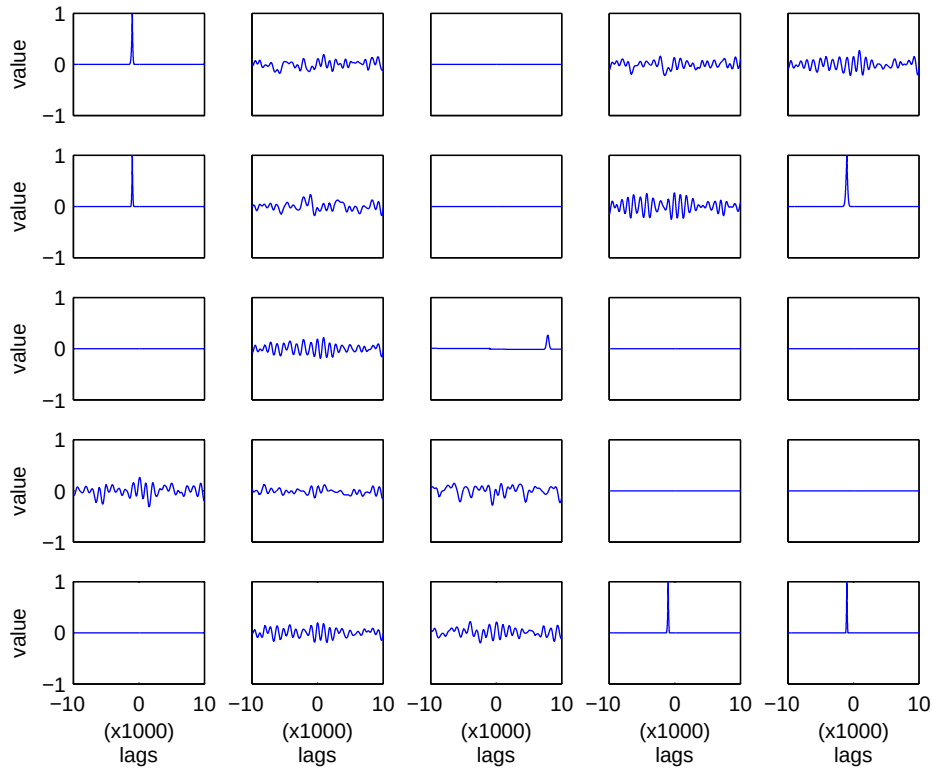

Figure G.10: Cross-correlation analysis for odour 1: trained input vs. +20% difference input. The Cross-correlation analysis was carried out between the response of the olfactory bulb of the trained input and the input minus a percentage of the difference between input value and the limit range for the input. Plots are sorted from left to right and from up to down, starting from the cross-corelation between for the first mitral cell (the first column and first row) up to the 25th mitral cell in the last column at the bottom. Plots with zero response result from Mitral cells which remain silent for this particular input. The time constants of both the ORN and mitral cells were set to $\tilde{\tau}_m \approx 10$ ms, with a threshold potential, $V_{th} = 50000$. The time constants of the excitatory synapses were set to $\tilde{\tau}_E \approx 4$ ms, whereas for the inhibitory synapses the time constants were set to $\tilde{\tau}_I \approx 16$ ms. For the ORNs, constant values randomly selected in a range between 500 and 1000, were used to represent a constant concentration of each odor stimulus. The total running time in terms of biological values is equivalent to 5 seconds at a sampling frequency of $f_{smp} = 10$ KHz. Although the clock frequency was set to $f_{clk} = 10$ MHz thus each run lasted for 5 ms of the FPGA processing time.

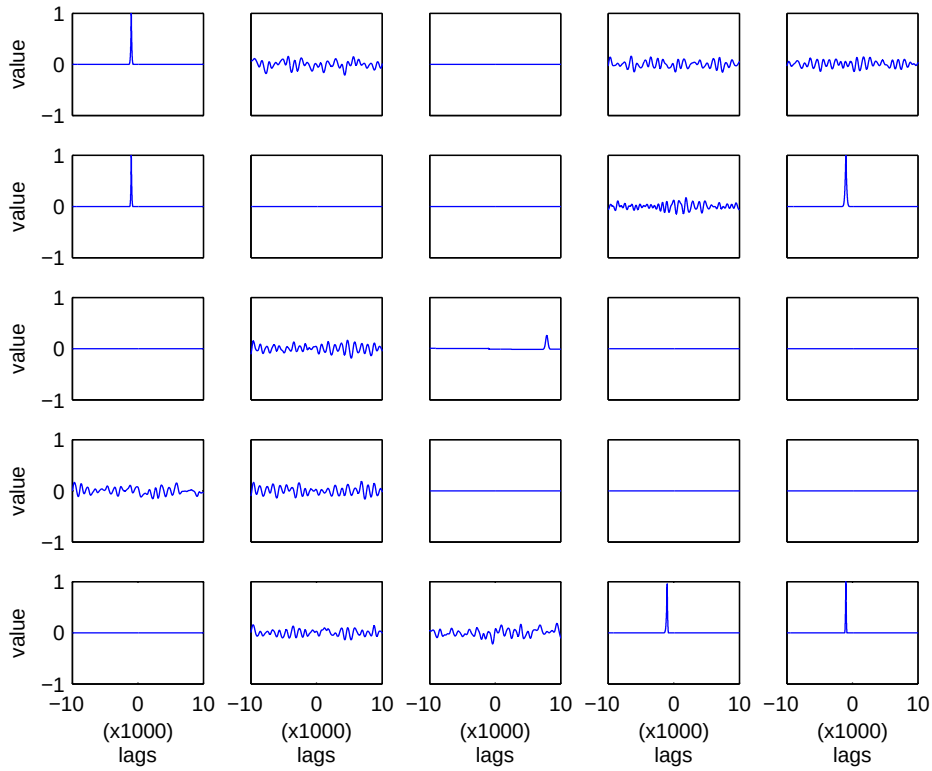

Figure G.11: Cross-correlation analysis for odour 1: trained input vs. +40% difference input. The Cross-correlation analysis was carried out between the response of the olfactory bulb of the trained input and the input minus a percentage of the difference between input value and the limit range for the input. Plots are sorted from left to right and from up to down, starting from the cross-corelation between for the first mitral cell (the first column and first row) up to the 25th mitral cell in the last column at the bottom. Plots with zero response result from Mitral cells which remain silent for this particular input. The time constants of both the ORN and mitral cells were set to $\tilde{\tau}_m \approx 10$ ms, with a threshold potential, $V_{th} = 50000$. The time constants of the excitatory synapses were set to $\tilde{\tau}_E \approx 4$ ms, whereas for the inhibitory synapses the time constants were set to $\tilde{\tau}_I \approx 16$ ms. For the ORNs, constant values randomly selected in a range between 500 and 1000, were used to represent a constant concentration of each odor stimulus. The total running time in terms of biological values is equivalent to 5 seconds at a sampling frequency of $f_{smp} = 10$ KHz. Although the clock frequency was set to $f_{clk} = 10$ MHz thus each run lasted for 5 ms of the FPGA processing time.

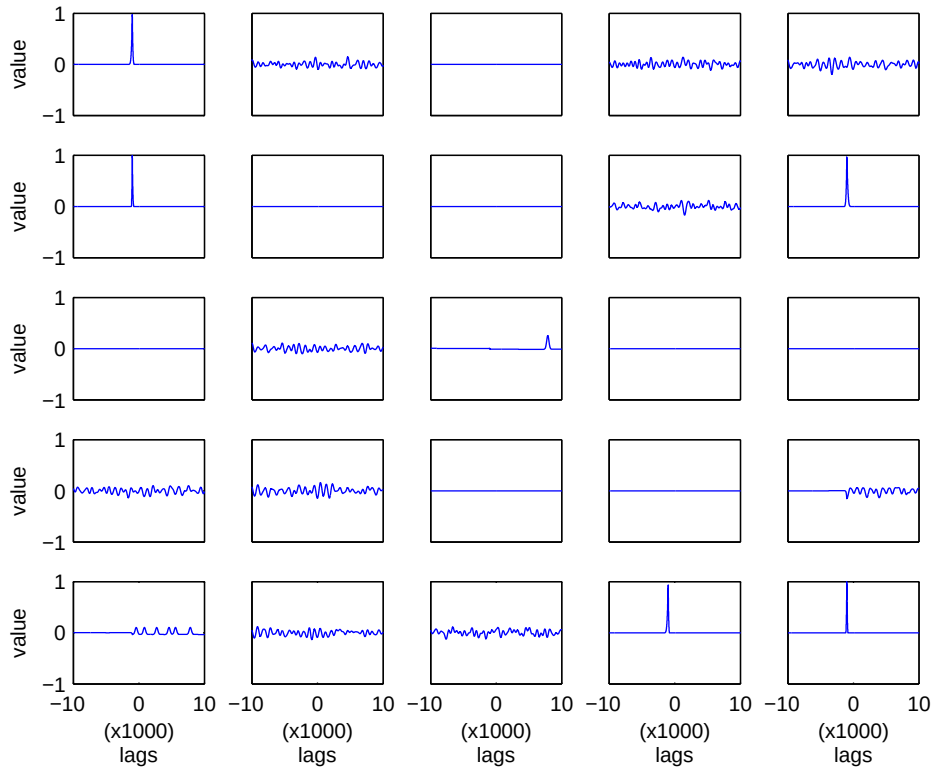

Figure G.12: Cross-correlation analysis for odour 1: trained input vs. +60% difference input. The Cross-correlation analysis was carried out between the response of the olfactory bulb of the trained input and the input minus a percentage of the difference between input value and the limit range for the input. Plots are sorted from left to right and from up to down, starting from the cross-corelation between for the first mitral cell (the first column and first row) up to the 25th mitral cell in the last column at the bottom. Plots with zero response result from Mitral cells which remain silent for this particular input. The time constants of both the ORN and mitral cells were set to $\tilde{\tau}_m \approx 10$ ms, with a threshold potential, $V_{th} = 50000$. The time constants of the excitatory synapses were set to $\tilde{\tau}_E \approx 4$ ms, whereas for the inhibitory synapses the time constants were set to $\tilde{\tau}_I \approx 16$ ms. For the ORNs, constant values randomly selected in a range between 500 and 1000, were used to represent a constant concentration of each odor stimulus. The total running time in terms of biological values is equivalent to 5 seconds at a sampling frequency of $f_{smp} = 10$ KHz. Although the clock frequency was set to $f_{clk} = 10$ MHz thus each run lasted for 5 ms of the FPGA processing time.

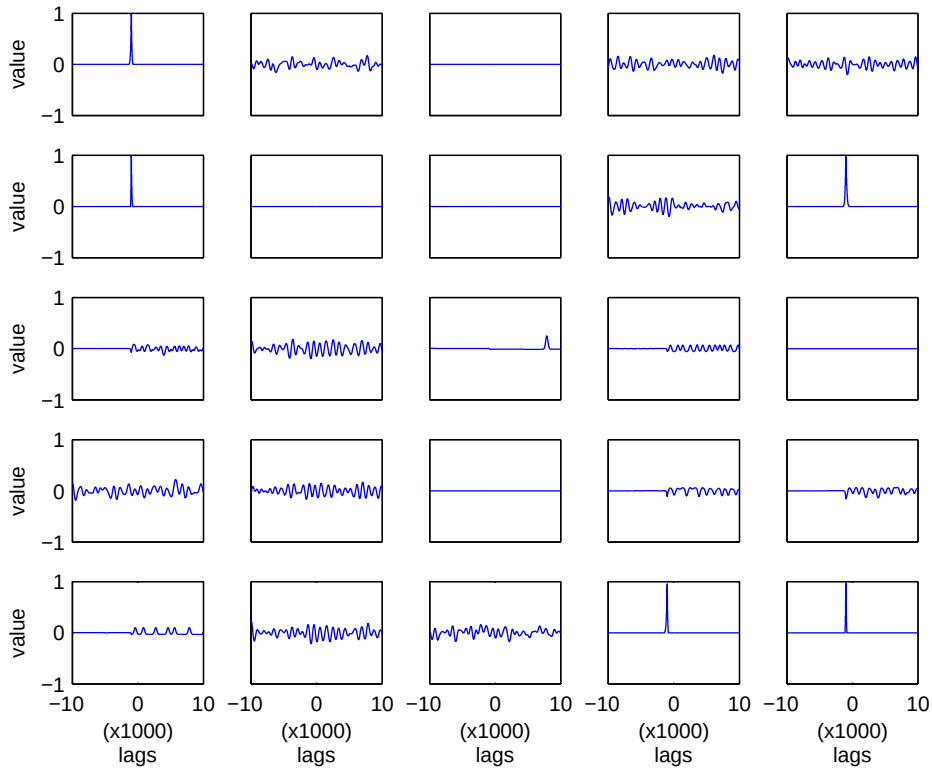

Figure G.13: Cross-correlation analysis for odour 1: trained input vs. +80% difference input. The Cross-correlation analysis was carried out between the response of the olfactory bulb of the trained input and the input minus a percentage of the difference between input value and the limit range for the input. Plots are sorted from left to right and from up to down, starting from the cross-corelation between for the first mitral cell (the first column and first row) up to the 25th mitral cell in the last column at the bottom. Plots with zero response result from Mitral cells which remain silent for this particular input. The time constants of both the ORN and mitral cells were set to $\tilde{\tau}_m \approx 10$ ms, with a threshold potential, $V_{th} = 50000$. The time constants of the excitatory synapses were set to $\tilde{\tau}_E \approx 4$ ms, whereas for the inhibitory synapses the time constants were set to $\tilde{\tau}_I \approx 16$ ms. For the ORNs, constant values randomly selected in a range between 500 and 1000, were used to represent a constant concentration of each odor stimulus. The total running time in terms of biological values is equivalent to 5 seconds at a sampling frequency of $f_{smp} = 10$ KHz. Although the clock frequency was set to $f_{clk} = 10$ MHz thus each run lasted for 5 ms of the FPGA processing time.

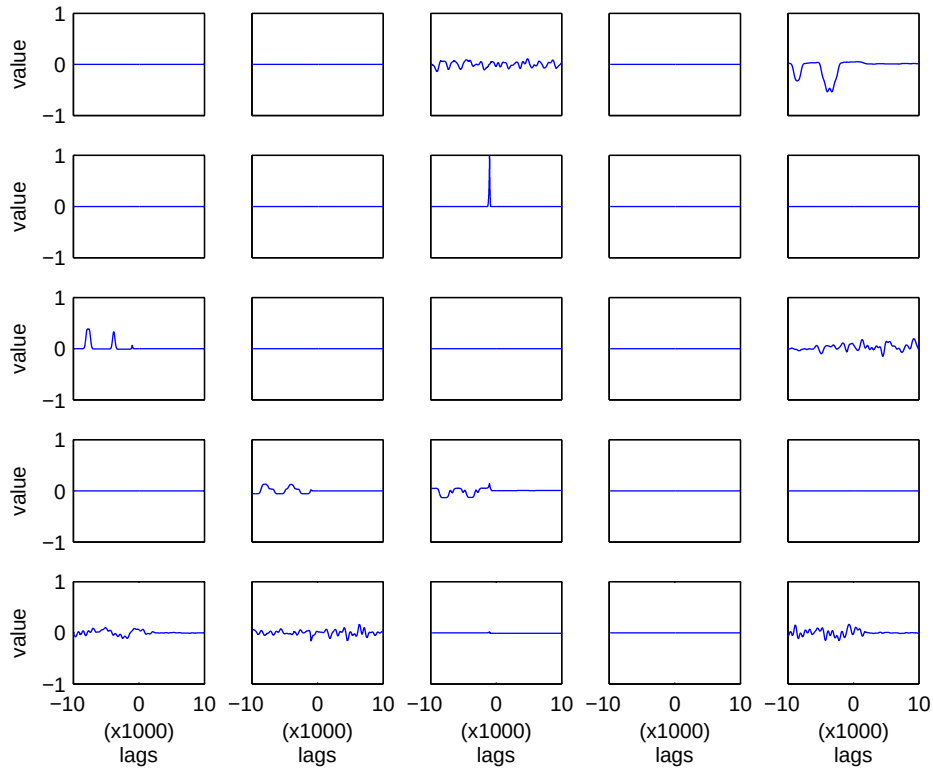

Figure G.14: Cross-correlation analysis for odour 2: trained input vs. -80% difference input. The Cross-correlation analysis was carried out between the response of the olfactory bulb of the trained input and the input minus a percentage of the difference between input value and the limit range for the input. Plots are sorted from left to right and from up to down, starting from the cross-corelation between for the first mitral cell (the first column and first row) up to the 25th mitral cell in the last column at the bottom. Plots with zero response result from Mitral cells which remain silent for this particular input. The time constants of both the ORN and mitral cells were set to $\tilde{\tau}_m \approx 10$ ms, with a threshold potential, $V_{th} = 50000$. The time constants of the excitatory synapses were set to $\tilde{\tau}_E \approx 4$ ms, whereas for the inhibitory synapses the time constants were set to $\tilde{\tau}_I \approx 16$ ms. For the ORNs, constant values randomly selected in a range between 500 and 1000, were used to represent a constant concentration of each odor stimulus. The total running time in terms of biological values is equivalent to 5 seconds at a sampling frequency of $f_{smp} = 10$ KHz. Although the clock frequency was set to $f_{clk} = 10$ MHz thus each run lasted for 5 ms of the FPGA processing time.

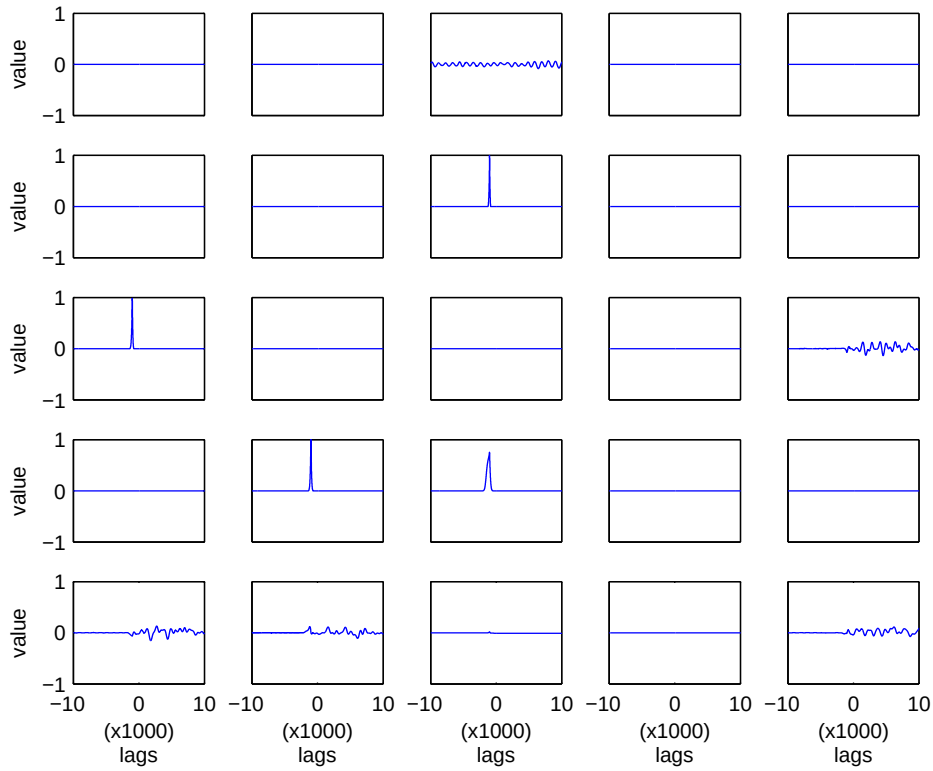

Figure G.15: Cross-correlation analysis for odour 2: trained input vs. -60% difference input. The Cross-correlation analysis was carried out between the response of the olfactory bulb of the trained input and the input minus a percentage of the difference between input value and the limit range for the input. Plots are sorted from left to right and from up to down, starting from the cross-corelation between for the first mitral cell (the first column and first row) up to the 25th mitral cell in the last column at the bottom. Plots with zero response result from Mitral cells which remain silent for this particular input. The time constants of both the ORN and mitral cells were set to $\tilde{\tau}_m \approx 10$ ms, with a threshold potential, $V_{th} = 50000$. The time constants of the excitatory synapses were set to $\tilde{\tau}_E \approx 4$ ms, whereas for the inhibitory synapses the time constants were set to $\tilde{\tau}_I \approx 16$ ms. For the ORNs, constant values randomly selected in a range between 500 and 1000, were used to represent a constant concentration of each odor stimulus. The total running time in terms of biological values is equivalent to 5 seconds at a sampling frequency of $f_{smp} = 10$ KHz. Although the clock frequency was set to $f_{clk} = 10$ MHz thus each run lasted for 5 ms of the FPGA processing time.

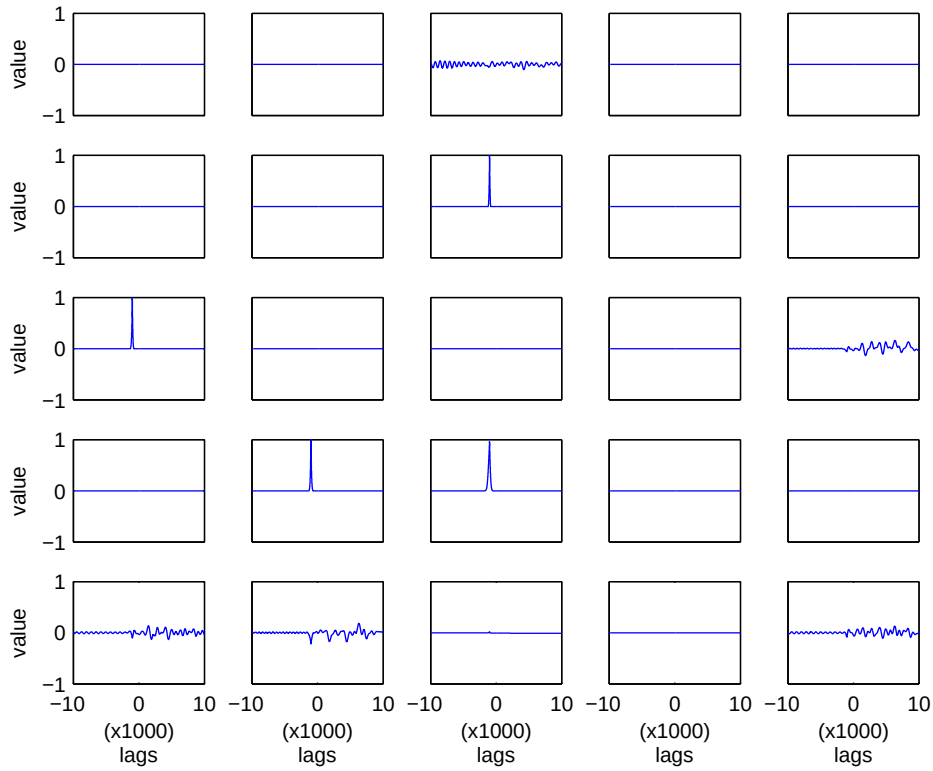

Figure G.16: Cross-correlation analysis for odour 2: trained input vs. -40% difference input. The Cross-correlation analysis was carried out between the response of the olfactory bulb of the trained input and the input minus a percentage of the difference between input value and the limit range for the input. Plots are sorted from left to right and from up to down, starting from the cross-corelation between for the first mitral cell (the first column and first row) up to the 25th mitral cell in the last column at the bottom. Plots with zero response result from Mitral cells which remain silent for this particular input. The time constants of both the ORN and mitral cells were set to $\tilde{\tau}_m \approx 10$ ms, with a threshold potential, $V_{th} = 50000$. The time constants of the excitatory synapses were set to $\tilde{\tau}_E \approx 4$ ms, whereas for the inhibitory synapses the time constants were set to $\tilde{\tau}_I \approx 16$ ms. For the ORNs, constant values randomly selected in a range between 500 and 1000, were used to represent a constant concentration of each odor stimulus. The total running time in terms of biological values is equivalent to 5 seconds at a sampling frequency of $f_{smp} = 10$ KHz. Although the clock frequency was set to $f_{clk} = 10$ MHz thus each run lasted for 5 ms of the FPGA processing time.

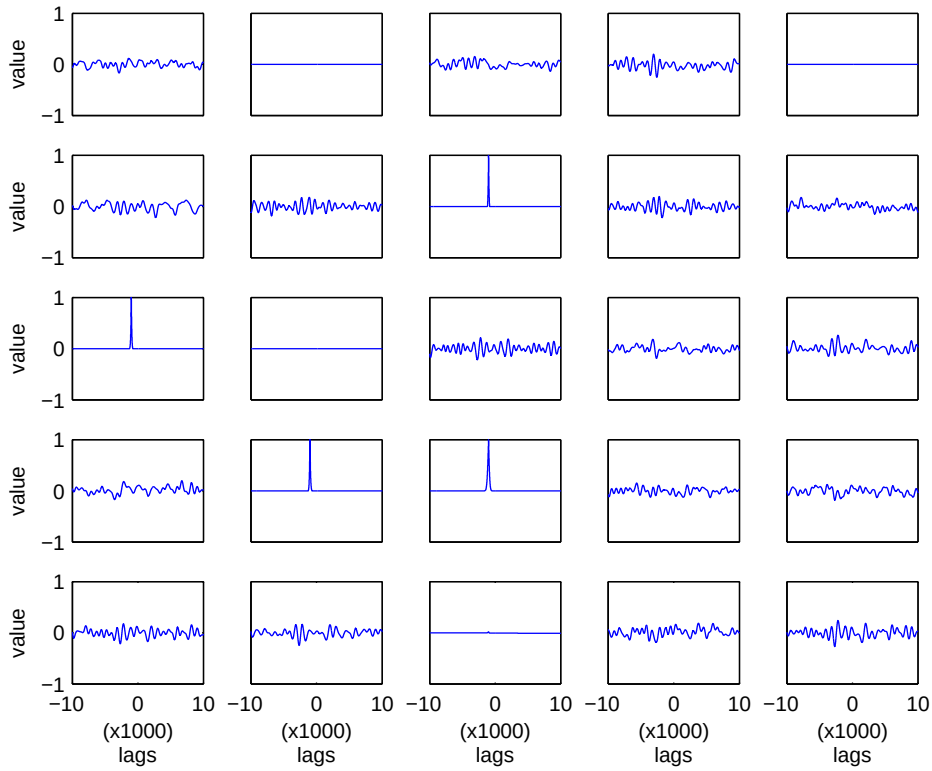

Figure G.17: Cross-correlation analysis for odour 2: trained input vs. -20% difference input. The Cross-correlation analysis was carried out between the response of the olfactory bulb of the trained input and the input minus a percentage of the difference between input value and the limit range for the input. Plots are sorted from left to right and from up to down, starting from the cross-corelation between for the first mitral cell (the first column and first row) up to the 25th mitral cell in the last column at the bottom. Plots with zero response result from Mitral cells which remain silent for this particular input. The time constants of both the ORN and mitral cells were set to $\tilde{\tau}_m \approx 10$ ms, with a threshold potential, $V_{th} = 50000$. The time constants of the excitatory synapses were set to $\tilde{\tau}_E \approx 4$ ms, whereas for the inhibitory synapses the time constants were set to $\tilde{\tau}_I \approx 16$ ms. For the ORNs, constant values randomly selected in a range between 500 and 1000, were used to represent a constant concentration of each odor stimulus. The total running time in terms of biological values is equivalent to 5 seconds at a sampling frequency of $f_{smp} = 10$ KHz. Although the clock frequency was set to $f_{clk} = 10$ MHz thus each run lasted for 5 ms of the FPGA processing time.

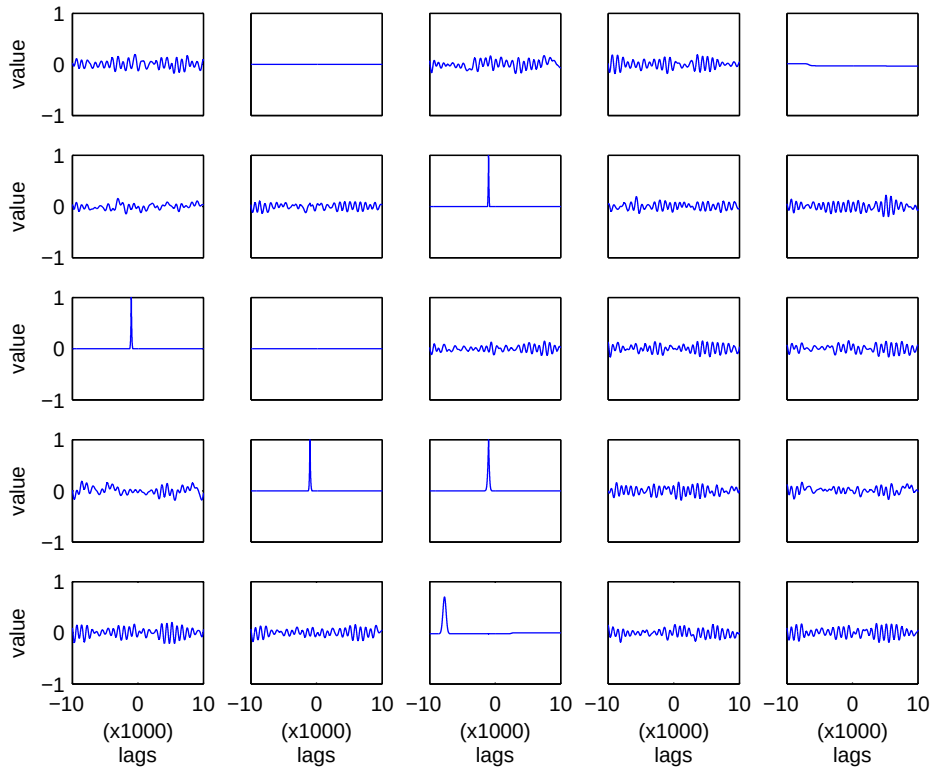

Figure G.18: Cross-correlation analysis for odour 2: trained input vs. -10% difference input. The Cross-correlation analysis was carried out between the response of the olfactory bulb of the trained input and the input minus a percentage of the difference between input value and the limit range for the input. Plots are sorted from left to right and from up to down, starting from the cross-corelation between for the first mitral cell (the first column and first row) up to the 25th mitral cell in the last column at the bottom. Plots with zero response result from Mitral cells which remain silent for this particular input. The time constants of both the ORN and mitral cells were set to $\tilde{\tau}_m \approx 10$ ms, with a threshold potential, $V_{th} = 50000$. The time constants of the excitatory synapses were set to $\tilde{\tau}_E \approx 4$ ms, whereas for the inhibitory synapses the time constants were set to $\tilde{\tau}_I \approx 16$ ms. For the ORNs, constant values randomly selected in a range between 500 and 1000, were used to represent a constant concentration of each odor stimulus. The total running time in terms of biological values is equivalent to 5 seconds at a sampling frequency of $f_{smp} = 10$ KHz. Although the clock frequency was set to $f_{clk} = 10$ MHz thus each run lasted for 5 ms of the FPGA processing time.

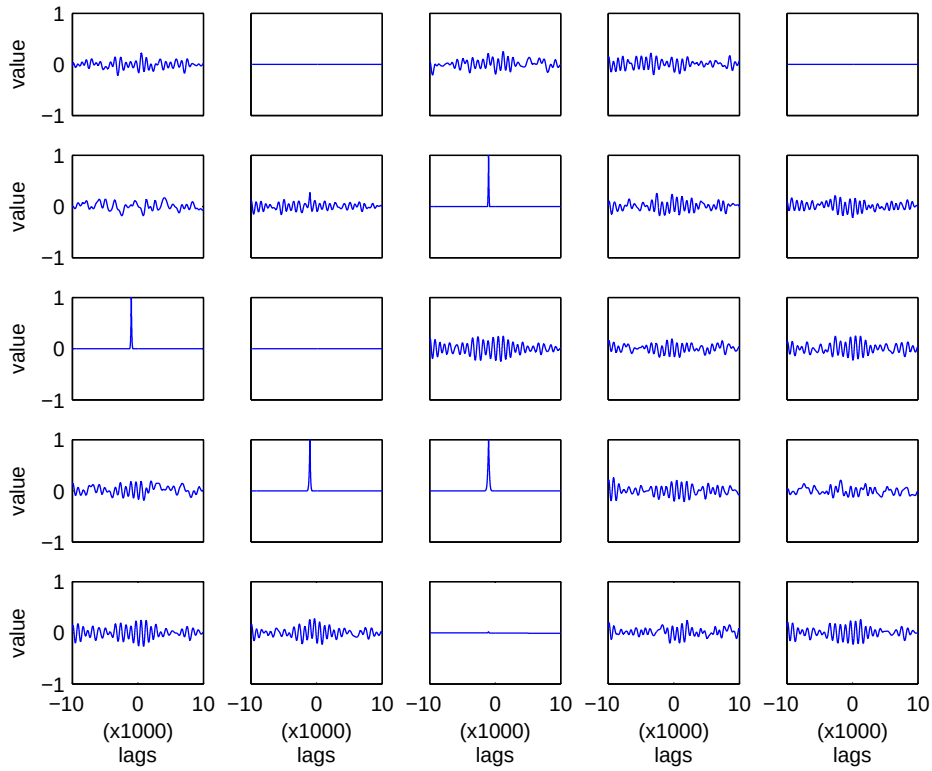

Figure G.19: Cross-correlation analysis for odour 2: trained input vs. -4% difference input. The Cross-correlation analysis was carried out between the response of the olfactory bulb of the trained input and the input minus a percentage of the difference between input value and the limit range for the input. Plots are sorted from left to right and from up to down, starting from the cross-corelation between for the first mitral cell (the first column and first row) up to the 25th mitral cell in the last column at the bottom. Plots with zero response result from Mitral cells which remain silent for this particular input. The time constants of both the ORN and mitral cells were set to $\tilde{\tau}_m \approx 10$ ms, with a threshold potential, $V_{th} = 50000$. The time constants of the excitatory synapses were set to $\tilde{\tau}_E \approx 4$ ms, whereas for the inhibitory synapses the time constants were set to $\tilde{\tau}_I \approx 16$ ms. For the ORNs, constant values randomly selected in a range between 500 and 1000, were used to represent a constant concentration of each odor stimulus. The total running time in terms of biological values is equivalent to 5 seconds at a sampling frequency of $f_{smp} = 10$ KHz. Although the clock frequency was set to $f_{clk} = 10$ MHz thus each run lasted for 5 ms of the FPGA processing time.

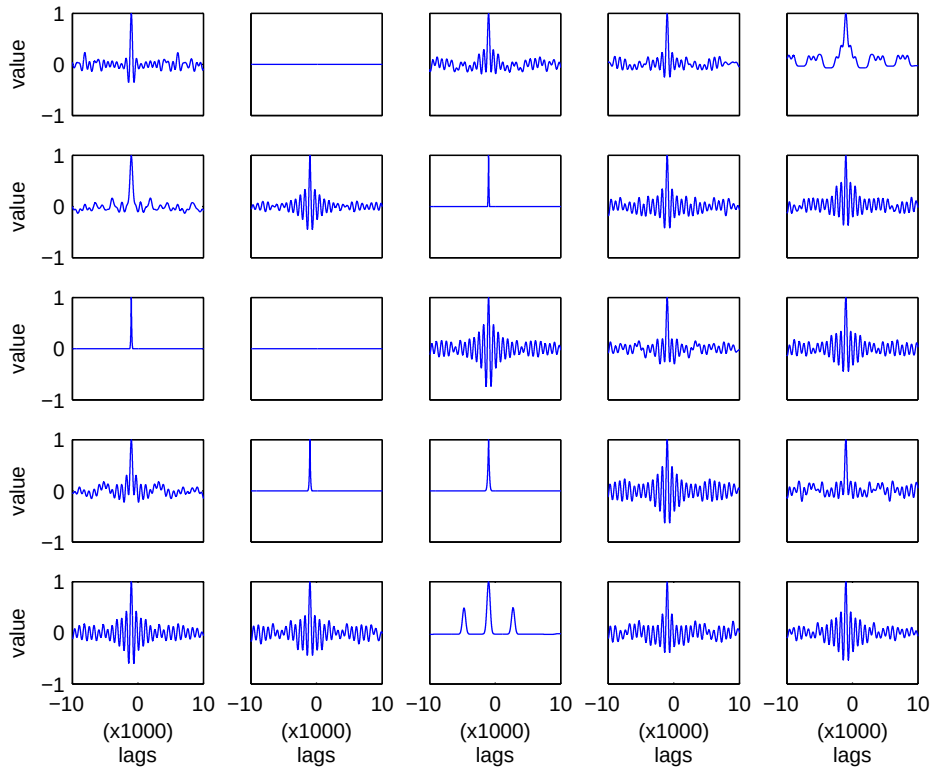

Figure G.20: Cross-correlation analysis for odour 2: trained input vs. 0% difference input. The Cross-correlation analysis was carried out between the response of the olfactory bulb of the trained input and the input minus a percentage of the difference between input value and the limit range for the input. Plots are sorted from left to right and from up to down, starting from the cross-corelation between for the first mitral cell (the first column and first row) up to the 25th mitral cell in the last column at the bottom. Plots with zero response result from Mitral cells which remain silent for this particular input. The time constants of both the ORN and mitral cells were set to $\tilde{\tau}_m \approx 10$ ms, with a threshold potential, $V_{th} = 50000$. The time constants of the excitatory synapses were set to $\tilde{\tau}_E \approx 4$ ms, whereas for the inhibitory synapses the time constants were set to $\tilde{\tau}_I \approx 16$ ms. For the ORNs, constant values randomly selected in a range between 500 and 1000, were used to represent a constant concentration of each odor stimulus. The total running time in terms of biological values is equivalent to 5 seconds at a sampling frequency of $f_{smp} = 10$ KHz. Although the clock frequency was set to $f_{clk} = 10$ MHz thus each run lasted for 5 ms of the FPGA processing time.

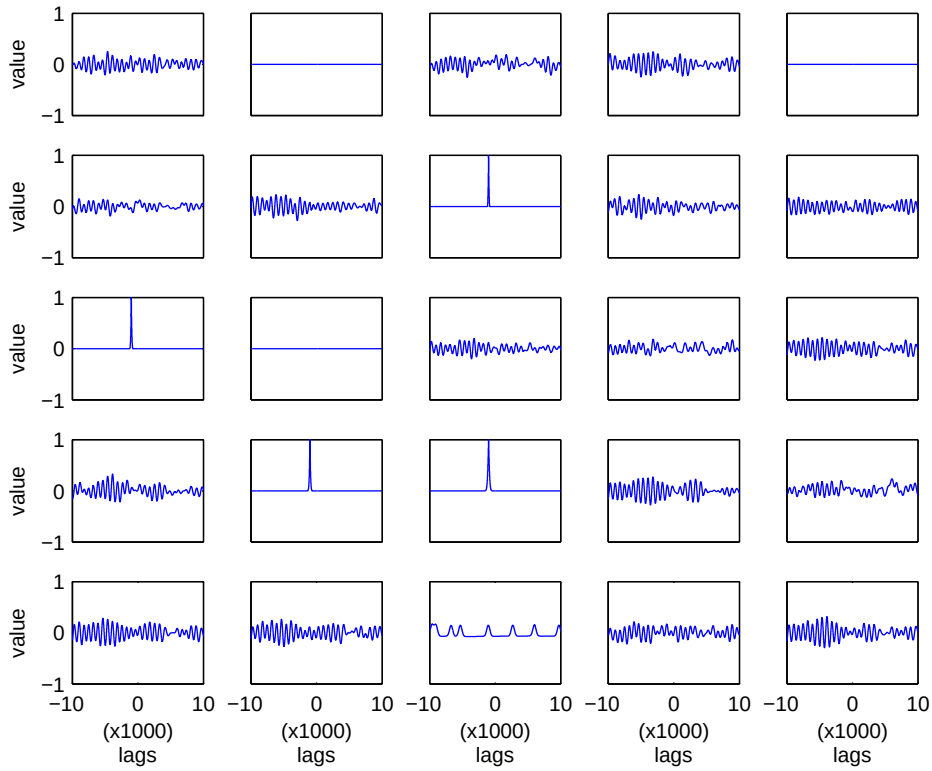

Figure G.21: Cross-correlation analysis for odour 2: trained input vs. +4% difference input. The Cross-correlation analysis was carried out between the response of the olfactory bulb of the trained input and the input minus a percentage of the difference between input value and the limit range for the input. Plots are sorted from left to right and from up to down, starting from the cross-corelation between for the first mitral cell (the first column and first row) up to the 25th mitral cell in the last column at the bottom. Plots with zero response result from Mitral cells which remain silent for this particular input. The time constants of both the ORN and mitral cells were set to $\tilde{\tau}_m \approx 10$ ms, with a threshold potential, $V_{th} = 50000$. The time constants of the excitatory synapses were set to $\tilde{\tau}_E \approx 4$ ms, whereas for the inhibitory synapses the time constants were set to $\tilde{\tau}_I \approx 16$ ms. For the ORNs, constant values randomly selected in a range between 500 and 1000, were used to represent a constant concentration of each odor stimulus. The total running time in terms of biological values is equivalent to 5 seconds at a sampling frequency of $f_{smp} = 10$ KHz. Although the clock frequency was set to $f_{clk} = 10$ MHz thus each run lasted for 5 ms of the FPGA processing time.

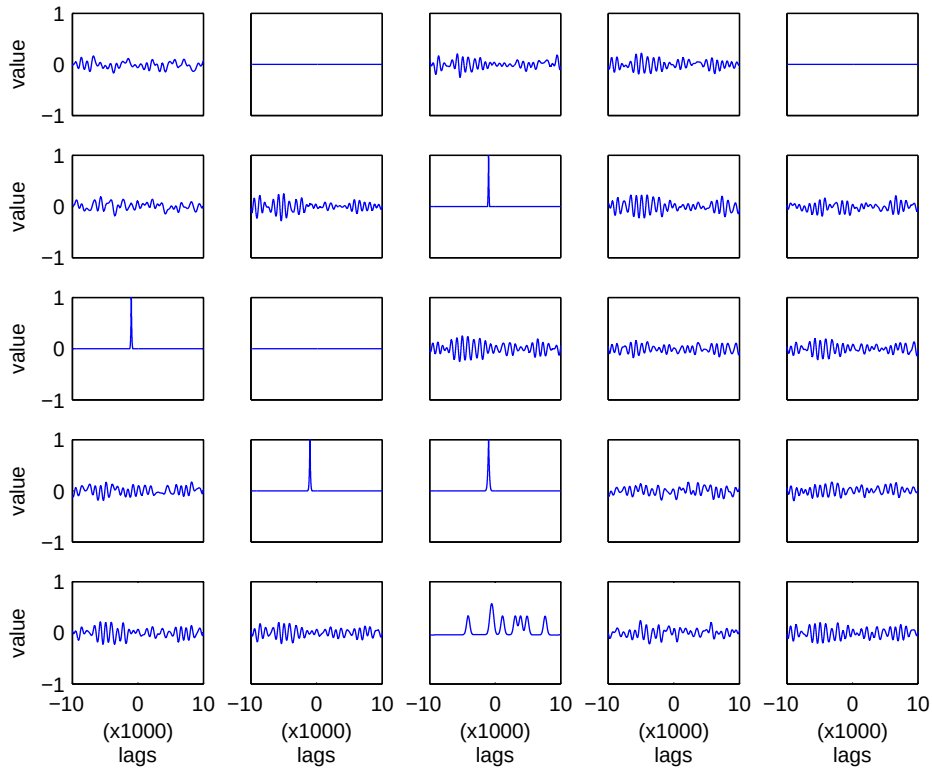

Figure G.22: Cross-correlation analysis for odour 2: trained input vs. +10% difference input. The Cross-correlation analysis was carried out between the response of the olfactory bulb of the trained input and the input minus a percentage of the difference between input value and the limit range for the input. Plots are sorted from left to right and from up to down, starting from the cross-corelation between for the first mitral cell (the first column and first row) up to the 25th mitral cell in the last column at the bottom. Plots with zero response result from Mitral cells which remain silent for this particular input. The time constants of both the ORN and mitral cells were set to $\tilde{\tau}_m \approx 10$ ms, with a threshold potential, $V_{th} = 50000$. The time constants of the excitatory synapses were set to $\tilde{\tau}_E \approx 4$ ms, whereas for the inhibitory synapses the time constants were set to $\tilde{\tau}_I \approx 16$ ms. For the ORNs, constant values randomly selected in a range between 500 and 1000, were used to represent a constant concentration of each odor stimulus. The total running time in terms of biological values is equivalent to 5 seconds at a sampling frequency of $f_{smp} = 10$ KHz. Although the clock frequency was set to $f_{clk} = 10$ MHz thus each run lasted for 5 ms of the FPGA processing time.

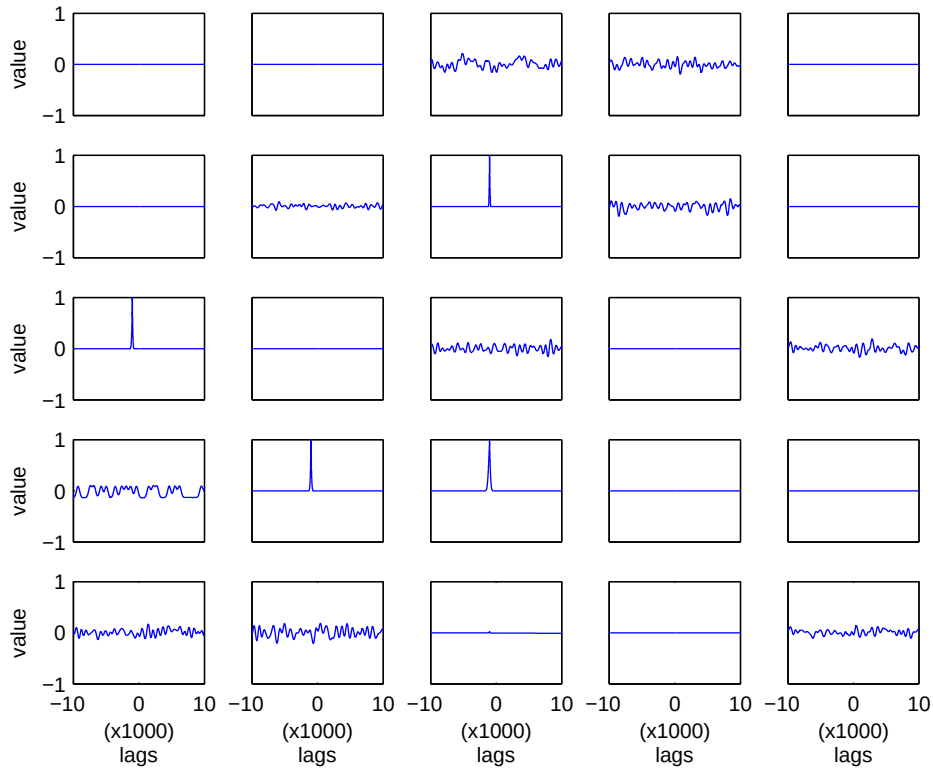

Figure G.23: Cross-correlation analysis for odour 2: trained input vs. +20% difference input. The Cross-correlation analysis was carried out between the response of the olfactory bulb of the trained input and the input minus a percentage of the difference between input value and the limit range for the input. Plots are sorted from left to right and from up to down, starting from the cross-corelation between for the first mitral cell (the first column and first row) up to the 25th mitral cell in the last column at the bottom. Plots with zero response result from Mitral cells which remain silent for this particular input. The time constants of both the ORN and mitral cells were set to $\tilde{\tau}_m \approx 10$ ms, with a threshold potential, $V_{th} = 50000$. The time constants of the excitatory synapses were set to $\tilde{\tau}_E \approx 4$ ms, whereas for the inhibitory synapses the time constants were set to $\tilde{\tau}_I \approx 16$ ms. For the ORNs, constant values randomly selected in a range between 500 and 1000, were used to represent a constant concentration of each odor stimulus. The total running time in terms of biological values is equivalent to 5 seconds at a sampling frequency of $f_{smp} = 10$ KHz. Although the clock frequency was set to $f_{clk} = 10$ MHz thus each run lasted for 5 ms of the FPGA processing time.

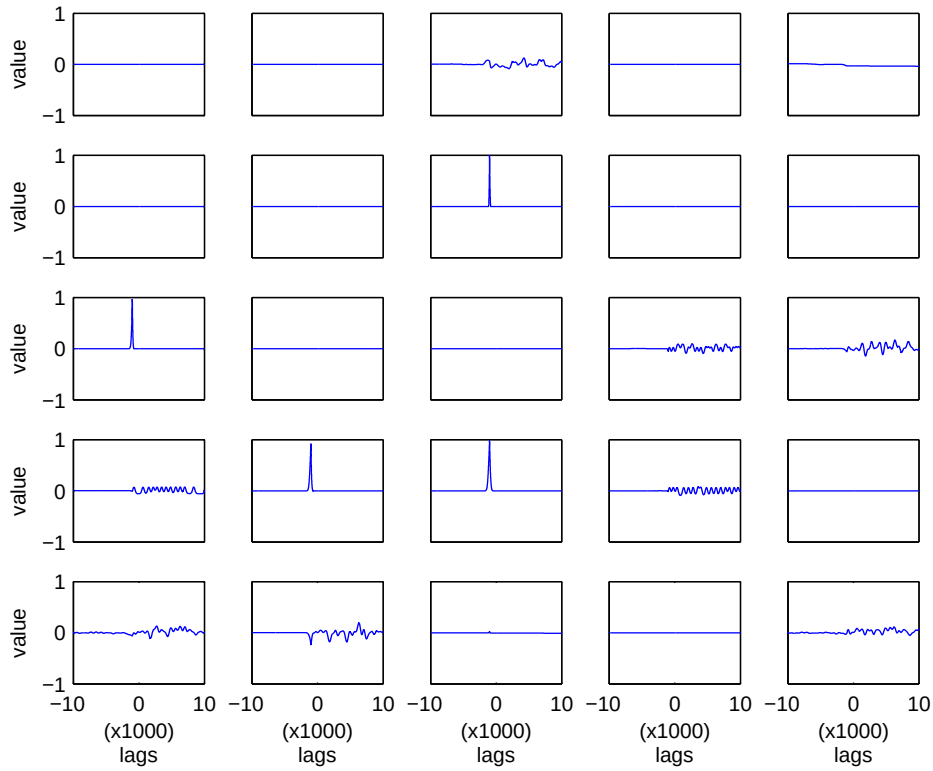

Figure G.24: Cross-correlation analysis for odour 2: trained input vs. +40% difference input. The Cross-correlation analysis was carried out between the response of the olfactory bulb of the trained input and the input minus a percentage of the difference between input value and the limit range for the input. Plots are sorted from left to right and from up to down, starting from the cross-corelation between for the first mitral cell (the first column and first row) up to the 25th mitral cell in the last column at the bottom. Plots with zero response result from Mitral cells which remain silent for this particular input. The time constants of both the ORN and mitral cells were set to $\tilde{\tau}_m \approx 10$ ms, with a threshold potential, $V_{th} = 50000$. The time constants of the excitatory synapses were set to $\tilde{\tau}_E \approx 4$ ms, whereas for the inhibitory synapses the time constants were set to $\tilde{\tau}_I \approx 16$ ms. For the ORNs, constant values randomly selected in a range between 500 and 1000, were used to represent a constant concentration of each odor stimulus. The total running time in terms of biological values is equivalent to 5 seconds at a sampling frequency of $f_{smp} = 10$ KHz. Although the clock frequency was set to $f_{clk} = 10$ MHz thus each run lasted for 5 ms of the FPGA processing time.

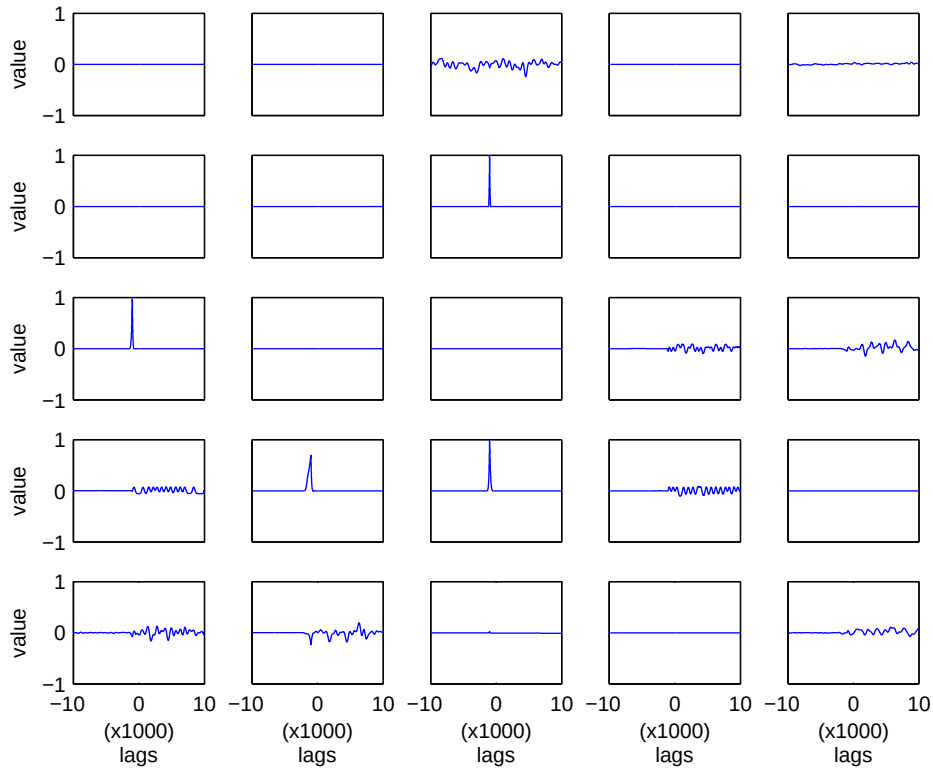

Figure G.25: Cross-correlation analysis for odour 2: trained input vs. +60% difference input. The Cross-correlation analysis was carried out between the response of the olfactory bulb of the trained input and the input minus a percentage of the difference between input value and the limit range for the input. Plots are sorted from left to right and from up to down, starting from the cross-corelation between for the first mitral cell (the first column and first row) up to the 25th mitral cell in the last column at the bottom. Plots with zero response result from Mitral cells which remain silent for this particular input. The time constants of both the ORN and mitral cells were set to $\tilde{\tau}_m \approx 10$ ms, with a threshold potential, $V_{th} = 50000$. The time constants of the excitatory synapses were set to $\tilde{\tau}_E \approx 4$ ms, whereas for the inhibitory synapses the time constants were set to $\tilde{\tau}_I \approx 16$ ms. For the ORNs, constant values randomly selected in a range between 500 and 1000, were used to represent a constant concentration of each odor stimulus. The total running time in terms of biological values is equivalent to 5 seconds at a sampling frequency of $f_{smp} = 10$ KHz. Although the clock frequency was set to $f_{clk} = 10$ MHz thus each run lasted for 5 ms of the FPGA processing time.

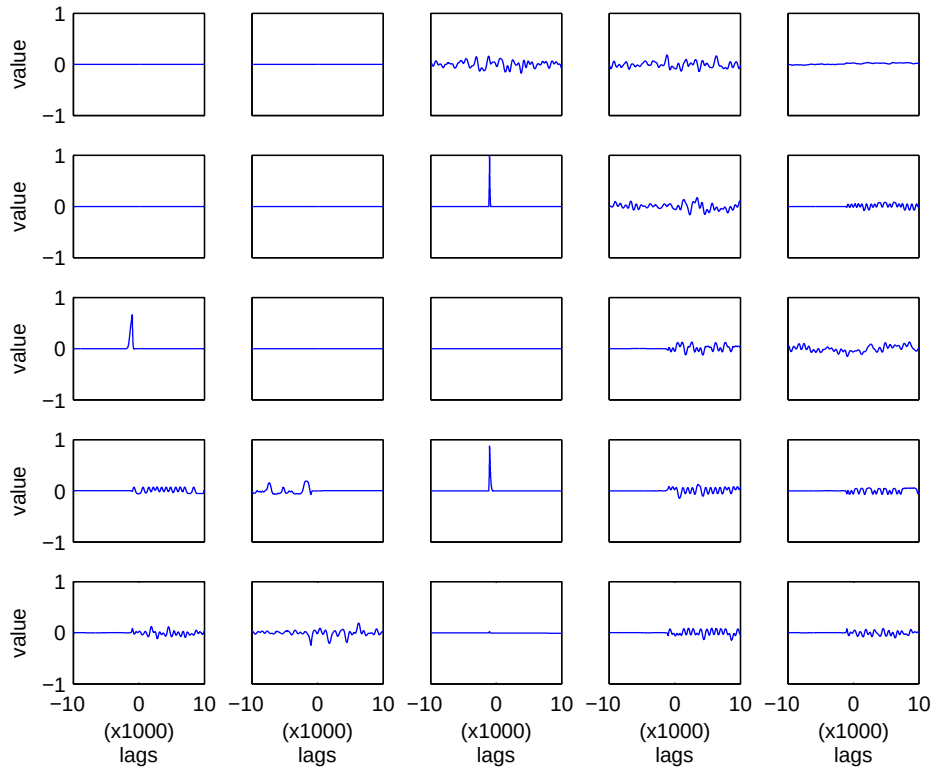

Figure G.26: Cross-correlation analysis for odour 2: trained input vs. +80% difference input. The Cross-correlation analysis was carried out between the response of the olfactory bulb of the trained input and the input minus a percentage of the difference between input value and the limit range for the input. Plots are sorted from left to right and from up to down, starting from the cross-corelation between for the first mitral cell (the first column and first row) up to the 25th mitral cell in the last column at the bottom. Plots with zero response result from Mitral cells which remain silent for this particular input. The time constants of both the ORN and mitral cells were set to $\tilde{\tau}_m \approx 10$ ms, with a threshold potential, $V_{th} = 50000$. The time constants of the excitatory synapses were set to $\tilde{\tau}_E \approx 4$ ms, whereas for the inhibitory synapses the time constants were set to $\tilde{\tau}_I \approx 16$ ms. For the ORNs, constant values randomly selected in a range between 500 and 1000, were used to represent a constant concentration of each odor stimulus. The total running time in terms of biological values is equivalent to 5 seconds at a sampling frequency of $f_{smp} = 10$ KHz. Although the clock frequency was set to $f_{clk} = 10$ MHz thus each run lasted for 5 ms of the FPGA processing time.

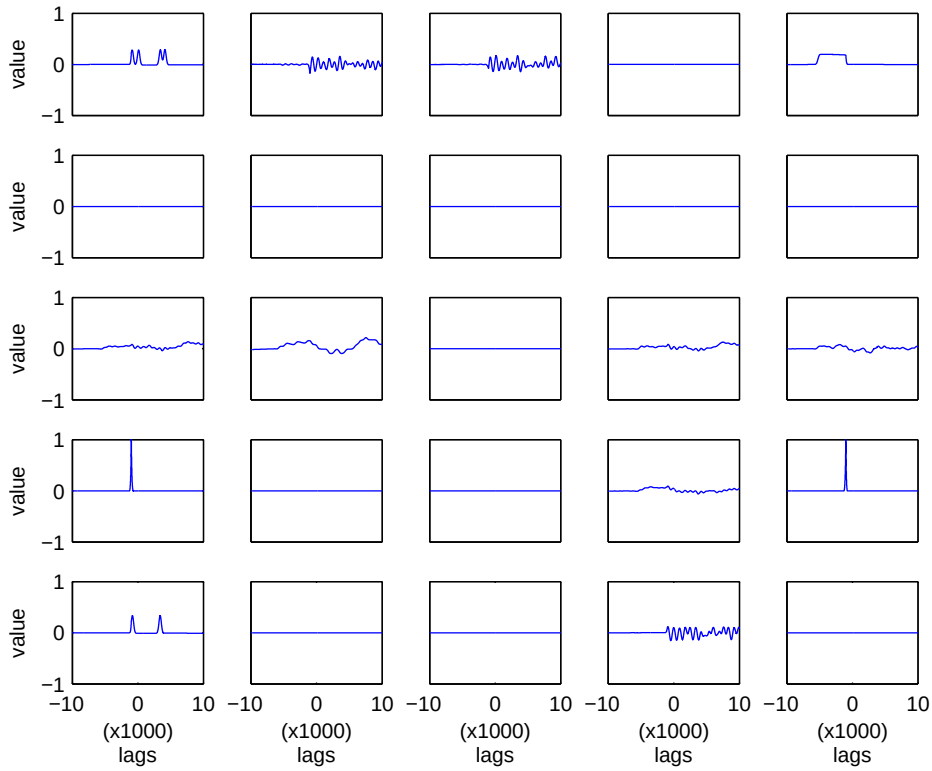

Figure G.27: Cross-correlation analysis for odour 3: trained input vs. -80% difference input. The Cross-correlation analysis was carried out between the response of the olfactory bulb of the trained input and the input minus a percentage of the difference between input value and the limit range for the input. Plots are sorted from left to right and from up to down, starting from the cross-corelation between for the first mitral cell (the first column and first row) up to the 25th mitral cell in the last column at the bottom. Plots with zero response result from Mitral cells which remain silent for this particular input. The time constants of both the ORN and mitral cells were set to $\tilde{\tau}_m \approx 10$ ms, with a threshold potential, $V_{th} = 50000$. The time constants of the excitatory synapses were set to $\tilde{\tau}_E \approx 4$ ms, whereas for the inhibitory synapses the time constants were set to $\tilde{\tau}_I \approx 16$ ms. For the ORNs, constant values randomly selected in a range between 500 and 1000, were used to represent a constant concentration of each odor stimulus. The total running time in terms of biological values is equivalent to 5 seconds at a sampling frequency of $f_{smp} = 10$ KHz. Although the clock frequency was set to $f_{clk} = 10$ MHz thus each run lasted for 5 ms of the FPGA processing time.

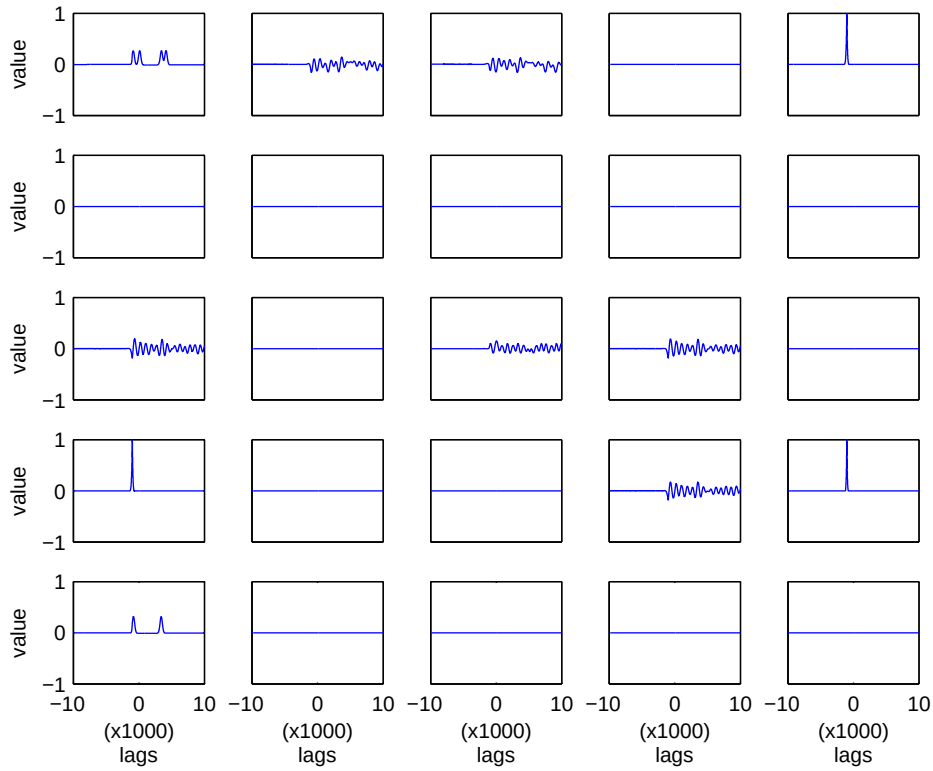

Figure G.28: Cross-correlation analysis for odour 3: trained input vs. -60% difference input. The Cross-correlation analysis was carried out between the response of the olfactory bulb of the trained input and the input minus a percentage of the difference between input value and the limit range for the input. Plots are sorted from left to right and from up to down, starting from the cross-corelation between for the first mitral cell (the first column and first row) up to the 25th mitral cell in the last column at the bottom. Plots with zero response result from Mitral cells which remain silent for this particular input. The time constants of both the ORN and mitral cells were set to $\tilde{\tau}_m \approx 10$ ms, with a threshold potential, $V_{th} = 50000$. The time constants of the excitatory synapses were set to $\tilde{\tau}_E \approx 4$ ms, whereas for the inhibitory synapses the time constants were set to $\tilde{\tau}_I \approx 16$ ms. For the ORNs, constant values randomly selected in a range between 500 and 1000, were used to represent a constant concentration of each odor stimulus. The total running time in terms of biological values is equivalent to 5 seconds at a sampling frequency of $f_{smp} = 10$ KHz. Although the clock frequency was set to $f_{clk} = 10$ MHz thus each run lasted for 5 ms of the FPGA processing time.

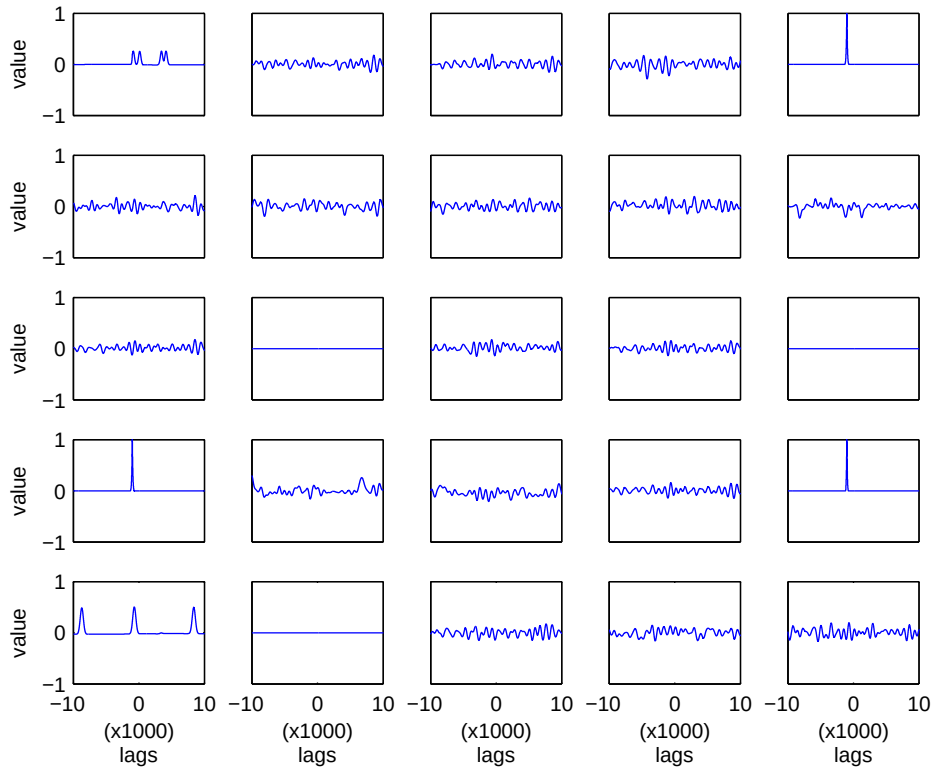

Figure G.29: Cross-correlation analysis for odour 3: trained input vs. -40% difference input. The Cross-correlation analysis was carried out between the response of the olfactory bulb of the trained input and the input minus a percentage of the difference between input value and the limit range for the input. Plots are sorted from left to right and from up to down, starting from the cross-corelation between for the first mitral cell (the first column and first row) up to the 25th mitral cell in the last column at the bottom. Plots with zero response result from Mitral cells which remain silent for this particular input. The time constants of both the ORN and mitral cells were set to $\tilde{\tau}_m \approx 10$ ms, with a threshold potential, $V_{th} = 50000$. The time constants of the excitatory synapses were set to $\tilde{\tau}_E \approx 4$ ms, whereas for the inhibitory synapses the time constants were set to $\tilde{\tau}_I \approx 16$ ms. For the ORNs, constant values randomly selected in a range between 500 and 1000, were used to represent a constant concentration of each odor stimulus. The total running time in terms of biological values is equivalent to 5 seconds at a sampling frequency of $f_{smp} = 10$ KHz. Although the clock frequency was set to $f_{clk} = 10$ MHz thus each run lasted for 5 ms of the FPGA processing time.

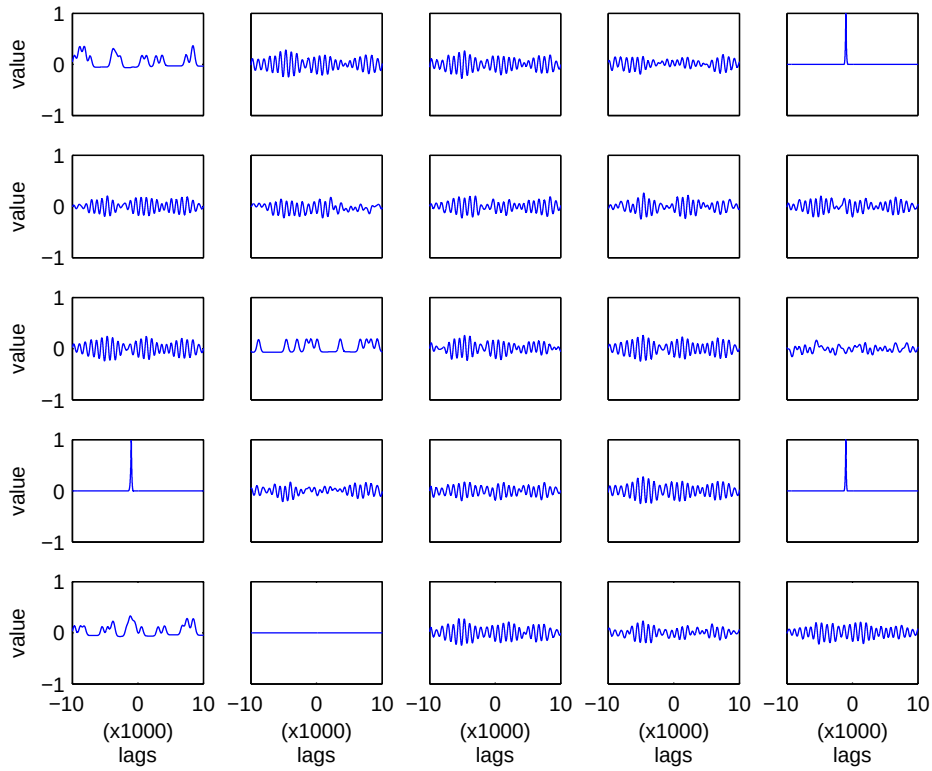

Figure G.30: Cross-correlation analysis for odour 3: trained input vs. -20% difference input. The Cross-correlation analysis was carried out between the response of the olfactory bulb of the trained input and the input minus a percentage of the difference between input value and the limit range for the input. Plots are sorted from left to right and from up to down, starting from the cross-corelation between for the first mitral cell (the first column and first row) up to the 25th mitral cell in the last column at the bottom. Plots with zero response result from Mitral cells which remain silent for this particular input. The time constants of both the ORN and mitral cells were set to $\tilde{\tau}_m \approx 10$ ms, with a threshold potential, $V_{th} = 50000$. The time constants of the excitatory synapses were set to $\tilde{\tau}_E \approx 4$ ms, whereas for the inhibitory synapses the time constants were set to $\tilde{\tau}_I \approx 16$ ms. For the ORNs, constant values randomly selected in a range between 500 and 1000, were used to represent a constant concentration of each odor stimulus. The total running time in terms of biological values is equivalent to 5 seconds at a sampling frequency of $f_{smp} = 10$ KHz. Although the clock frequency was set to $f_{clk} = 10$ MHz thus each run lasted for 5 ms of the FPGA processing time.

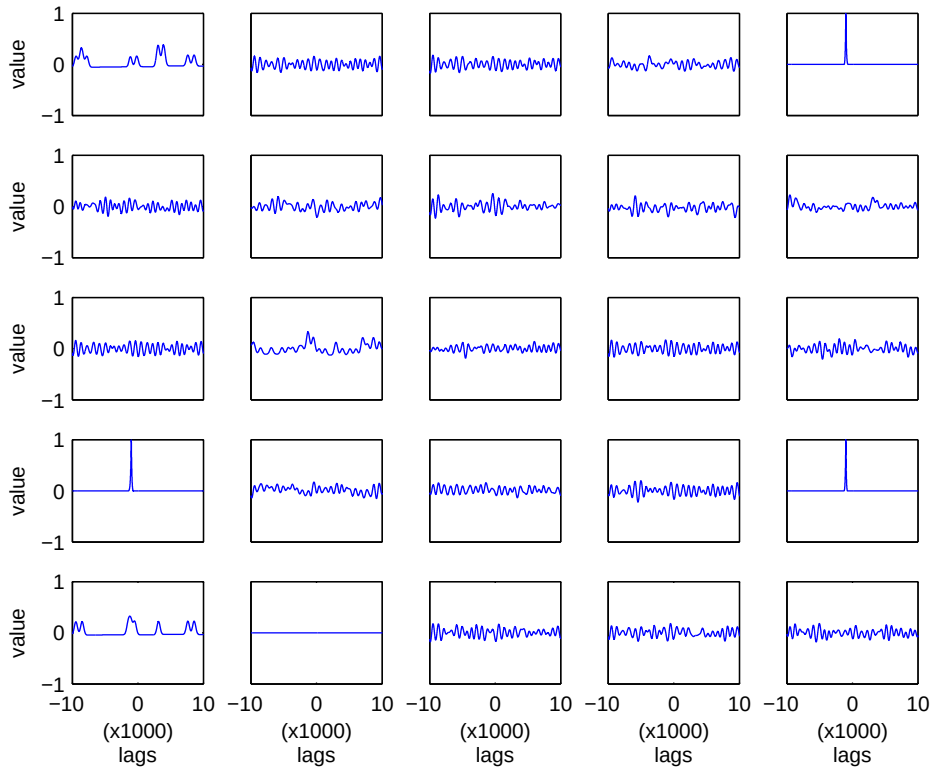

Figure G.31: Cross-correlation analysis for odour 3: trained input vs. -10% difference input. The Cross-correlation analysis was carried out between the response of the olfactory bulb of the trained input and the input minus a percentage of the difference between input value and the limit range for the input. Plots are sorted from left to right and from up to down, starting from the cross-corelation between for the first mitral cell (the first column and first row) up to the 25th mitral cell in the last column at the bottom. Plots with zero response result from Mitral cells which remain silent for this particular input. The time constants of both the ORN and mitral cells were set to $\tilde{\tau}_m \approx 10$ ms, with a threshold potential, $V_{th} = 50000$. The time constants of the excitatory synapses were set to $\tilde{\tau}_E \approx 4$ ms, whereas for the inhibitory synapses the time constants were set to $\tilde{\tau}_I \approx 16$ ms. For the ORNs, constant values randomly selected in a range between 500 and 1000, were used to represent a constant concentration of each odor stimulus. The total running time in terms of biological values is equivalent to 5 seconds at a sampling frequency of $f_{smp} = 10$ KHz. Although the clock frequency was set to $f_{clk} = 10$ MHz thus each run lasted for 5 ms of the FPGA processing time.

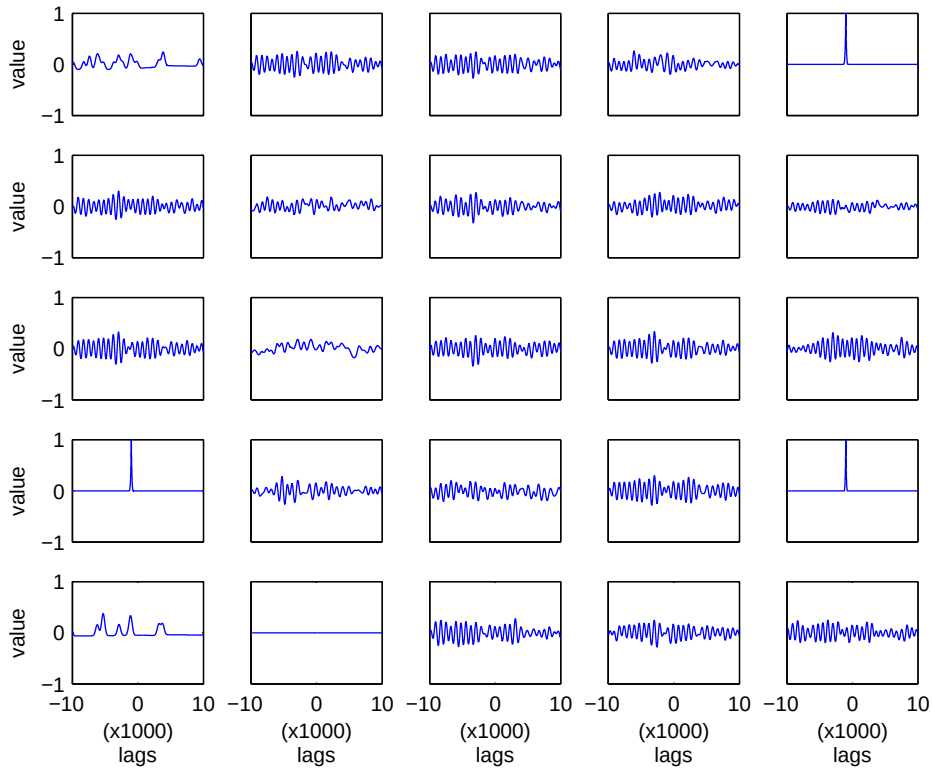

Figure G.32: Cross-correlation analysis for odour 3: trained input vs. -4% difference input. The Cross-correlation analysis was carried out between the response of the olfactory bulb of the trained input and the input minus a percentage of the difference between input value and the limit range for the input. Plots are sorted from left to right and from up to down, starting from the cross-corelation between for the first mitral cell (the first column and first row) up to the 25th mitral cell in the last column at the bottom. Plots with zero response result from Mitral cells which remain silent for this particular input. The time constants of both the ORN and mitral cells were set to $\tilde{\tau}_m \approx 10$ ms, with a threshold potential, $V_{th} = 50000$. The time constants of the excitatory synapses were set to $\tilde{\tau}_E \approx 4$ ms, whereas for the inhibitory synapses the time constants were set to $\tilde{\tau}_I \approx 16$ ms. For the ORNs, constant values randomly selected in a range between 500 and 1000, were used to represent a constant concentration of each odor stimulus. The total running time in terms of biological values is equivalent to 5 seconds at a sampling frequency of $f_{smp} = 10$ KHz. Although the clock frequency was set to $f_{clk} = 10$ MHz thus each run lasted for 5 ms of the FPGA processing time.

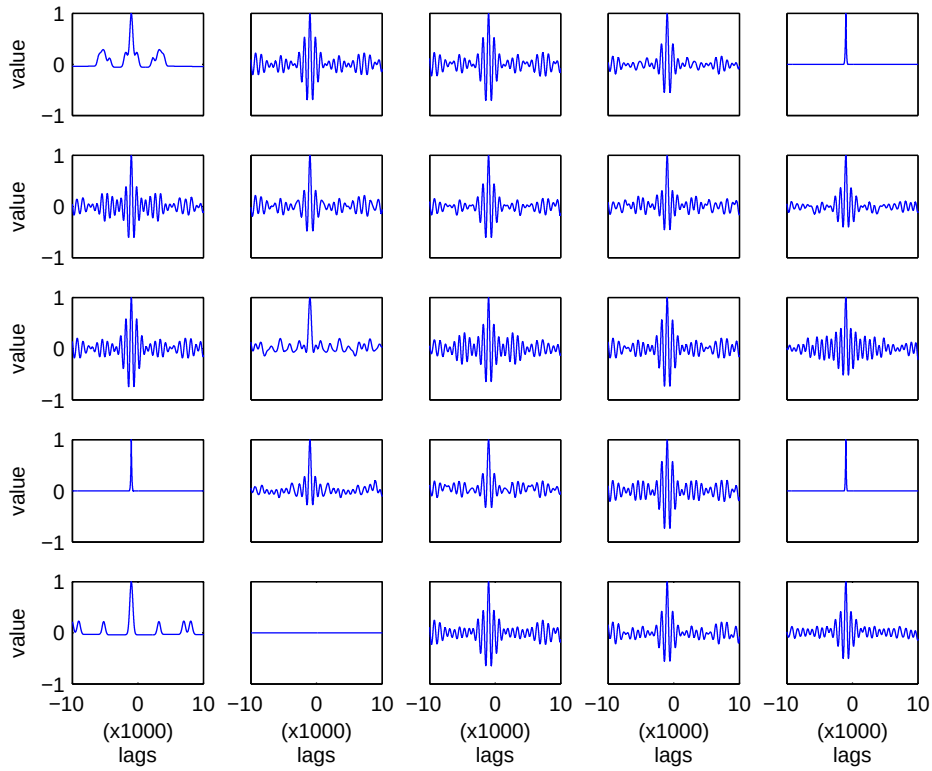

Figure G.33: Cross-correlation analysis for odour 3: trained input vs. 0% difference input. The Cross-correlation analysis was carried out between the response of the olfactory bulb of the trained input and the input minus a percentage of the difference between input value and the limit range for the input. Plots are sorted from left to right and from up to down, starting from the cross-corelation between for the first mitral cell (the first column and first row) up to the 25th mitral cell in the last column at the bottom. Plots with zero response result from Mitral cells which remain silent for this particular input. The time constants of both the ORN and mitral cells were set to $\tilde{\tau}_m \approx 10$ ms, with a threshold potential, $V_{th} = 50000$. The time constants of the excitatory synapses were set to $\tilde{\tau}_E \approx 4$ ms, whereas for the inhibitory synapses the time constants were set to $\tilde{\tau}_I \approx 16$ ms. For the ORNs, constant values randomly selected in a range between 500 and 1000, were used to represent a constant concentration of each odor stimulus. The total running time in terms of biological values is equivalent to 5 seconds at a sampling frequency of $f_{smp} = 10$ KHz. Although the clock frequency was set to $f_{clk} = 10$ MHz thus each run lasted for 5 ms of the FPGA processing time.

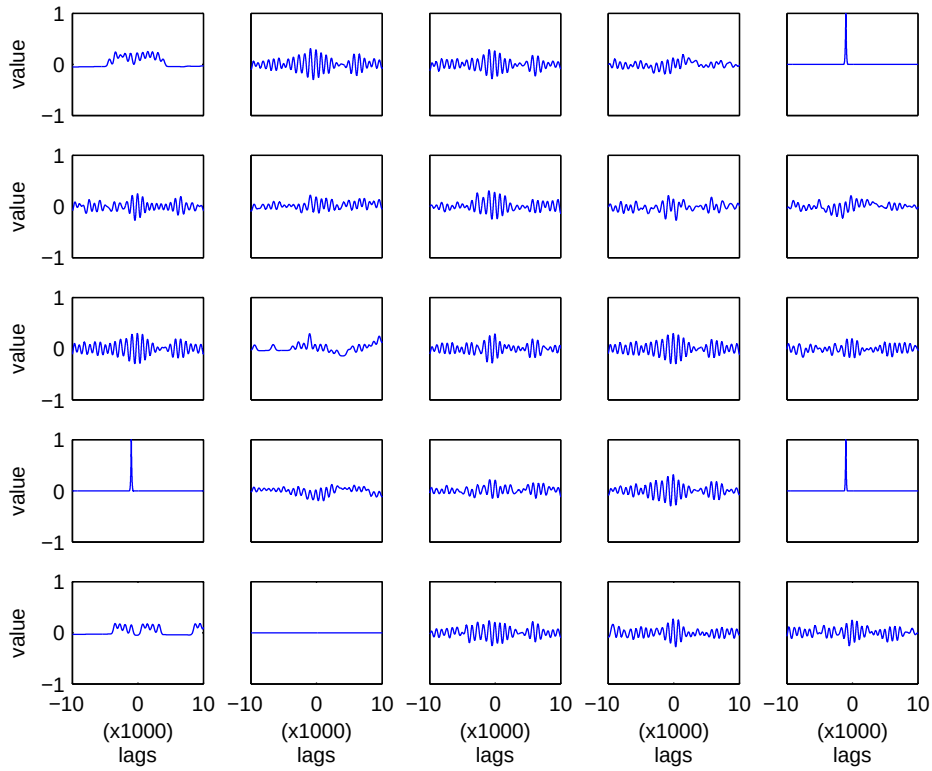

Figure G.34: Cross-correlation analysis for odour 3: trained input vs. +4% difference input. The Cross-correlation analysis was carried out between the response of the olfactory bulb of the trained input and the input minus a percentage of the difference between input value and the limit range for the input. Plots are sorted from left to right and from up to down, starting from the cross-corelation between for the first mitral cell (the first column and first row) up to the 25th mitral cell in the last column at the bottom. Plots with zero response result from Mitral cells which remain silent for this particular input. The time constants of both the ORN and mitral cells were set to $\tilde{\tau}_m \approx 10$ ms, with a threshold potential, $V_{th} = 50000$. The time constants of the excitatory synapses were set to $\tilde{\tau}_E \approx 4$ ms, whereas for the inhibitory synapses the time constants were set to $\tilde{\tau}_I \approx 16$ ms. For the ORNs, constant values randomly selected in a range between 500 and 1000, were used to represent a constant concentration of each odor stimulus. The total running time in terms of biological values is equivalent to 5 seconds at a sampling frequency of $f_{smp} = 10$ KHz. Although the clock frequency was set to $f_{clk} = 10$ MHz thus each run lasted for 5 ms of the FPGA processing time.

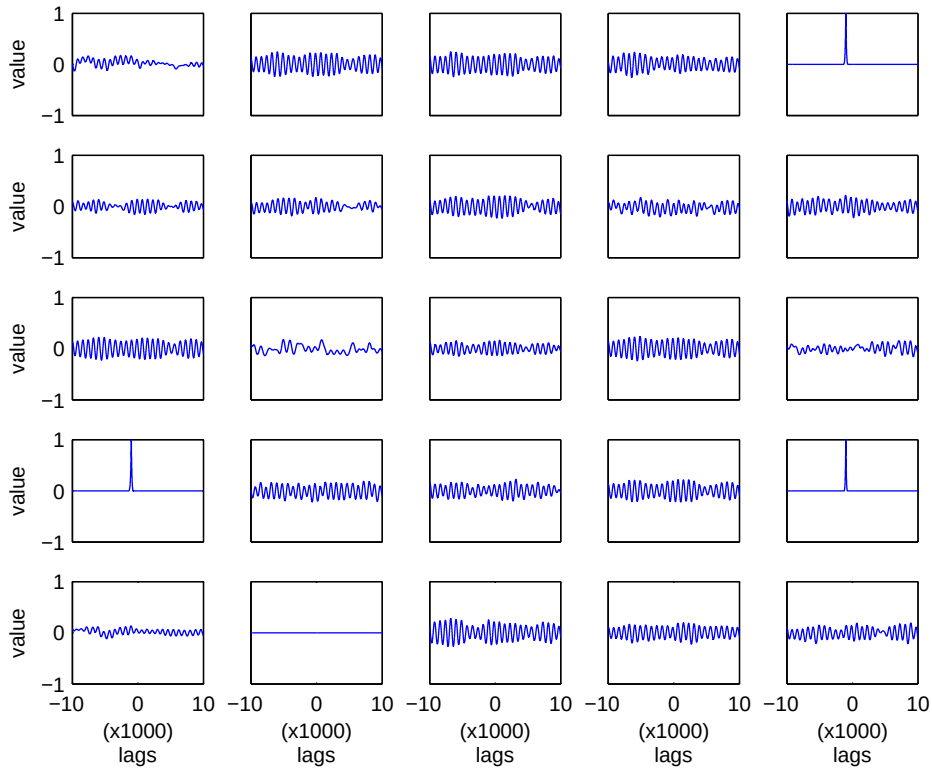

Figure G.35: Cross-correlation analysis for odour 3: trained input vs. +10% difference input. The Cross-correlation analysis was carried out between the response of the olfactory bulb of the trained input and the input minus a percentage of the difference between input value and the limit range for the input. Plots are sorted from left to right and from up to down, starting from the cross-corelation between for the first mitral cell (the first column and first row) up to the 25th mitral cell in the last column at the bottom. Plots with zero response result from Mitral cells which remain silent for this particular input. The time constants of both the ORN and mitral cells were set to $\tilde{\tau}_m \approx 10$ ms, with a threshold potential, $V_{th} = 50000$. The time constants of the excitatory synapses were set to $\tilde{\tau}_E \approx 4$ ms, whereas for the inhibitory synapses the time constants were set to $\tilde{\tau}_I \approx 16$ ms. For the ORNs, constant values randomly selected in a range between 500 and 1000, were used to represent a constant concentration of each odor stimulus. The total running time in terms of biological values is equivalent to 5 seconds at a sampling frequency of $f_{smp} = 10$ KHz. Although the clock frequency was set to $f_{clk} = 10$ MHz thus each run lasted for 5 ms of the FPGA processing time.

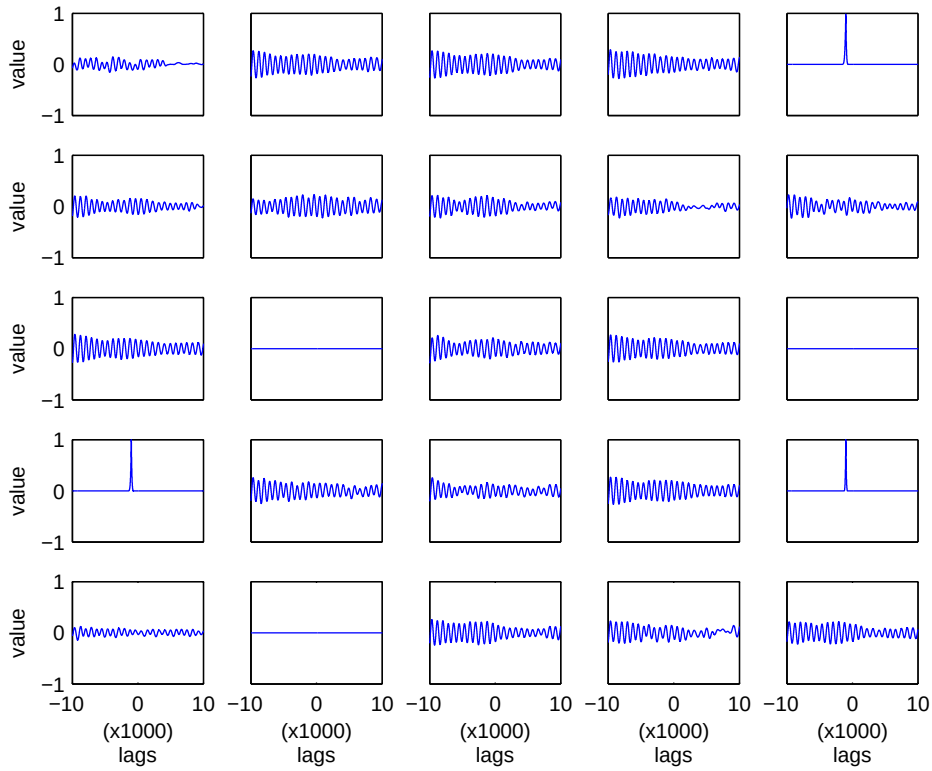

Figure G.36: Cross-correlation analysis for odour 3: trained input vs. +20% difference input. The Cross-correlation analysis was carried out between the response of the olfactory bulb of the trained input and the input minus a percentage of the difference between input value and the limit range for the input. Plots are sorted from left to right and from up to down, starting from the cross-corelation between for the first mitral cell (the first column and first row) up to the 25th mitral cell in the last column at the bottom. Plots with zero response result from Mitral cells which remain silent for this particular input. The time constants of both the ORN and mitral cells were set to $\tilde{\tau}_m \approx 10$ ms, with a threshold potential, $V_{th} = 50000$. The time constants of the excitatory synapses were set to $\tilde{\tau}_E \approx 4$ ms, whereas for the inhibitory synapses the time constants were set to $\tilde{\tau}_I \approx 16$ ms. For the ORNs, constant values randomly selected in a range between 500 and 1000, were used to represent a constant concentration of each odor stimulus. The total running time in terms of biological values is equivalent to 5 seconds at a sampling frequency of $f_{smp} = 10$ KHz. Although the clock frequency was set to $f_{clk} = 10$ MHz thus each run lasted for 5 ms of the FPGA processing time.

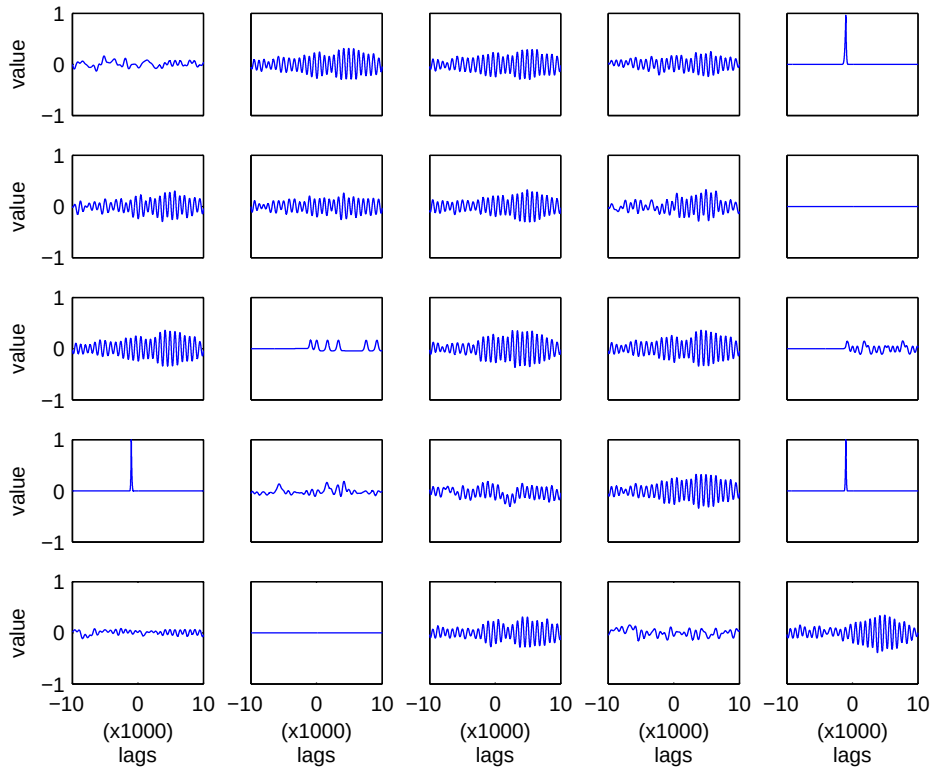

Figure G.37: Cross-correlation analysis for odour 3: trained input vs. +40% difference input. The Cross-correlation analysis was carried out between the response of the olfactory bulb of the trained input and the input minus a percentage of the difference between input value and the limit range for the input. Plots are sorted from left to right and from up to down, starting from the cross-corelation between for the first mitral cell (the first column and first row) up to the 25th mitral cell in the last column at the bottom. Plots with zero response result from Mitral cells which remain silent for this particular input. The time constants of both the ORN and mitral cells were set to $\tilde{\tau}_m \approx 10$ ms, with a threshold potential, $V_{th} = 50000$. The time constants of the excitatory synapses were set to $\tilde{\tau}_E \approx 4$ ms, whereas for the inhibitory synapses the time constants were set to $\tilde{\tau}_I \approx 16$ ms. For the ORNs, constant values randomly selected in a range between 500 and 1000, were used to represent a constant concentration of each odor stimulus. The total running time in terms of biological values is equivalent to 5 seconds at a sampling frequency of $f_{smp} = 10$ KHz. Although the clock frequency was set to $f_{clk} = 10$ MHz thus each run lasted for 5 ms of the FPGA processing time.

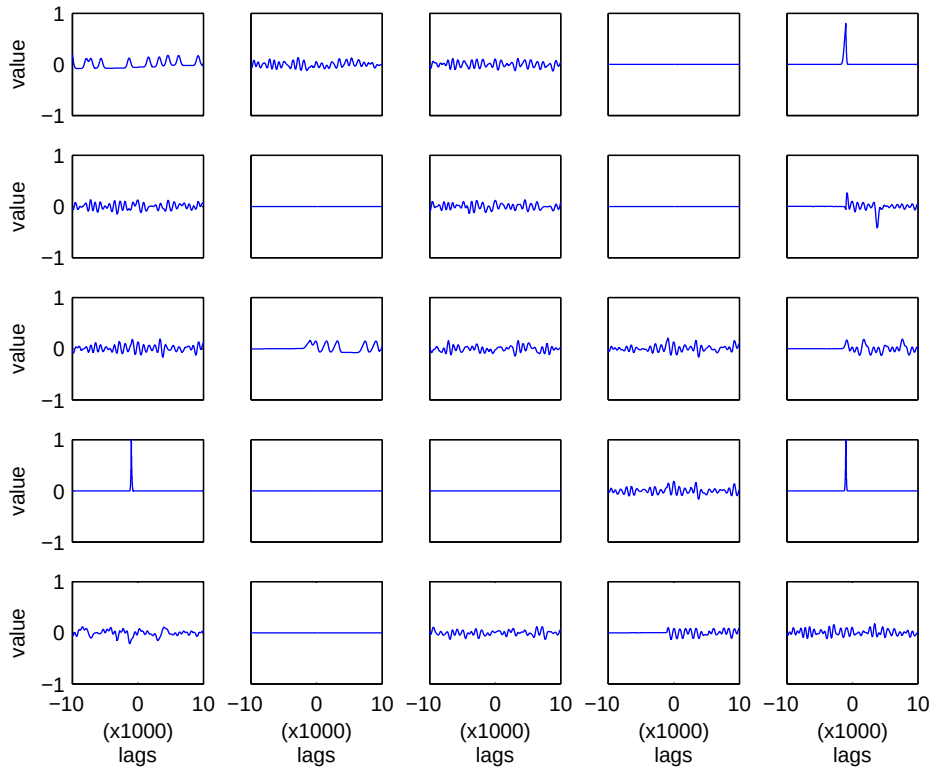

Figure G.38: Cross-correlation analysis for odour 3: trained input vs. +60% difference input. The Cross-correlation analysis was carried out between the response of the olfactory bulb of the trained input and the input minus a percentage of the difference between input value and the limit range for the input. Plots are sorted from left to right and from up to down, starting from the cross-corelation between for the first mitral cell (the first column and first row) up to the 25th mitral cell in the last column at the bottom. Plots with zero response result from Mitral cells which remain silent for this particular input. The time constants of both the ORN and mitral cells were set to $\tilde{\tau}_m \approx 10$ ms, with a threshold potential, $V_{th} = 50000$. The time constants of the excitatory synapses were set to $\tilde{\tau}_E \approx 4$ ms, whereas for the inhibitory synapses the time constants were set to $\tilde{\tau}_I \approx 16$ ms. For the ORNs, constant values randomly selected in a range between 500 and 1000, were used to represent a constant concentration of each odor stimulus. The total running time in terms of biological values is equivalent to 5 seconds at a sampling frequency of $f_{smp} = 10$ KHz. Although the clock frequency was set to $f_{clk} = 10$ MHz thus each run lasted for 5 ms of the FPGA processing time.

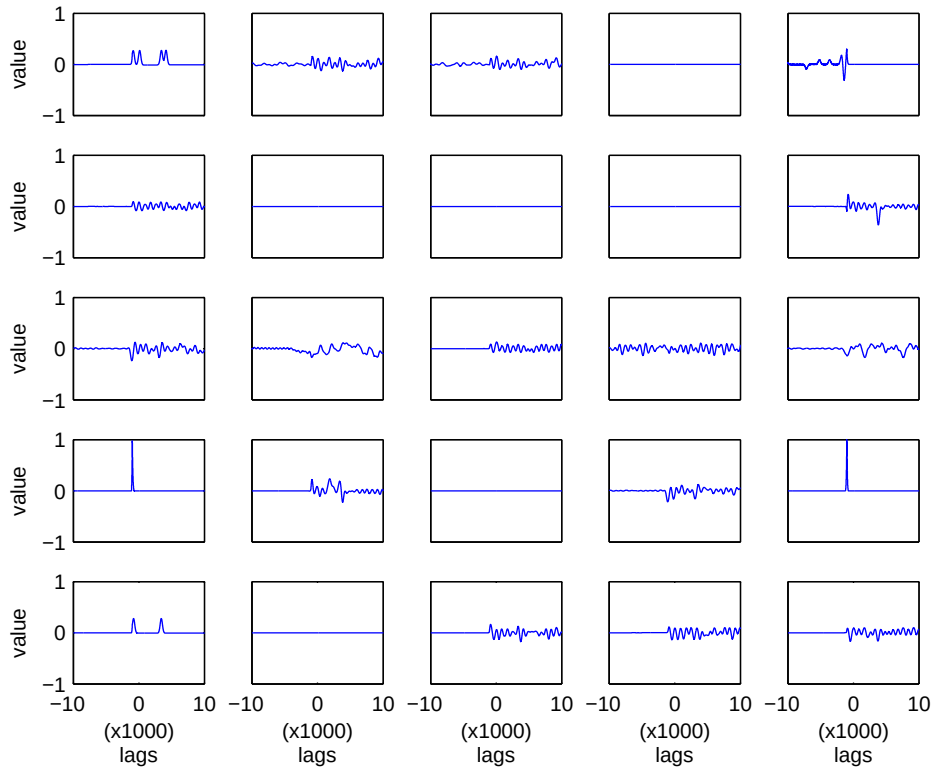

Figure G.39: Cross-correlation analysis for odour 3: trained input vs. +80% difference input. The Cross-correlation analysis was carried out between the response of the olfactory bulb of the trained input and the input minus a percentage of the difference between input value and the limit range for the input. Plots are sorted from left to right and from up to down, starting from the cross-corelation between for the first mitral cell (the first column and first row) up to the 25th mitral cell in the last column at the bottom. Plots with zero response result from Mitral cells which remain silent for this particular input. The time constants of both the ORN and mitral cells were set to $\tilde{\tau}_m \approx 10$ ms, with a threshold potential, $V_{th} = 50000$. The time constants of the excitatory synapses were set to $\tilde{\tau}_E \approx 4$ ms, whereas for the inhibitory synapses the time constants were set to $\tilde{\tau}_I \approx 16$ ms. For the ORNs, constant values randomly selected in a range between 500 and 1000, were used to represent a constant concentration of each odor stimulus. The total running time in terms of biological values is equivalent to 5 seconds at a sampling frequency of $f_{smp} = 10$ KHz. Although the clock frequency was set to $f_{clk} = 10$ MHz thus each run lasted for 5 ms of the FPGA processing time.

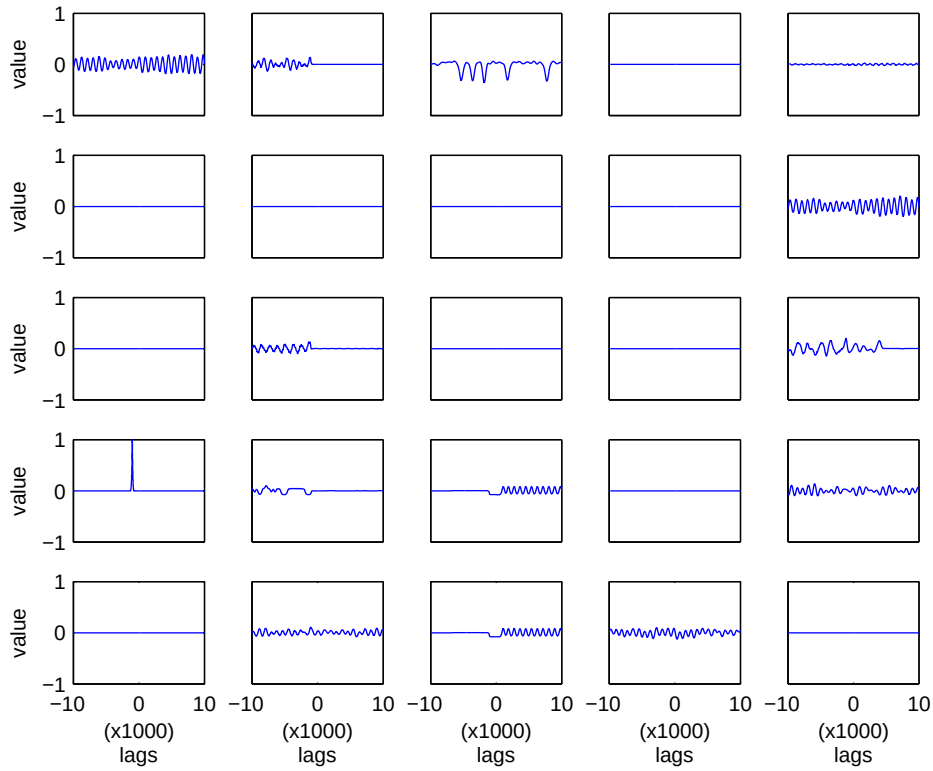

Figure G.40: Cross-correlation analysis for odour 4: trained input vs. -80% difference input. The Cross-correlation analysis was carried out between the response of the olfactory bulb of the trained input and the input minus a percentage of the difference between input value and the limit range for the input. Plots are sorted from left to right and from up to down, starting from the cross-corelation between for the first mitral cell (the first column and first row) up to the 25th mitral cell in the last column at the bottom. Plots with zero response result from Mitral cells which remain silent for this particular input. The time constants of both the ORN and mitral cells were set to $\tilde{\tau}_m \approx 10$ ms, with a threshold potential, $V_{th} = 50000$. The time constants of the excitatory synapses were set to $\tilde{\tau}_E \approx 4$ ms, whereas for the inhibitory synapses the time constants were set to $\tilde{\tau}_I \approx 16$ ms. For the ORNs, constant values randomly selected in a range between 500 and 1000, were used to represent a constant concentration of each odor stimulus. The total running time in terms of biological values is equivalent to 5 seconds at a sampling frequency of $f_{smp} = 10$ KHz. Although the clock frequency was set to $f_{clk} = 10$ MHz thus each run lasted for 5 ms of the FPGA processing time.

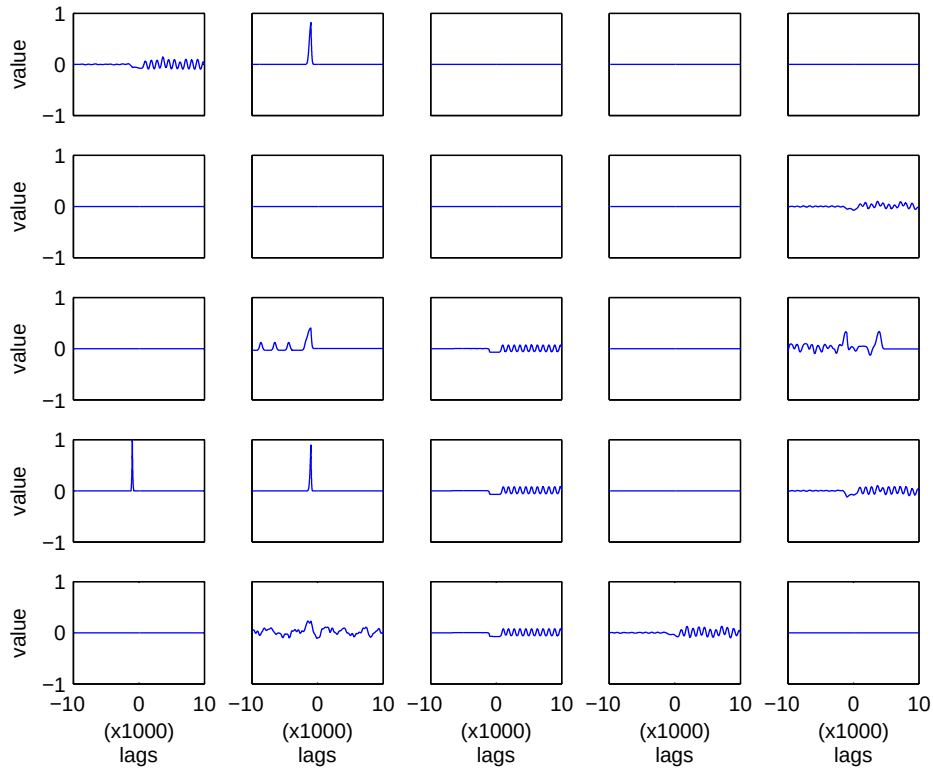

Figure G.41: Cross-correlation analysis for odour 4: trained input vs. -60% difference input. The Cross-correlation analysis was carried out between the response of the olfactory bulb of the trained input and the input minus a percentage of the difference between input value and the limit range for the input. Plots are sorted from left to right and from up to down, starting from the cross-corelation between for the first mitral cell (the first column and first row) up to the 25th mitral cell in the last column at the bottom. Plots with zero response result from Mitral cells which remain silent for this particular input. The time constants of both the ORN and mitral cells were set to $\tilde{\tau}_m \approx 10$ ms, with a threshold potential, $V_{th} = 50000$. The time constants of the excitatory synapses were set to $\tilde{\tau}_E \approx 4$ ms, whereas for the inhibitory synapses the time constants were set to $\tilde{\tau}_I \approx 16$ ms. For the ORNs, constant values randomly selected in a range between 500 and 1000, were used to represent a constant concentration of each odor stimulus. The total running time in terms of biological values is equivalent to 5 seconds at a sampling frequency of $f_{smp} = 10$ KHz. Although the clock frequency was set to $f_{clk} = 10$ MHz thus each run lasted for 5 ms of the FPGA processing time.

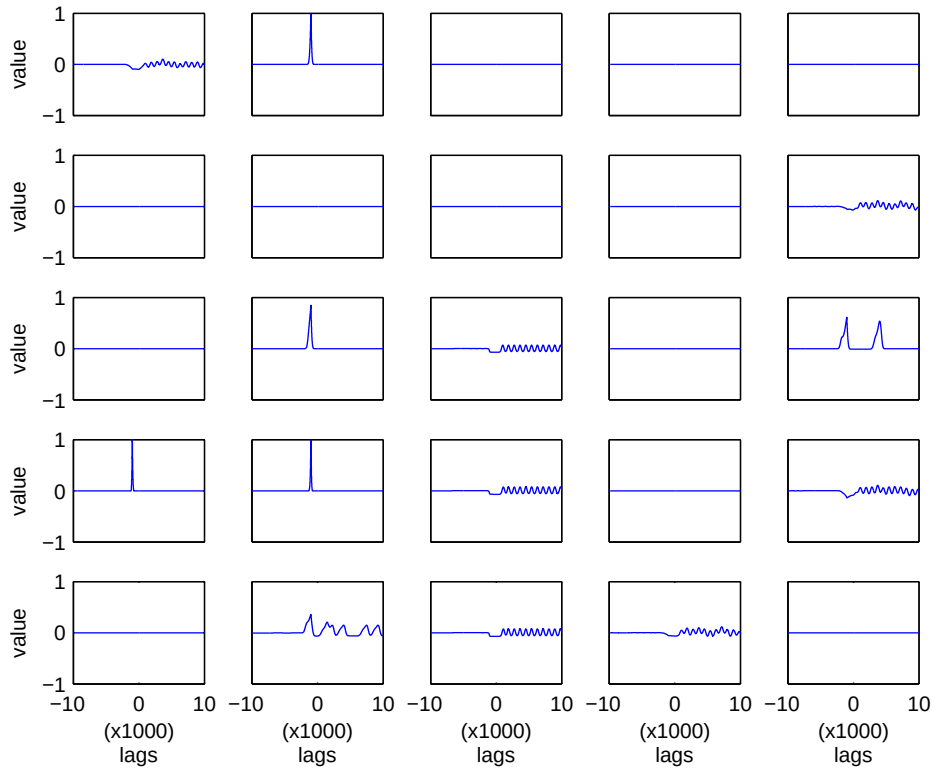

Figure G.42: Cross-correlation analysis for odour 4: trained input vs. -40% difference input. The Cross-correlation analysis was carried out between the response of the olfactory bulb of the trained input and the input minus a percentage of the difference between input value and the limit range for the input. Plots are sorted from left to right and from up to down, starting from the cross-corelation between for the first mitral cell (the first column and first row) up to the 25th mitral cell in the last column at the bottom. Plots with zero response result from Mitral cells which remain silent for this particular input. The time constants of both the ORN and mitral cells were set to $\tilde{\tau}_m \approx 10$ ms, with a threshold potential, $V_{th} = 50000$. The time constants of the excitatory synapses were set to $\tilde{\tau}_E \approx 4$ ms, whereas for the inhibitory synapses the time constants were set to $\tilde{\tau}_I \approx 16$ ms. For the ORNs, constant values randomly selected in a range between 500 and 1000, were used to represent a constant concentration of each odor stimulus. The total running time in terms of biological values is equivalent to 5 seconds at a sampling frequency of $f_{smp} = 10$ KHz. Although the clock frequency was set to $f_{clk} = 10$ MHz thus each run lasted for 5 ms of the FPGA processing time.

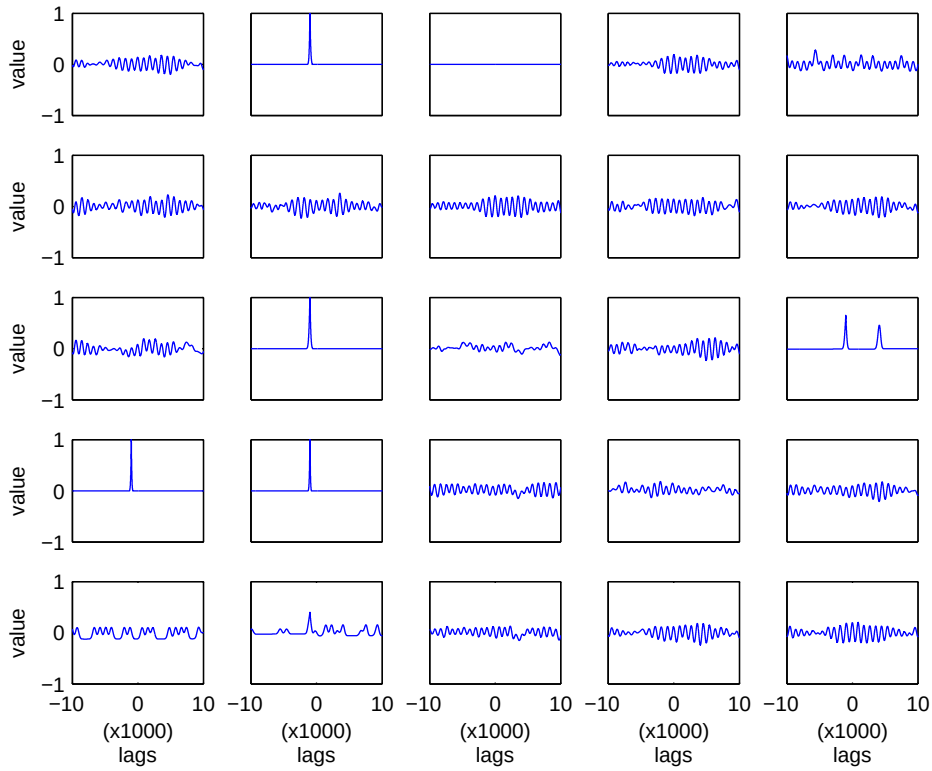

Figure G.43: Cross-correlation analysis for odour 4: trained input vs. -20% difference input. The Cross-correlation analysis was carried out between the response of the olfactory bulb of the trained input and the input minus a percentage of the difference between input value and the limit range for the input. Plots are sorted from left to right and from up to down, starting from the cross-corelation between for the first mitral cell (the first column and first row) up to the 25th mitral cell in the last column at the bottom. Plots with zero response result from Mitral cells which remain silent for this particular input. The time constants of both the ORN and mitral cells were set to $\tilde{\tau}_m \approx 10$ ms, with a threshold potential, $V_{th} = 50000$. The time constants of the excitatory synapses were set to $\tilde{\tau}_E \approx 4$ ms, whereas for the inhibitory synapses the time constants were set to $\tilde{\tau}_I \approx 16$ ms. For the ORNs, constant values randomly selected in a range between 500 and 1000, were used to represent a constant concentration of each odor stimulus. The total running time in terms of biological values is equivalent to 5 seconds at a sampling frequency of $f_{smp} = 10$ KHz. Although the clock frequency was set to $f_{clk} = 10$ MHz thus each run lasted for 5 ms of the FPGA processing time.

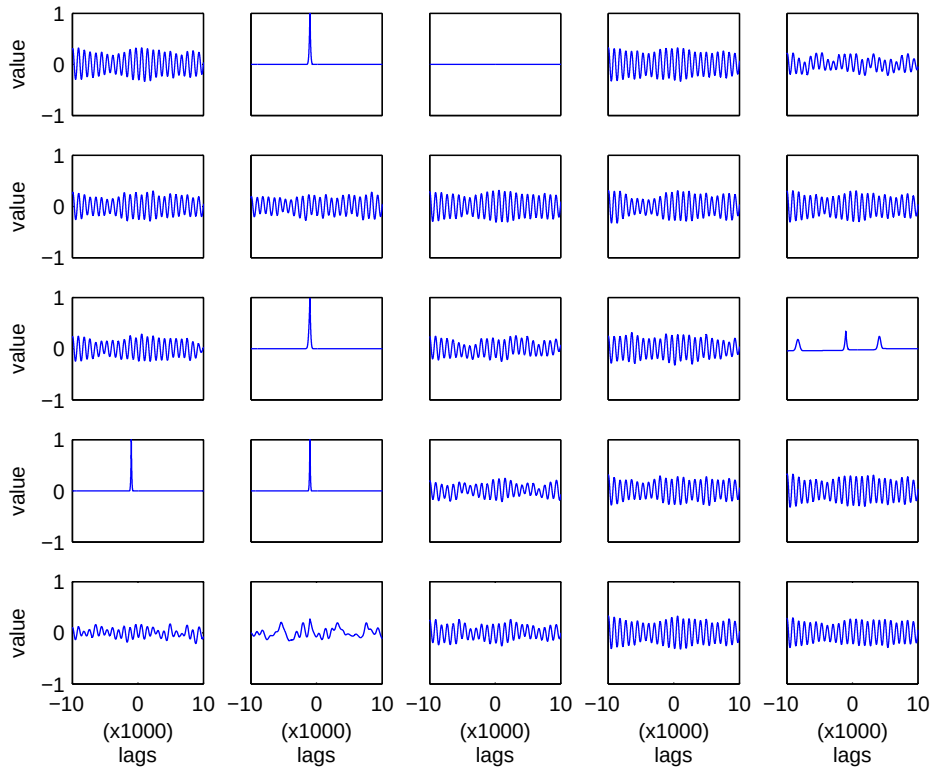

Figure G.44: Cross-correlation analysis for odour 4: trained input vs. -10% difference input. The Cross-correlation analysis was carried out between the response of the olfactory bulb of the trained input and the input minus a percentage of the difference between input value and the limit range for the input. Plots are sorted from left to right and from up to down, starting from the cross-corelation between for the first mitral cell (the first column and first row) up to the 25th mitral cell in the last column at the bottom. Plots with zero response result from Mitral cells which remain silent for this particular input. The time constants of both the ORN and mitral cells were set to $\tilde{\tau}_m \approx 10$ ms, with a threshold potential, $V_{th} = 50000$. The time constants of the excitatory synapses were set to $\tilde{\tau}_E \approx 4$ ms, whereas for the inhibitory synapses the time constants were set to $\tilde{\tau}_I \approx 16$ ms. For the ORNs, constant values randomly selected in a range between 500 and 1000, were used to represent a constant concentration of each odor stimulus. The total running time in terms of biological values is equivalent to 5 seconds at a sampling frequency of $f_{smp} = 10$ KHz. Although the clock frequency was set to $f_{clk} = 10$ MHz thus each run lasted for 5 ms of the FPGA processing time.

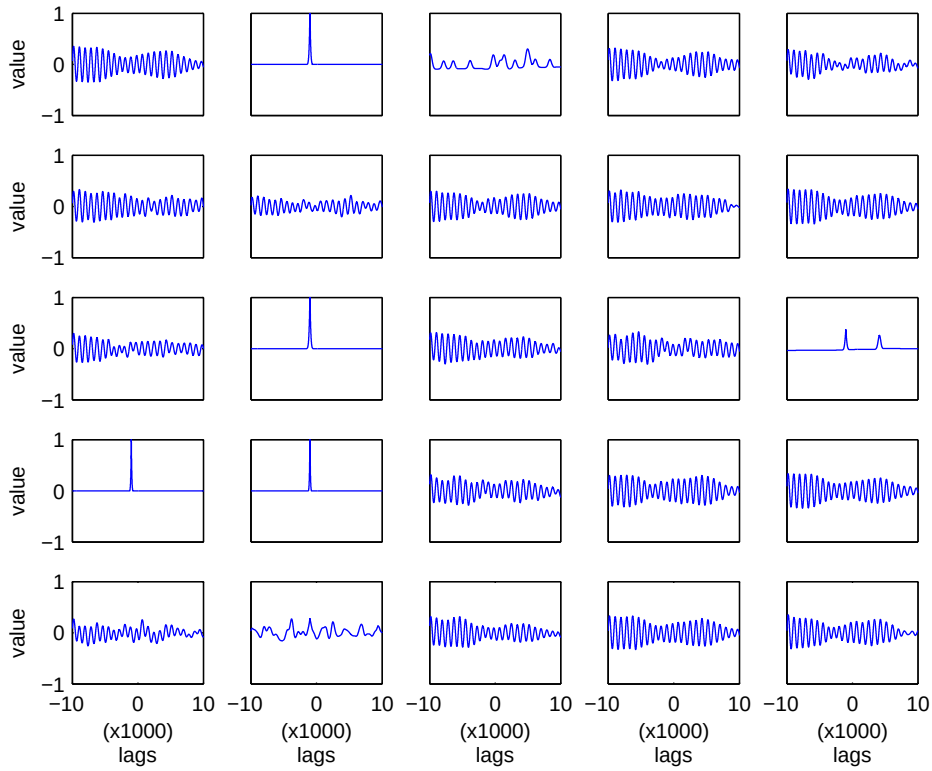

Figure G.45: Cross-correlation analysis for odour 4: trained input vs. -4% difference input. The Cross-correlation analysis was carried out between the response of the olfactory bulb of the trained input and the input minus a percentage of the difference between input value and the limit range for the input. Plots are sorted from left to right and from up to down, starting from the cross-corelation between for the first mitral cell (the first column and first row) up to the 25th mitral cell in the last column at the bottom. Plots with zero response result from Mitral cells which remain silent for this particular input. The time constants of both the ORN and mitral cells were set to $\tilde{\tau}_m \approx 10$ ms, with a threshold potential, $V_{th} = 50000$. The time constants of the excitatory synapses were set to $\tilde{\tau}_E \approx 4$ ms, whereas for the inhibitory synapses the time constants were set to $\tilde{\tau}_I \approx 16$ ms. For the ORNs, constant values randomly selected in a range between 500 and 1000, were used to represent a constant concentration of each odor stimulus. The total running time in terms of biological values is equivalent to 5 seconds at a sampling frequency of $f_{smp} = 10$ KHz. Although the clock frequency was set to $f_{clk} = 10$ MHz thus each run lasted for 5 ms of the FPGA processing time.

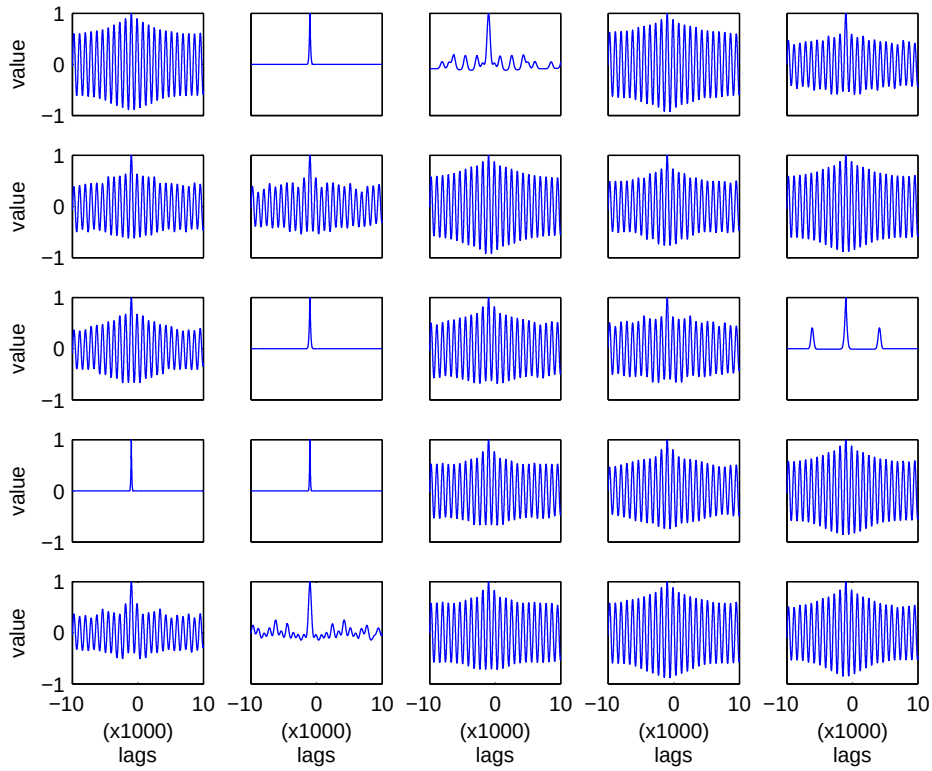

Figure G.46: Cross-correlation analysis for odour 4: trained input vs. 0% difference input. The Cross-correlation analysis was carried out between the response of the olfactory bulb of the trained input and the input minus a percentage of the difference between input value and the limit range for the input. Plots are sorted from left to right and from up to down, starting from the cross-corelation between for the first mitral cell (the first column and first row) up to the 25th mitral cell in the last column at the bottom. Plots with zero response result from Mitral cells which remain silent for this particular input. The time constants of both the ORN and mitral cells were set to $\tilde{\tau}_m \approx 10$ ms, with a threshold potential, $V_{th} = 50000$. The time constants of the excitatory synapses were set to $\tilde{\tau}_E \approx 4$ ms, whereas for the inhibitory synapses the time constants were set to $\tilde{\tau}_I \approx 16$ ms. For the ORNs, constant values randomly selected in a range between 500 and 1000, were used to represent a constant concentration of each odor stimulus. The total running time in terms of biological values is equivalent to 5 seconds at a sampling frequency of $f_{smp} = 10$ kHz. Although the clock frequency was set to $f_{clk} = 10$ MHz thus each run lasted for 5 ms of the FPGA processing time.

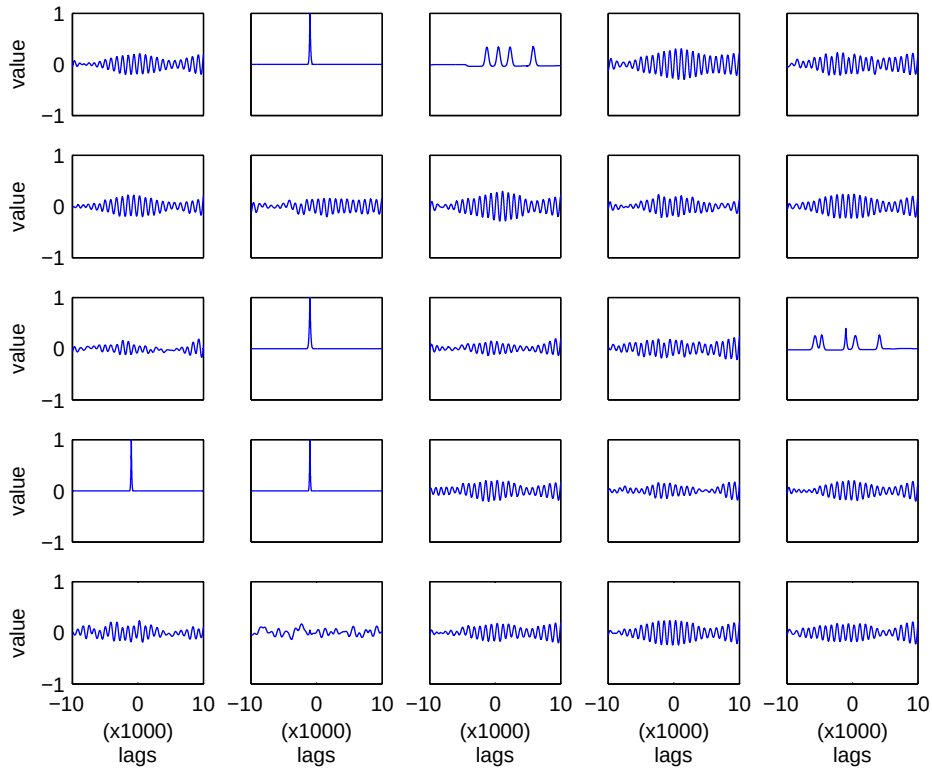

Figure G.47: Cross-correlation analysis for odour 4: trained input vs. +4% difference input. The Cross-correlation analysis was carried out between the response of the olfactory bulb of the trained input and the input minus a percentage of the difference between input value and the limit range for the input. Plots are sorted from left to right and from up to down, starting from the cross-corelation between for the first mitral cell (the first column and first row) up to the 25th mitral cell in the last column at the bottom. Plots with zero response result from Mitral cells which remain silent for this particular input. The time constants of both the ORN and mitral cells were set to $\tilde{\tau}_m \approx 10$ ms, with a threshold potential, $V_{th} = 50000$. The time constants of the excitatory synapses were set to $\tilde{\tau}_E \approx 4$ ms, whereas for the inhibitory synapses the time constants were set to $\tilde{\tau}_I \approx 16$ ms. For the ORNs, constant values randomly selected in a range between 500 and 1000, were used to represent a constant concentration of each odor stimulus. The total running time in terms of biological values is equivalent to 5 seconds at a sampling frequency of $f_{smp} = 10$ kHz. Although the clock frequency was set to $f_{clk} = 10$ MHz thus each run lasted for 5 ms of the FPGA processing time.

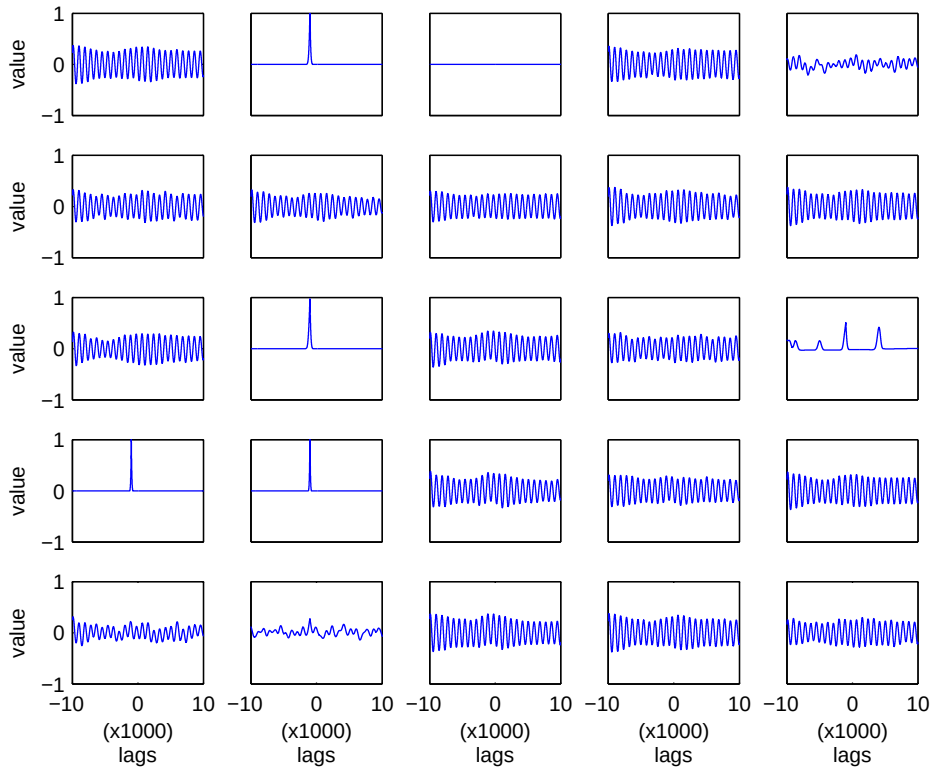

Figure G.48: Cross-correlation analysis for odour 4: trained input vs. +10% difference input. The Cross-correlation analysis was carried out between the response of the olfactory bulb of the trained input and the input minus a percentage of the difference between input value and the limit range for the input. Plots are sorted from left to right and from up to down, starting from the cross-corelation between for the first mitral cell (the first column and first row) up to the 25th mitral cell in the last column at the bottom. Plots with zero response result from Mitral cells which remain silent for this particular input. The time constants of both the ORN and mitral cells were set to $\tilde{\tau}_m \approx 10$ ms, with a threshold potential, $V_{th} = 50000$. The time constants of the excitatory synapses were set to $\tilde{\tau}_E \approx 4$ ms, whereas for the inhibitory synapses the time constants were set to $\tilde{\tau}_I \approx 16$ ms. For the ORNs, constant values randomly selected in a range between 500 and 1000, were used to represent a constant concentration of each odor stimulus. The total running time in terms of biological values is equivalent to 5 seconds at a sampling frequency of $f_{smp} = 10$ kHz. Although the clock frequency was set to $f_{clk} = 10$ MHz thus each run lasted for 5 ms of the FPGA processing time.

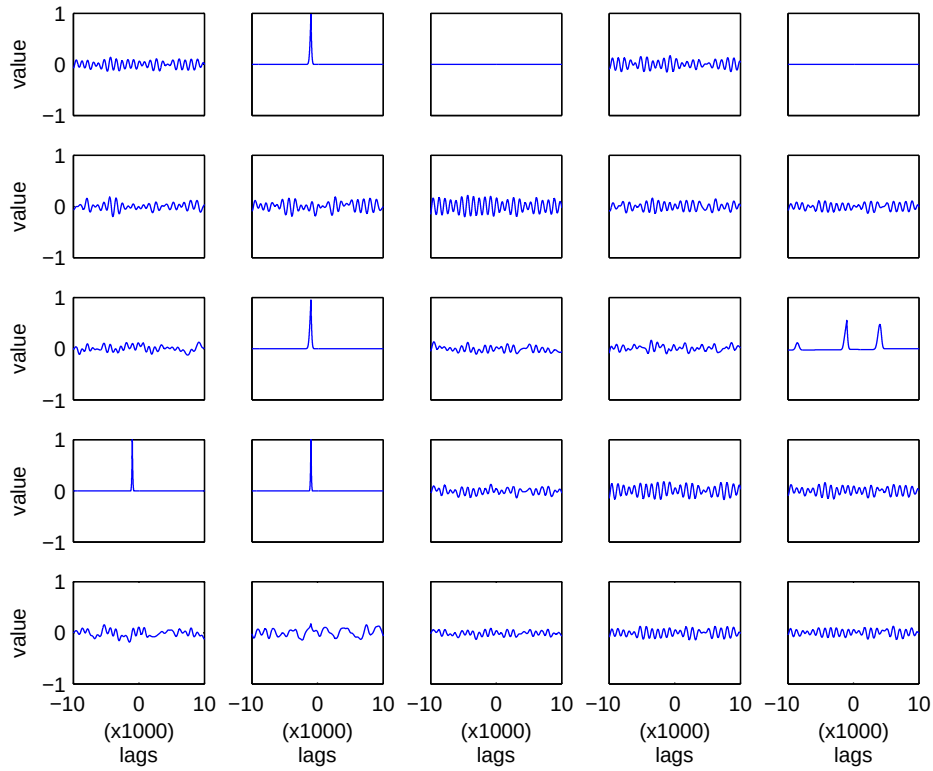

Figure G.49: Cross-correlation analysis for odour 4: trained input vs. +20% difference input. The Cross-correlation analysis was carried out between the response of the olfactory bulb of the trained input and the input minus a percentage of the difference between input value and the limit range for the input. Plots are sorted from left to right and from up to down, starting from the cross-corelation between for the first mitral cell (the first column and first row) up to the 25th mitral cell in the last column at the bottom. Plots with zero response result from Mitral cells which remain silent for this particular input. The time constants of both the ORN and mitral cells were set to $\tilde{\tau}_m \approx 10$ ms, with a threshold potential, $V_{th} = 50000$. The time constants of the excitatory synapses were set to $\tilde{\tau}_E \approx 4$ ms, whereas for the inhibitory synapses the time constants were set to $\tilde{\tau}_I \approx 16$ ms. For the ORNs, constant values randomly selected in a range between 500 and 1000, were used to represent a constant concentration of each odor stimulus. The total running time in terms of biological values is equivalent to 5 seconds at a sampling frequency of $f_{smp} = 10$ kHz. Although the clock frequency was set to $f_{clk} = 10$ MHz thus each run lasted for 5 ms of the FPGA processing time.

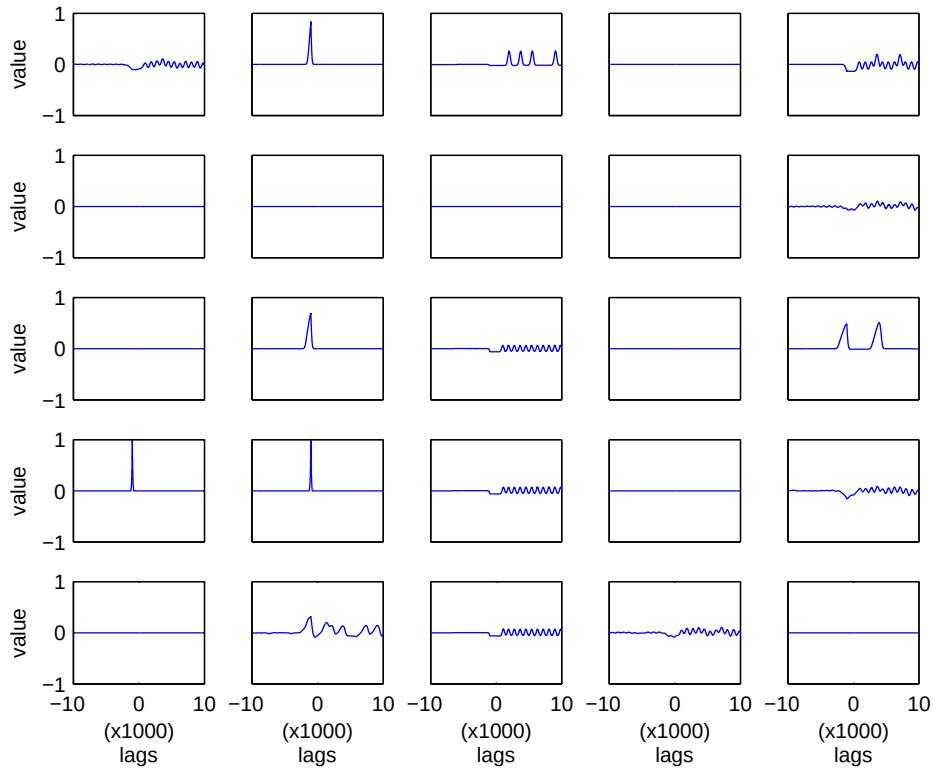

Figure G.50: Cross-correlation analysis for odour 4: trained input vs. +40% difference input. The Cross-correlation analysis was carried out between the response of the olfactory bulb of the trained input and the input minus a percentage of the difference between input value and the limit range for the input. Plots are sorted from left to right and from up to down, starting from the cross-corelation between for the first mitral cell (the first column and first row) up to the 25th mitral cell in the last column at the bottom. Plots with zero response result from Mitral cells which remain silent for this particular input. The time constants of both the ORN and mitral cells were set to $\tilde{\tau}_m \approx 10$ ms, with a threshold potential, $V_{th} = 50000$. The time constants of the excitatory synapses were set to $\tilde{\tau}_E \approx 4$ ms, whereas for the inhibitory synapses the time constants were set to $\tilde{\tau}_I \approx 16$ ms. For the ORNs, constant values randomly selected in a range between 500 and 1000, were used to represent a constant concentration of each odor stimulus. The total running time in terms of biological values is equivalent to 5 seconds at a sampling frequency of $f_{smp} = 10$ kHz. Although the clock frequency was set to $f_{clk} = 10$ MHz thus each run lasted for 5 ms of the FPGA processing time.

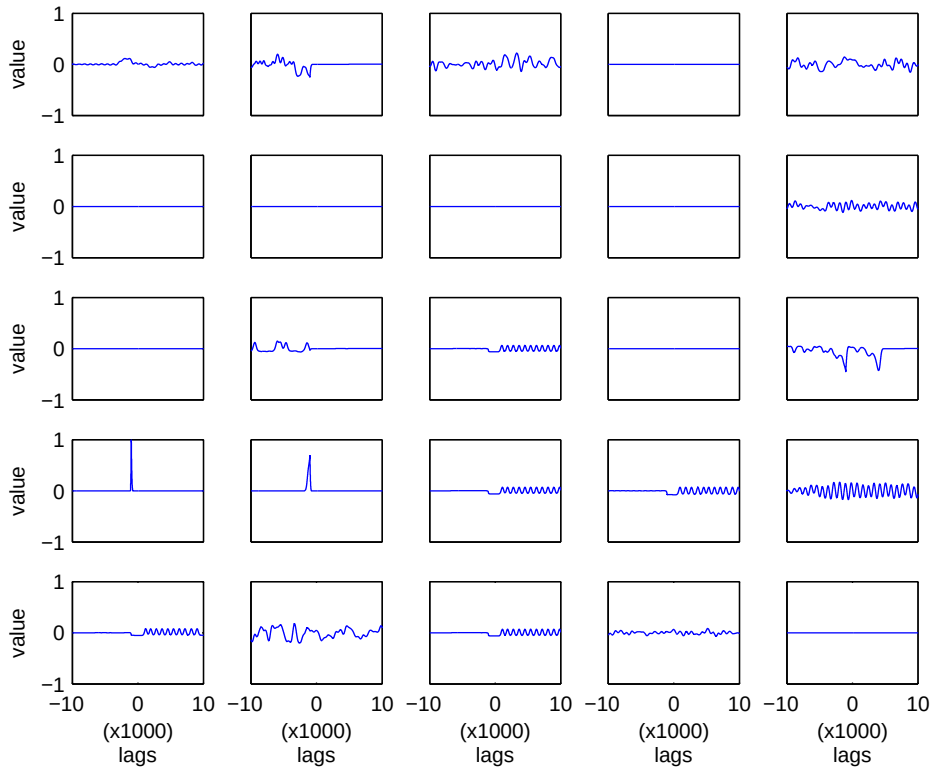

Figure G.51: Cross-correlation analysis for odour 4: trained input vs. +60% difference input. The Cross-correlation analysis was carried out between the response of the olfactory bulb of the trained input and the input minus a percentage of the difference between input value and the limit range for the input. Plots are sorted from left to right and from up to down, starting from the cross-corelation between for the first mitral cell (the first column and first row) up to the 25th mitral cell in the last column at the bottom. Plots with zero response result from Mitral cells which remain silent for this particular input. The time constants of both the ORN and mitral cells were set to $\tilde{\tau}_m \approx 10$ ms, with a threshold potential, $V_{th} = 50000$. The time constants of the excitatory synapses were set to $\tilde{\tau}_E \approx 4$ ms, whereas for the inhibitory synapses the time constants were set to $\tilde{\tau}_I \approx 16$ ms. For the ORNs, constant values randomly selected in a range between 500 and 1000, were used to represent a constant concentration of each odor stimulus. The total running time in terms of biological values is equivalent to 5 seconds at a sampling frequency of $f_{smp} = 10$ kHz. Although the clock frequency was set to $f_{clk} = 10$ MHz thus each run lasted for 5 ms of the FPGA processing time.

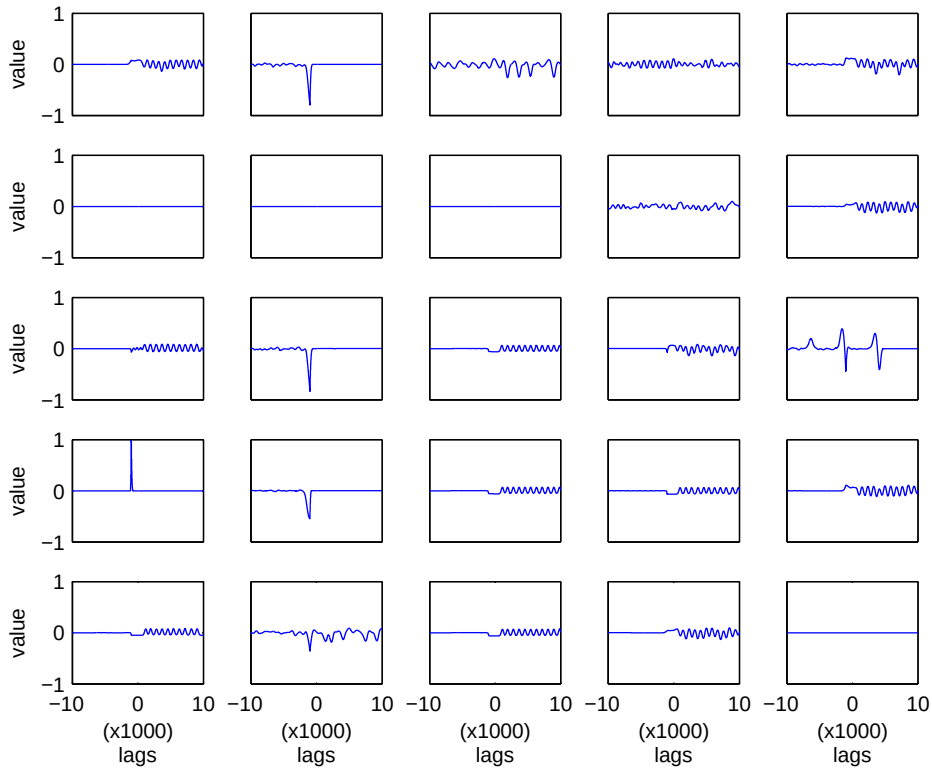

Figure G.52: Cross-correlation analysis for odour 4: trained input vs. +80% difference input. The Cross-correlation analysis was carried out between the response of the olfactory bulb of the trained input and the input minus a percentage of the difference between input value and the limit range for the input. Plots are sorted from left to right and from up to down, starting from the cross-corelation between for the first mitral cell (the first column and first row) up to the 25th mitral cell in the last column at the bottom. Plots with zero response result from Mitral cells which remain silent for this particular input. The time constants of both the ORN and mitral cells were set to $\tilde{\tau}_m \approx 10$ ms, with a threshold potential, $V_{th} = 50000$. The time constants of the excitatory synapses were set to $\tilde{\tau}_E \approx 4$ ms, whereas for the inhibitory synapses the time constants were set to $\tilde{\tau}_I \approx 16$ ms. For the ORNs, constant values randomly selected in a range between 500 and 1000, were used to represent a constant concentration of each odor stimulus. The total running time in terms of biological values is equivalent to 5 seconds at a sampling frequency of $f_{smp} = 10$ kHz. Although the clock frequency was set to $f_{clk} = 10$ MHz thus each run lasted for 5 ms of the FPGA processing time.

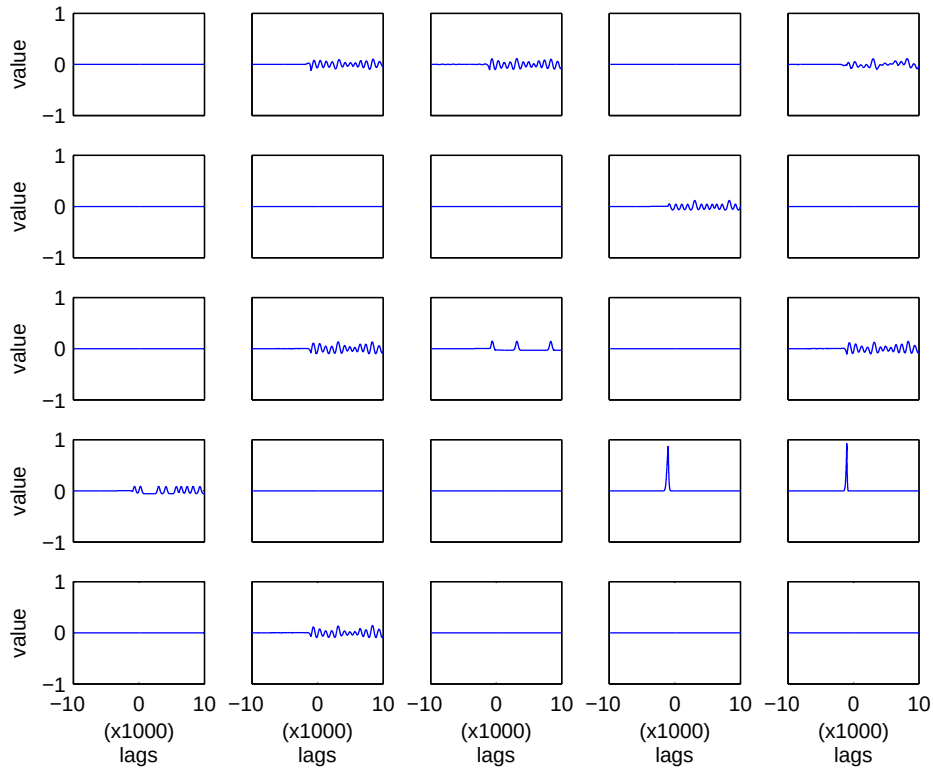

Figure G.53: Cross-correlation analysis for odour 5: trained input vs. -80% difference input. The Cross-correlation analysis was carried out between the response of the olfactory bulb of the trained input and the input minus a percentage of the difference between input value and the limit range for the input. Plots are sorted from left to right and from up to down, starting from the cross-corelation between for the first mitral cell (the first column and first row) up to the 25th mitral cell in the last column at the bottom. Plots with zero response result from Mitral cells which remain silent for this particular input. The time constants of both the ORN and mitral cells were set to $\tilde{\tau}_m \approx 10$ ms, with a threshold potential, $V_{th} = 50000$. The time constants of the excitatory synapses were set to $\tilde{\tau}_E \approx 4$ ms, whereas for the inhibitory synapses the time constants were set to $\tilde{\tau}_I \approx 16$ ms. For the ORNs, constant values randomly selected in a range between 500 and 1000, were used to represent a constant concentration of each odor stimulus. The total running time in terms of biological values is equivalent to 5 seconds at a sampling frequency of $f_{smp} = 10$ kHz. Although the clock frequency was set to $f_{clk} = 10$ MHz thus each run lasted for 5 ms of the FPGA processing time.

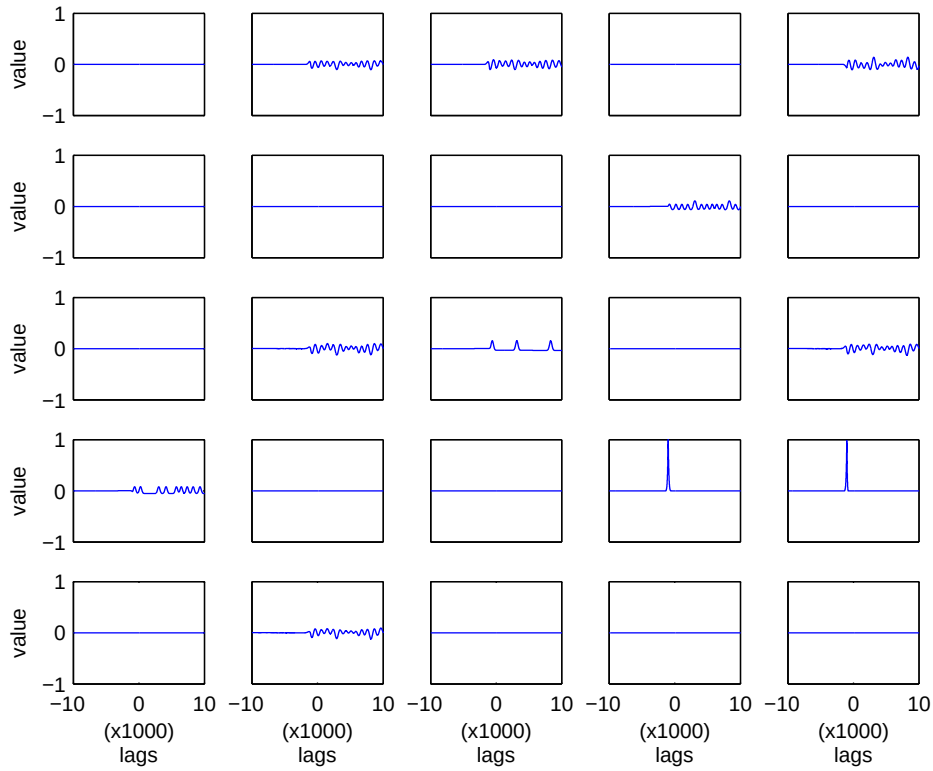

Figure G.54: Cross-correlation analysis for odour 5: trained input vs. -60% difference input. The Cross-correlation analysis was carried out between the response of the olfactory bulb of the trained input and the input minus a percentage of the difference between input value and the limit range for the input. Plots are sorted from left to right and from up to down, starting from the cross-corelation between for the first mitral cell (the first column and first row) up to the 25th mitral cell in the last column at the bottom. Plots with zero response result from Mitral cells which remain silent for this particular input. The time constants of both the ORN and mitral cells were set to $\tilde{\tau}_m \approx 10$ ms, with a threshold potential, $V_{th} = 50000$. The time constants of the excitatory synapses were set to $\tilde{\tau}_E \approx 4$ ms, whereas for the inhibitory synapses the time constants were set to $\tilde{\tau}_I \approx 16$ ms. For the ORNs, constant values randomly selected in a range between 500 and 1000, were used to represent a constant concentration of each odor stimulus. The total running time in terms of biological values is equivalent to 5 seconds at a sampling frequency of $f_{smp} = 10$ kHz. Although the clock frequency was set to $f_{clk} = 10$ MHz thus each run lasted for 5 ms of the FPGA processing time.

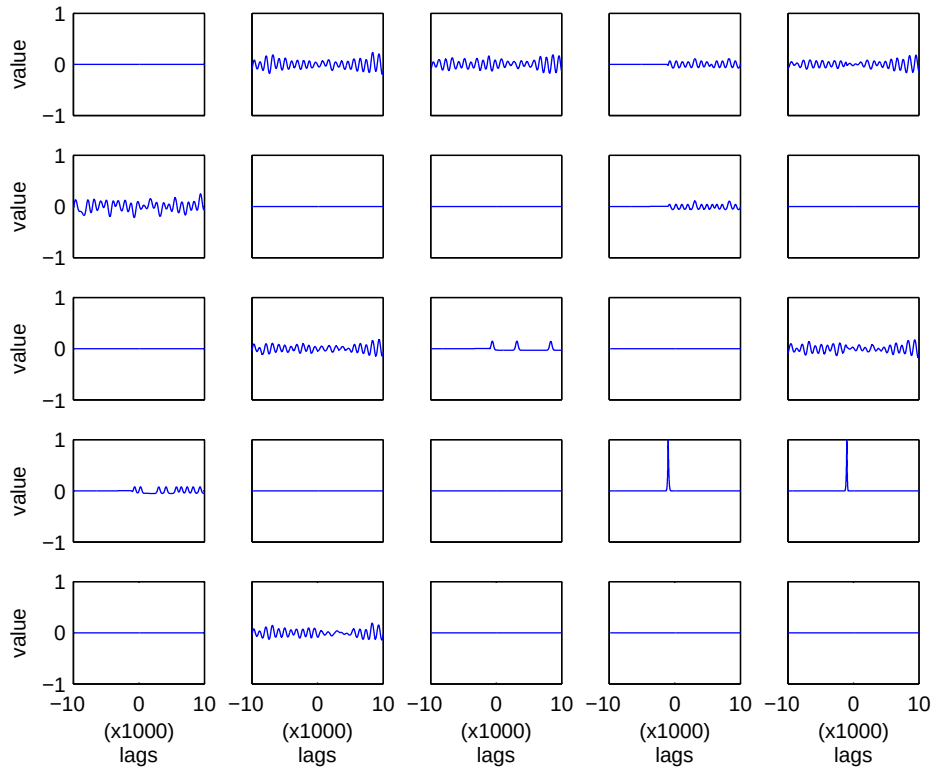

Figure G.55: Cross-correlation analysis for odour 5: trained input vs. -40% difference input. The Cross-correlation analysis was carried out between the response of the olfactory bulb of the trained input and the input minus a percentage of the difference between input value and the limit range for the input. Plots are sorted from left to right and from up to down, starting from the cross-corelation between for the first mitral cell (the first column and first row) up to the 25th mitral cell in the last column at the bottom. Plots with zero response result from Mitral cells which remain silent for this particular input. The time constants of both the ORN and mitral cells were set to $\tilde{\tau}_m \approx 10$ ms, with a threshold potential, $V_{th} = 50000$. The time constants of the excitatory synapses were set to $\tilde{\tau}_E \approx 4$ ms, whereas for the inhibitory synapses the time constants were set to $\tilde{\tau}_I \approx 16$ ms. For the ORNs, constant values randomly selected in a range between 500 and 1000, were used to represent a constant concentration of each odor stimulus. The total running time in terms of biological values is equivalent to 5 seconds at a sampling frequency of $f_{smp} = 10$ kHz. Although the clock frequency was set to $f_{clk} = 10$ MHz thus each run lasted for 5 ms of the FPGA processing time.

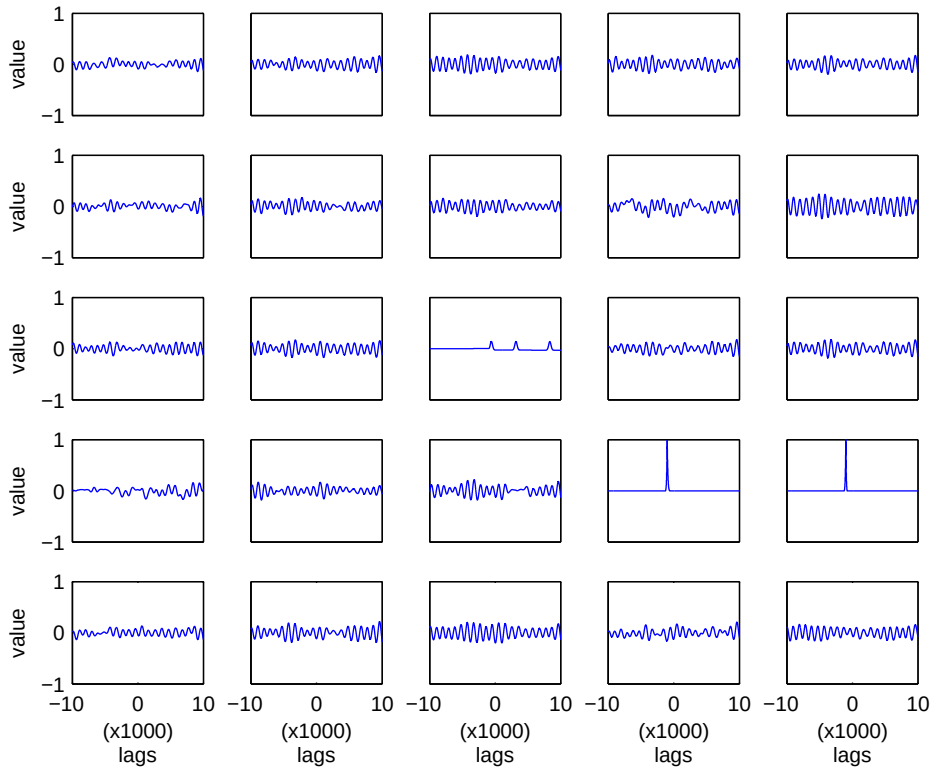

Figure G.56: Cross-correlation analysis for odour 5: trained input vs. -20% difference input. The Cross-correlation analysis was carried out between the response of the olfactory bulb of the trained input and the input minus a percentage of the difference between input value and the limit range for the input. Plots are sorted from left to right and from up to down, starting from the cross-corelation between for the first mitral cell (the first column and first row) up to the 25th mitral cell in the last column at the bottom. Plots with zero response result from Mitral cells which remain silent for this particular input. The time constants of both the ORN and mitral cells were set to $\tilde{\tau}_m \approx 10$ ms, with a threshold potential, $V_{th} = 50000$. The time constants of the excitatory synapses were set to $\tilde{\tau}_E \approx 4$ ms, whereas for the inhibitory synapses the time constants were set to $\tilde{\tau}_I \approx 16$ ms. For the ORNs, constant values randomly selected in a range between 500 and 1000, were used to represent a constant concentration of each odor stimulus. The total running time in terms of biological values is equivalent to 5 seconds at a sampling frequency of $f_{smp} = 10$ kHz. Although the clock frequency was set to $f_{clk} = 10$ MHz thus each run lasted for 5 ms of the FPGA processing time.

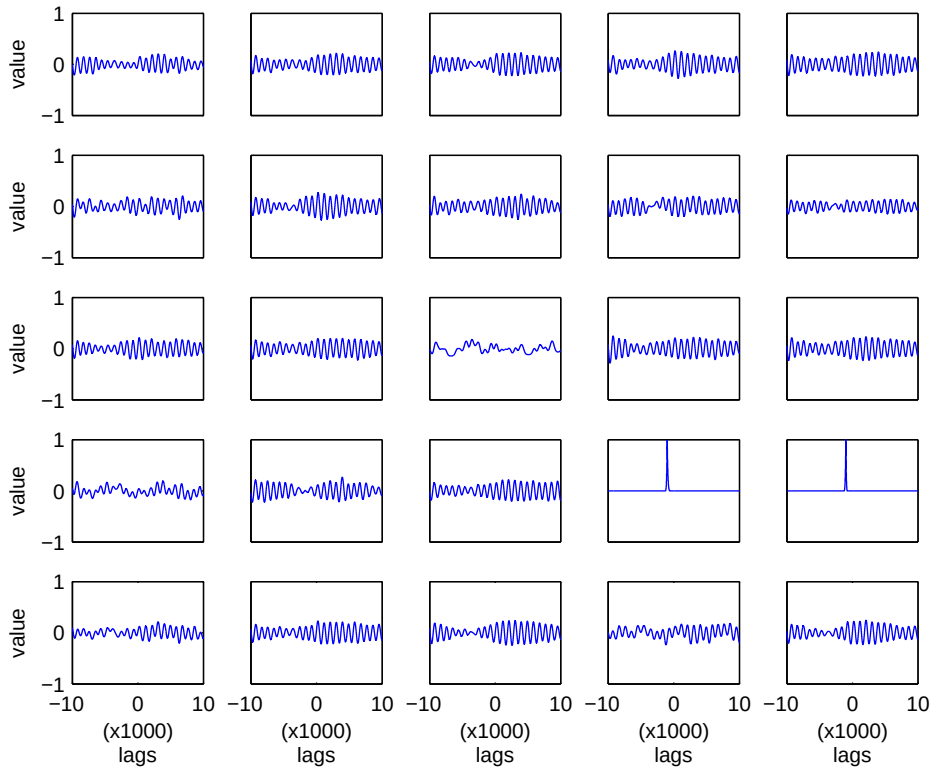

Figure G.57: Cross-correlation analysis for odour 5: trained input vs. -10% difference input. The Cross-correlation analysis was carried out between the response of the olfactory bulb of the trained input and the input minus a percentage of the difference between input value and the limit range for the input. Plots are sorted from left to right and from up to down, starting from the cross-corelation between for the first mitral cell (the first column and first row) up to the 25th mitral cell in the last column at the bottom. Plots with zero response result from Mitral cells which remain silent for this particular input. The time constants of both the ORN and mitral cells were set to $\tilde{\tau}_m \approx 10$ ms, with a threshold potential, $V_{th} = 50000$. The time constants of the excitatory synapses were set to $\tilde{\tau}_E \approx 4$ ms, whereas for the inhibitory synapses the time constants were set to $\tilde{\tau}_I \approx 16$ ms. For the ORNs, constant values randomly selected in a range between 500 and 1000, were used to represent a constant concentration of each odor stimulus. The total running time in terms of biological values is equivalent to 5 seconds at a sampling frequency of $f_{smp} = 10$ kHz. Although the clock frequency was set to $f_{clk} = 10$ MHz thus each run lasted for 5 ms of the FPGA processing time.

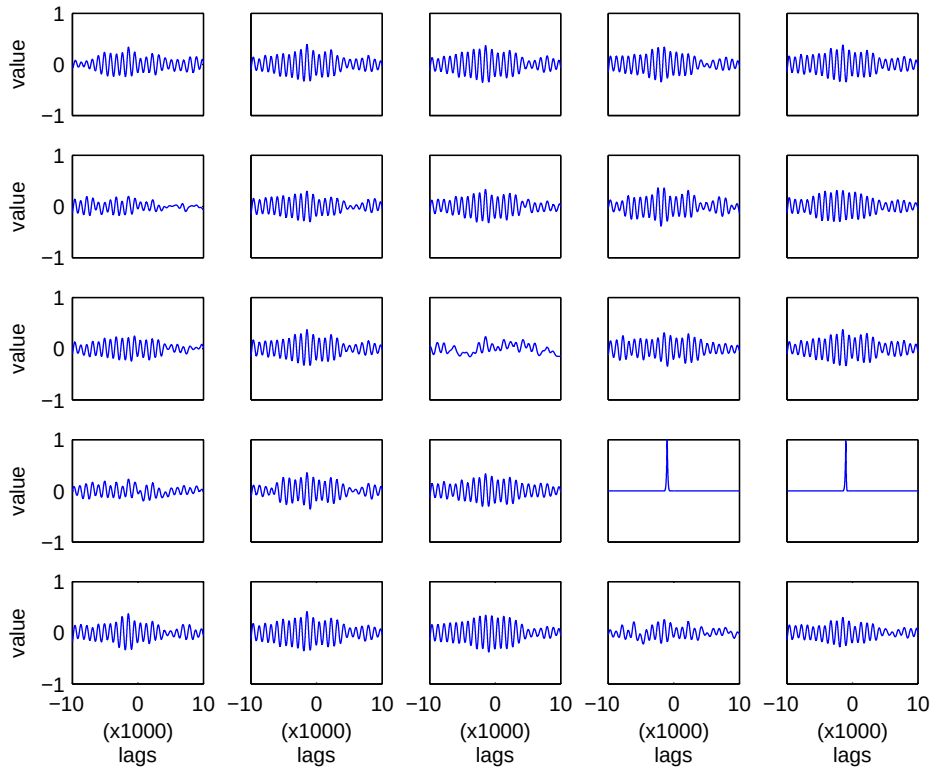

Figure G.58: Cross-correlation analysis for odour 5: trained input vs. -4% difference input. The Cross-correlation analysis was carried out between the response of the olfactory bulb of the trained input and the input minus a percentage of the difference between input value and the limit range for the input. Plots are sorted from left to right and from up to down, starting from the cross-corelation between for the first mitral cell (the first column and first row) up to the 25th mitral cell in the last column at the bottom. Plots with zero response result from Mitral cells which remain silent for this particular input. The time constants of both the ORN and mitral cells were set to $\tilde{\tau}_m \approx 10$ ms, with a threshold potential, $V_{th} = 50000$. The time constants of the excitatory synapses were set to $\tilde{\tau}_E \approx 4$ ms, whereas for the inhibitory synapses the time constants were set to $\tilde{\tau}_I \approx 16$ ms. For the ORNs, constant values randomly selected in a range between 500 and 1000, were used to represent a constant concentration of each odor stimulus. The total running time in terms of biological values is equivalent to 5 seconds at a sampling frequency of $f_{smp} = 10$ kHz. Although the clock frequency was set to $f_{clk} = 10$ MHz thus each run lasted for 5 ms of the FPGA processing time.

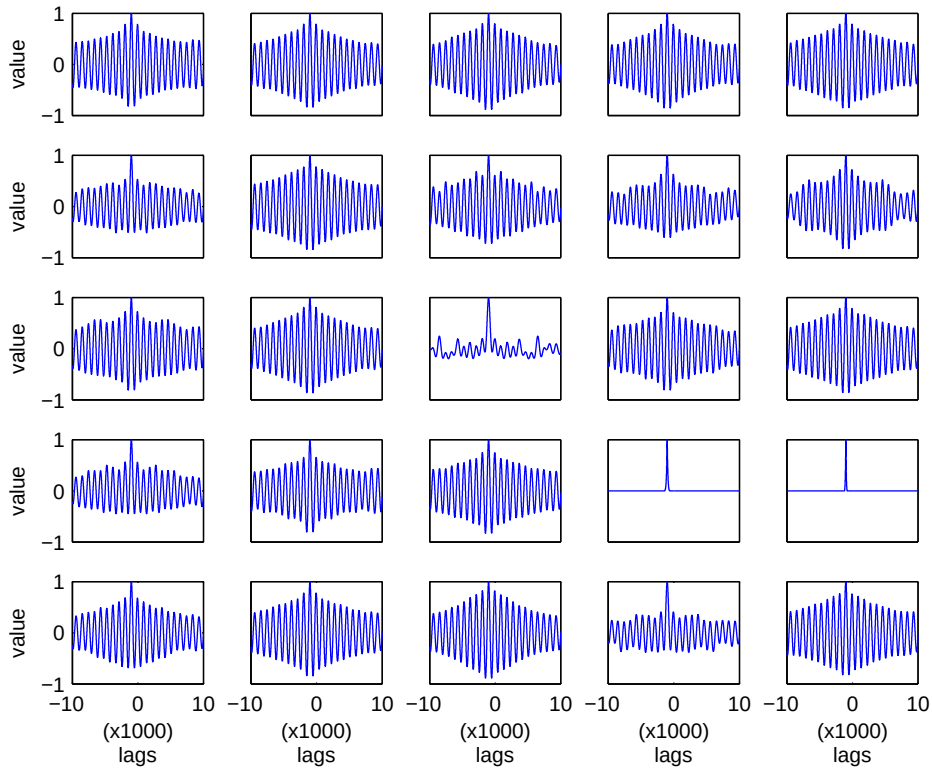

Figure G.59: Cross-correlation analysis for odour 5: trained input vs. 0% difference input. The Cross-correlation analysis was carried out between the response of the olfactory bulb of the trained input and the input minus a percentage of the difference between input value and the limit range for the input. Plots are sorted from left to right and from up to down, starting from the cross-corelation between for the first mitral cell (the first column and first row) up to the 25th mitral cell in the last column at the bottom. Plots with zero response result from Mitral cells which remain silent for this particular input. The time constants of both the ORN and mitral cells were set to $\tilde{\tau}_m \approx 10$ ms, with a threshold potential, $V_{th} = 50000$. The time constants of the excitatory synapses were set to $\tilde{\tau}_E \approx 4$ ms, whereas for the inhibitory synapses the time constants were set to $\tilde{\tau}_I \approx 16$ ms. For the ORNs, constant values randomly selected in a range between 500 and 1000, were used to represent a constant concentration of each odor stimulus. The total running time in terms of biological values is equivalent to 5 seconds at a sampling frequency of $f_{smp} = 10$ kHz. Although the clock frequency was set to $f_{clk} = 10$ MHz thus each run lasted for 5 ms of the FPGA processing time.

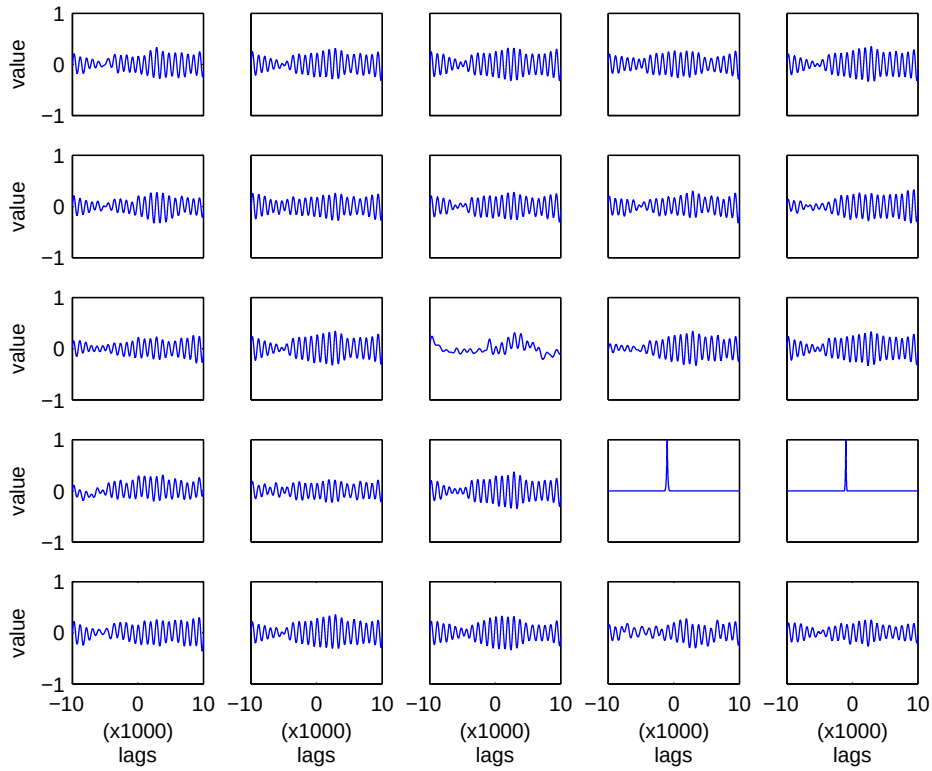

Figure G.60: Cross-correlation analysis for odour 5: trained input vs. +4% difference input. The Cross-correlation analysis was carried out between the response of the olfactory bulb of the trained input and the input minus a percentage of the difference between input value and the limit range for the input. Plots are sorted from left to right and from up to down, starting from the cross-corelation between for the first mitral cell (the first column and first row) up to the 25th mitral cell in the last column at the bottom. Plots with zero response result from Mitral cells which remain silent for this particular input. The time constants of both the ORN and mitral cells were set to $\tilde{\tau}_m \approx 10$ ms, with a threshold potential, $V_{th} = 50000$. The time constants of the excitatory synapses were set to $\tilde{\tau}_E \approx 4$ ms, whereas for the inhibitory synapses the time constants were set to $\tilde{\tau}_I \approx 16$ ms. For the ORNs, constant values randomly selected in a range between 500 and 1000, were used to represent a constant concentration of each odor stimulus. The total running time in terms of biological values is equivalent to 5 seconds at a sampling frequency of $f_{smp} = 10$ kHz. Although the clock frequency was set to $f_{clk} = 10$ MHz thus each run lasted for 5 ms of the FPGA processing time.

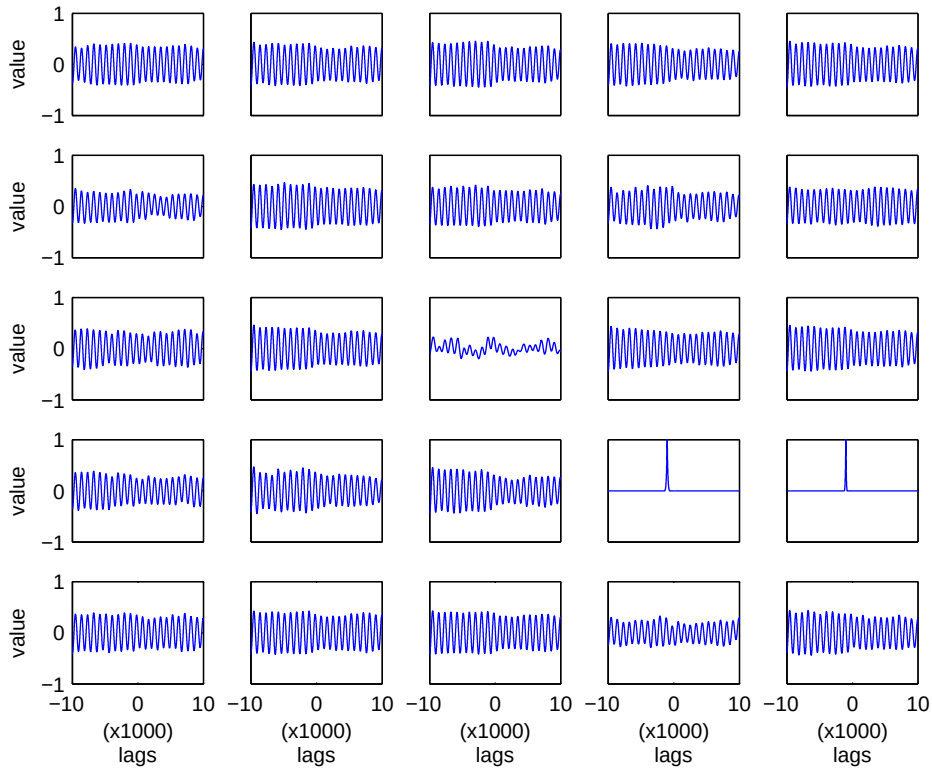

Figure G.61: Cross-correlation analysis for odour 5: trained input vs. +10% difference input. The Cross-correlation analysis was carried out between the response of the olfactory bulb of the trained input and the input minus a percentage of the difference between input value and the limit range for the input. Plots are sorted from left to right and from up to down, starting from the cross-corelation between for the first mitral cell (the first column and first row) up to the 25th mitral cell in the last column at the bottom. Plots with zero response result from Mitral cells which remain silent for this particular input. The time constants of both the ORN and mitral cells were set to $\tilde{\tau}_m \approx 10$ ms, with a threshold potential, $V_{th} = 50000$. The time constants of the excitatory synapses were set to $\tilde{\tau}_E \approx 4$ ms, whereas for the inhibitory synapses the time constants were set to $\tilde{\tau}_I \approx 16$ ms. For the ORNs, constant values randomly selected in a range between 500 and 1000, were used to represent a constant concentration of each odor stimulus. The total running time in terms of biological values is equivalent to 5 seconds at a sampling frequency of $f_{smp} = 10$ kHz. Although the clock frequency was set to $f_{clk} = 10$ MHz thus each run lasted for 5 ms of the FPGA processing time.

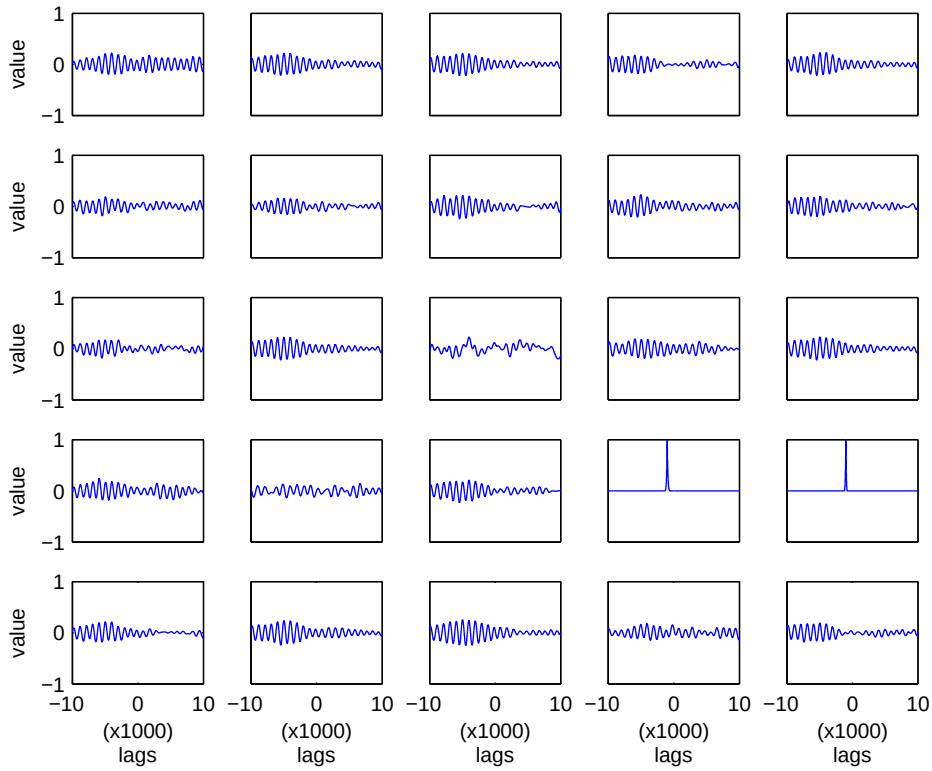

Figure G.62: Cross-correlation analysis for odour 5: trained input vs. +20% difference input. The Cross-correlation analysis was carried out between the response of the olfactory bulb of the trained input and the input minus a percentage of the difference between input value and the limit range for the input. Plots are sorted from left to right and from up to down, starting from the cross-corelation between for the first mitral cell (the first column and first row) up to the 25th mitral cell in the last column at the bottom. Plots with zero response result from Mitral cells which remain silent for this particular input. The time constants of both the ORN and mitral cells were set to $\tilde{\tau}_m \approx 10$ ms, with a threshold potential, $V_{th} = 50000$. The time constants of the excitatory synapses were set to $\tilde{\tau}_E \approx 4$ ms, whereas for the inhibitory synapses the time constants were set to $\tilde{\tau}_I \approx 16$ ms. For the ORNs, constant values randomly selected in a range between 500 and 1000, were used to represent a constant concentration of each odor stimulus. The total running time in terms of biological values is equivalent to 5 seconds at a sampling frequency of $f_{smp} = 10$ kHz. Although the clock frequency was set to $f_{clk} = 10$ MHz thus each run lasted for 5 ms of the FPGA processing time.

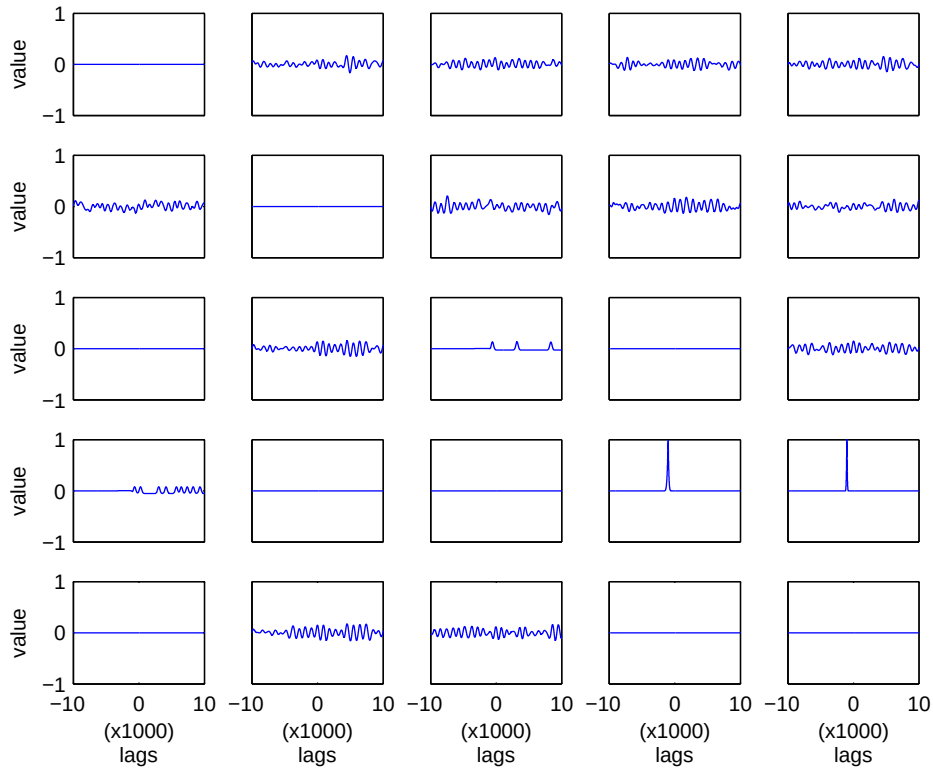

Figure G.63: Cross-correlation analysis for odour 5: trained input vs. +40% difference input. The Cross-correlation analysis was carried out between the response of the olfactory bulb of the trained input and the input minus a percentage of the difference between input value and the limit range for the input. Plots are sorted from left to right and from up to down, starting from the cross-corelation between for the first mitral cell (the first column and first row) up to the 25th mitral cell in the last column at the bottom. Plots with zero response result from Mitral cells which remain silent for this particular input. The time constants of both the ORN and mitral cells were set to $\tilde{\tau}_m \approx 10$ ms, with a threshold potential, $V_{th} = 50000$. The time constants of the excitatory synapses were set to $\tilde{\tau}_E \approx 4$ ms, whereas for the inhibitory synapses the time constants were set to $\tilde{\tau}_I \approx 16$ ms. For the ORNs, constant values randomly selected in a range between 500 and 1000, were used to represent a constant concentration of each odor stimulus. The total running time in terms of biological values is equivalent to 5 seconds at a sampling frequency of $f_{smp} = 10$ kHz. Although the clock frequency was set to $f_{clk} = 10$ MHz thus each run lasted for 5 ms of the FPGA processing time.

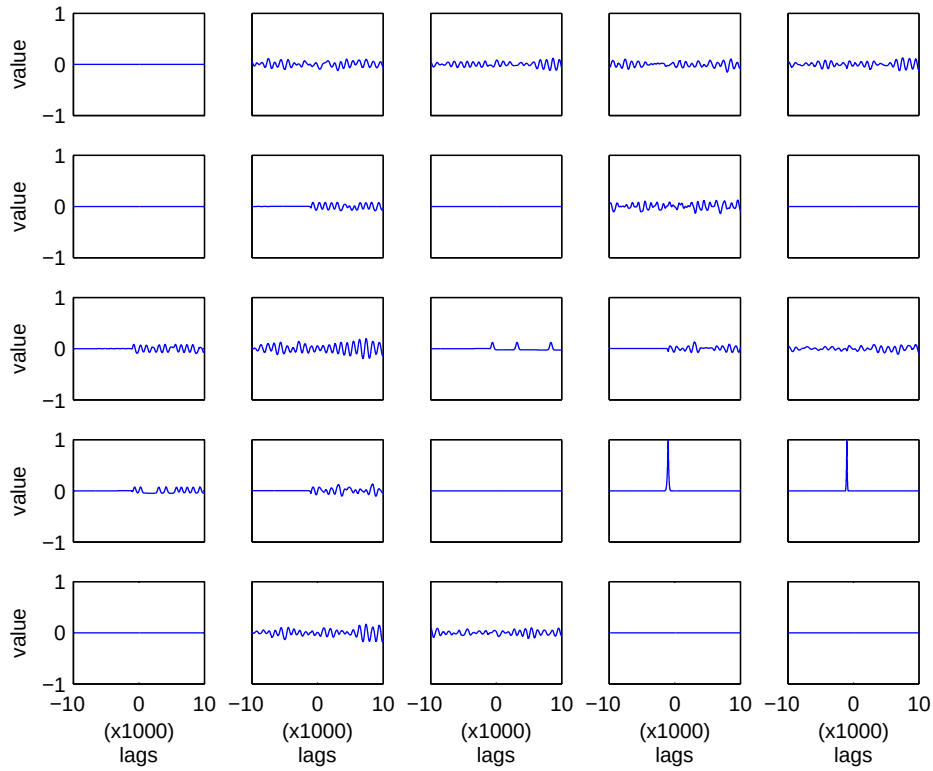

Figure G.64: Cross-correlation analysis for odour 5: trained input vs. +60% difference input. The Cross-correlation analysis was carried out between the response of the olfactory bulb of the trained input and the input minus a percentage of the difference between input value and the limit range for the input. Plots are sorted from left to right and from up to down, starting from the cross-corelation between for the first mitral cell (the first column and first row) up to the 25th mitral cell in the last column at the bottom. Plots with zero response result from Mitral cells which remain silent for this particular input. The time constants of both the ORN and mitral cells were set to $\tilde{\tau}_m \approx 10$ ms, with a threshold potential, $V_{th} = 50000$. The time constants of the excitatory synapses were set to $\tilde{\tau}_E \approx 4$ ms, whereas for the inhibitory synapses the time constants were set to $\tilde{\tau}_I \approx 16$ ms. For the ORNs, constant values randomly selected in a range between 500 and 1000, were used to represent a constant concentration of each odor stimulus. The total running time in terms of biological values is equivalent to 5 seconds at a sampling frequency of $f_{smp} = 10$ kHz. Although the clock frequency was set to $f_{clk} = 10$ MHz thus each run lasted for 5 ms of the FPGA processing time.

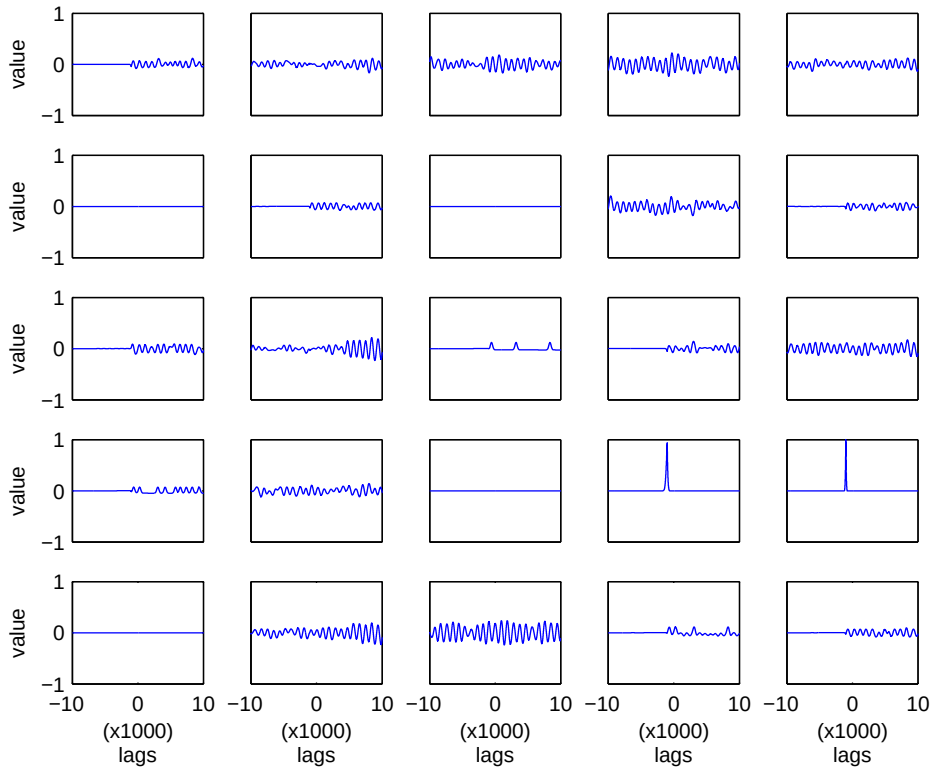

Figure G.65: Cross-correlation analysis for odour 5: trained input vs. +80% difference input. The Cross-correlation analysis was carried out between the response of the olfactory bulb of the trained input and the input minus a percentage of the difference between input value and the limit range for the input. Plots are sorted from left to right and from up to down, starting from the cross-corelation between for the first mitral cell (the first column and first row) up to the 25th mitral cell in the last column at the bottom. Plots with zero response result from Mitral cells which remain silent for this particular input. The time constants of both the ORN and mitral cells were set to $\tilde{\tau}_m \approx 10$ ms, with a threshold potential, $V_{th} = 50000$. The time constants of the excitatory synapses were set to $\tilde{\tau}_E \approx 4$ ms, whereas for the inhibitory synapses the time constants were set to $\tilde{\tau}_I \approx 16$ ms. For the ORNs, constant values randomly selected in a range between 500 and 1000, were used to represent a constant concentration of each odor stimulus. The total running time in terms of biological values is equivalent to 5 seconds at a sampling frequency of $f_{smp} = 10$ kHz. Although the clock frequency was set to $f_{clk} = 10$ MHz thus each run lasted for 5 ms of the FPGA processing time.

H. Evolution of the Cross-correlation over the progressive scanning of the inhibitory weights.

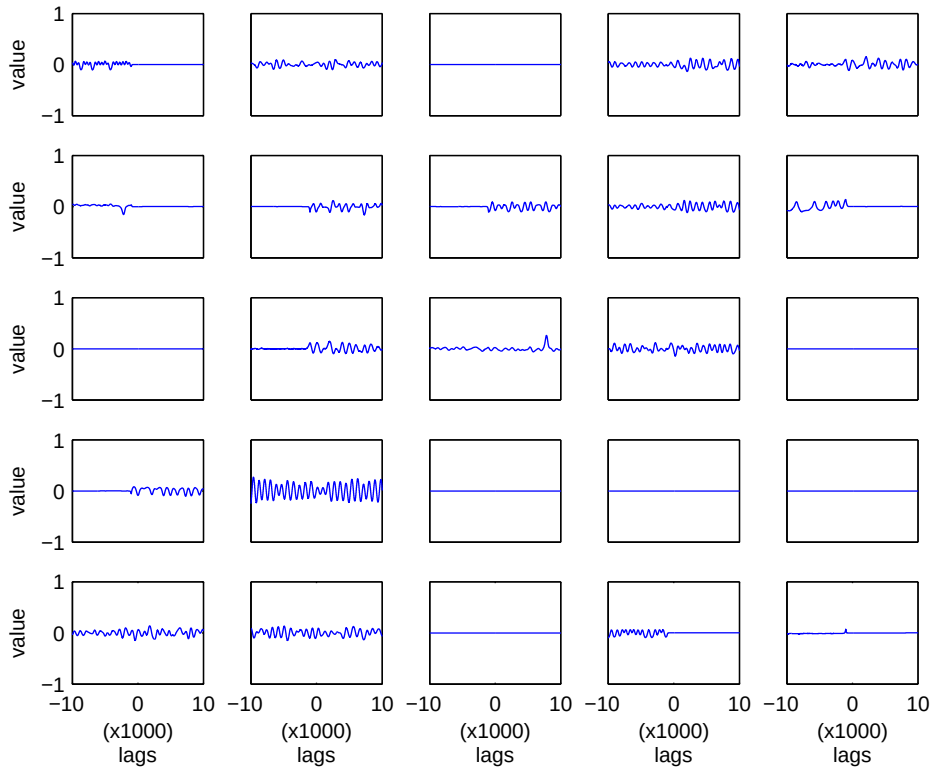

Figure H.1: Cross-correlation analysis for odour 1: trained weights vs. -80% difference weights. The Cross-correlation analysis was carried out between the response of the olfactory bulb of the trained weights and the weights minus a percentage of the difference between weight values and the limit range for the weights. Plots are sorted from left to right and from up to down, starting from the cross-corelation between for the first mitral cell (the first column and first row) up to the 25th mitral cell in the last column at the bottom. Plots with zero response result from Mitral cells which remain silent for these particular weight values. The time constants of both the ORN and mitral cells were set to $\tilde{\tau}_m \approx 10$ ms, with a threshold potential, $V_{th} = 50000$. The time constants of the excitatory synapses were set to $\tilde{\tau}_E \approx 4$ ms, whereas for the inhibitory synapses the time constants were set to $\tilde{\tau}_I \approx 16$ ms. For the ORNs, constant values randomly selected in a range between 500 and 1000, were used to represent a constant concentration of each odor stimulus. The total running time in terms of biological values is equivalent to 5 seconds at a sampling frequency of $f_{smp} = 10$ kHz. Although the clock frequency was set to $f_{clk} = 10$ MHz thus each run lasted for 5 ms of the FPGA processing time.

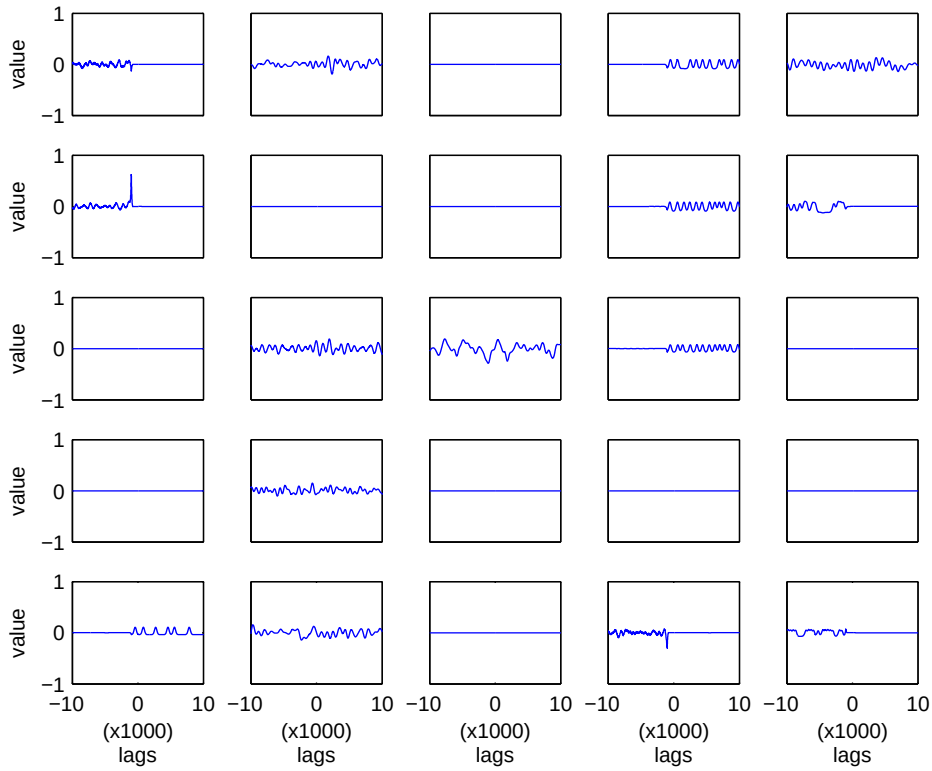

Figure H.2: Cross-correlation analysis for odour 1: trained weights vs. -60% difference weights. The Cross-correlation analysis was carried out between the response of the olfactory bulb of the trained weights and the weights minus a percentage of the difference between weight values and the limit range for the weights. Plots are sorted from left to right and from up to down, starting from the cross-corelation between for the first mitral cell (the first column and first row) up to the 25th mitral cell in the last column at the bottom. Plots with zero response result from Mitral cells which remain silent for these particular weight values. The time constants of both the ORN and mitral cells were set to $\tilde{\tau}_m \approx 10$ ms, with a threshold potential, $V_{th} = 50000$. The time constants of the excitatory synapses were set to $\tilde{\tau}_E \approx 4$ ms, whereas for the inhibitory synapses the time constants were set to $\tilde{\tau}_I \approx 16$ ms. For the ORNs, constant values randomly selected in a range between 500 and 1000, were used to represent a constant concentration of each odor stimulus. The total running time in terms of biological values is equivalent to 5 seconds at a sampling frequency of $f_{smp} = 10$ kHz. Although the clock frequency was set to $f_{clk} = 10$ MHz thus each run lasted for 5 ms of the FPGA processing time.

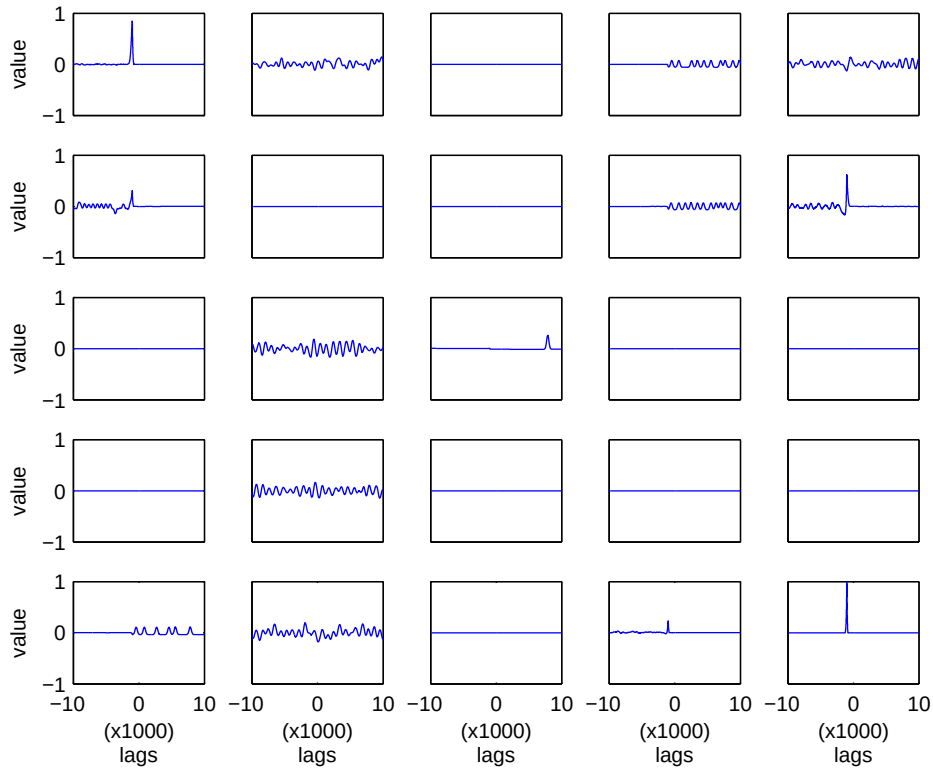

Figure H.3: Cross-correlation analysis for odour 1: trained weights vs. -40% difference weights. The Cross-correlation analysis was carried out between the response of the olfactory bulb of the trained weights and the weights minus a percentage of the difference between weight values and the limit range for the weights. Plots are sorted from left to right and from up to down, starting from the cross-corelation between for the first mitral cell (the first column and first row) up to the 25th mitral cell in the last column at the bottom. Plots with zero response result from Mitral cells which remain silent for these particular weight values. The time constants of both the ORN and mitral cells were set to $\tilde{\tau}_m \approx 10$ ms, with a threshold potential, $V_{th} = 50000$. The time constants of the excitatory synapses were set to $\tilde{\tau}_E \approx 4$ ms, whereas for the inhibitory synapses the time constants were set to $\tilde{\tau}_I \approx 16$ ms. For the ORNs, constant values randomly selected in a range between 500 and 1000, were used to represent a constant concentration of each odor stimulus. The total running time in terms of biological values is equivalent to 5 seconds at a sampling frequency of $f_{smp} = 10$ kHz. Although the clock frequency was set to $f_{clk} = 10$ MHz thus each run lasted for 5 ms of the FPGA processing time.

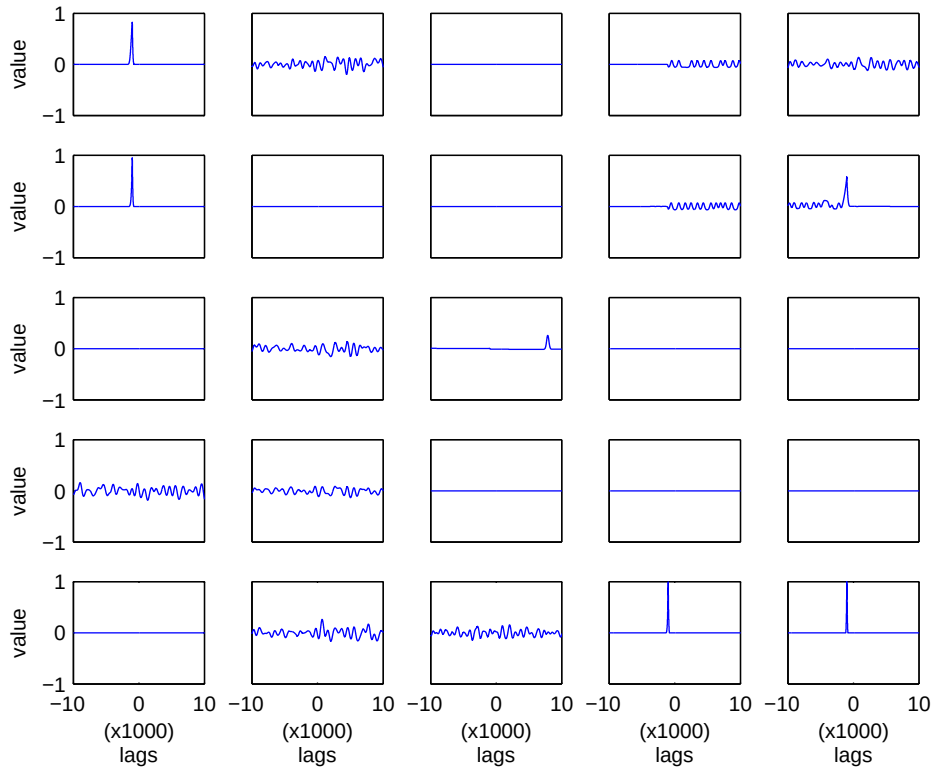

Figure H.4: Cross-correlation analysis for odour 1: trained weights vs. -20% difference weights. The Cross-correlation analysis was carried out between the response of the olfactory bulb of the trained weights and the weights minus a percentage of the difference between weight values and the limit range for the weights. Plots are sorted from left to right and from up to down, starting from the cross-corelation between for the first mitral cell (the first column and first row) up to the 25th mitral cell in the last column at the bottom. Plots with zero response result from Mitral cells which remain silent for these particular weight values. The time constants of both the ORN and mitral cells were set to $\tilde{\tau}_m \approx 10$ ms, with a threshold potential, $V_{th} = 50000$. The time constants of the excitatory synapses were set to $\tilde{\tau}_E \approx 4$ ms, whereas for the inhibitory synapses the time constants were set to $\tilde{\tau}_I \approx 16$ ms. For the ORNs, constant values randomly selected in a range between 500 and 1000, were used to represent a constant concentration of each odor stimulus. The total running time in terms of biological values is equivalent to 5 seconds at a sampling frequency of $f_{smp} = 10$ kHz. Although the clock frequency was set to $f_{clk} = 10$ MHz thus each run lasted for 5 ms of the FPGA processing time.

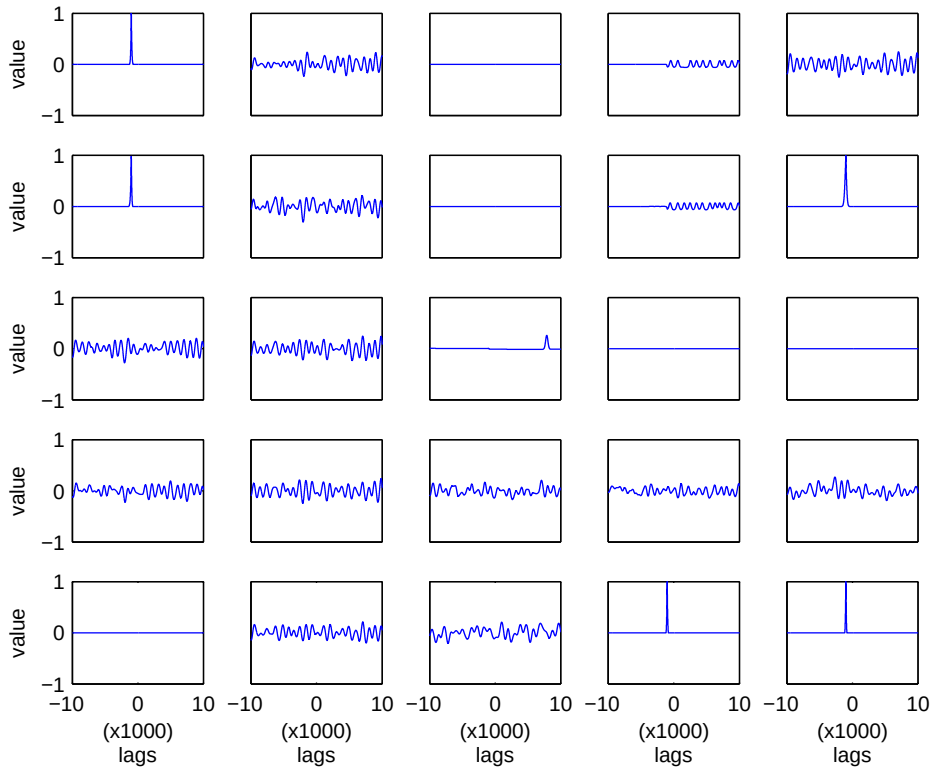

Figure H.5: Cross-correlation analysis for odour 1: trained weights vs. -10% difference weights. The Cross-correlation analysis was carried out between the response of the olfactory bulb of the trained weights and the weights minus a percentage of the difference between weight values and the limit range for the weights. Plots are sorted from left to right and from up to down, starting from the cross-corelation between for the first mitral cell (the first column and first row) up to the 25th mitral cell in the last column at the bottom. Plots with zero response result from Mitral cells which remain silent for these particular weight values. The time constants of both the ORN and mitral cells were set to $\tilde{\tau}_m \approx 10$ ms, with a threshold potential, $V_{th} = 50000$. The time constants of the excitatory synapses were set to $\tilde{\tau}_E \approx 4$ ms, whereas for the inhibitory synapses the time constants were set to $\tilde{\tau}_I \approx 16$ ms. For the ORNs, constant values randomly selected in a range between 500 and 1000, were used to represent a constant concentration of each odor stimulus. The total running time in terms of biological values is equivalent to 5 seconds at a sampling frequency of $f_{smp} = 10$ kHz. Although the clock frequency was set to $f_{clk} = 10$ MHz thus each run lasted for 5 ms of the FPGA processing time.

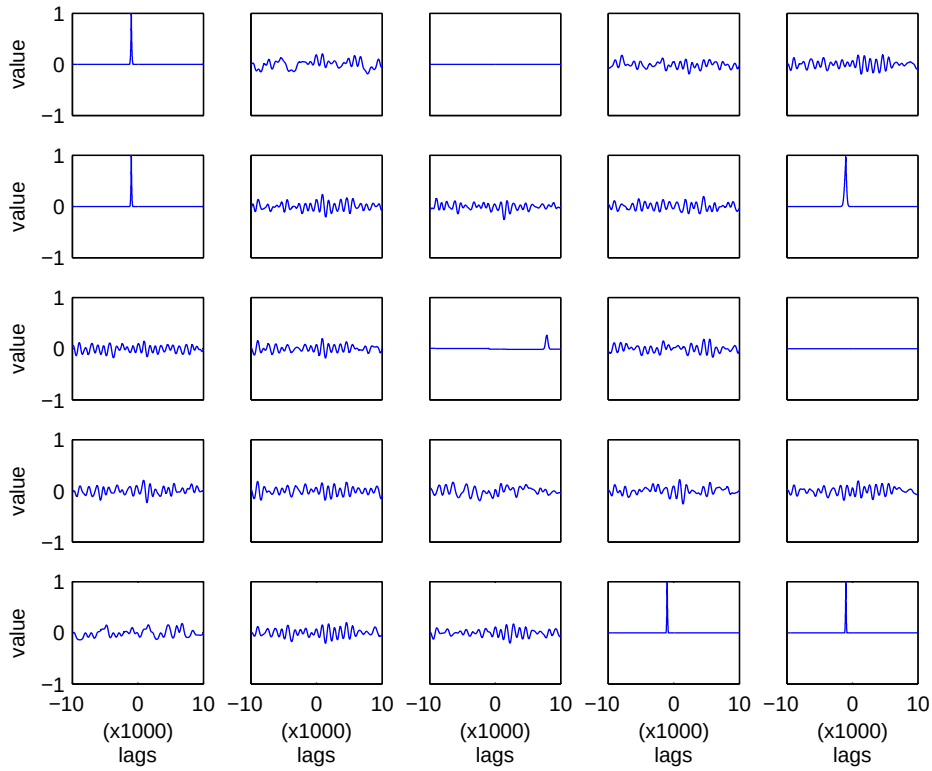

Figure H.6: Cross-correlation analysis for odour 1: trained weights vs. -4% difference weights. The Cross-correlation analysis was carried out between the response of the olfactory bulb of the trained weights and the weights minus a percentage of the difference between weight values and the limit range for the weights. Plots are sorted from left to right and from up to down, starting from the cross-corelation between for the first mitral cell (the first column and first row) up to the 25th mitral cell in the last column at the bottom. Plots with zero response result from Mitral cells which remain silent for these particular weight values. The time constants of both the ORN and mitral cells were set to $\tilde{\tau}_m \approx 10$ ms, with a threshold potential, $V_{th} = 50000$. The time constants of the excitatory synapses were set to $\tilde{\tau}_E \approx 4$ ms, whereas for the inhibitory synapses the time constants were set to $\tilde{\tau}_I \approx 16$ ms. For the ORNs, constant values randomly selected in a range between 500 and 1000, were used to represent a constant concentration of each odor stimulus. The total running time in terms of biological values is equivalent to 5 seconds at a sampling frequency of $f_{smp} = 10$ kHz. Although the clock frequency was set to $f_{clk} = 10$ MHz thus each run lasted for 5 ms of the FPGA processing time.

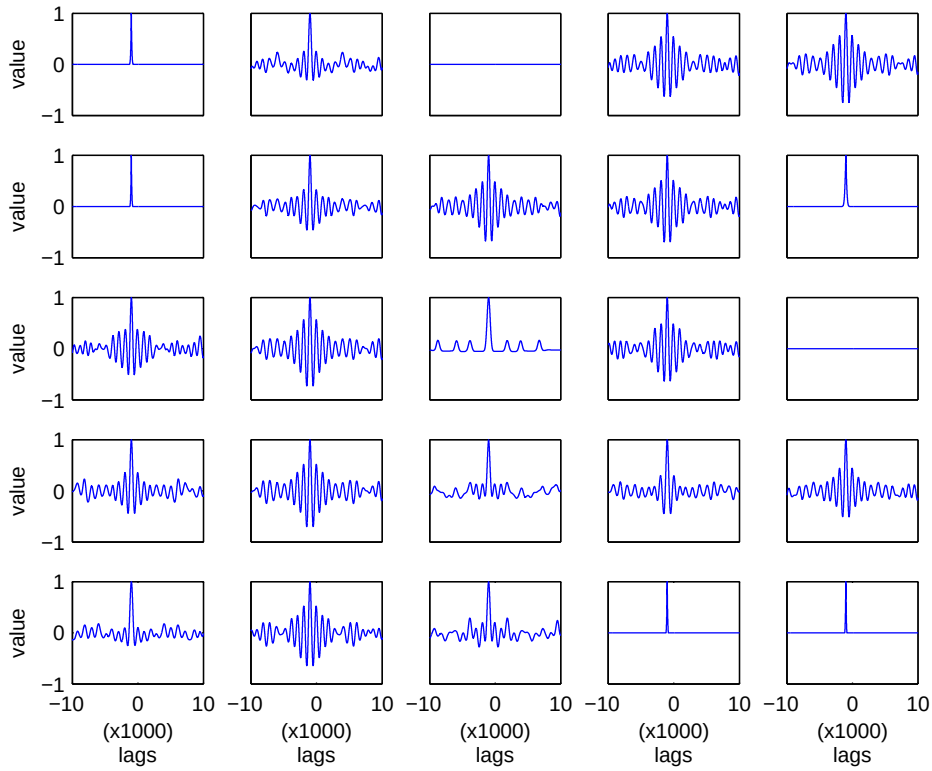

Figure H.7: Cross-correlation analysis for odour 1: trained weights vs. 0% difference weights. The Cross-correlation analysis was carried out between the response of the olfactory bulb of the trained weights and the weights minus a percentage of the difference between weight values and the limit range for the weights. Plots are sorted from left to right and from up to down, starting from the cross-corelation between for the first mitral cell (the first column and first row) up to the 25th mitral cell in the last column at the bottom. Plots with zero response result from Mitral cells which remain silent for these particular weight values. The time constants of both the ORN and mitral cells were set to $\tilde{\tau}_m \approx 10$ ms, with a threshold potential, $V_{th} = 50000$. The time constants of the excitatory synapses were set to $\tilde{\tau}_E \approx 4$ ms, whereas for the inhibitory synapses the time constants were set to $\tilde{\tau}_I \approx 16$ ms. For the ORNs, constant values randomly selected in a range between 500 and 1000, were used to represent a constant concentration of each odor stimulus. The total running time in terms of biological values is equivalent to 5 seconds at a sampling frequency of $f_{smp} = 10$ kHz. Although the clock frequency was set to $f_{clk} = 10$ MHz thus each run lasted for 5 ms of the FPGA processing time.

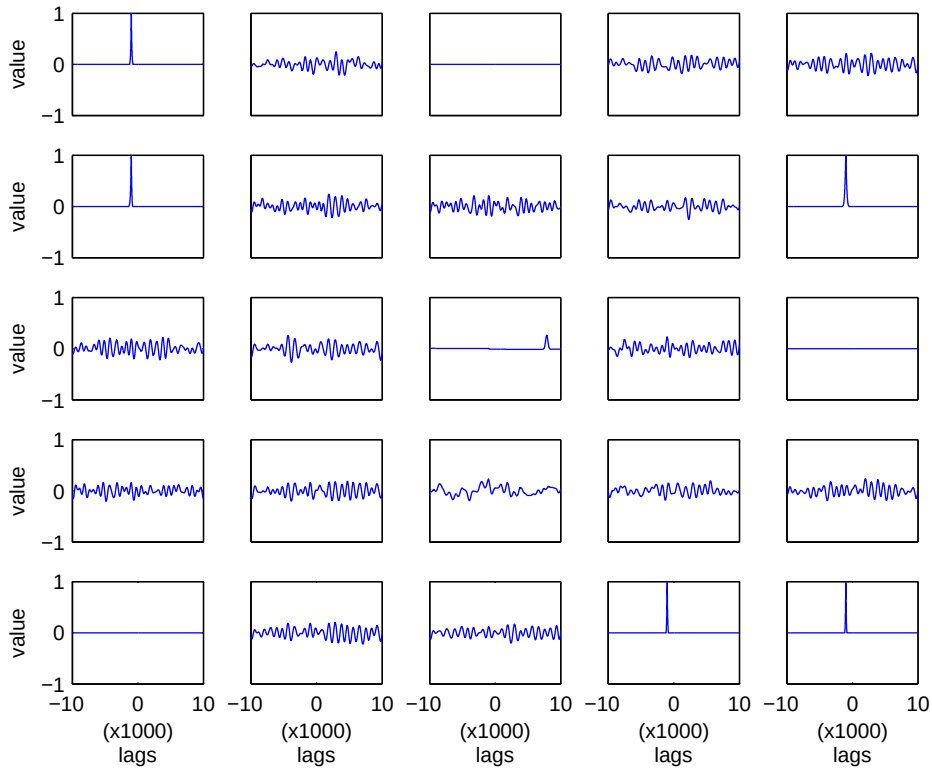

Figure H.8: Cross-correlation analysis for odour 1: trained weights vs. +4% difference weights. The Cross-correlation analysis was carried out between the response of the olfactory bulb of the trained weights and the weights minus a percentage of the difference between weight values and the limit range for the weights. Plots are sorted from left to right and from up to down, starting from the cross-corelation between for the first mitral cell (the first column and first row) up to the 25th mitral cell in the last column at the bottom. Plots with zero response result from Mitral cells which remain silent for these particular weight values. The time constants of both the ORN and mitral cells were set to $\tilde{\tau}_m \approx 10$ ms, with a threshold potential, $V_{th} = 50000$. The time constants of the excitatory synapses were set to $\tilde{\tau}_E \approx 4$ ms, whereas for the inhibitory synapses the time constants were set to $\tilde{\tau}_I \approx 16$ ms. For the ORNs, constant values randomly selected in a range between 500 and 1000, were used to represent a constant concentration of each odor stimulus. The total running time in terms of biological values is equivalent to 5 seconds at a sampling frequency of $f_{smp} = 10$ kHz. Although the clock frequency was set to $f_{clk} = 10$ MHz thus each run lasted for 5 ms of the FPGA processing time.

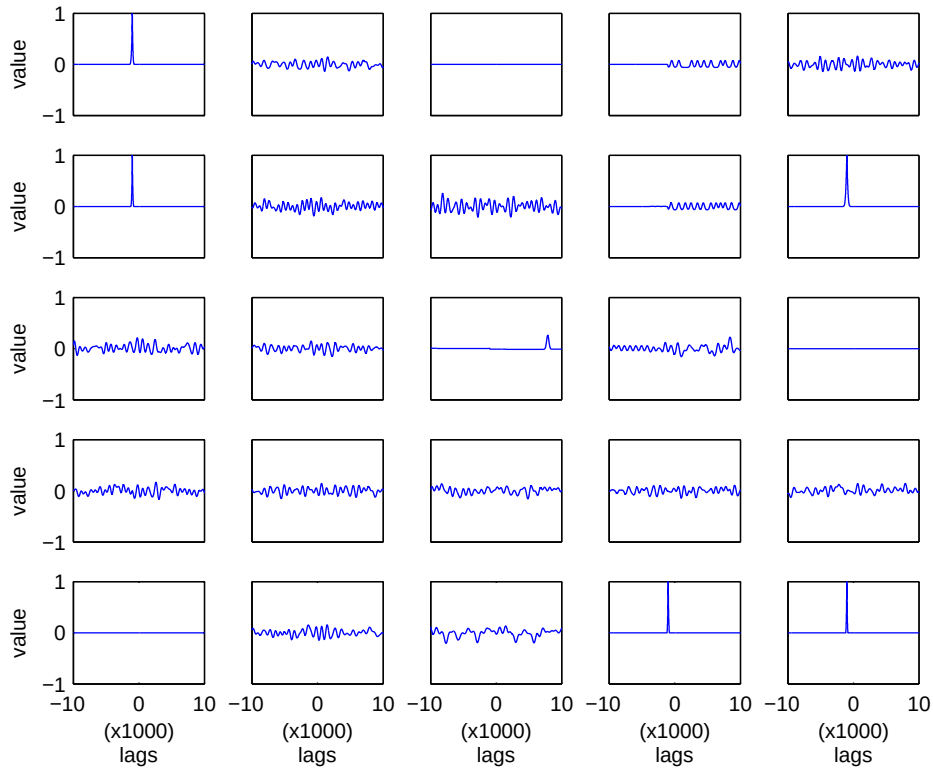

Figure H.9: Cross-correlation analysis for odour 1: trained weights vs. +10% difference weights. The Cross-correlation analysis was carried out between the response of the olfactory bulb of the trained weights and the weights minus a percentage of the difference between weight values and the limit range for the weights. Plots are sorted from left to right and from up to down, starting from the cross-corelation between for the first mitral cell (the first column and first row) up to the 25th mitral cell in the last column at the bottom. Plots with zero response result from Mitral cells which remain silent for these particular weight values. The time constants of both the ORN and mitral cells were set to $\tilde{\tau}_m \approx 10$ ms, with a threshold potential, $V_{th} = 50000$. The time constants of the excitatory synapses were set to $\tilde{\tau}_E \approx 4$ ms, whereas for the inhibitory synapses the time constants were set to $\tilde{\tau}_I \approx 16$ ms. For the ORNs, constant values randomly selected in a range between 500 and 1000, were used to represent a constant concentration of each odor stimulus. The total running time in terms of biological values is equivalent to 5 seconds at a sampling frequency of $f_{smp} = 10$ kHz. Although the clock frequency was set to $f_{clk} = 10$ MHz thus each run lasted for 5 ms of the FPGA processing time.

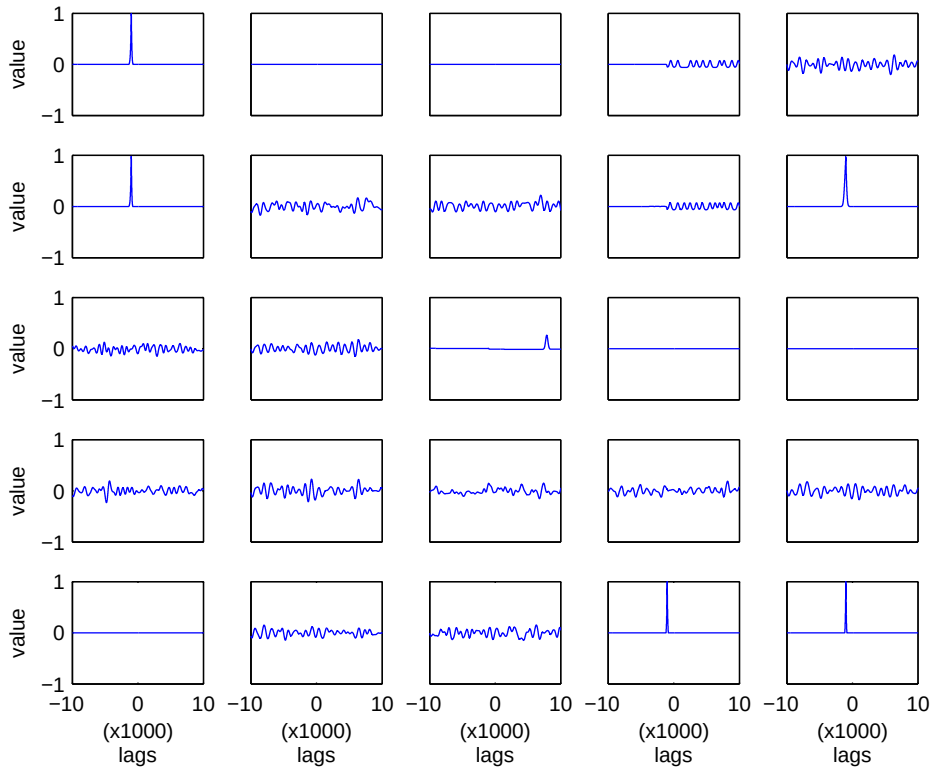

Figure H.10: Cross-correlation analysis for odour 1: trained weights vs. +20% difference weights. The Cross-correlation analysis was carried out between the response of the olfactory bulb of the trained weights and the weights minus a percentage of the difference between weight values and the limit range for the weights. Plots are sorted from left to right and from up to down, starting from the cross-corelation between for the first mitral cell (the first column and first row) up to the 25th mitral cell in the last column at the bottom. Plots with zero response result from Mitral cells which remain silent for these particular weight values. The time constants of both the ORN and mitral cells were set to $\tilde{\tau}_m \approx 10$ ms, with a threshold potential, $V_{th} = 50000$. The time constants of the excitatory synapses were set to $\tilde{\tau}_E \approx 4$ ms, whereas for the inhibitory synapses the time constants were set to $\tilde{\tau}_I \approx 16$ ms. For the ORNs, constant values randomly selected in a range between 500 and 1000, were used to represent a constant concentration of each odor stimulus. The total running time in terms of biological values is equivalent to 5 seconds at a sampling frequency of $f_{smp} = 10$ kHz. Although the clock frequency was set to $f_{clk} = 10$ MHz thus each run lasted for 5 ms of the FPGA processing time.

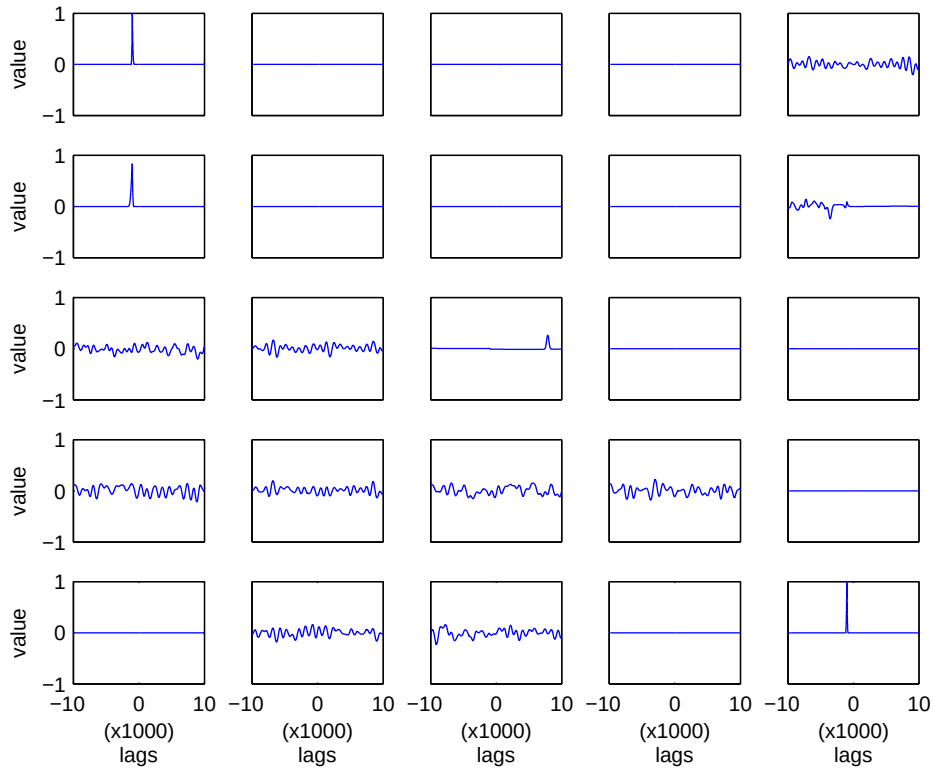

Figure H.11: Cross-correlation analysis for odour 1: trained weights vs. +40% difference weights. The Cross-correlation analysis was carried out between the response of the olfactory bulb of the trained weights and the weights minus a percentage of the difference between weight values and the limit range for the weights. Plots are sorted from left to right and from up to down, starting from the cross-corelation between for the first mitral cell (the first column and first row) up to the 25th mitral cell in the last column at the bottom. Plots with zero response result from Mitral cells which remain silent for these particular weight values. The time constants of both the ORN and mitral cells were set to $\tilde{\tau}_m \approx 10$ ms, with a threshold potential, $V_{th} = 50000$. The time constants of the excitatory synapses were set to $\tilde{\tau}_E \approx 4$ ms, whereas for the inhibitory synapses the time constants were set to $\tilde{\tau}_I \approx 16$ ms. For the ORNs, constant values randomly selected in a range between 500 and 1000, were used to represent a constant concentration of each odor stimulus. The total running time in terms of biological values is equivalent to 5 seconds at a sampling frequency of $f_{smp} = 10$ kHz. Although the clock frequency was set to $f_{clk} = 10$ MHz thus each run lasted for 5 ms of the FPGA processing time.

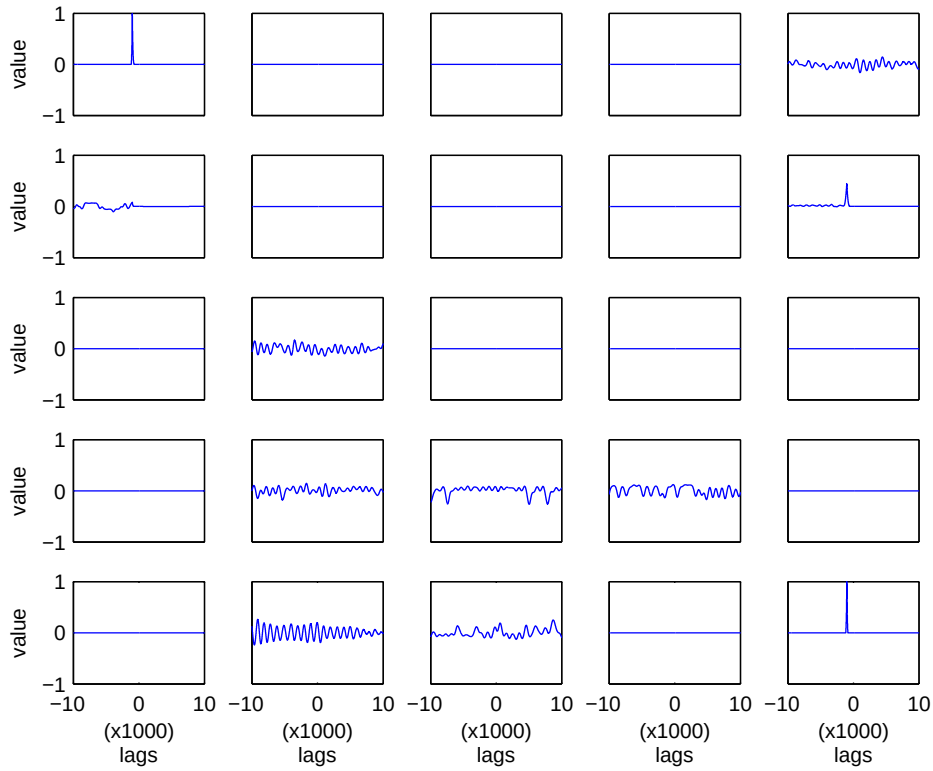

Figure H.12: Cross-correlation analysis for odour 1: trained weights vs. +60% difference weights. The Cross-correlation analysis was carried out between the response of the olfactory bulb of the trained weights and the weights minus a percentage of the difference between weight values and the limit range for the weights. Plots are sorted from left to right and from up to down, starting from the cross-corelation between for the first mitral cell (the first column and first row) up to the 25th mitral cell in the last column at the bottom. Plots with zero response result from Mitral cells which remain silent for these particular weight values. The time constants of both the ORN and mitral cells were set to $\tilde{\tau}_m \approx 10$ ms, with a threshold potential, $V_{th} = 50000$. The time constants of the excitatory synapses were set to $\tilde{\tau}_E \approx 4$ ms, whereas for the inhibitory synapses the time constants were set to $\tilde{\tau}_I \approx 16$ ms. For the ORNs, constant values randomly selected in a range between 500 and 1000, were used to represent a constant concentration of each odor stimulus. The total running time in terms of biological values is equivalent to 5 seconds at a sampling frequency of $f_{smp} = 10$ kHz. Although the clock frequency was set to $f_{clk} = 10$ MHz thus each run lasted for 5 ms of the FPGA processing time.

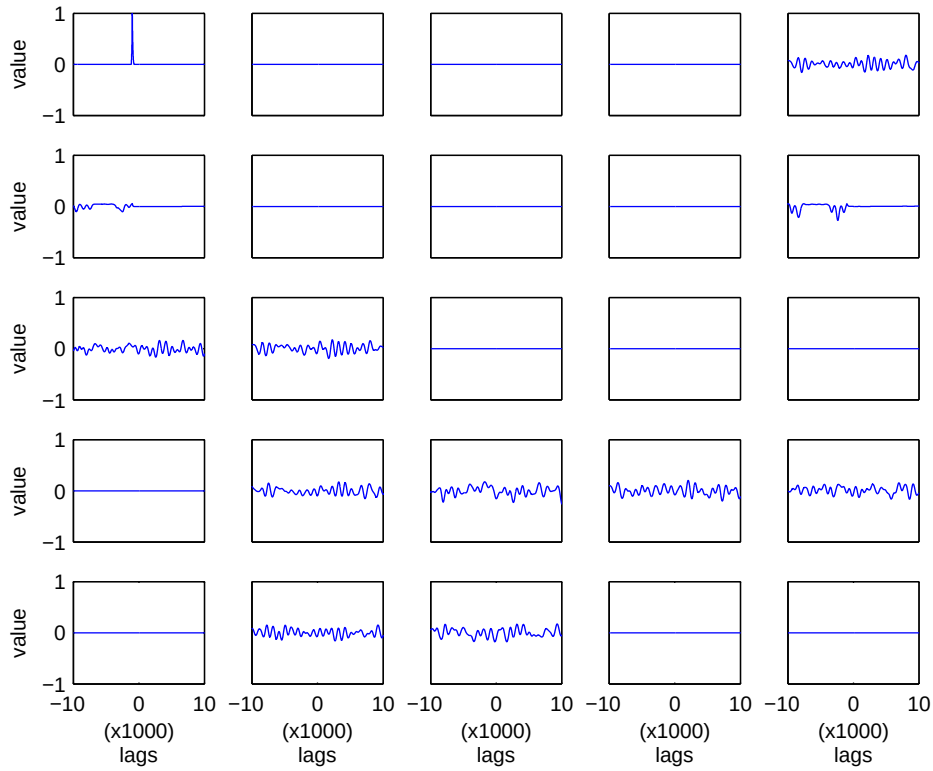

Figure H.13: Cross-correlation analysis for odour 1: trained weights vs. +80% difference weights. The Cross-correlation analysis was carried out between the response of the olfactory bulb of the trained weights and the weights minus a percentage of the difference between weight values and the limit range for the weights. Plots are sorted from left to right and from up to down, starting from the cross-corelation between for the first mitral cell (the first column and first row) up to the 25th mitral cell in the last column at the bottom. Plots with zero response result from Mitral cells which remain silent for these particular weight values. The time constants of both the ORN and mitral cells were set to $\tilde{\tau}_m \approx 10$ ms, with a threshold potential, $V_{th} = 50000$. The time constants of the excitatory synapses were set to $\tilde{\tau}_E \approx 4$ ms, whereas for the inhibitory synapses the time constants were set to $\tilde{\tau}_I \approx 16$ ms. For the ORNs, constant values randomly selected in a range between 500 and 1000, were used to represent a constant concentration of each odor stimulus. The total running time in terms of biological values is equivalent to 5 seconds at a sampling frequency of $f_{smp} = 10$ kHz. Although the clock frequency was set to $f_{clk} = 10$ MHz thus each run lasted for 5 ms of the FPGA processing time.

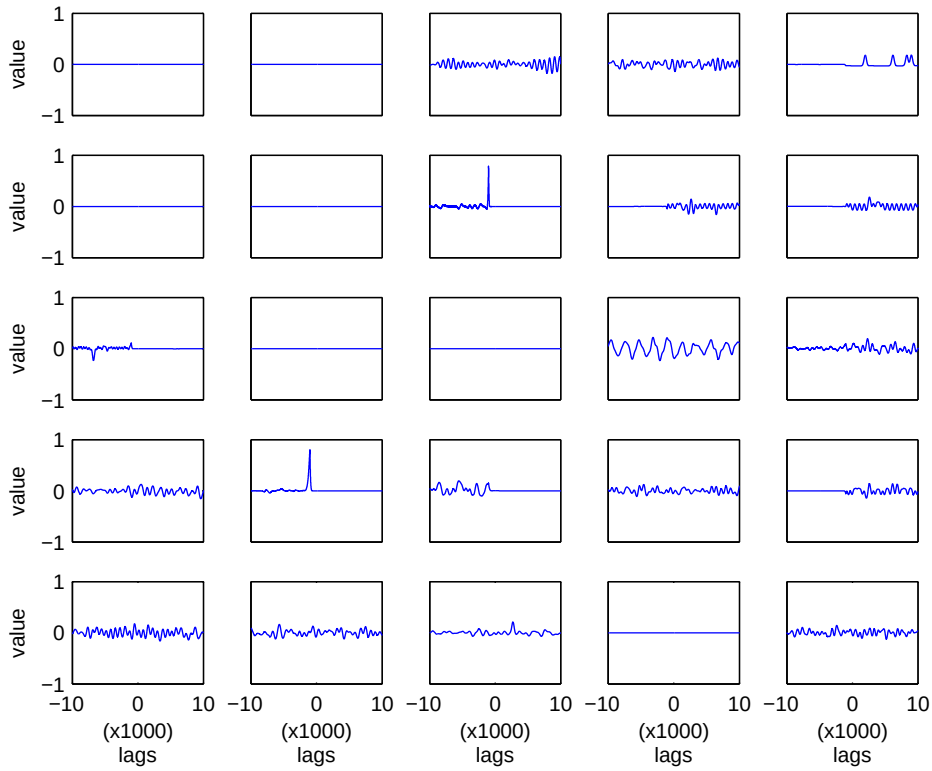

Figure H.14: Cross-correlation analysis for odour 2: trained weights vs. -80% difference weights. The Cross-correlation analysis was carried out between the response of the olfactory bulb of the trained weights and the weights minus a percentage of the difference between weight values and the limit range for the weights. Plots are sorted from left to right and from up to down, starting from the cross-corelation between for the first mitral cell (the first column and first row) up to the 25th mitral cell in the last column at the bottom. Plots with zero response result from Mitral cells which remain silent for these particular weight values. The time constants of both the ORN and mitral cells were set to $\tilde{\tau}_m \approx 10$ ms, with a threshold potential, $V_{th} = 50000$. The time constants of the excitatory synapses were set to $\tilde{\tau}_E \approx 4$ ms, whereas for the inhibitory synapses the time constants were set to $\tilde{\tau}_I \approx 16$ ms. For the ORNs, constant values randomly selected in a range between 500 and 1000, were used to represent a constant concentration of each odor stimulus. The total running time in terms of biological values is equivalent to 5 seconds at a sampling frequency of $f_{smp} = 10$ kHz. Although the clock frequency was set to $f_{clk} = 10$ MHz thus each run lasted for 5 ms of the FPGA processing time.

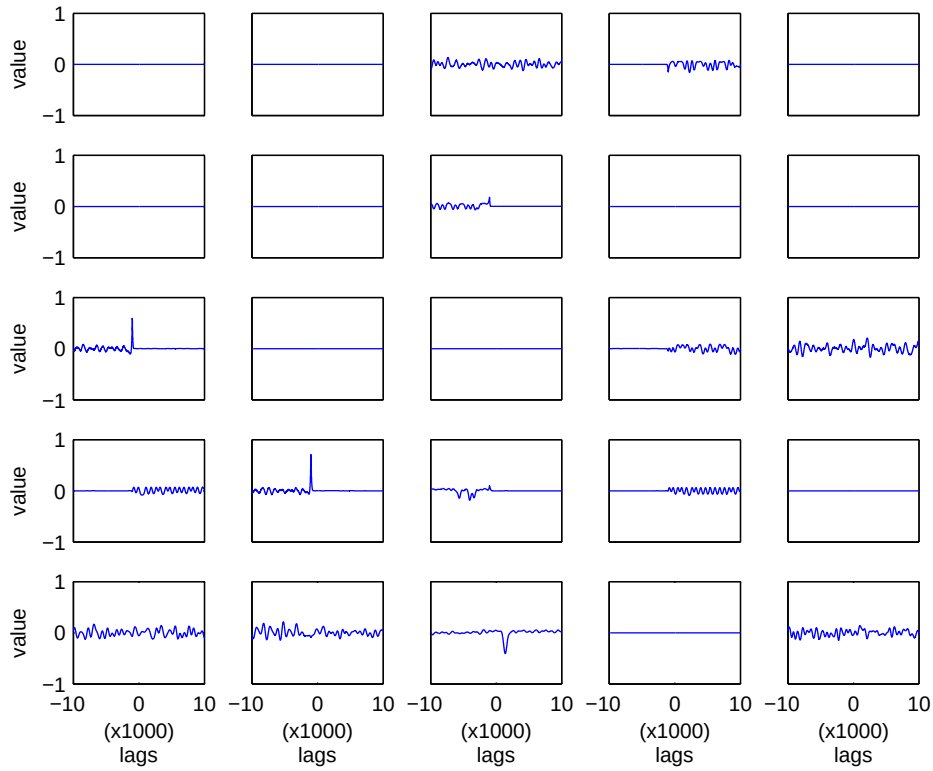

Figure H.15: Cross-correlation analysis for odour 2: trained weights vs. -60% difference weights. The Cross-correlation analysis was carried out between the response of the olfactory bulb of the trained weights and the weights minus a percentage of the difference between weight values and the limit range for the weights. Plots are sorted from left to right and from up to down, starting from the cross-corelation between for the first mitral cell (the first column and first row) up to the 25th mitral cell in the last column at the bottom. Plots with zero response result from Mitral cells which remain silent for these particular weight values. The time constants of both the ORN and mitral cells were set to $\tilde{\tau}_m \approx 10$ ms, with a threshold potential, $V_{th} = 50000$. The time constants of the excitatory synapses were set to $\tilde{\tau}_E \approx 4$ ms, whereas for the inhibitory synapses the time constants were set to $\tilde{\tau}_I \approx 16$ ms. For the ORNs, constant values randomly selected in a range between 500 and 1000, were used to represent a constant concentration of each odor stimulus. The total running time in terms of biological values is equivalent to 5 seconds at a sampling frequency of $f_{smp} = 10$ kHz. Although the clock frequency was set to $f_{clk} = 10$ MHz thus each run lasted for 5 ms of the FPGA processing time.

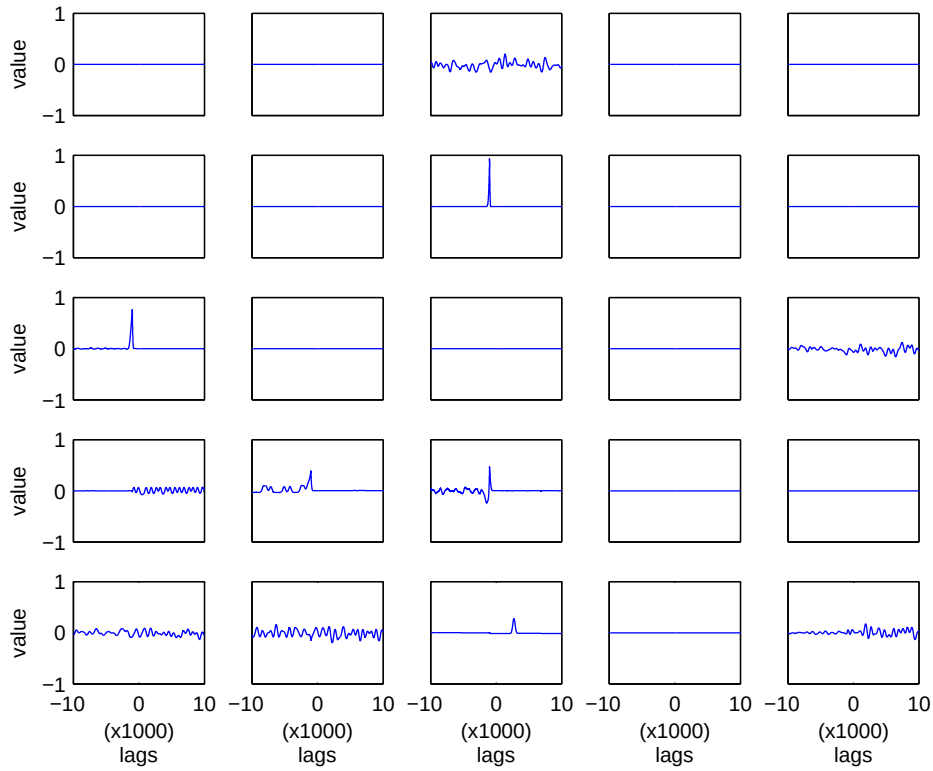

Figure H.16: Cross-correlation analysis for odour 2: trained weights vs. -40% difference weights. The Cross-correlation analysis was carried out between the response of the olfactory bulb of the trained weights and the weights minus a percentage of the difference between weight values and the limit range for the weights. Plots are sorted from left to right and from up to down, starting from the cross-corelation between for the first mitral cell (the first column and first row) up to the 25th mitral cell in the last column at the bottom. Plots with zero response result from Mitral cells which remain silent for these particular weight values. The time constants of both the ORN and mitral cells were set to $\tilde{\tau}_m \approx 10$ ms, with a threshold potential, $V_{th} = 50000$. The time constants of the excitatory synapses were set to $\tilde{\tau}_E \approx 4$ ms, whereas for the inhibitory synapses the time constants were set to $\tilde{\tau}_I \approx 16$ ms. For the ORNs, constant values randomly selected in a range between 500 and 1000, were used to represent a constant concentration of each odor stimulus. The total running time in terms of biological values is equivalent to 5 seconds at a sampling frequency of $f_{smp} = 10$ kHz. Although the clock frequency was set to $f_{clk} = 10$ MHz thus each run lasted for 5 ms of the FPGA processing time.

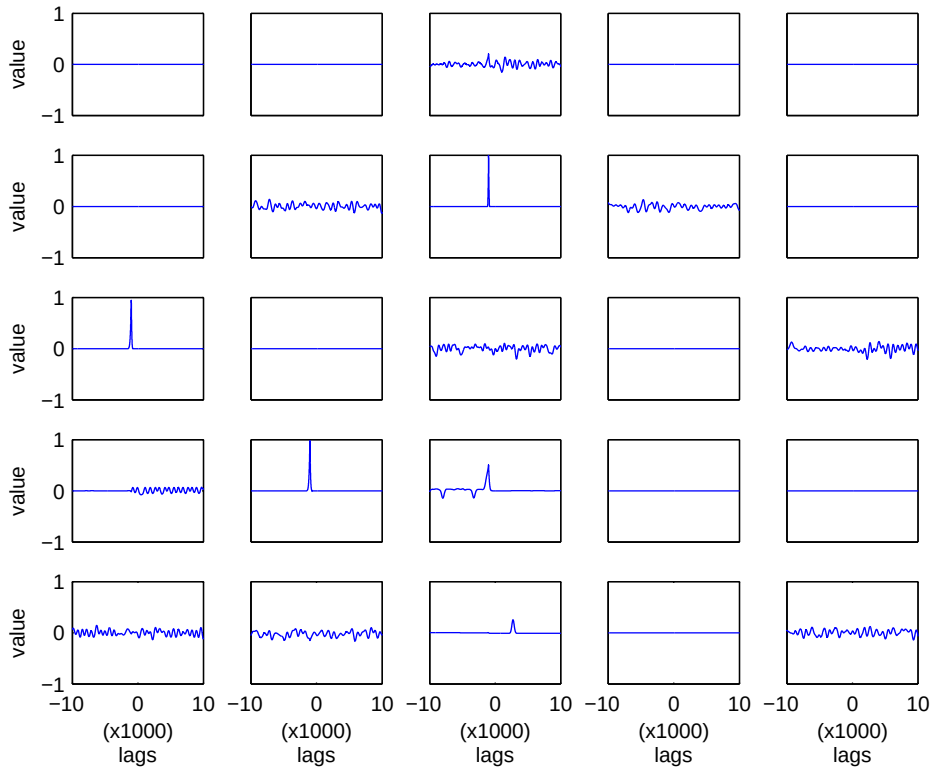

Figure H.17: Cross-correlation analysis for odour 2: trained weights vs. -20% difference weights. The Cross-correlation analysis was carried out between the response of the olfactory bulb of the trained weights and the weights minus a percentage of the difference between weight values and the limit range for the weights. Plots are sorted from left to right and from up to down, starting from the cross-corelation between for the first mitral cell (the first column and first row) up to the 25th mitral cell in the last column at the bottom. Plots with zero response result from Mitral cells which remain silent for these particular weight values. The time constants of both the ORN and mitral cells were set to $\tilde{\tau}_m \approx 10$ ms, with a threshold potential, $V_{th} = 50000$. The time constants of the excitatory synapses were set to $\tilde{\tau}_E \approx 4$ ms, whereas for the inhibitory synapses the time constants were set to $\tilde{\tau}_I \approx 16$ ms. For the ORNs, constant values randomly selected in a range between 500 and 1000, were used to represent a constant concentration of each odor stimulus. The total running time in terms of biological values is equivalent to 5 seconds at a sampling frequency of $f_{smp} = 10$ kHz. Although the clock frequency was set to $f_{clk} = 10$ MHz thus each run lasted for 5 ms of the FPGA processing time.

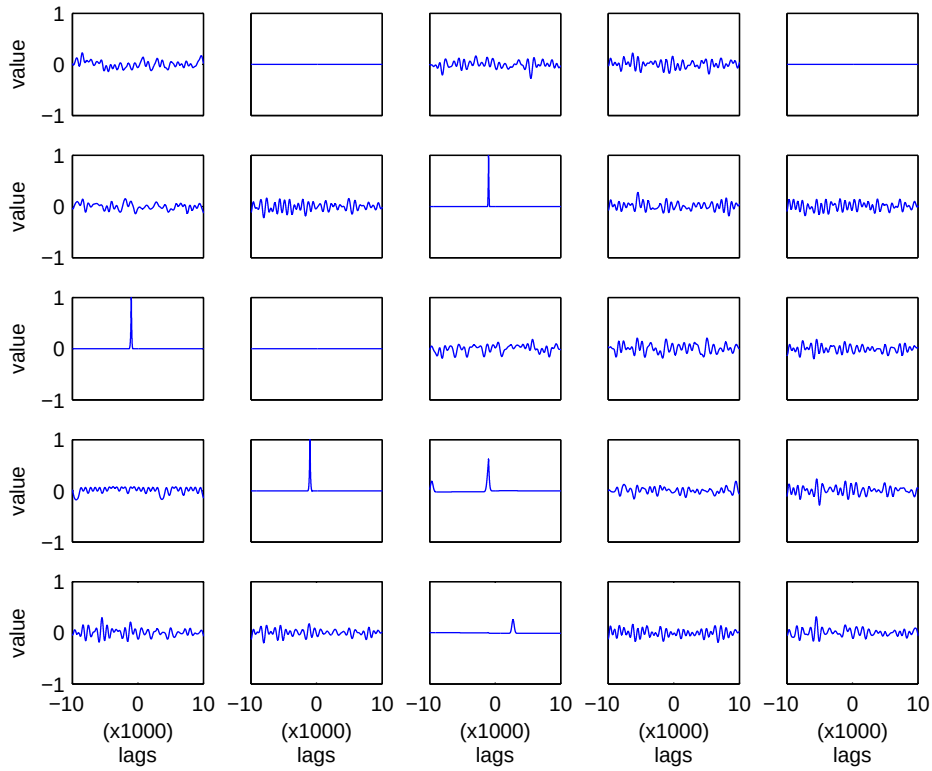

Figure H.18: Cross-correlation analysis for odour 2: trained weights vs. -10% difference weights. The Cross-correlation analysis was carried out between the response of the olfactory bulb of the trained weights and the weights minus a percentage of the difference between weight values and the limit range for the weights. Plots are sorted from left to right and from up to down, starting from the cross-corelation between for the first mitral cell (the first column and first row) up to the 25th mitral cell in the last column at the bottom. Plots with zero response result from Mitral cells which remain silent for these particular weight values. The time constants of both the ORN and mitral cells were set to $\tilde{\tau}_m \approx 10$ ms, with a threshold potential, $V_{th} = 50000$. The time constants of the excitatory synapses were set to $\tilde{\tau}_E \approx 4$ ms, whereas for the inhibitory synapses the time constants were set to $\tilde{\tau}_I \approx 16$ ms. For the ORNs, constant values randomly selected in a range between 500 and 1000, were used to represent a constant concentration of each odor stimulus. The total running time in terms of biological values is equivalent to 5 seconds at a sampling frequency of $f_{smp} = 10$ kHz. Although the clock frequency was set to $f_{clk} = 10$ MHz thus each run lasted for 5 ms of the FPGA processing time.

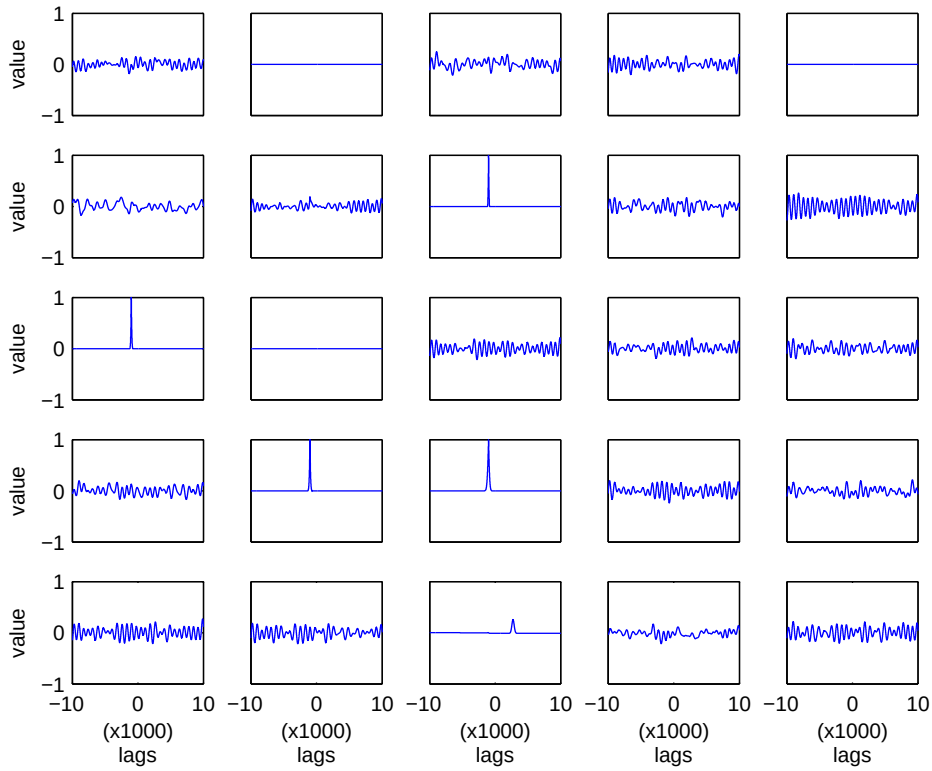

Figure H.19: Cross-correlation analysis for odour 2: trained weights vs. -4% difference weights. The Cross-correlation analysis was carried out between the response of the olfactory bulb of the trained weights and the weights minus a percentage of the difference between weight values and the limit range for the weights. Plots are sorted from left to right and from up to down, starting from the cross-corelation between for the first mitral cell (the first column and first row) up to the 25th mitral cell in the last column at the bottom. Plots with zero response result from Mitral cells which remain silent for these particular weight values. The time constants of both the ORN and mitral cells were set to $\tilde{\tau}_m \approx 10$ ms, with a threshold potential, $V_{th} = 50000$. The time constants of the excitatory synapses were set to $\tilde{\tau}_E \approx 4$ ms, whereas for the inhibitory synapses the time constants were set to $\tilde{\tau}_I \approx 16$ ms. For the ORNs, constant values randomly selected in a range between 500 and 1000, were used to represent a constant concentration of each odor stimulus. The total running time in terms of biological values is equivalent to 5 seconds at a sampling frequency of $f_{smp} = 10$ kHz. Although the clock frequency was set to $f_{clk} = 10$ MHz thus each run lasted for 5 ms of the FPGA processing time.

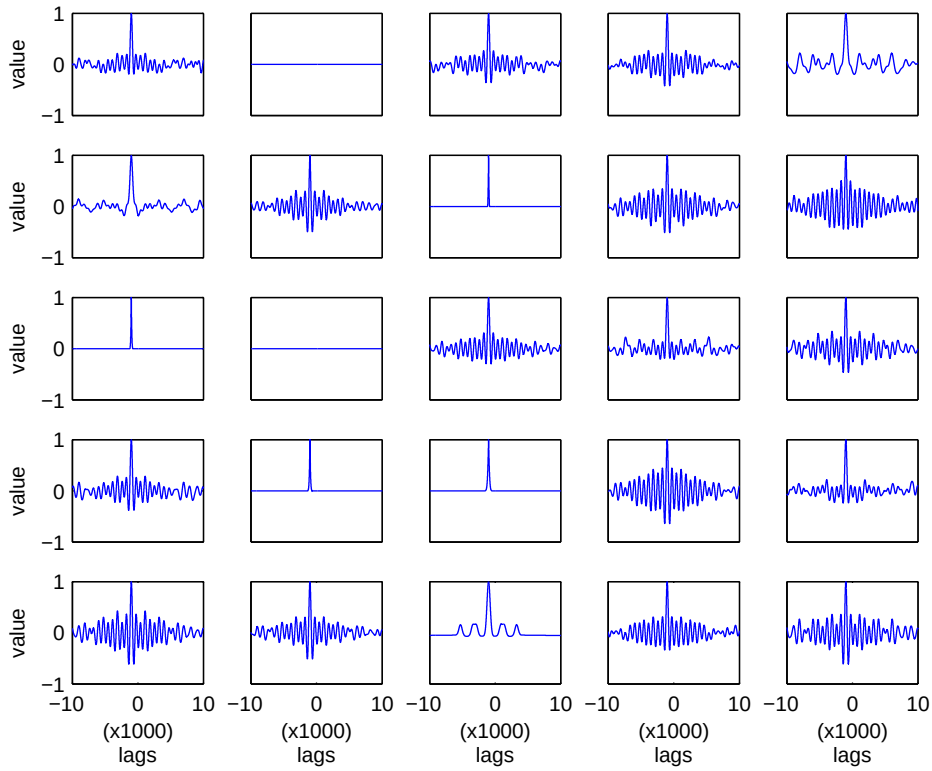

Figure H.20: Cross-correlation analysis for odour 2: trained weights vs. 0% difference weights. The Cross-correlation analysis was carried out between the response of the olfactory bulb of the trained weights and the weights minus a percentage of the difference between weight values and the limit range for the weights. Plots are sorted from left to right and from up to down, starting from the cross-corelation between for the first mitral cell (the first column and first row) up to the 25th mitral cell in the last column at the bottom. Plots with zero response result from Mitral cells which remain silent for these particular weight values. The time constants of both the ORN and mitral cells were set to $\tilde{\tau}_m \approx 10$ ms, with a threshold potential, $V_{th} = 50000$. The time constants of the excitatory synapses were set to $\tilde{\tau}_E \approx 4$ ms, whereas for the inhibitory synapses the time constants were set to $\tilde{\tau}_I \approx 16$ ms. For the ORNs, constant values randomly selected in a range between 500 and 1000, were used to represent a constant concentration of each odor stimulus. The total running time in terms of biological values is equivalent to 5 seconds at a sampling frequency of $f_{smp} = 10$ kHz. Although the clock frequency was set to $f_{clk} = 10$ MHz thus each run lasted for 5 ms of the FPGA processing time.

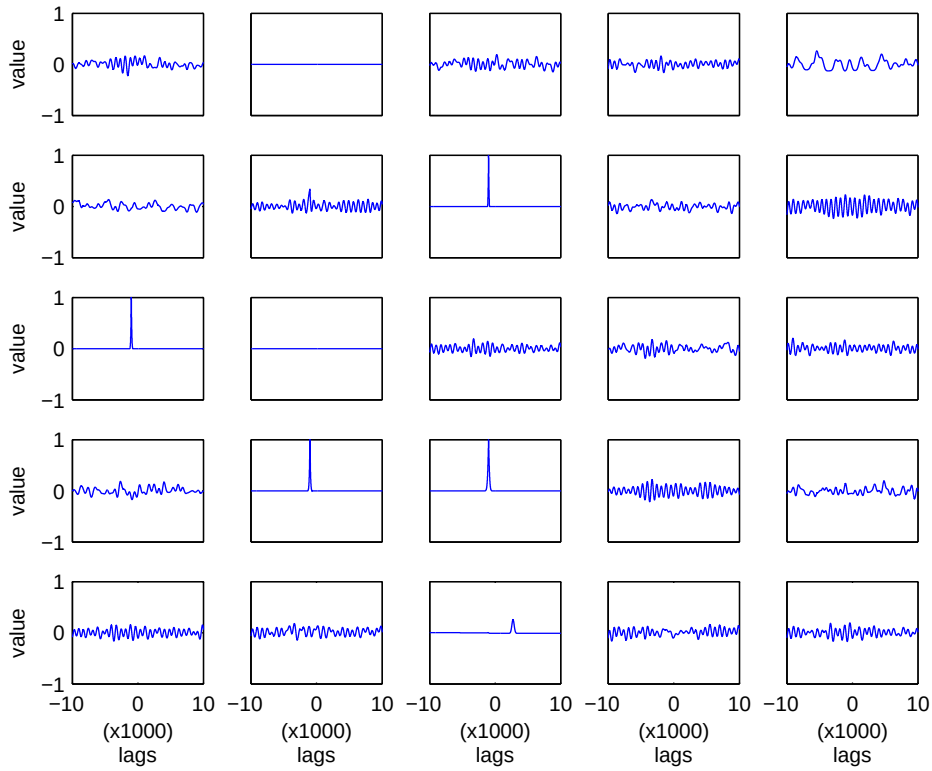

Figure H.21: Cross-correlation analysis for odour 2: trained weights vs. +4% difference weights. The Cross-correlation analysis was carried out between the response of the olfactory bulb of the trained weights and the weights minus a percentage of the difference between weight values and the limit range for the weights. Plots are sorted from left to right and from up to down, starting from the cross-corelation between for the first mitral cell (the first column and first row) up to the 25th mitral cell in the last column at the bottom. Plots with zero response result from Mitral cells which remain silent for these particular weight values. The time constants of both the ORN and mitral cells were set to $\tilde{\tau}_m \approx 10$ ms, with a threshold potential, $V_{th} = 50000$. The time constants of the excitatory synapses were set to $\tilde{\tau}_E \approx 4$ ms, whereas for the inhibitory synapses the time constants were set to $\tilde{\tau}_I \approx 16$ ms. For the ORNs, constant values randomly selected in a range between 500 and 1000, were used to represent a constant concentration of each odor stimulus. The total running time in terms of biological values is equivalent to 5 seconds at a sampling frequency of $f_{smp} = 10$ kHz. Although the clock frequency was set to $f_{clk} = 10$ MHz thus each run lasted for 5 ms of the FPGA processing time.

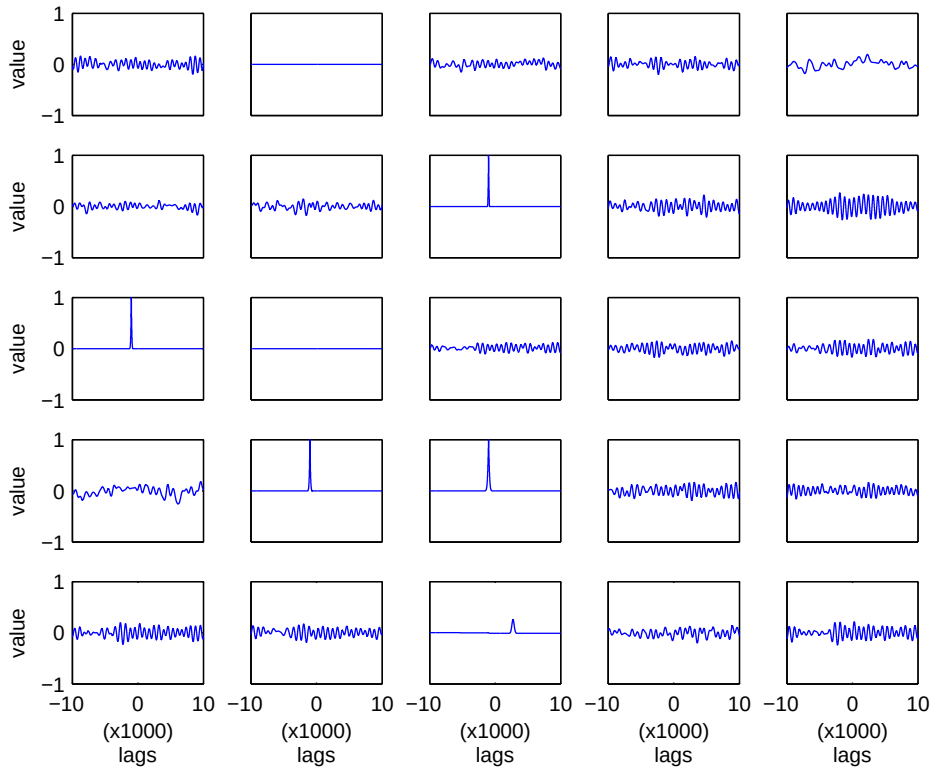

Figure H.22: Cross-correlation analysis for odour 2: trained weights vs. +10% difference weights. The Cross-correlation analysis was carried out between the response of the olfactory bulb of the trained weights and the weights minus a percentage of the difference between weight values and the limit range for the weights. Plots are sorted from left to right and from up to down, starting from the cross-corelation between for the first mitral cell (the first column and first row) up to the 25th mitral cell in the last column at the bottom. Plots with zero response result from Mitral cells which remain silent for these particular weight values. The time constants of both the ORN and mitral cells were set to $\tilde{\tau}_m \approx 10$ ms, with a threshold potential, $V_{th} = 50000$. The time constants of the excitatory synapses were set to $\tilde{\tau}_E \approx 4$ ms, whereas for the inhibitory synapses the time constants were set to $\tilde{\tau}_I \approx 16$ ms. For the ORNs, constant values randomly selected in a range between 500 and 1000, were used to represent a constant concentration of each odor stimulus. The total running time in terms of biological values is equivalent to 5 seconds at a sampling frequency of $f_{smp} = 10$ kHz. Although the clock frequency was set to $f_{clk} = 10$ MHz thus each run lasted for 5 ms of the FPGA processing time.

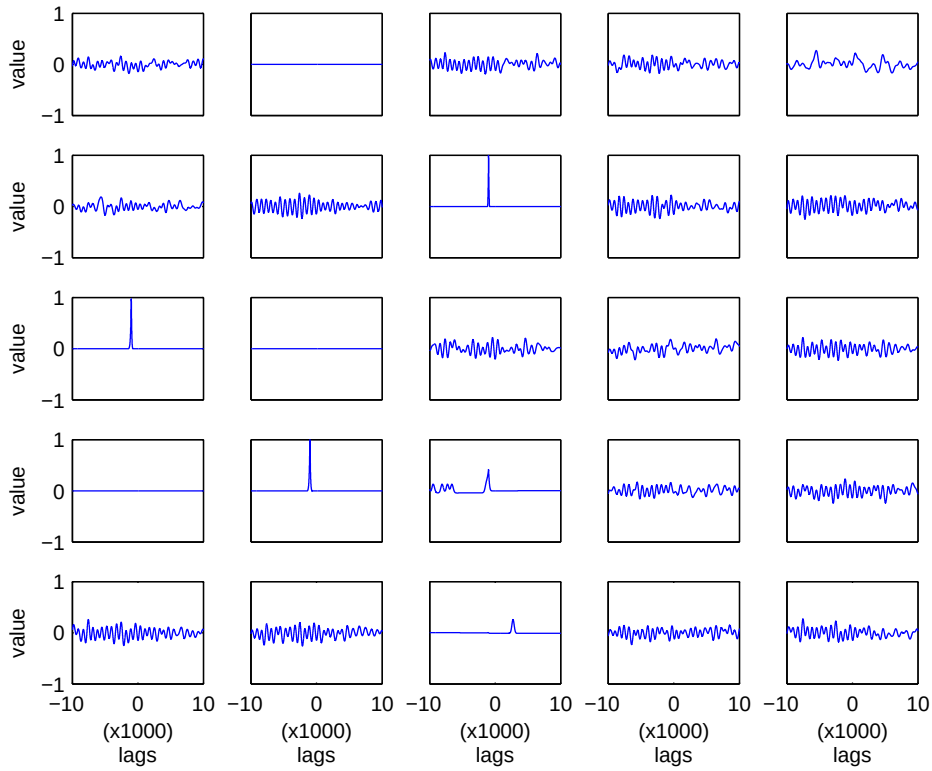

Figure H.23: Cross-correlation analysis for odour 2: trained weights vs. +20% difference weights. The Cross-correlation analysis was carried out between the response of the olfactory bulb of the trained weights and the weights minus a percentage of the difference between weight values and the limit range for the weights. Plots are sorted from left to right and from up to down, starting from the cross-corelation between for the first mitral cell (the first column and first row) up to the 25th mitral cell in the last column at the bottom. Plots with zero response result from Mitral cells which remain silent for these particular weight values. The time constants of both the ORN and mitral cells were set to $\tilde{\tau}_m \approx 10$ ms, with a threshold potential, $V_{th} = 50000$. The time constants of the excitatory synapses were set to $\tilde{\tau}_E \approx 4$ ms, whereas for the inhibitory synapses the time constants were set to $\tilde{\tau}_I \approx 16$ ms. For the ORNs, constant values randomly selected in a range between 500 and 1000, were used to represent a constant concentration of each odor stimulus. The total running time in terms of biological values is equivalent to 5 seconds at a sampling frequency of $f_{smp} = 10$ kHz. Although the clock frequency was set to $f_{clk} = 10$ MHz thus each run lasted for 5 ms of the FPGA processing time.

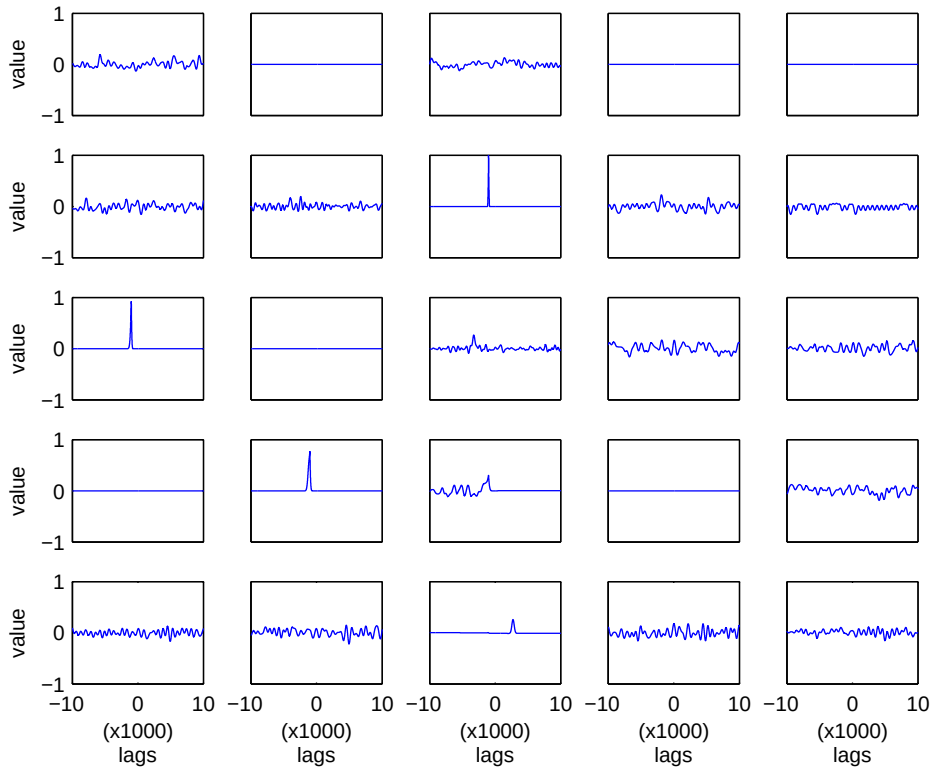

Figure H.24: Cross-correlation analysis for odour 2: trained weights vs. +40% difference weights. The Cross-correlation analysis was carried out between the response of the olfactory bulb of the trained weights and the weights minus a percentage of the difference between weight values and the limit range for the weights. Plots are sorted from left to right and from up to down, starting from the cross-corelation between for the first mitral cell (the first column and first row) up to the 25th mitral cell in the last column at the bottom. Plots with zero response result from Mitral cells which remain silent for these particular weight values. The time constants of both the ORN and mitral cells were set to $\tilde{\tau}_m \approx 10$ ms, with a threshold potential, $V_{th} = 50000$. The time constants of the excitatory synapses were set to $\tilde{\tau}_E \approx 4$ ms, whereas for the inhibitory synapses the time constants were set to $\tilde{\tau}_I \approx 16$ ms. For the ORNs, constant values randomly selected in a range between 500 and 1000, were used to represent a constant concentration of each odor stimulus. The total running time in terms of biological values is equivalent to 5 seconds at a sampling frequency of $f_{smp} = 10$ kHz. Although the clock frequency was set to $f_{clk} = 10$ MHz thus each run lasted for 5 ms of the FPGA processing time.

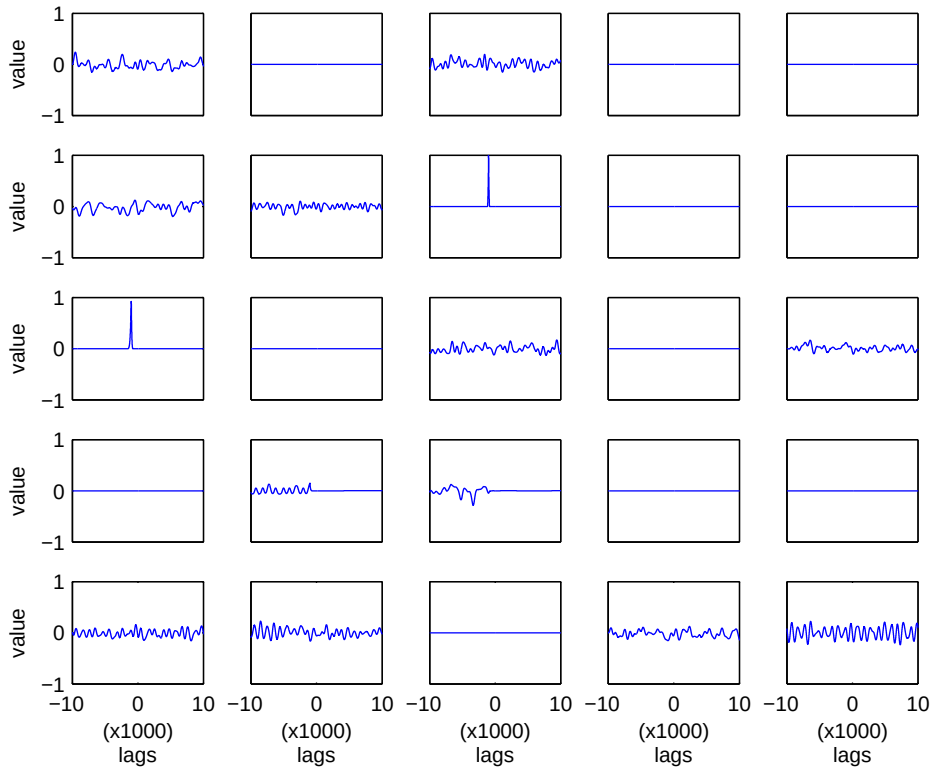

Figure H.25: Cross-correlation analysis for odour 2: trained weights vs. +60% difference weights. The Cross-correlation analysis was carried out between the response of the olfactory bulb of the trained weights and the weights minus a percentage of the difference between weight values and the limit range for the weights. Plots are sorted from left to right and from up to down, starting from the cross-corelation between for the first mitral cell (the first column and first row) up to the 25th mitral cell in the last column at the bottom. Plots with zero response result from Mitral cells which remain silent for these particular weight values. The time constants of both the ORN and mitral cells were set to $\tilde{\tau}_m \approx 10$ ms, with a threshold potential, $V_{th} = 50000$. The time constants of the excitatory synapses were set to $\tilde{\tau}_E \approx 4$ ms, whereas for the inhibitory synapses the time constants were set to $\tilde{\tau}_I \approx 16$ ms. For the ORNs, constant values randomly selected in a range between 500 and 1000, were used to represent a constant concentration of each odor stimulus. The total running time in terms of biological values is equivalent to 5 seconds at a sampling frequency of $f_{smp} = 10$ kHz. Although the clock frequency was set to $f_{clk} = 10$ MHz thus each run lasted for 5 ms of the FPGA processing time.

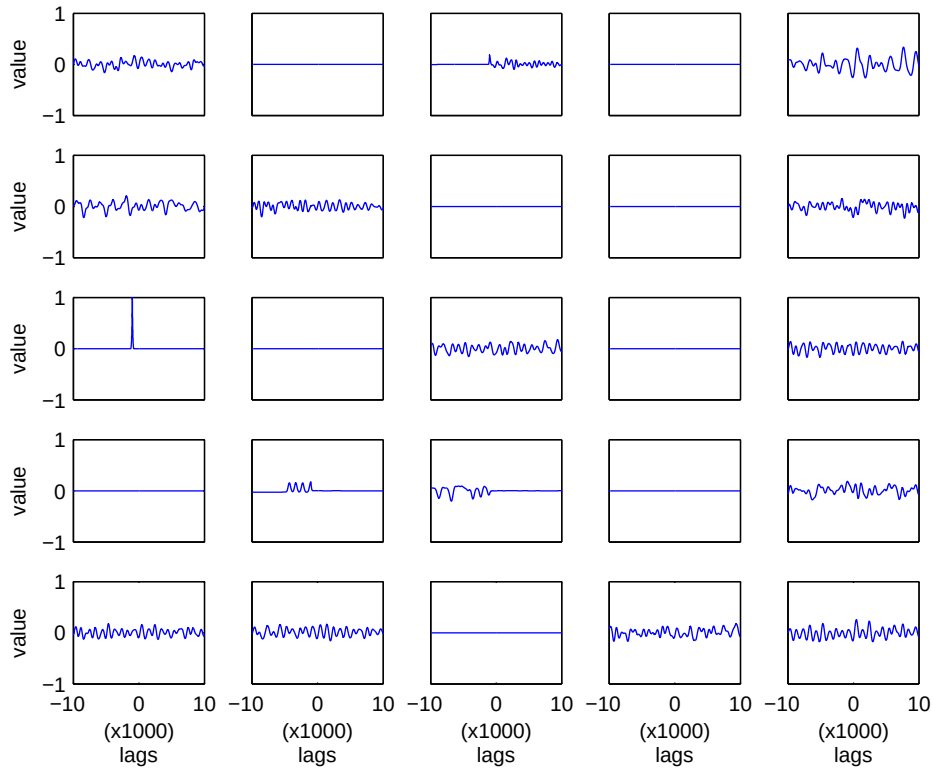

Figure H.26: Cross-correlation analysis for odour 2: trained weights vs. +80% difference weights. The Cross-correlation analysis was carried out between the response of the olfactory bulb of the trained weights and the weights minus a percentage of the difference between weight values and the limit range for the weights. Plots are sorted from left to right and from up to down, starting from the cross-corelation between for the first mitral cell (the first column and first row) up to the 25th mitral cell in the last column at the bottom. Plots with zero response result from Mitral cells which remain silent for these particular weight values. The time constants of both the ORN and mitral cells were set to $\tilde{\tau}_m \approx 10$ ms, with a threshold potential, $V_{th} = 50000$. The time constants of the excitatory synapses were set to $\tilde{\tau}_E \approx 4$ ms, whereas for the inhibitory synapses the time constants were set to $\tilde{\tau}_I \approx 16$ ms. For the ORNs, constant values randomly selected in a range between 500 and 1000, were used to represent a constant concentration of each odor stimulus. The total running time in terms of biological values is equivalent to 5 seconds at a sampling frequency of $f_{smp} = 10$ kHz. Although the clock frequency was set to $f_{clk} = 10$ MHz thus each run lasted for 5 ms of the FPGA processing time.

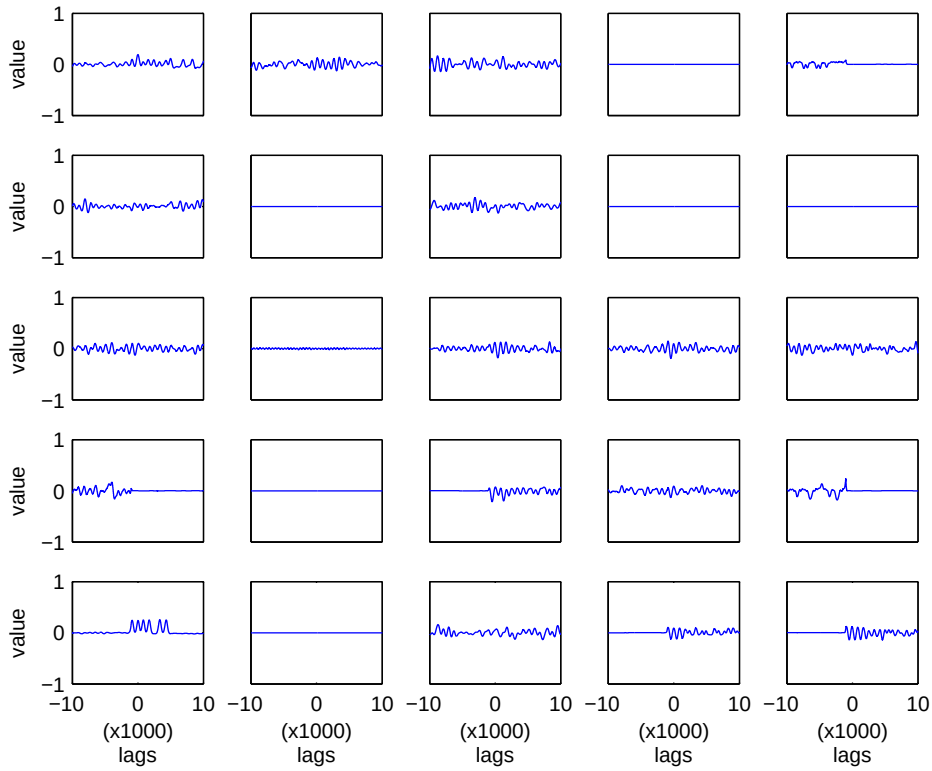

Figure H.27: Cross-correlation analysis for odour 3: trained weights vs. -80% difference weights. The Cross-correlation analysis was carried out between the response of the olfactory bulb of the trained weights and the weights minus a percentage of the difference between weight values and the limit range for the weights. Plots are sorted from left to right and from up to down, starting from the cross-corelation between for the first mitral cell (the first column and first row) up to the 25th mitral cell in the last column at the bottom. Plots with zero response result from Mitral cells which remain silent for these particular weight values. The time constants of both the ORN and mitral cells were set to $\tilde{\tau}_m \approx 10$ ms, with a threshold potential, $V_{th} = 50000$. The time constants of the excitatory synapses were set to $\tilde{\tau}_E \approx 4$ ms, whereas for the inhibitory synapses the time constants were set to $\tilde{\tau}_I \approx 16$ ms. For the ORNs, constant values randomly selected in a range between 500 and 1000, were used to represent a constant concentration of each odor stimulus. The total running time in terms of biological values is equivalent to 5 seconds at a sampling frequency of $f_{smp} = 10$ kHz. Although the clock frequency was set to $f_{clk} = 10$ MHz thus each run lasted for 5 ms of the FPGA processing time.

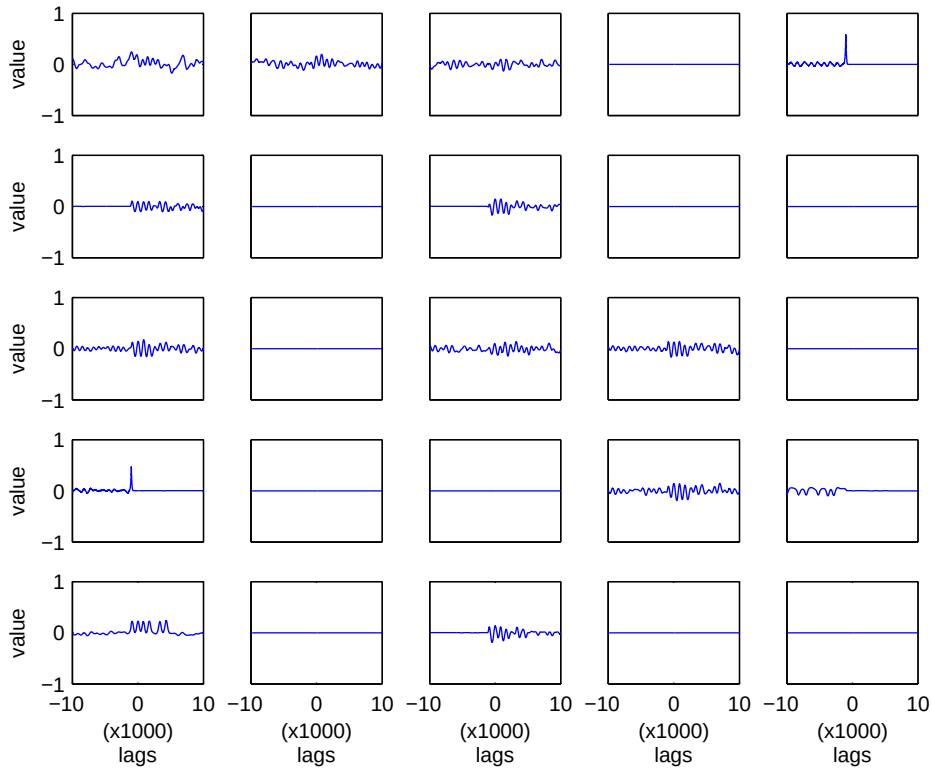

Figure H.28: Cross-correlation analysis for odour 3: trained weights vs. -60% difference weights. The Cross-correlation analysis was carried out between the response of the olfactory bulb of the trained weights and the weights minus a percentage of the difference between weight values and the limit range for the weights. Plots are sorted from left to right and from up to down, starting from the cross-corelation between for the first mitral cell (the first column and first row) up to the 25th mitral cell in the last column at the bottom. Plots with zero response result from Mitral cells which remain silent for these particular weight values. The time constants of both the ORN and mitral cells were set to $\tilde{\tau}_m \approx 10$ ms, with a threshold potential, $V_{th} = 50000$. The time constants of the excitatory synapses were set to $\tilde{\tau}_E \approx 4$ ms, whereas for the inhibitory synapses the time constants were set to $\tilde{\tau}_I \approx 16$ ms. For the ORNs, constant values randomly selected in a range between 500 and 1000, were used to represent a constant concentration of each odor stimulus. The total running time in terms of biological values is equivalent to 5 seconds at a sampling frequency of $f_{smp} = 10$ kHz. Although the clock frequency was set to $f_{clk} = 10$ MHz thus each run lasted for 5 ms of the FPGA processing time.

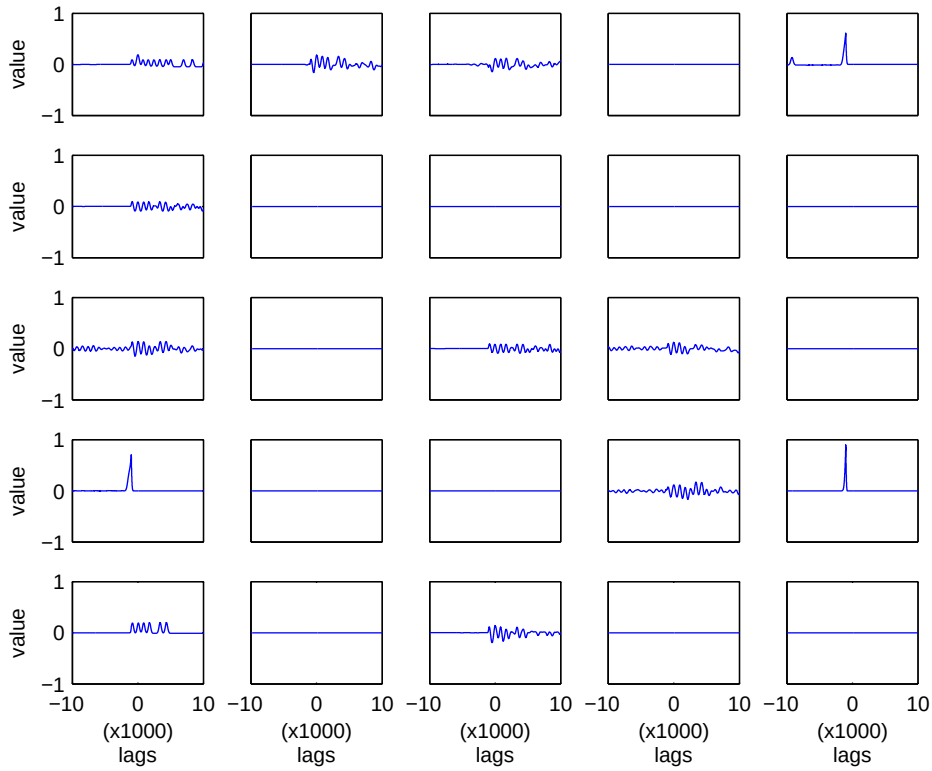

Figure H.29: Cross-correlation analysis for odour 3: trained weights vs. -40% difference weights. The Cross-correlation analysis was carried out between the response of the olfactory bulb of the trained weights and the weights minus a percentage of the difference between weight values and the limit range for the weights. Plots are sorted from left to right and from up to down, starting from the cross-corelation between for the first mitral cell (the first column and first row) up to the 25th mitral cell in the last column at the bottom. Plots with zero response result from Mitral cells which remain silent for these particular weight values. The time constants of both the ORN and mitral cells were set to $\tilde{\tau}_m \approx 10$ ms, with a threshold potential, $V_{th} = 50000$. The time constants of the excitatory synapses were set to $\tilde{\tau}_E \approx 4$ ms, whereas for the inhibitory synapses the time constants were set to $\tilde{\tau}_I \approx 16$ ms. For the ORNs, constant values randomly selected in a range between 500 and 1000, were used to represent a constant concentration of each odor stimulus. The total running time in terms of biological values is equivalent to 5 seconds at a sampling frequency of $f_{smp} = 10$ kHz. Although the clock frequency was set to $f_{clk} = 10$ MHz thus each run lasted for 5 ms of the FPGA processing time.

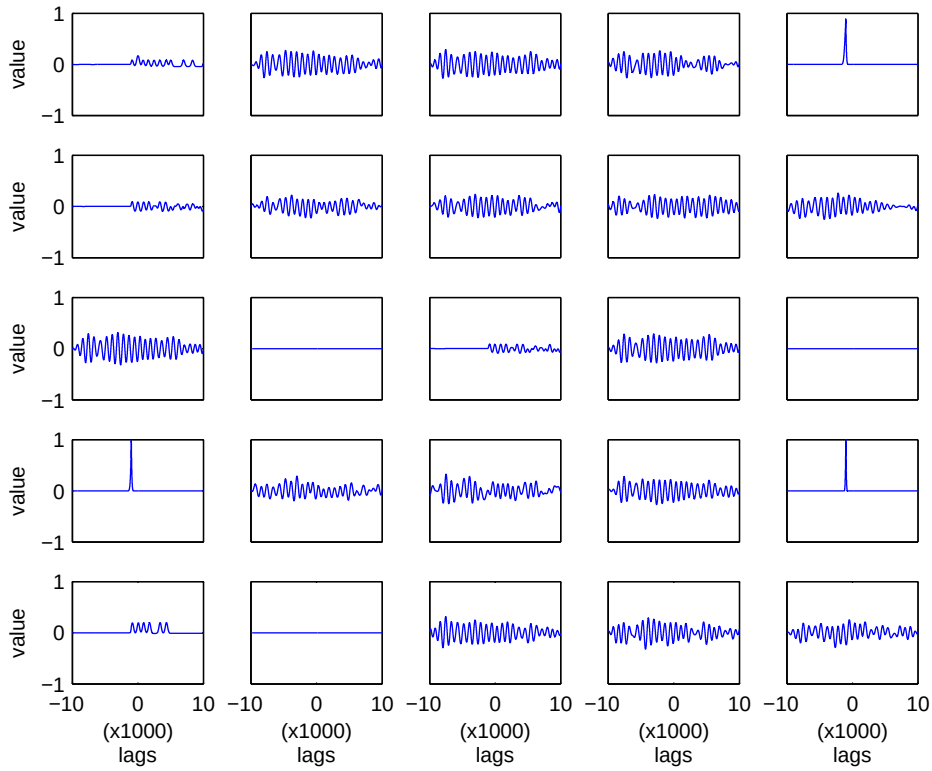

Figure H.30: Cross-correlation analysis for odour 3: trained weights vs. -20% difference weights. The Cross-correlation analysis was carried out between the response of the olfactory bulb of the trained weights and the weights minus a percentage of the difference between weight values and the limit range for the weights. Plots are sorted from left to right and from up to down, starting from the cross-corelation between for the first mitral cell (the first column and first row) up to the 25th mitral cell in the last column at the bottom. Plots with zero response result from Mitral cells which remain silent for these particular weight values. The time constants of both the ORN and mitral cells were set to $\tilde{\tau}_m \approx 10$ ms, with a threshold potential, $V_{th} = 50000$. The time constants of the excitatory synapses were set to $\tilde{\tau}_E \approx 4$ ms, whereas for the inhibitory synapses the time constants were set to $\tilde{\tau}_I \approx 16$ ms. For the ORNs, constant values randomly selected in a range between 500 and 1000, were used to represent a constant concentration of each odor stimulus. The total running time in terms of biological values is equivalent to 5 seconds at a sampling frequency of $f_{smp} = 10$ kHz. Although the clock frequency was set to $f_{clk} = 10$ MHz thus each run lasted for 5 ms of the FPGA processing time.

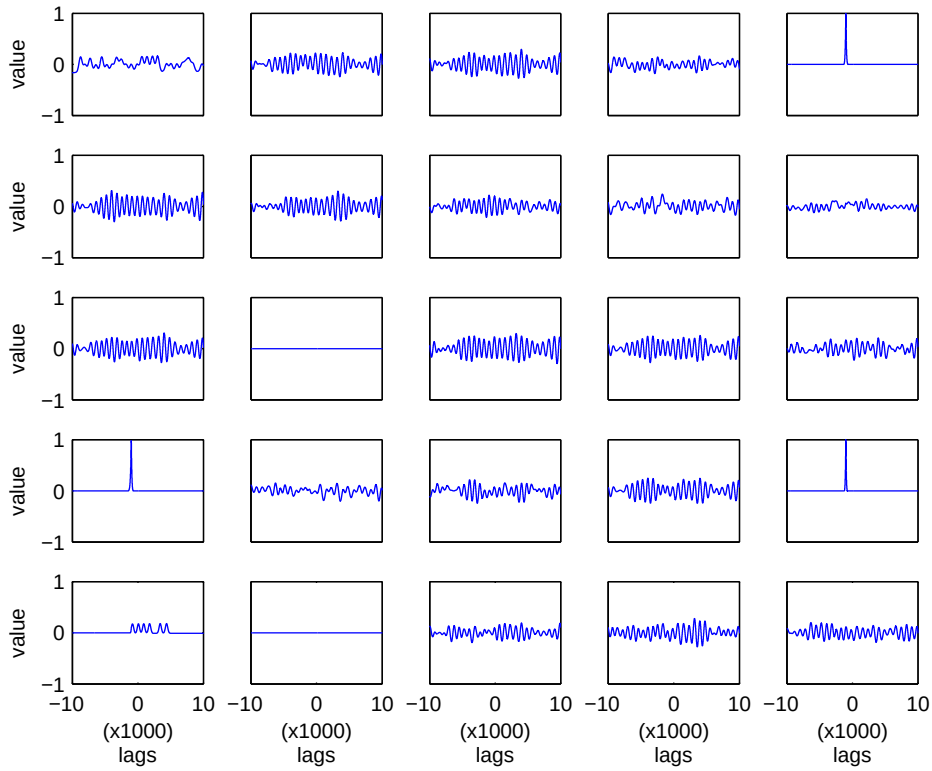

Figure H.31: Cross-correlation analysis for odour 3: trained weights vs. -10% difference weights. The Cross-correlation analysis was carried out between the response of the olfactory bulb of the trained weights and the weights minus a percentage of the difference between weight values and the limit range for the weights. Plots are sorted from left to right and from up to down, starting from the cross-corelation between for the first mitral cell (the first column and first row) up to the 25th mitral cell in the last column at the bottom. Plots with zero response result from Mitral cells which remain silent for these particular weight values. The time constants of both the ORN and mitral cells were set to $\tilde{\tau}_m \approx 10$ ms, with a threshold potential, $V_{th} = 50000$. The time constants of the excitatory synapses were set to $\tilde{\tau}_E \approx 4$ ms, whereas for the inhibitory synapses the time constants were set to $\tilde{\tau}_I \approx 16$ ms. For the ORNs, constant values randomly selected in a range between 500 and 1000, were used to represent a constant concentration of each odor stimulus. The total running time in terms of biological values is equivalent to 5 seconds at a sampling frequency of $f_{smp} = 10$ kHz. Although the clock frequency was set to $f_{clk} = 10$ MHz thus each run lasted for 5 ms of the FPGA processing time.

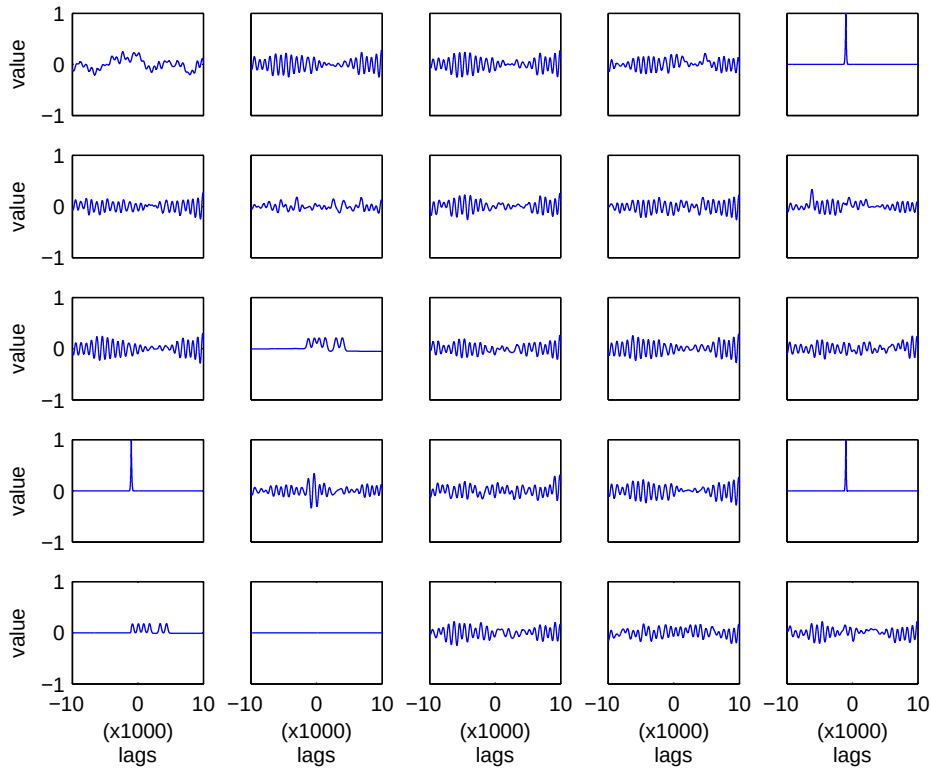

Figure H.32: Cross-correlation analysis for odour 3: trained weights vs. -4% difference weights. The Cross-correlation analysis was carried out between the response of the olfactory bulb of the trained weights and the weights minus a percentage of the difference between weight values and the limit range for the weights. Plots are sorted from left to right and from up to down, starting from the cross-corelation between for the first mitral cell (the first column and first row) up to the 25th mitral cell in the last column at the bottom. Plots with zero response result from Mitral cells which remain silent for these particular weight values. The time constants of both the ORN and mitral cells were set to $\tilde{\tau}_m \approx 10$ ms, with a threshold potential, $V_{th} = 50000$. The time constants of the excitatory synapses were set to $\tilde{\tau}_E \approx 4$ ms, whereas for the inhibitory synapses the time constants were set to $\tilde{\tau}_I \approx 16$ ms. For the ORNs, constant values randomly selected in a range between 500 and 1000, were used to represent a constant concentration of each odor stimulus. The total running time in terms of biological values is equivalent to 5 seconds at a sampling frequency of $f_{smp} = 10$ kHz. Although the clock frequency was set to $f_{clk} = 10$ MHz thus each run lasted for 5 ms of the FPGA processing time.

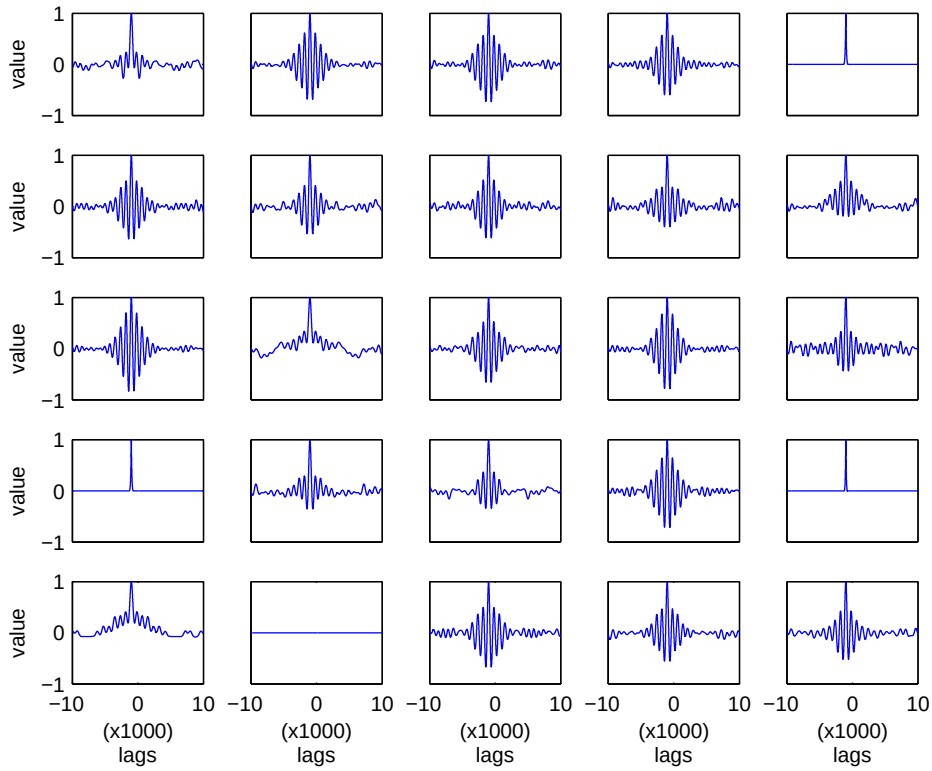

Figure H.33: Cross-correlation analysis for odour 3: trained weights vs. 0% difference weights. The Cross-correlation analysis was carried out between the response of the olfactory bulb of the trained weights and the weights minus a percentage of the difference between weight values and the limit range for the weights. Plots are sorted from left to right and from up to down, starting from the cross-corelation between for the first mitral cell (the first column and first row) up to the 25th mitral cell in the last column at the bottom. Plots with zero response result from Mitral cells which remain silent for these particular weight values. The time constants of both the ORN and mitral cells were set to $\tilde{\tau}_m \approx 10$ ms, with a threshold potential, $V_{th} = 50000$. The time constants of the excitatory synapses were set to $\tilde{\tau}_E \approx 4$ ms, whereas for the inhibitory synapses the time constants were set to $\tilde{\tau}_I \approx 16$ ms. For the ORNs, constant values randomly selected in a range between 500 and 1000, were used to represent a constant concentration of each odor stimulus. The total running time in terms of biological values is equivalent to 5 seconds at a sampling frequency of $f_{smp} = 10$ kHz. Although the clock frequency was set to $f_{clk} = 10$ MHz thus each run lasted for 5 ms of the FPGA processing time.

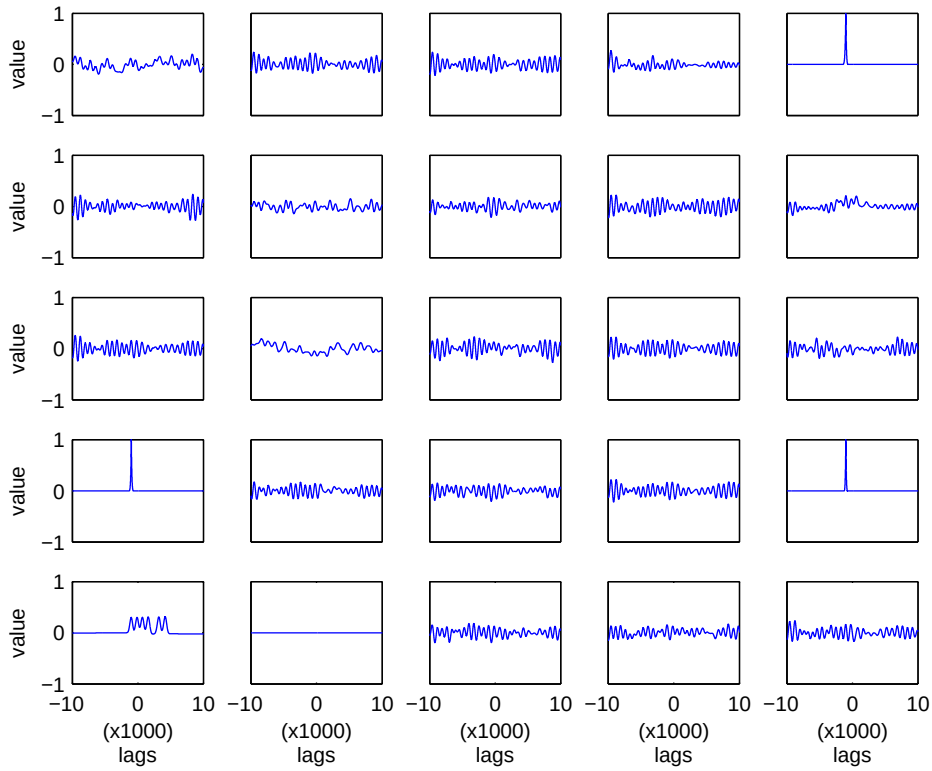

Figure H.34: Cross-correlation analysis for odour 3: trained weights vs. +4% difference weights. The Cross-correlation analysis was carried out between the response of the olfactory bulb of the trained weights and the weights minus a percentage of the difference between weight values and the limit range for the weights. Plots are sorted from left to right and from up to down, starting from the cross-corelation between for the first mitral cell (the first column and first row) up to the 25th mitral cell in the last column at the bottom. Plots with zero response result from Mitral cells which remain silent for these particular weight values. The time constants of both the ORN and mitral cells were set to $\tilde{\tau}_m \approx 10$ ms, with a threshold potential, $V_{th} = 50000$. The time constants of the excitatory synapses were set to $\tilde{\tau}_E \approx 4$ ms, whereas for the inhibitory synapses the time constants were set to $\tilde{\tau}_I \approx 16$ ms. For the ORNs, constant values randomly selected in a range between 500 and 1000, were used to represent a constant concentration of each odor stimulus. The total running time in terms of biological values is equivalent to 5 seconds at a sampling frequency of $f_{smp} = 10$ kHz. Although the clock frequency was set to $f_{clk} = 10$ MHz thus each run lasted for 5 ms of the FPGA processing time.

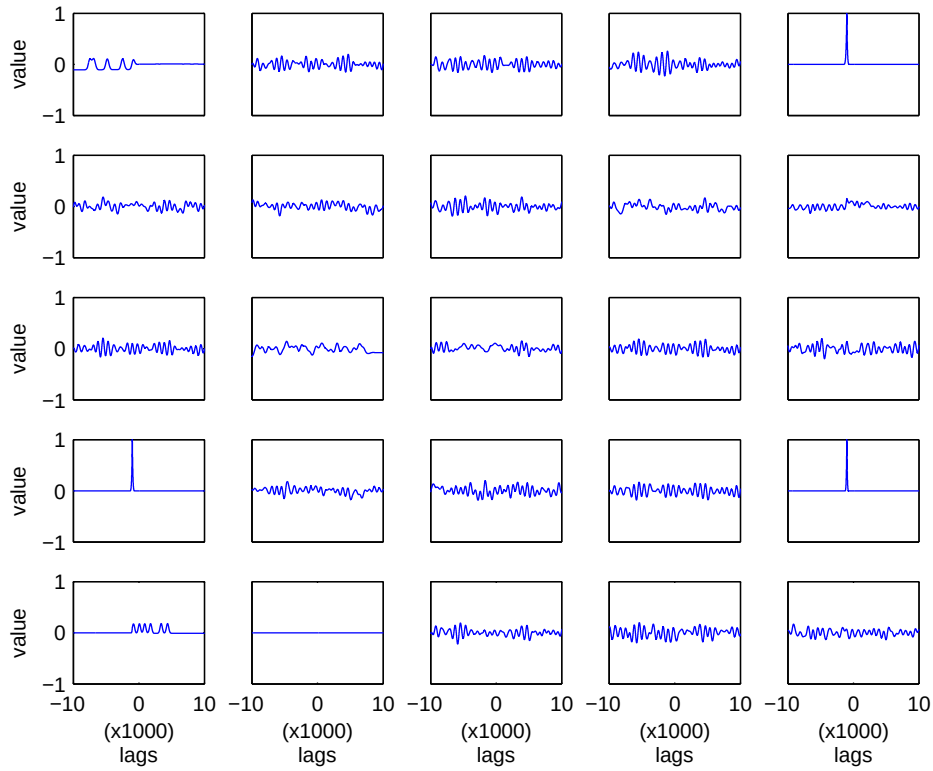

Figure H.35: Cross-correlation analysis for odour 3: trained weights vs. +10% difference weights. The Cross-correlation analysis was carried out between the response of the olfactory bulb of the trained weights and the weights minus a percentage of the difference between weight values and the limit range for the weights. Plots are sorted from left to right and from up to down, starting from the cross-corelation between for the first mitral cell (the first column and first row) up to the 25th mitral cell in the last column at the bottom. Plots with zero response result from Mitral cells which remain silent for these particular weight values. The time constants of both the ORN and mitral cells were set to $\tilde{\tau}_m \approx 10$ ms, with a threshold potential, $V_{th} = 50000$. The time constants of the excitatory synapses were set to $\tilde{\tau}_E \approx 4$ ms, whereas for the inhibitory synapses the time constants were set to $\tilde{\tau}_I \approx 16$ ms. For the ORNs, constant values randomly selected in a range between 500 and 1000, were used to represent a constant concentration of each odor stimulus. The total running time in terms of biological values is equivalent to 5 seconds at a sampling frequency of $f_{smp} = 10$ kHz. Although the clock frequency was set to $f_{clk} = 10$ MHz thus each run lasted for 5 ms of the FPGA processing time.

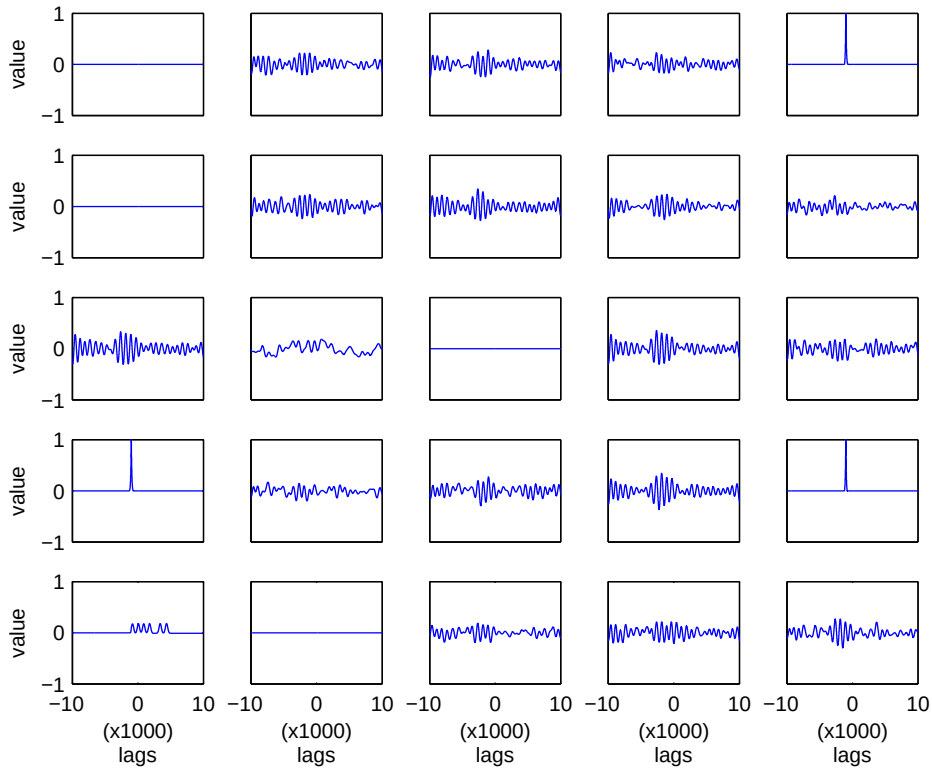

Figure H.36: Cross-correlation analysis for odour 3: trained weights vs. +20% difference weights. The Cross-correlation analysis was carried out between the response of the olfactory bulb of the trained weights and the weights minus a percentage of the difference between weight values and the limit range for the weights. Plots are sorted from left to right and from up to down, starting from the cross-corelation between for the first mitral cell (the first column and first row) up to the 25th mitral cell in the last column at the bottom. Plots with zero response result from Mitral cells which remain silent for these particular weight values. The time constants of both the ORN and mitral cells were set to $\tilde{\tau}_m \approx 10$ ms, with a threshold potential, $V_{th} = 50000$. The time constants of the excitatory synapses were set to $\tilde{\tau}_E \approx 4$ ms, whereas for the inhibitory synapses the time constants were set to $\tilde{\tau}_I \approx 16$ ms. For the ORNs, constant values randomly selected in a range between 500 and 1000, were used to represent a constant concentration of each odor stimulus. The total running time in terms of biological values is equivalent to 5 seconds at a sampling frequency of $f_{smp} = 10$ kHz. Although the clock frequency was set to $f_{clk} = 10$ MHz thus each run lasted for 5 ms of the FPGA processing time.

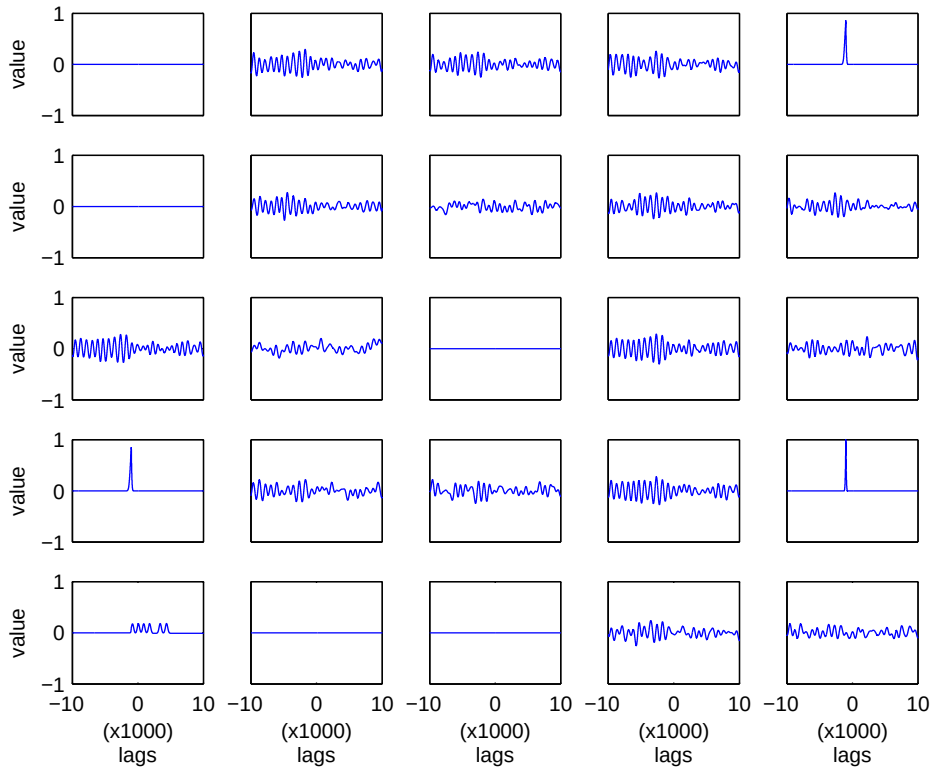

Figure H.37: Cross-correlation analysis for odour 3: trained weights vs. +40% difference weights. The Cross-correlation analysis was carried out between the response of the olfactory bulb of the trained weights and the weights minus a percentage of the difference between weight values and the limit range for the weights. Plots are sorted from left to right and from up to down, starting from the cross-corelation between for the first mitral cell (the first column and first row) up to the 25th mitral cell in the last column at the bottom. Plots with zero response result from Mitral cells which remain silent for these particular weight values. The time constants of both the ORN and mitral cells were set to $\tilde{\tau}_m \approx 10$ ms, with a threshold potential, $V_{th} = 50000$. The time constants of the excitatory synapses were set to $\tilde{\tau}_E \approx 4$ ms, whereas for the inhibitory synapses the time constants were set to $\tilde{\tau}_I \approx 16$ ms. For the ORNs, constant values randomly selected in a range between 500 and 1000, were used to represent a constant concentration of each odor stimulus. The total running time in terms of biological values is equivalent to 5 seconds at a sampling frequency of $f_{smp} = 10$ kHz. Although the clock frequency was set to $f_{clk} = 10$ MHz thus each run lasted for 5 ms of the FPGA processing time.

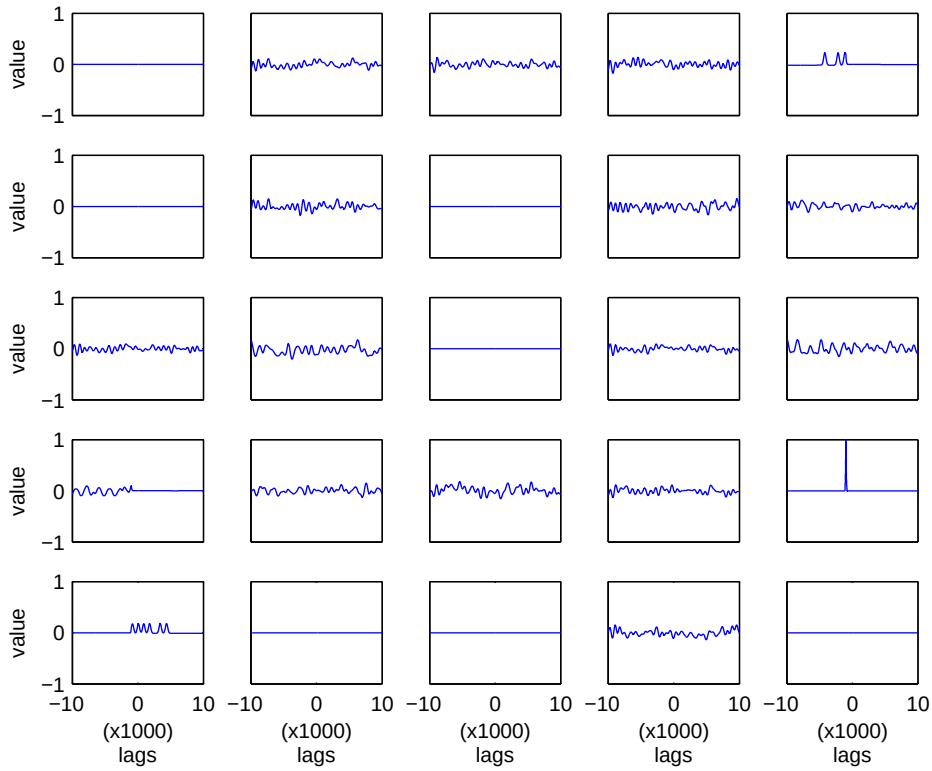

Figure H.38: Cross-correlation analysis for odour 3: trained weights vs. +60% difference weights. The Cross-correlation analysis was carried out between the response of the olfactory bulb of the trained weights and the weights minus a percentage of the difference between weight values and the limit range for the weights. Plots are sorted from left to right and from up to down, starting from the cross-corelation between for the first mitral cell (the first column and first row) up to the 25th mitral cell in the last column at the bottom. Plots with zero response result from Mitral cells which remain silent for these particular weight values. The time constants of both the ORN and mitral cells were set to $\tilde{\tau}_m \approx 10$ ms, with a threshold potential, $V_{th} = 50000$. The time constants of the excitatory synapses were set to $\tilde{\tau}_E \approx 4$ ms, whereas for the inhibitory synapses the time constants were set to $\tilde{\tau}_I \approx 16$ ms. For the ORNs, constant values randomly selected in a range between 500 and 1000, were used to represent a constant concentration of each odor stimulus. The total running time in terms of biological values is equivalent to 5 seconds at a sampling frequency of $f_{smp} = 10$ kHz. Although the clock frequency was set to $f_{clk} = 10$ MHz thus each run lasted for 5 ms of the FPGA processing time.

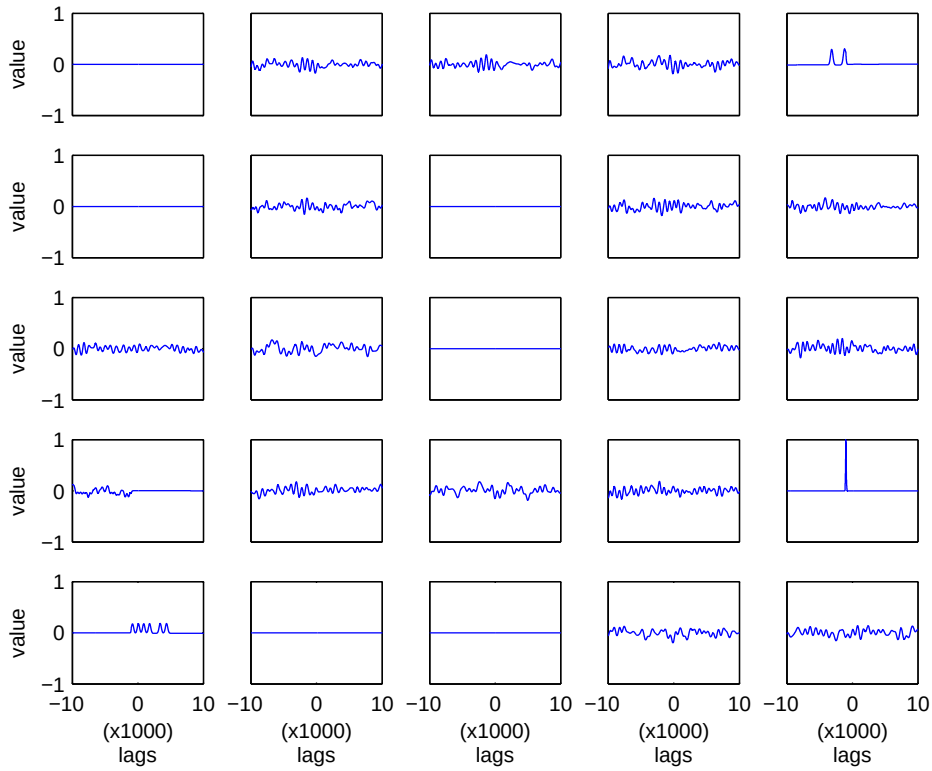

Figure H.39: Cross-correlation analysis for odour 3: trained weights vs. +80% difference weights. The Cross-correlation analysis was carried out between the response of the olfactory bulb of the trained weights and the weights minus a percentage of the difference between weight values and the limit range for the weights. Plots are sorted from left to right and from up to down, starting from the cross-corelation between for the first mitral cell (the first column and first row) up to the 25th mitral cell in the last column at the bottom. Plots with zero response result from Mitral cells which remain silent for these particular weight values. The time constants of both the ORN and mitral cells were set to $\tilde{\tau}_m \approx 10$ ms, with a threshold potential, $V_{th} = 50000$. The time constants of the excitatory synapses were set to $\tilde{\tau}_E \approx 4$ ms, whereas for the inhibitory synapses the time constants were set to $\tilde{\tau}_I \approx 16$ ms. For the ORNs, constant values randomly selected in a range between 500 and 1000, were used to represent a constant concentration of each odor stimulus. The total running time in terms of biological values is equivalent to 5 seconds at a sampling frequency of $f_{smp} = 10$ kHz. Although the clock frequency was set to $f_{clk} = 10$ MHz thus each run lasted for 5 ms of the FPGA processing time.

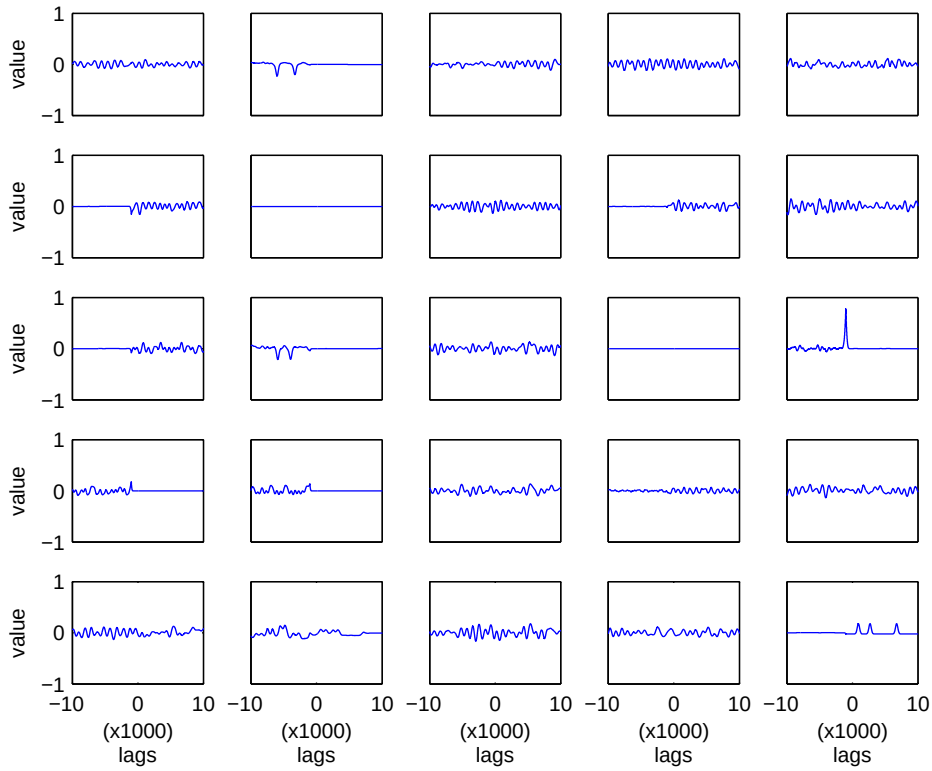

Figure H.40: Cross-correlation analysis for odour 4: trained weights vs. -80% difference weights. The Cross-correlation analysis was carried out between the response of the olfactory bulb of the trained weights and the weights minus a percentage of the difference between weight values and the limit range for the weights. Plots are sorted from left to right and from up to down, starting from the cross-corelation between for the first mitral cell (the first column and first row) up to the 25th mitral cell in the last column at the bottom. Plots with zero response result from Mitral cells which remain silent for these particular weight values. The time constants of both the ORN and mitral cells were set to $\tilde{\tau}_m \approx 10$ ms, with a threshold potential, $V_{th} = 50000$. The time constants of the excitatory synapses were set to $\tilde{\tau}_E \approx 4$ ms, whereas for the inhibitory synapses the time constants were set to $\tilde{\tau}_I \approx 16$ ms. For the ORNs, constant values randomly selected in a range between 500 and 1000, were used to represent a constant concentration of each odor stimulus. The total running time in terms of biological values is equivalent to 5 seconds at a sampling frequency of $f_{smp} = 10$ kHz. Although the clock frequency was set to $f_{clk} = 10$ MHz thus each run lasted for 5 ms of the FPGA processing time.

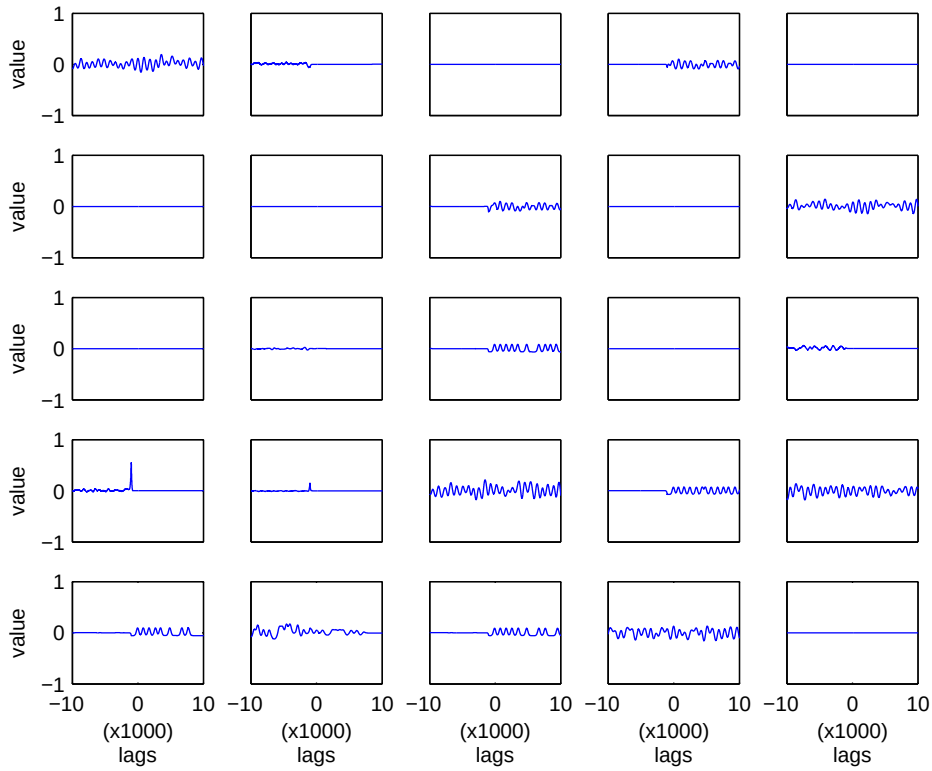

Figure H.41: Cross-correlation analysis for odour 4: trained weights vs. -60% difference weights. The Cross-correlation analysis was carried out between the response of the olfactory bulb of the trained weights and the weights minus a percentage of the difference between weight values and the limit range for the weights. Plots are sorted from left to right and from up to down, starting from the cross-corelation between for the first mitral cell (the first column and first row) up to the 25th mitral cell in the last column at the bottom. Plots with zero response result from Mitral cells which remain silent for these particular weight values. The time constants of both the ORN and mitral cells were set to $\tilde{\tau}_m \approx 10$ ms, with a threshold potential, $V_{th} = 50000$. The time constants of the excitatory synapses were set to $\tilde{\tau}_E \approx 4$ ms, whereas for the inhibitory synapses the time constants were set to $\tilde{\tau}_I \approx 16$ ms. For the ORNs, constant values randomly selected in a range between 500 and 1000, were used to represent a constant concentration of each odor stimulus. The total running time in terms of biological values is equivalent to 5 seconds at a sampling frequency of $f_{smp} = 10$ kHz. Although the clock frequency was set to $f_{clk} = 10$ MHz thus each run lasted for 5 ms of the FPGA processing time.

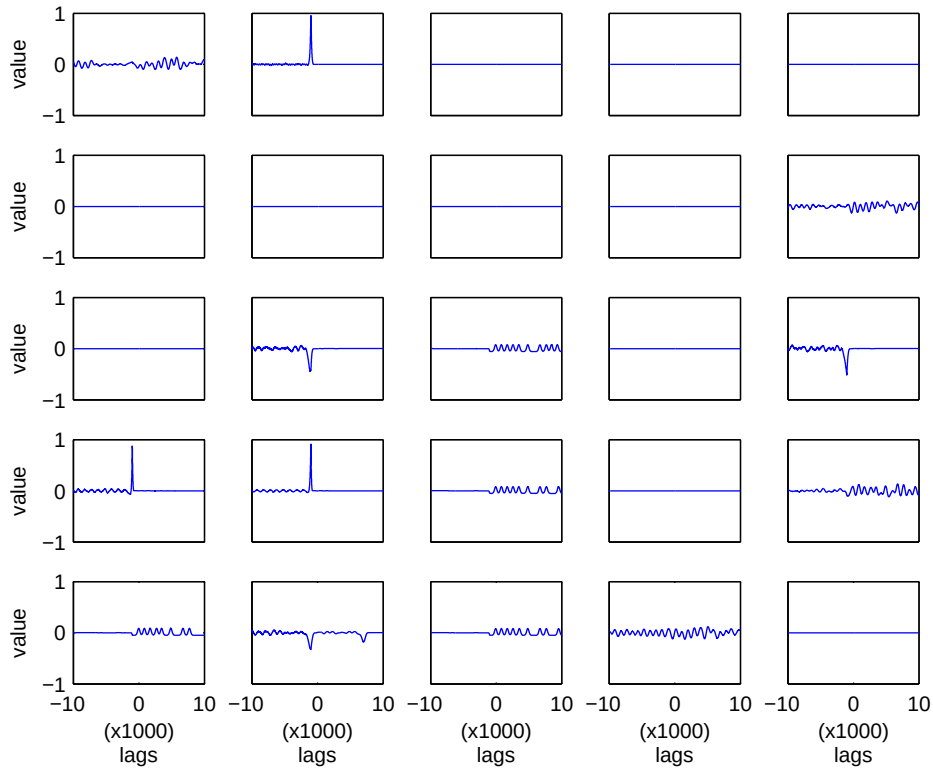

Figure H.42: Cross-correlation analysis for odour 4: trained weights vs. -40% difference weights. The Cross-correlation analysis was carried out between the response of the olfactory bulb of the trained weights and the weights minus a percentage of the difference between weight values and the limit range for the weights. Plots are sorted from left to right and from up to down, starting from the cross-corelation between for the first mitral cell (the first column and first row) up to the 25th mitral cell in the last column at the bottom. Plots with zero response result from Mitral cells which remain silent for these particular weight values. The time constants of both the ORN and mitral cells were set to $\tilde{\tau}_m \approx 10$ ms, with a threshold potential, $V_{th} = 50000$. The time constants of the excitatory synapses were set to $\tilde{\tau}_E \approx 4$ ms, whereas for the inhibitory synapses the time constants were set to $\tilde{\tau}_I \approx 16$ ms. For the ORNs, constant values randomly selected in a range between 500 and 1000, were used to represent a constant concentration of each odor stimulus. The total running time in terms of biological values is equivalent to 5 seconds at a sampling frequency of $f_{smp} = 10$ kHz. Although the clock frequency was set to $f_{clk} = 10$ MHz thus each run lasted for 5 ms of the FPGA processing time.

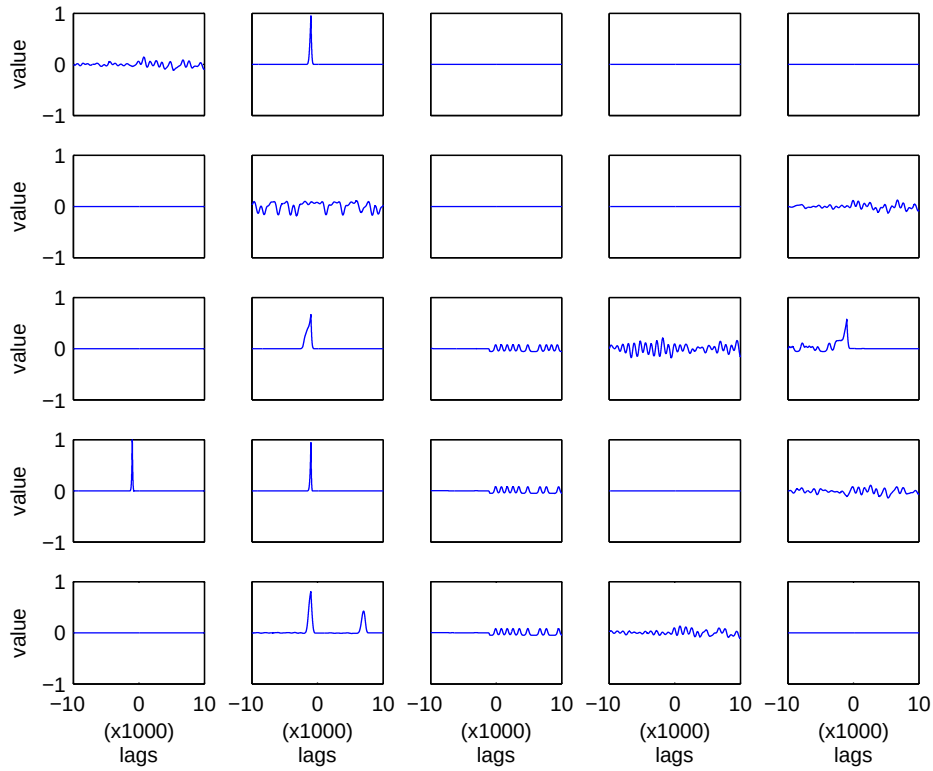

Figure H.43: Cross-correlation analysis for odour 4: trained weights vs. -20% difference weights. The Cross-correlation analysis was carried out between the response of the olfactory bulb of the trained weights and the weights minus a percentage of the difference between weight values and the limit range for the weights. Plots are sorted from left to right and from up to down, starting from the cross-corelation between for the first mitral cell (the first column and first row) up to the 25th mitral cell in the last column at the bottom. Plots with zero response result from Mitral cells which remain silent for these particular weight values. The time constants of both the ORN and mitral cells were set to $\tilde{\tau}_m \approx 10$ ms, with a threshold potential, $V_{th} = 50000$. The time constants of the excitatory synapses were set to $\tilde{\tau}_E \approx 4$ ms, whereas for the inhibitory synapses the time constants were set to $\tilde{\tau}_I \approx 16$ ms. For the ORNs, constant values randomly selected in a range between 500 and 1000, were used to represent a constant concentration of each odor stimulus. The total running time in terms of biological values is equivalent to 5 seconds at a sampling frequency of $f_{smp} = 10$ kHz. Although the clock frequency was set to $f_{clk} = 10$ MHz thus each run lasted for 5 ms of the FPGA processing time.

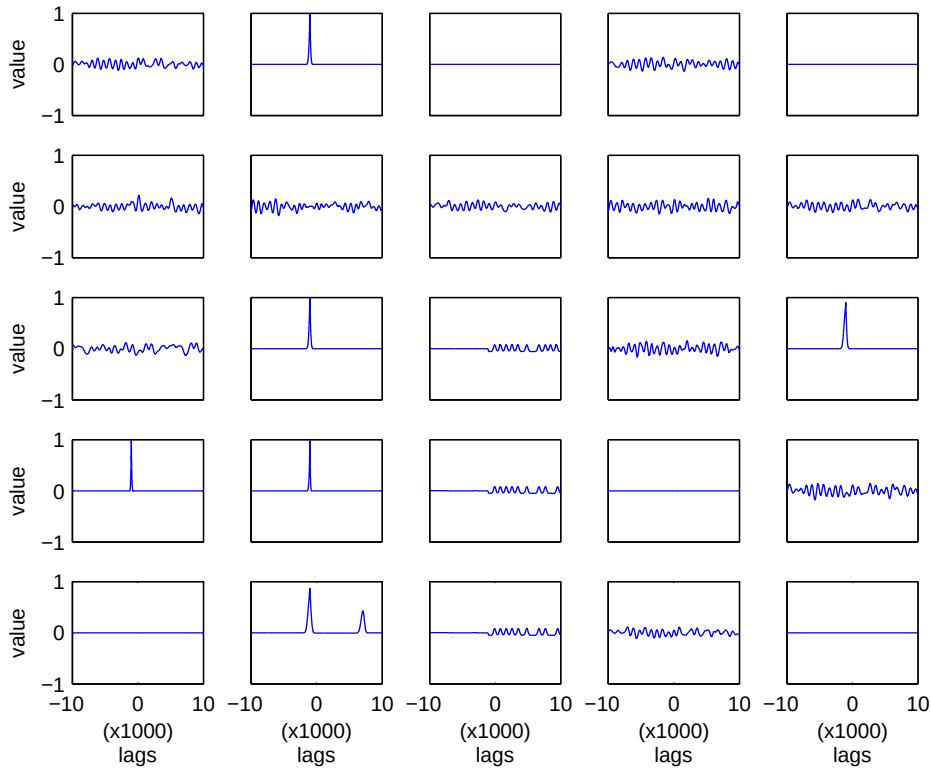

Figure H.44: Cross-correlation analysis for odour 4: trained weights vs. -10% difference weights. The Cross-correlation analysis was carried out between the response of the olfactory bulb of the trained weights and the weights minus a percentage of the difference between weight values and the limit range for the weights. Plots are sorted from left to right and from up to down, starting from the cross-corelation between for the first mitral cell (the first column and first row) up to the 25th mitral cell in the last column at the bottom. Plots with zero response result from Mitral cells which remain silent for these particular weight values. The time constants of both the ORN and mitral cells were set to $\tilde{\tau}_m \approx 10$ ms, with a threshold potential, $V_{th} = 50000$. The time constants of the excitatory synapses were set to $\tilde{\tau}_E \approx 4$ ms, whereas for the inhibitory synapses the time constants were set to $\tilde{\tau}_I \approx 16$ ms. For the ORNs, constant values randomly selected in a range between 500 and 1000, were used to represent a constant concentration of each odor stimulus. The total running time in terms of biological values is equivalent to 5 seconds at a sampling frequency of $f_{smp} = 10$ kHz. Although the clock frequency was set to $f_{clk} = 10$ MHz thus each run lasted for 5 ms of the FPGA processing time.

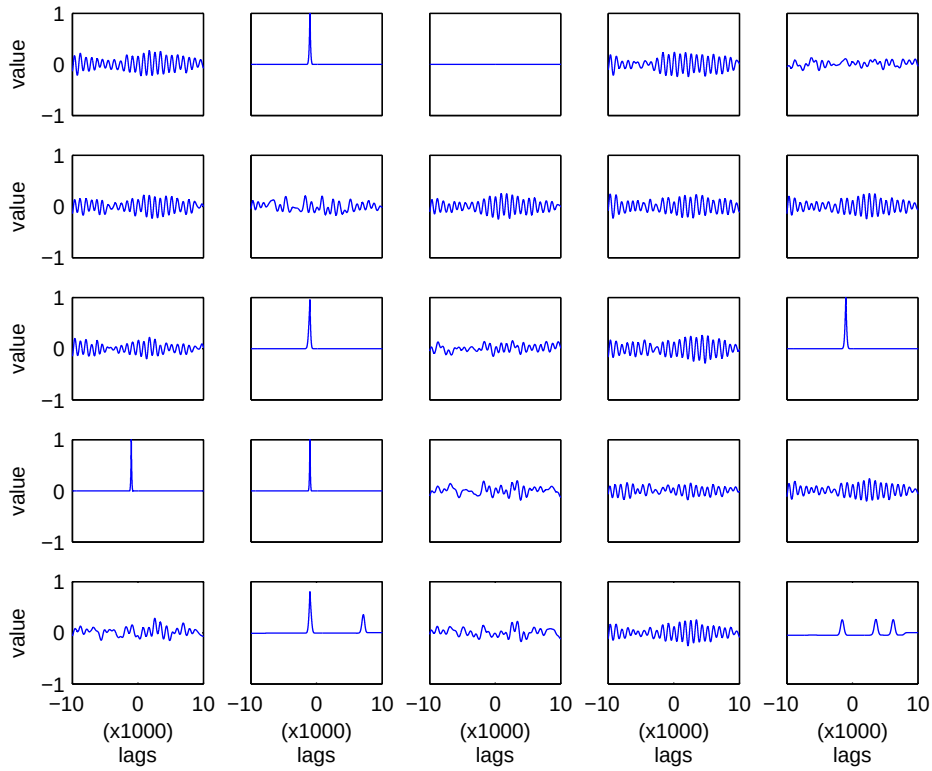

Figure H.45: Cross-correlation analysis for odour 4: trained weights vs. -4% difference weights. The Cross-correlation analysis was carried out between the response of the olfactory bulb of the trained weights and the weights minus a percentage of the difference between weight values and the limit range for the weights. Plots are sorted from left to right and from up to down, starting from the cross-corelation between for the first mitral cell (the first column and first row) up to the 25th mitral cell in the last column at the bottom. Plots with zero response result from Mitral cells which remain silent for these particular weight values. The time constants of both the ORN and mitral cells were set to $\tilde{\tau}_m \approx 10$ ms, with a threshold potential, $V_{th} = 50000$. The time constants of the excitatory synapses were set to $\tilde{\tau}_E \approx 4$ ms, whereas for the inhibitory synapses the time constants were set to $\tilde{\tau}_I \approx 16$ ms. For the ORNs, constant values randomly selected in a range between 500 and 1000, were used to represent a constant concentration of each odor stimulus. The total running time in terms of biological values is equivalent to 5 seconds at a sampling frequency of $f_{smp} = 10$ kHz. Although the clock frequency was set to $f_{clk} = 10$ MHz thus each run lasted for 5 ms of the FPGA processing time.

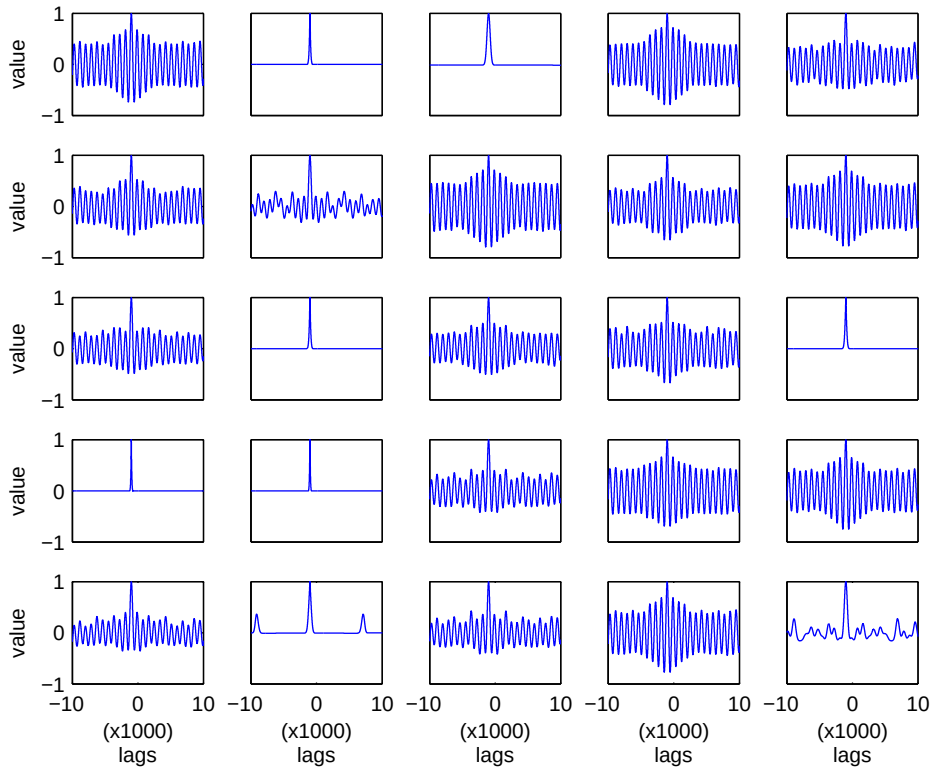

Figure H.46: Cross-correlation analysis for odour 4: trained weights vs. 0% difference weights. The Cross-correlation analysis was carried out between the response of the olfactory bulb of the trained weights and the weights minus a percentage of the difference between weight values and the limit range for the weights. Plots are sorted from left to right and from up to down, starting from the cross-corelation between for the first mitral cell (the first column and first row) up to the 25th mitral cell in the last column at the bottom. Plots with zero response result from Mitral cells which remain silent for these particular weight values. The time constants of both the ORN and mitral cells were set to $\tilde{\tau}_m \approx 10$ ms, with a threshold potential, $V_{th} = 50000$. The time constants of the excitatory synapses were set to $\tilde{\tau}_E \approx 4$ ms, whereas for the inhibitory synapses the time constants were set to $\tilde{\tau}_I \approx 16$ ms. For the ORNs, constant values randomly selected in a range between 500 and 1000, were used to represent a constant concentration of each odor stimulus. The total running time in terms of biological values is equivalent to 5 seconds at a sampling frequency of $f_{smp} = 10$ kHz. Although the clock frequency was set to $f_{clk} = 10$ MHz thus each run lasted for 5 ms of the FPGA processing time.

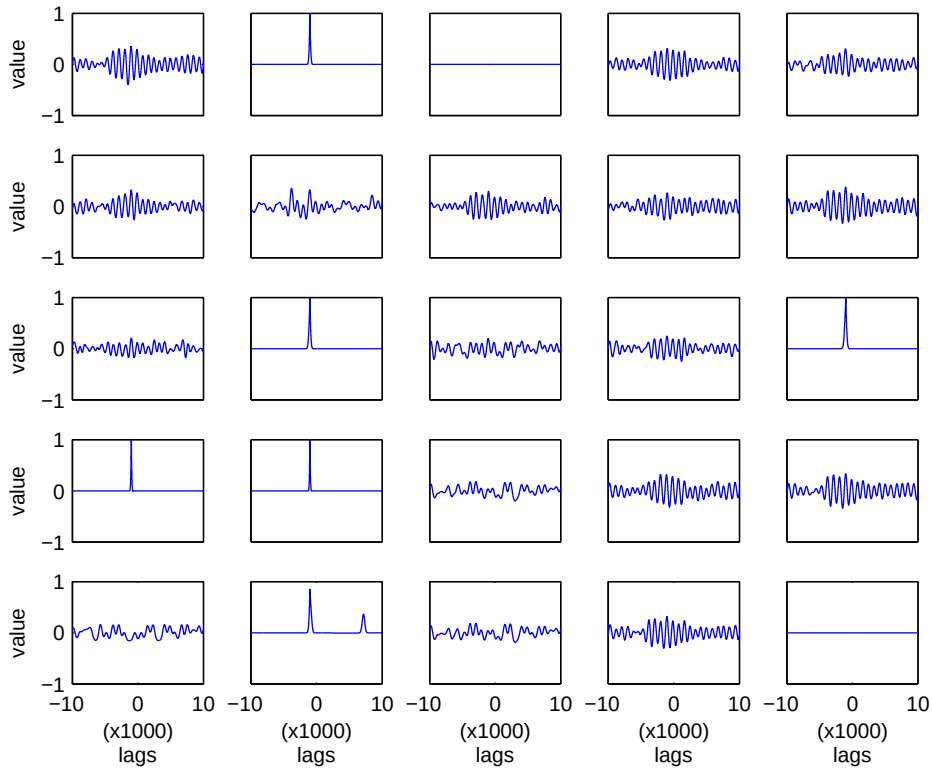

Figure H.47: Cross-correlation analysis for odour 4: trained weights vs. +4% difference weights. The Cross-correlation analysis was carried out between the response of the olfactory bulb of the trained weights and the weights minus a percentage of the difference between weight values and the limit range for the weights. Plots are sorted from left to right and from up to down, starting from the cross-corelation between for the first mitral cell (the first column and first row) up to the 25th mitral cell in the last column at the bottom. Plots with zero response result from Mitral cells which remain silent for these particular weight values. The time constants of both the ORN and mitral cells were set to $\tilde{\tau}_m \approx 10$ ms, with a threshold potential, $V_{th} = 50000$. The time constants of the excitatory synapses were set to $\tilde{\tau}_E \approx 4$ ms, whereas for the inhibitory synapses the time constants were set to $\tilde{\tau}_I \approx 16$ ms. For the ORNs, constant values randomly selected in a range between 500 and 1000, were used to represent a constant concentration of each odor stimulus. The total running time in terms of biological values is equivalent to 5 seconds at a sampling frequency of $f_{smp} = 10$ kHz. Although the clock frequency was set to $f_{clk} = 10$ MHz thus each run lasted for 5 ms of the FPGA processing time.

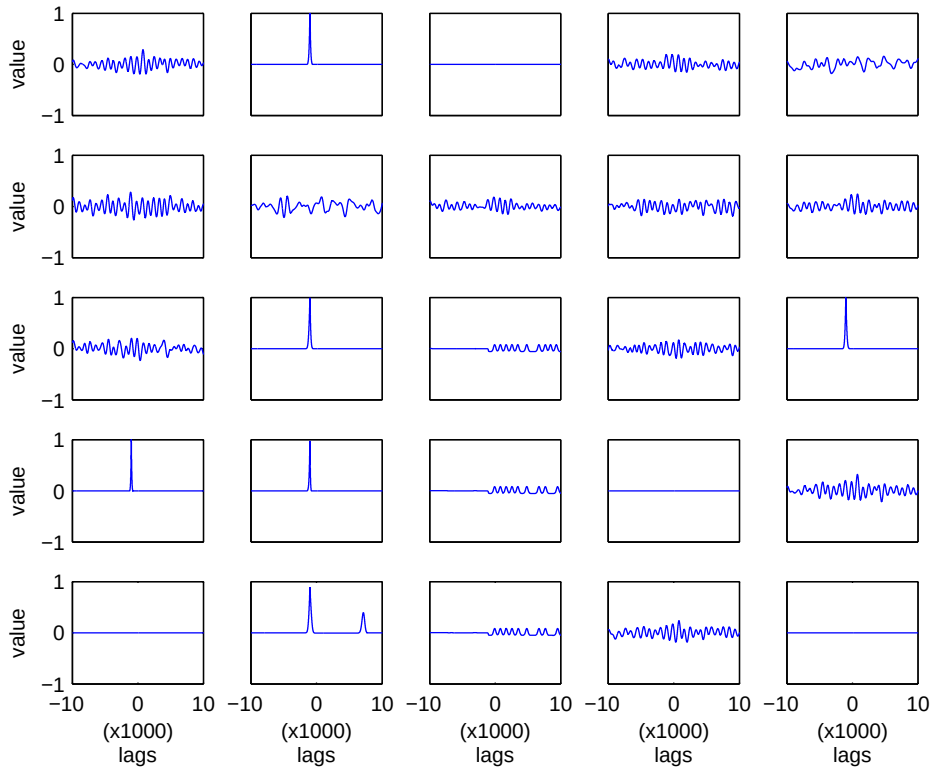

Figure H.48: Cross-correlation analysis for odour 4: trained weights vs. +10% difference weights. The Cross-correlation analysis was carried out between the response of the olfactory bulb of the trained weights and the weights minus a percentage of the difference between weight values and the limit range for the weights. Plots are sorted from left to right and from up to down, starting from the cross-corelation between for the first mitral cell (the first column and first row) up to the 25th mitral cell in the last column at the bottom. Plots with zero response result from Mitral cells which remain silent for these particular weight values. The time constants of both the ORN and mitral cells were set to $\tilde{\tau}_m \approx 10$ ms, with a threshold potential, $V_{th} = 50000$. The time constants of the excitatory synapses were set to $\tilde{\tau}_E \approx 4$ ms, whereas for the inhibitory synapses the time constants were set to $\tilde{\tau}_I \approx 16$ ms. For the ORNs, constant values randomly selected in a range between 500 and 1000, were used to represent a constant concentration of each odor stimulus. The total running time in terms of biological values is equivalent to 5 seconds at a sampling frequency of $f_{smp} = 10$ kHz. Although the clock frequency was set to $f_{clk} = 10$ MHz thus each run lasted for 5 ms of the FPGA processing time.

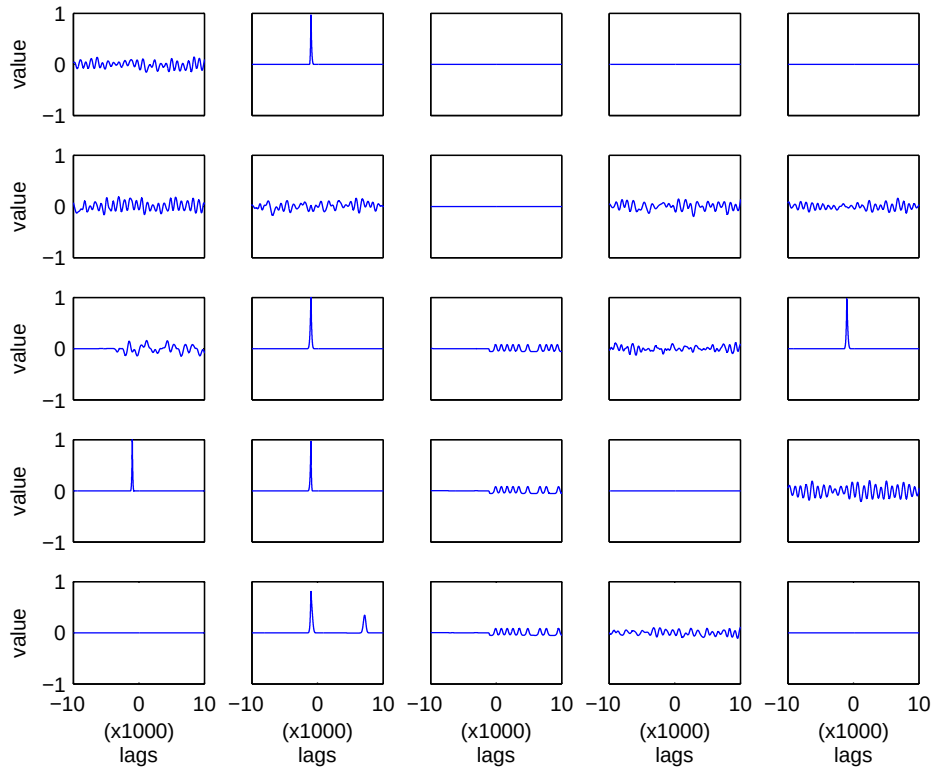

Figure H.49: Cross-correlation analysis for odour 4: trained weights vs. +20% difference weights. The Cross-correlation analysis was carried out between the response of the olfactory bulb of the trained weights and the weights minus a percentage of the difference between weight values and the limit range for the weights. Plots are sorted from left to right and from up to down, starting from the cross-corelation between for the first mitral cell (the first column and first row) up to the 25th mitral cell in the last column at the bottom. Plots with zero response result from Mitral cells which remain silent for these particular weight values. The time constants of both the ORN and mitral cells were set to $\tilde{\tau}_m \approx 10$ ms, with a threshold potential, $V_{th} = 50000$. The time constants of the excitatory synapses were set to $\tilde{\tau}_E \approx 4$ ms, whereas for the inhibitory synapses the time constants were set to $\tilde{\tau}_I \approx 16$ ms. For the ORNs, constant values randomly selected in a range between 500 and 1000, were used to represent a constant concentration of each odor stimulus. The total running time in terms of biological values is equivalent to 5 seconds at a sampling frequency of $f_{smp} = 10$ kHz. Although the clock frequency was set to $f_{clk} = 10$ MHz thus each run lasted for 5 ms of the FPGA processing time.

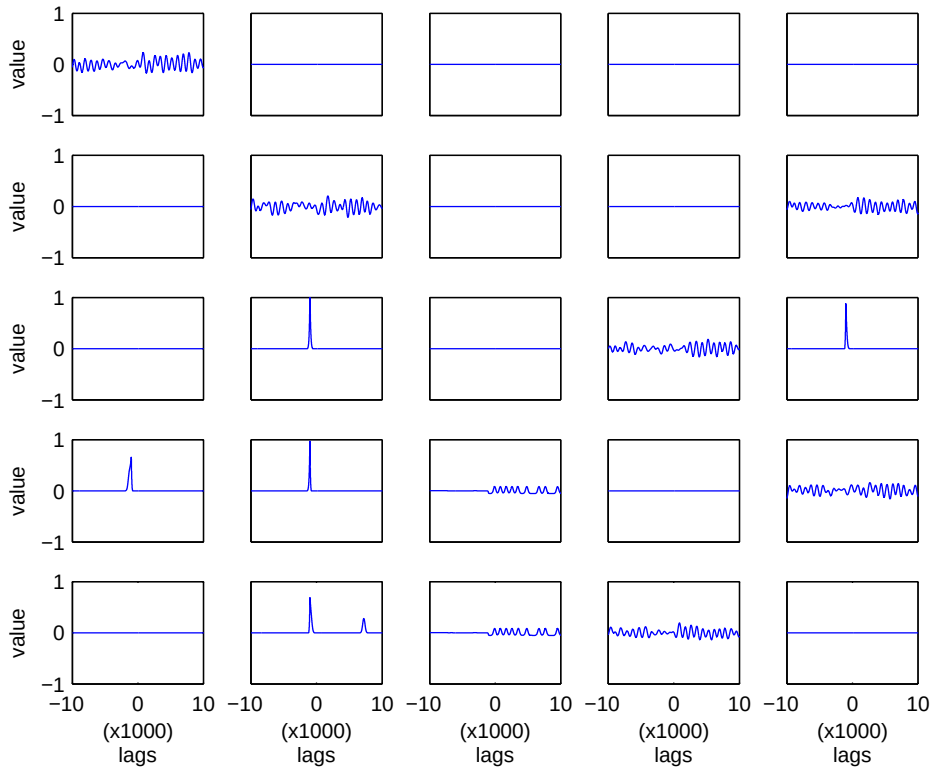

Figure H.50: Cross-correlation analysis for odour 4: trained weights vs. +40% difference weights. The Cross-correlation analysis was carried out between the response of the olfactory bulb of the trained weights and the weights minus a percentage of the difference between weight values and the limit range for the weights. Plots are sorted from left to right and from up to down, starting from the cross-corelation between for the first mitral cell (the first column and first row) up to the 25th mitral cell in the last column at the bottom. Plots with zero response result from Mitral cells which remain silent for these particular weight values. The time constants of both the ORN and mitral cells were set to $\tilde{\tau}_m \approx 10$ ms, with a threshold potential, $V_{th} = 50000$. The time constants of the excitatory synapses were set to $\tilde{\tau}_E \approx 4$ ms, whereas for the inhibitory synapses the time constants were set to $\tilde{\tau}_I \approx 16$ ms. For the ORNs, constant values randomly selected in a range between 500 and 1000, were used to represent a constant concentration of each odor stimulus. The total running time in terms of biological values is equivalent to 5 seconds at a sampling frequency of $f_{smp} = 10$ kHz. Although the clock frequency was set to $f_{clk} = 10$ MHz thus each run lasted for 5 ms of the FPGA processing time.

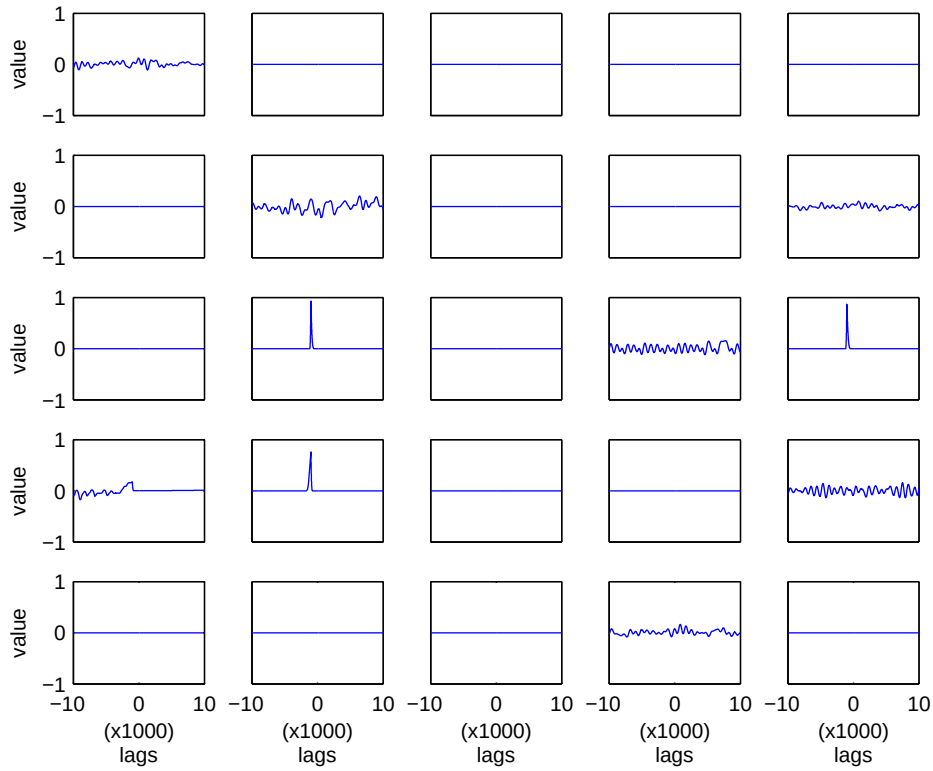

Figure H.51: Cross-correlation analysis for odour 4: trained weights vs. +60% difference weights. The Cross-correlation analysis was carried out between the response of the olfactory bulb of the trained weights and the weights minus a percentage of the difference between weight values and the limit range for the weights. Plots are sorted from left to right and from up to down, starting from the cross-corelation between for the first mitral cell (the first column and first row) up to the 25th mitral cell in the last column at the bottom. Plots with zero response result from Mitral cells which remain silent for these particular weight values. The time constants of both the ORN and mitral cells were set to $\tilde{\tau}_m \approx 10$ ms, with a threshold potential, $V_{th} = 50000$. The time constants of the excitatory synapses were set to $\tilde{\tau}_E \approx 4$ ms, whereas for the inhibitory synapses the time constants were set to $\tilde{\tau}_I \approx 16$ ms. For the ORNs, constant values randomly selected in a range between 500 and 1000, were used to represent a constant concentration of each odor stimulus. The total running time in terms of biological values is equivalent to 5 seconds at a sampling frequency of $f_{smp} = 10$ kHz. Although the clock frequency was set to $f_{clk} = 10$ MHz thus each run lasted for 5 ms of the FPGA processing time.

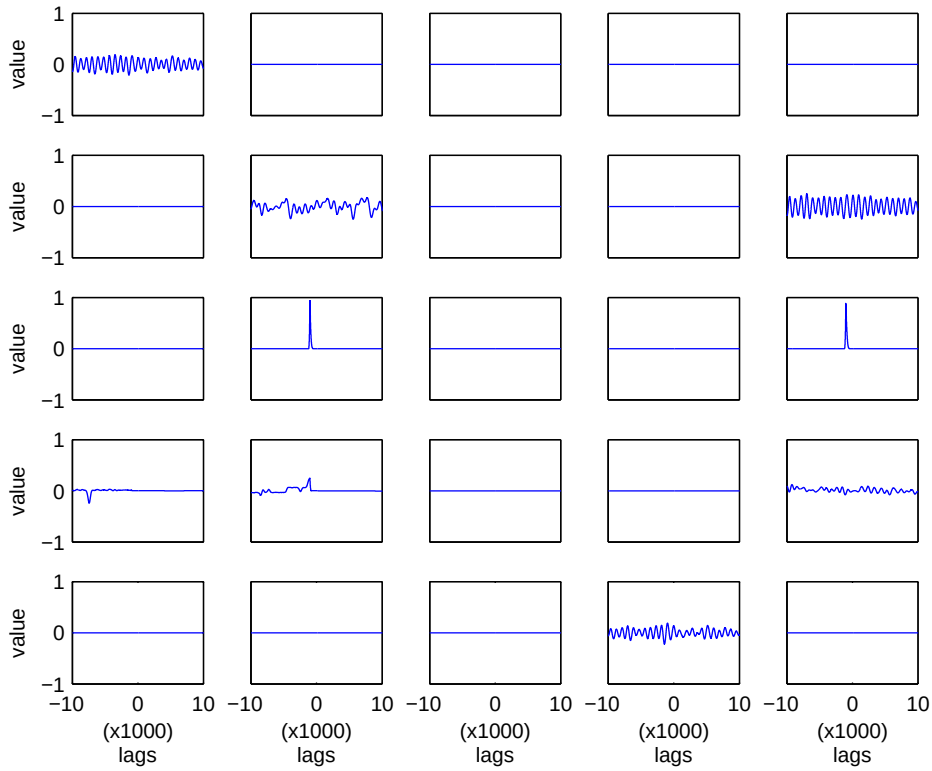

Figure H.52: Cross-correlation analysis for odour 4: trained weights vs. +80% difference weights. The Cross-correlation analysis was carried out between the response of the olfactory bulb of the trained weights and the weights minus a percentage of the difference between weight values and the limit range for the weights. Plots are sorted from left to right and from up to down, starting from the cross-corelation between for the first mitral cell (the first column and first row) up to the 25th mitral cell in the last column at the bottom. Plots with zero response result from Mitral cells which remain silent for these particular weight values. The time constants of both the ORN and mitral cells were set to $\tilde{\tau}_m \approx 10$ ms, with a threshold potential, $V_{th} = 50000$. The time constants of the excitatory synapses were set to $\tilde{\tau}_E \approx 4$ ms, whereas for the inhibitory synapses the time constants were set to $\tilde{\tau}_I \approx 16$ ms. For the ORNs, constant values randomly selected in a range between 500 and 1000, were used to represent a constant concentration of each odor stimulus. The total running time in terms of biological values is equivalent to 5 seconds at a sampling frequency of $f_{smp} = 10$ kHz. Although the clock frequency was set to $f_{clk} = 10$ MHz thus each run lasted for 5 ms of the FPGA processing time.

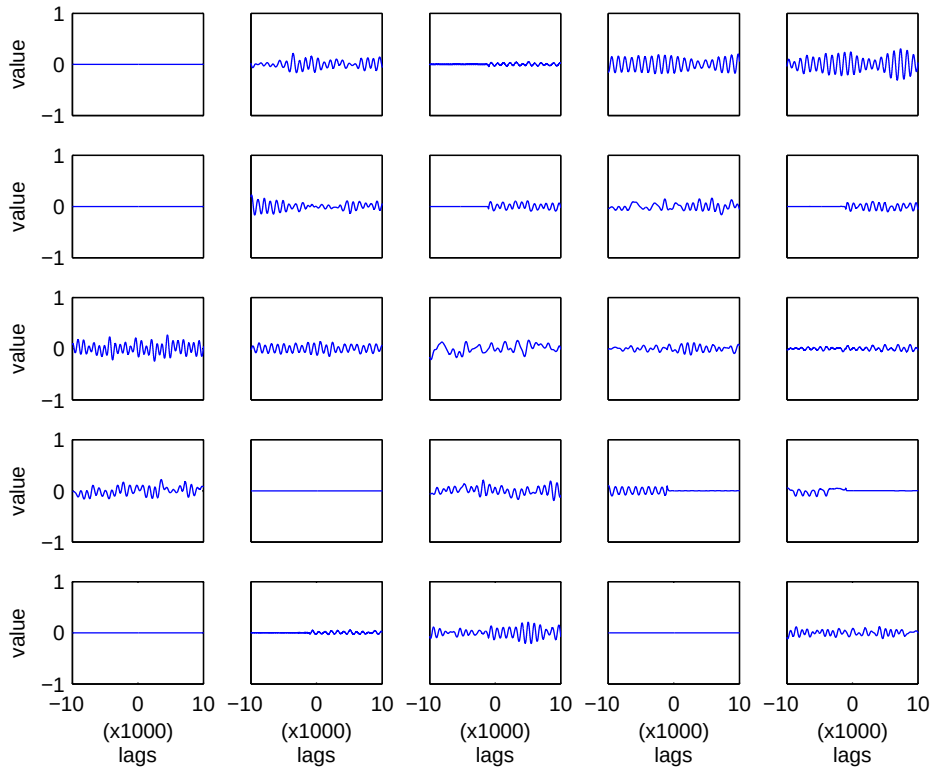

Figure H.53: Cross-correlation analysis for odour 5: trained weights vs. -80% difference weights. The Cross-correlation analysis was carried out between the response of the olfactory bulb of the trained weights and the weights minus a percentage of the difference between weight values and the limit range for the weights. Plots are sorted from left to right and from up to down, starting from the cross-corelation between for the first mitral cell (the first column and first row) up to the 25th mitral cell in the last column at the bottom. Plots with zero response result from Mitral cells which remain silent for these particular weight values. The time constants of both the ORN and mitral cells were set to $\tilde{\tau}_m \approx 10$ ms, with a threshold potential, $V_{th} = 50000$. The time constants of the excitatory synapses were set to $\tilde{\tau}_E \approx 4$ ms, whereas for the inhibitory synapses the time constants were set to $\tilde{\tau}_I \approx 16$ ms. For the ORNs, constant values randomly selected in a range between 500 and 1000, were used to represent a constant concentration of each odor stimulus. The total running time in terms of biological values is equivalent to 5 seconds at a sampling frequency of $f_{smp} = 10$ kHz. Although the clock frequency was set to $f_{clk} = 10$ MHz thus each run lasted for 5 ms of the FPGA processing time.

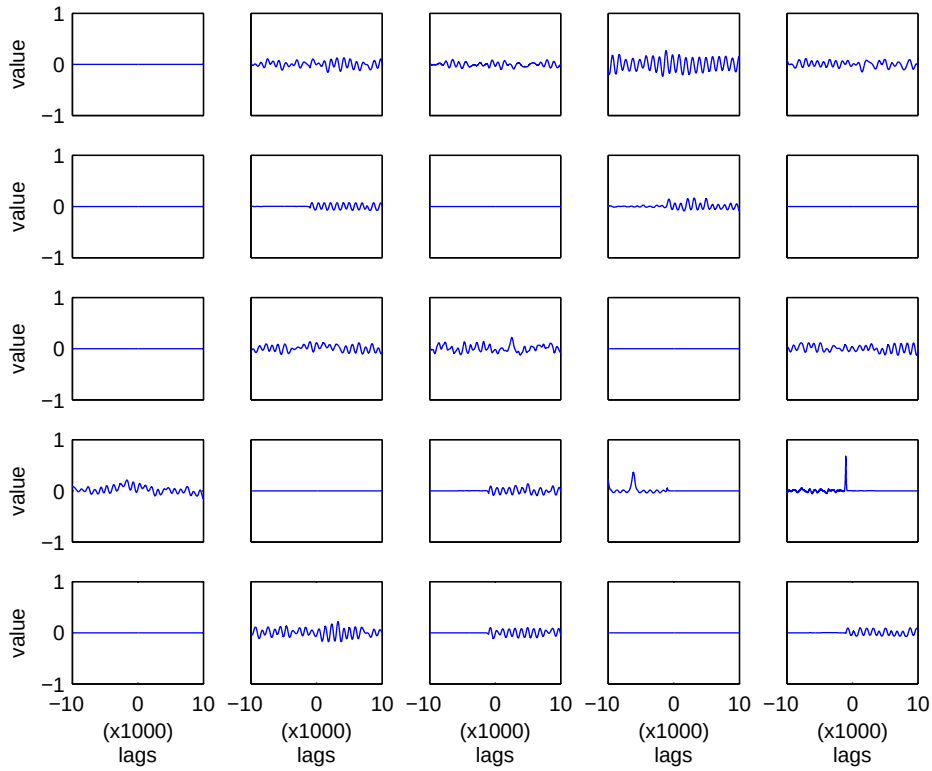

Figure H.54: Cross-correlation analysis for odour 5: trained weights vs. -60% difference weights. The Cross-correlation analysis was carried out between the response of the olfactory bulb of the trained weights and the weights minus a percentage of the difference between weight values and the limit range for the weights. Plots are sorted from left to right and from up to down, starting from the cross-corelation between for the first mitral cell (the first column and first row) up to the 25th mitral cell in the last column at the bottom. Plots with zero response result from Mitral cells which remain silent for these particular weight values. The time constants of both the ORN and mitral cells were set to $\tilde{\tau}_m \approx 10$ ms, with a threshold potential, $V_{th} = 50000$. The time constants of the excitatory synapses were set to $\tilde{\tau}_E \approx 4$ ms, whereas for the inhibitory synapses the time constants were set to $\tilde{\tau}_I \approx 16$ ms. For the ORNs, constant values randomly selected in a range between 500 and 1000, were used to represent a constant concentration of each odor stimulus. The total running time in terms of biological values is equivalent to 5 seconds at a sampling frequency of $f_{smp} = 10$ kHz. Although the clock frequency was set to $f_{clk} = 10$ MHz thus each run lasted for 5 ms of the FPGA processing time.

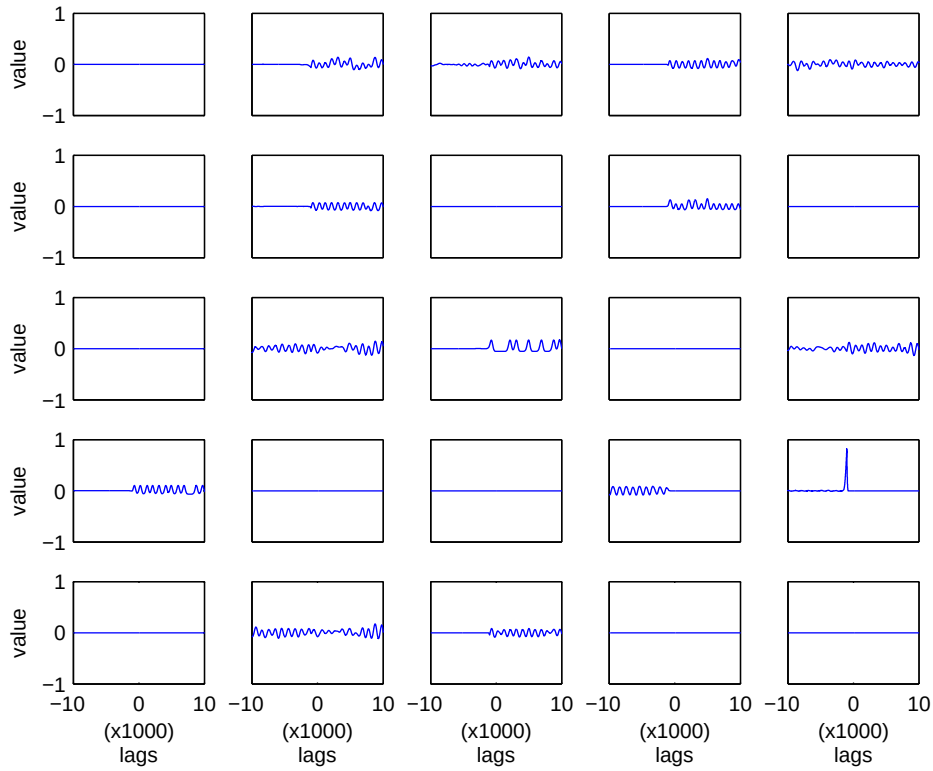

Figure H.55: Cross-correlation analysis for odour 5: trained weights vs. -40% difference weights. The Cross-correlation analysis was carried out between the response of the olfactory bulb of the trained weights and the weights minus a percentage of the difference between weight values and the limit range for the weights. Plots are sorted from left to right and from up to down, starting from the cross-corelation between for the first mitral cell (the first column and first row) up to the 25th mitral cell in the last column at the bottom. Plots with zero response result from Mitral cells which remain silent for these particular weight values. The time constants of both the ORN and mitral cells were set to $\tilde{\tau}_m \approx 10$ ms, with a threshold potential, $V_{th} = 50000$. The time constants of the excitatory synapses were set to $\tilde{\tau}_E \approx 4$ ms, whereas for the inhibitory synapses the time constants were set to $\tilde{\tau}_I \approx 16$ ms. For the ORNs, constant values randomly selected in a range between 500 and 1000, were used to represent a constant concentration of each odor stimulus. The total running time in terms of biological values is equivalent to 5 seconds at a sampling frequency of $f_{smp} = 10$ kHz. Although the clock frequency was set to $f_{clk} = 10$ MHz thus each run lasted for 5 ms of the FPGA processing time.

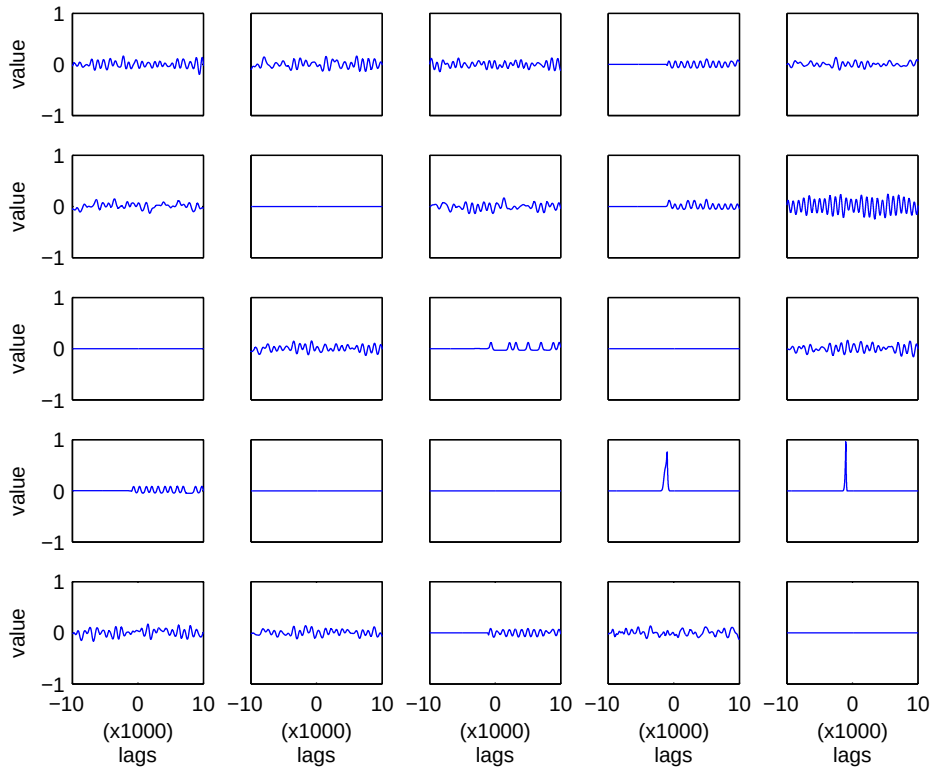

Figure H.56: Cross-correlation analysis for odour 5: trained weights vs. -20% difference weights. The Cross-correlation analysis was carried out between the response of the olfactory bulb of the trained weights and the weights minus a percentage of the difference between weight values and the limit range for the weights. Plots are sorted from left to right and from up to down, starting from the cross-corelation between for the first mitral cell (the first column and first row) up to the 25th mitral cell in the last column at the bottom. Plots with zero response result from Mitral cells which remain silent for these particular weight values. The time constants of both the ORN and mitral cells were set to $\tilde{\tau}_m \approx 10$ ms, with a threshold potential, $V_{th} = 50000$. The time constants of the excitatory synapses were set to $\tilde{\tau}_E \approx 4$ ms, whereas for the inhibitory synapses the time constants were set to $\tilde{\tau}_I \approx 16$ ms. For the ORNs, constant values randomly selected in a range between 500 and 1000, were used to represent a constant concentration of each odor stimulus. The total running time in terms of biological values is equivalent to 5 seconds at a sampling frequency of $f_{smp} = 10$ kHz. Although the clock frequency was set to $f_{clk} = 10$ MHz thus each run lasted for 5 ms of the FPGA processing time.

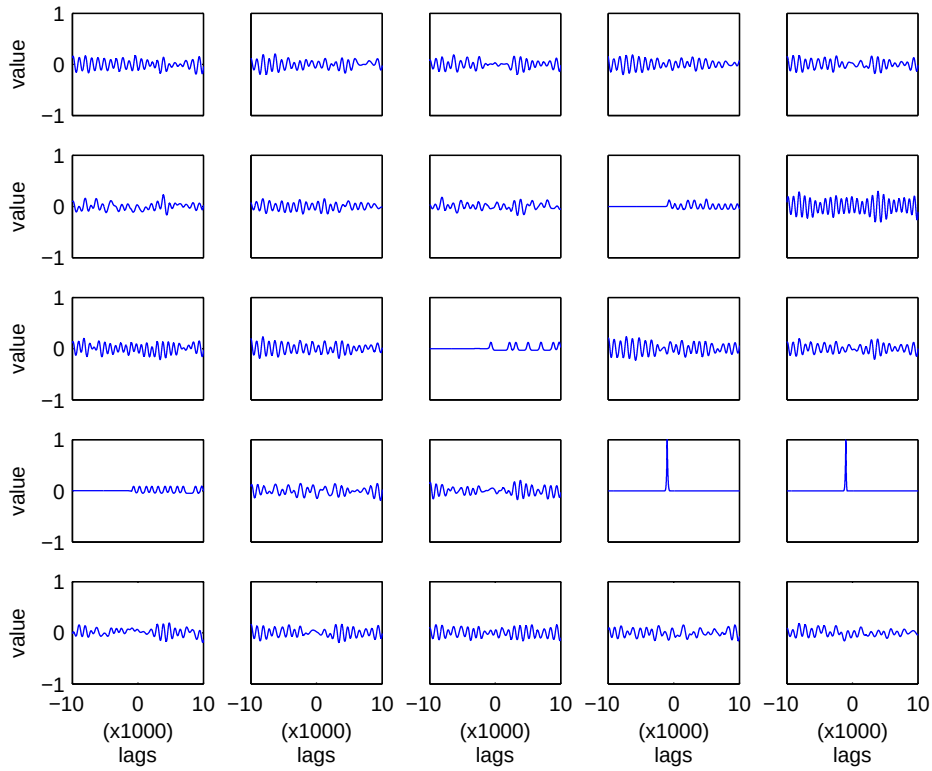

Figure H.57: Cross-correlation analysis for odour 5: trained weights vs. -10% difference weights. The Cross-correlation analysis was carried out between the response of the olfactory bulb of the trained weights and the weights minus a percentage of the difference between weight values and the limit range for the weights. Plots are sorted from left to right and from up to down, starting from the cross-corelation between for the first mitral cell (the first column and first row) up to the 25th mitral cell in the last column at the bottom. Plots with zero response result from Mitral cells which remain silent for these particular weight values. The time constants of both the ORN and mitral cells were set to $\tilde{\tau}_m \approx 10$ ms, with a threshold potential, $V_{th} = 50000$. The time constants of the excitatory synapses were set to $\tilde{\tau}_E \approx 4$ ms, whereas for the inhibitory synapses the time constants were set to $\tilde{\tau}_I \approx 16$ ms. For the ORNs, constant values randomly selected in a range between 500 and 1000, were used to represent a constant concentration of each odor stimulus. The total running time in terms of biological values is equivalent to 5 seconds at a sampling frequency of $f_{smp} = 10$ kHz. Although the clock frequency was set to $f_{clk} = 10$ MHz thus each run lasted for 5 ms of the FPGA processing time.

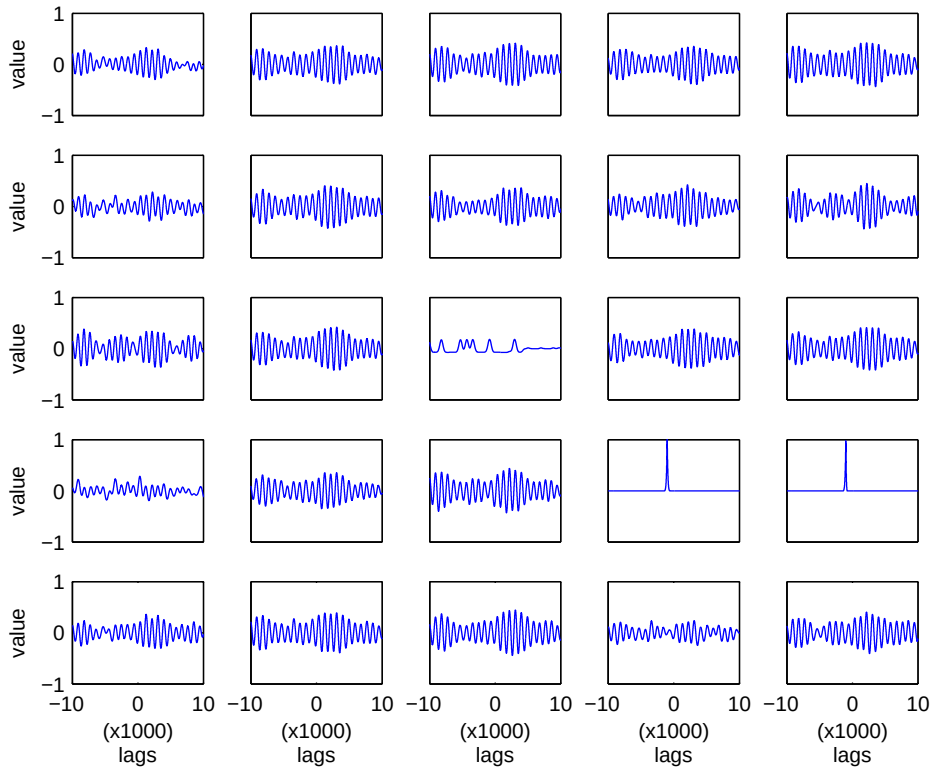

Figure H.58: Cross-correlation analysis for odour 5: trained weights vs. -4% difference weights. The Cross-correlation analysis was carried out between the response of the olfactory bulb of the trained weights and the weights minus a percentage of the difference between weight values and the limit range for the weights. Plots are sorted from left to right and from up to down, starting from the cross-corelation between for the first mitral cell (the first column and first row) up to the 25th mitral cell in the last column at the bottom. Plots with zero response result from Mitral cells which remain silent for these particular weight values. The time constants of both the ORN and mitral cells were set to $\tilde{\tau}_m \approx 10$ ms, with a threshold potential, $V_{th} = 50000$. The time constants of the excitatory synapses were set to $\tilde{\tau}_E \approx 4$ ms, whereas for the inhibitory synapses the time constants were set to $\tilde{\tau}_I \approx 16$ ms. For the ORNs, constant values randomly selected in a range between 500 and 1000, were used to represent a constant concentration of each odor stimulus. The total running time in terms of biological values is equivalent to 5 seconds at a sampling frequency of $f_{smp} = 10$ kHz. Although the clock frequency was set to $f_{clk} = 10$ MHz thus each run lasted for 5 ms of the FPGA processing time.

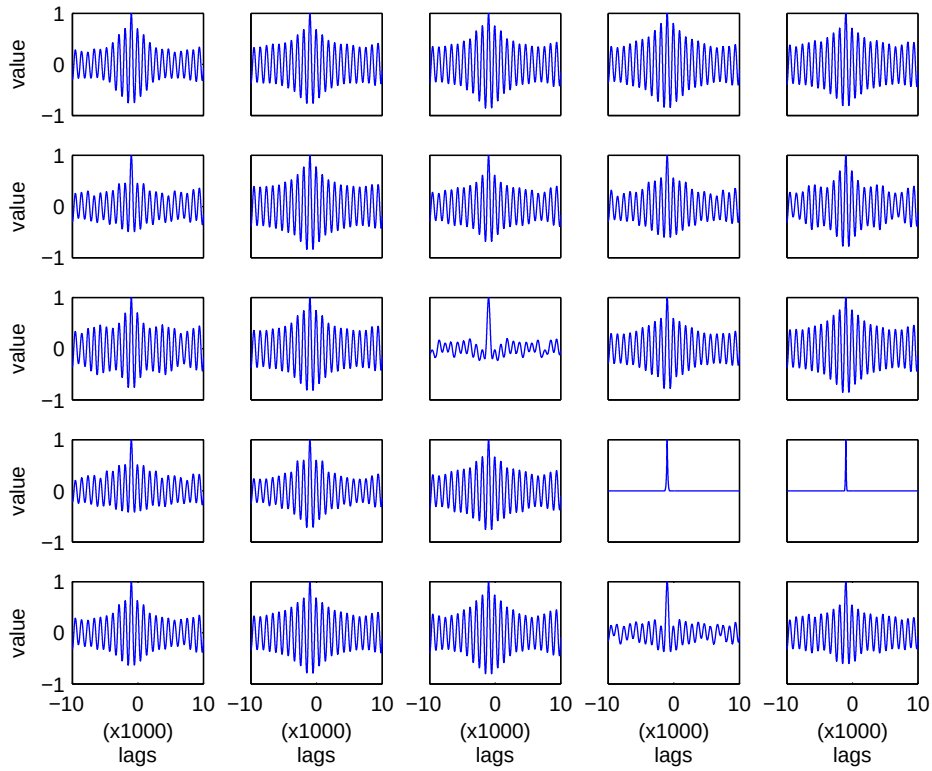

Figure H.59: Cross-correlation analysis for odour 5: trained weights vs. 0% difference weights. The Cross-correlation analysis was carried out between the response of the olfactory bulb of the trained weights and the weights minus a percentage of the difference between weight values and the limit range for the weights. Plots are sorted from left to right and from up to down, starting from the cross-corelation between for the first mitral cell (the first column and first row) up to the 25th mitral cell in the last column at the bottom. Plots with zero response result from Mitral cells which remain silent for these particular weight values. The time constants of both the ORN and mitral cells were set to $\tilde{\tau}_m \approx 10$ ms, with a threshold potential, $V_{th} = 50000$. The time constants of the excitatory synapses were set to $\tilde{\tau}_E \approx 4$ ms, whereas for the inhibitory synapses the time constants were set to $\tilde{\tau}_I \approx 16$ ms. For the ORNs, constant values randomly selected in a range between 500 and 1000, were used to represent a constant concentration of each odor stimulus. The total running time in terms of biological values is equivalent to 5 seconds at a sampling frequency of $f_{smp} = 10$ kHz. Although the clock frequency was set to $f_{clk} = 10$ MHz thus each run lasted for 5 ms of the FPGA processing time.

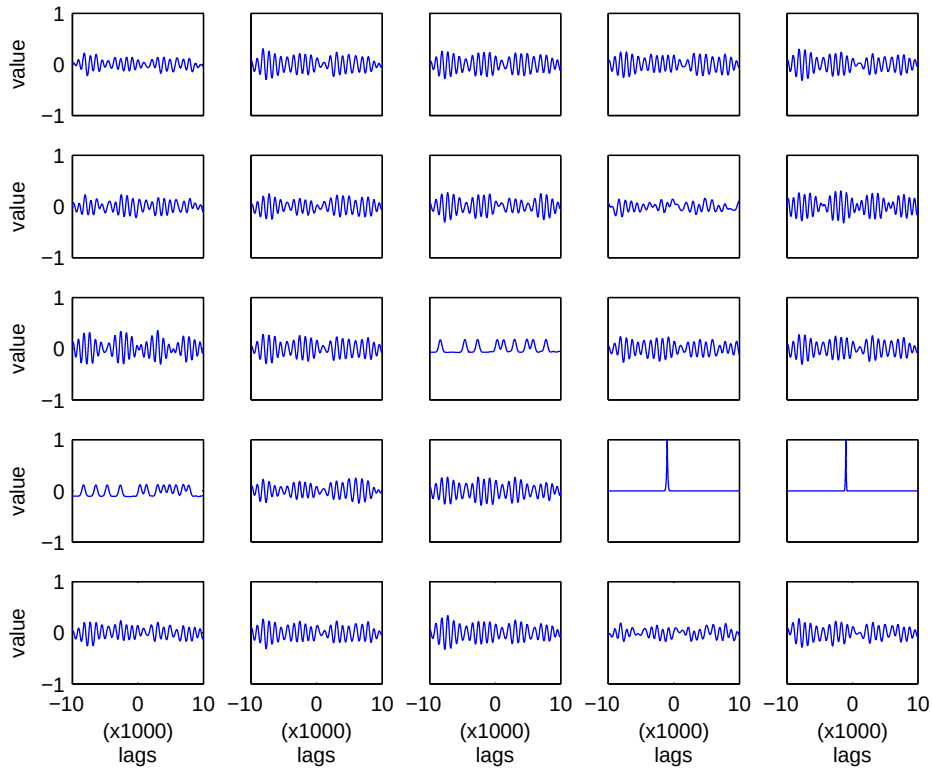

Figure H.60: Cross-correlation analysis for odour 5: trained weights vs. +4% difference weights. The Cross-correlation analysis was carried out between the response of the olfactory bulb of the trained weights and the weights minus a percentage of the difference between weight values and the limit range for the weights. Plots are sorted from left to right and from up to down, starting from the cross-corelation between for the first mitral cell (the first column and first row) up to the 25th mitral cell in the last column at the bottom. Plots with zero response result from Mitral cells which remain silent for these particular weight values. The time constants of both the ORN and mitral cells were set to $\tilde{\tau}_m \approx 10$ ms, with a threshold potential, $V_{th} = 50000$. The time constants of the excitatory synapses were set to $\tilde{\tau}_E \approx 4$ ms, whereas for the inhibitory synapses the time constants were set to $\tilde{\tau}_I \approx 16$ ms. For the ORNs, constant values randomly selected in a range between 500 and 1000, were used to represent a constant concentration of each odor stimulus. The total running time in terms of biological values is equivalent to 5 seconds at a sampling frequency of $f_{smp} = 10$ kHz. Although the clock frequency was set to $f_{clk} = 10$ MHz thus each run lasted for 5 ms of the FPGA processing time.

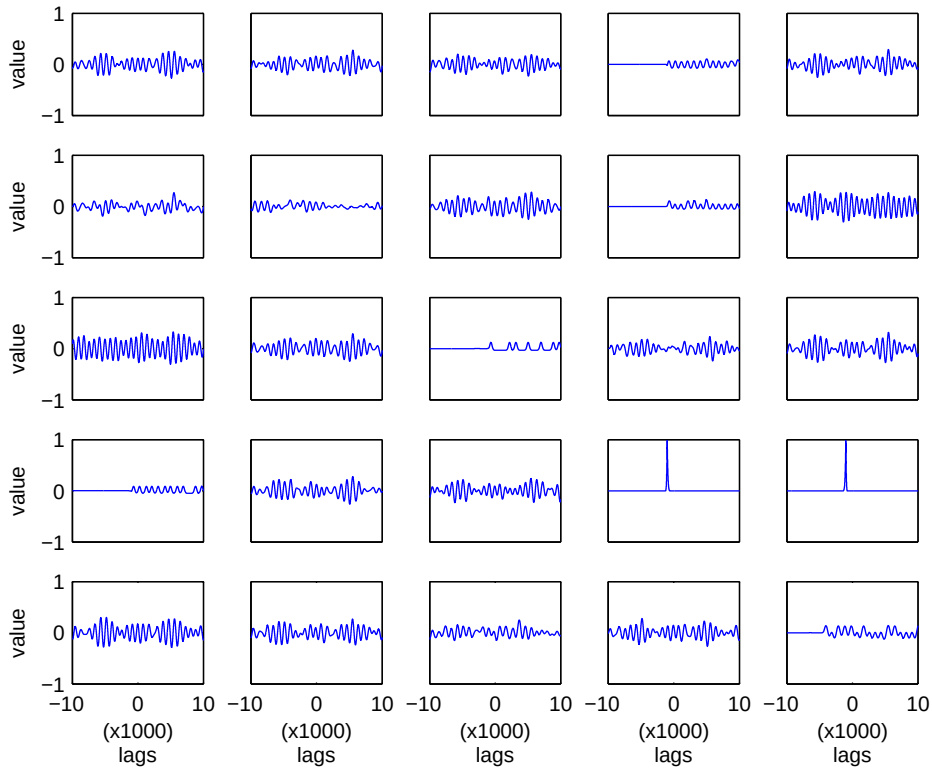

Figure H.61: Cross-correlation analysis for odour 5: trained weights vs. +10% difference weights. The Cross-correlation analysis was carried out between the response of the olfactory bulb of the trained weights and the weights minus a percentage of the difference between weight values and the limit range for the weights. Plots are sorted from left to right and from up to down, starting from the cross-corelation between for the first mitral cell (the first column and first row) up to the 25th mitral cell in the last column at the bottom. Plots with zero response result from Mitral cells which remain silent for these particular weight values. The time constants of both the ORN and mitral cells were set to $\tilde{\tau}_m \approx 10$ ms, with a threshold potential, $V_{th} = 50000$. The time constants of the excitatory synapses were set to $\tilde{\tau}_E \approx 4$ ms, whereas for the inhibitory synapses the time constants were set to $\tilde{\tau}_I \approx 16$ ms. For the ORNs, constant values randomly selected in a range between 500 and 1000, were used to represent a constant concentration of each odor stimulus. The total running time in terms of biological values is equivalent to 5 seconds at a sampling frequency of $f_{smp} = 10$ kHz. Although the clock frequency was set to $f_{clk} = 10$ MHz thus each run lasted for 5 ms of the FPGA processing time.

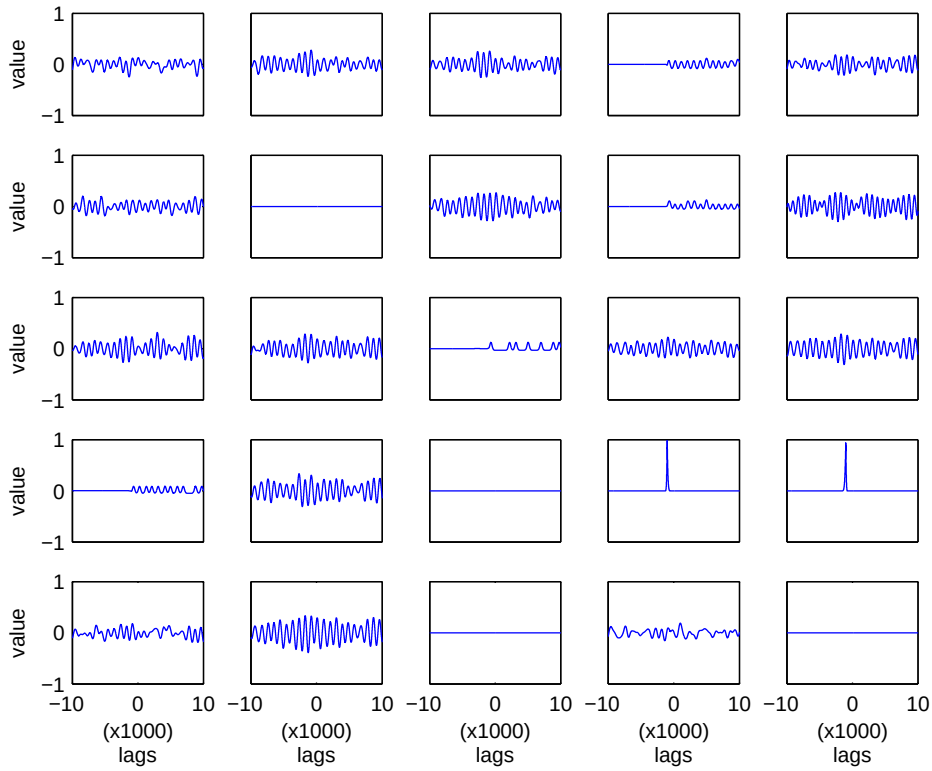

Figure H.62: Cross-correlation analysis for odour 5: trained weights vs. +20% difference weights. The Cross-correlation analysis was carried out between the response of the olfactory bulb of the trained weights and the weights minus a percentage of the difference between weight values and the limit range for the weights. Plots are sorted from left to right and from up to down, starting from the cross-corelation between for the first mitral cell (the first column and first row) up to the 25th mitral cell in the last column at the bottom. Plots with zero response result from Mitral cells which remain silent for these particular weight values. The time constants of both the ORN and mitral cells were set to $\tilde{\tau}_m \approx 10$ ms, with a threshold potential, $V_{th} = 50000$. The time constants of the excitatory synapses were set to $\tilde{\tau}_E \approx 4$ ms, whereas for the inhibitory synapses the time constants were set to $\tilde{\tau}_I \approx 16$ ms. For the ORNs, constant values randomly selected in a range between 500 and 1000, were used to represent a constant concentration of each odor stimulus. The total running time in terms of biological values is equivalent to 5 seconds at a sampling frequency of $f_{smp} = 10$ kHz. Although the clock frequency was set to $f_{clk} = 10$ MHz thus each run lasted for 5 ms of the FPGA processing time.

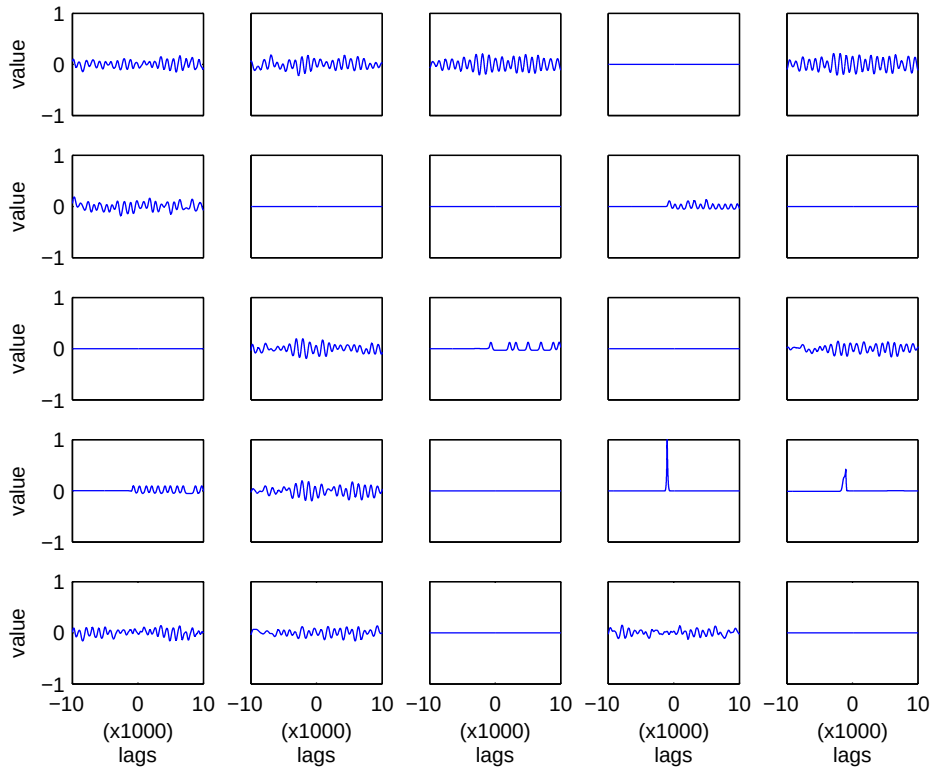

Figure H.63: Cross-correlation analysis for odour 5: trained weights vs. +40% difference weights. The Cross-correlation analysis was carried out between the response of the olfactory bulb of the trained weights and the weights minus a percentage of the difference between weight values and the limit range for the weights. Plots are sorted from left to right and from up to down, starting from the cross-corelation between for the first mitral cell (the first column and first row) up to the 25th mitral cell in the last column at the bottom. Plots with zero response result from Mitral cells which remain silent for these particular weight values. The time constants of both the ORN and mitral cells were set to $\tilde{\tau}_m \approx 10$ ms, with a threshold potential, $V_{th} = 50000$. The time constants of the excitatory synapses were set to $\tilde{\tau}_E \approx 4$ ms, whereas for the inhibitory synapses the time constants were set to $\tilde{\tau}_I \approx 16$ ms. For the ORNs, constant values randomly selected in a range between 500 and 1000, were used to represent a constant concentration of each odor stimulus. The total running time in terms of biological values is equivalent to 5 seconds at a sampling frequency of $f_{smp} = 10$ kHz. Although the clock frequency was set to $f_{clk} = 10$ MHz thus each run lasted for 5 ms of the FPGA processing time.

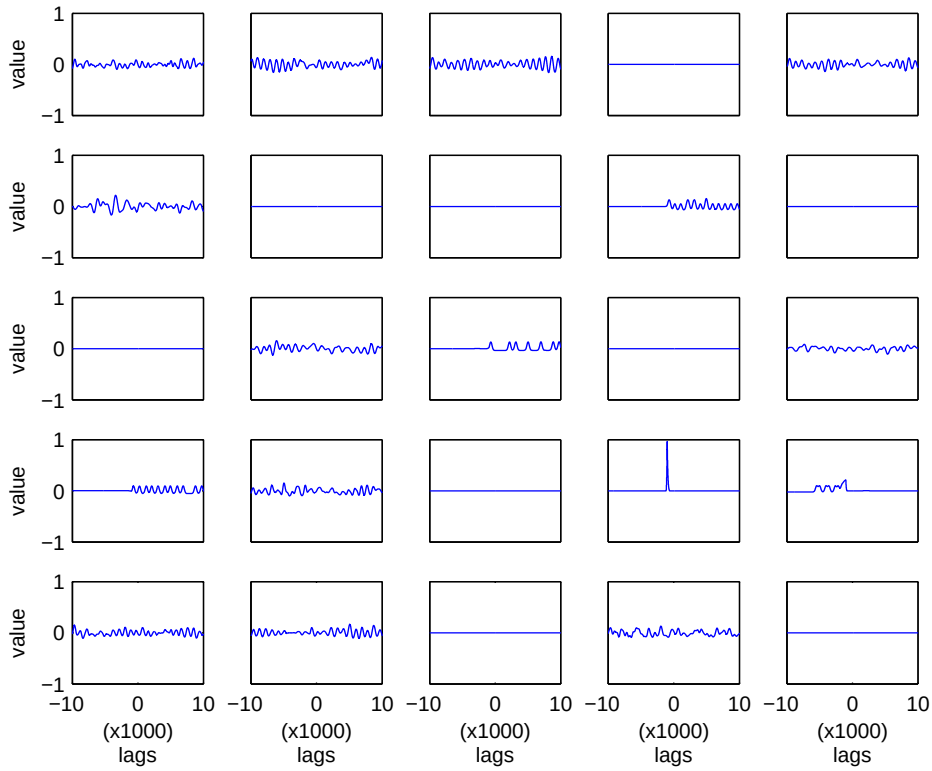

Figure H.64: Cross-correlation analysis for odour 5: trained weights vs. +60% difference weights. The Cross-correlation analysis was carried out between the response of the olfactory bulb of the trained weights and the weights minus a percentage of the difference between weight values and the limit range for the weights. Plots are sorted from left to right and from up to down, starting from the cross-corelation between for the first mitral cell (the first column and first row) up to the 25th mitral cell in the last column at the bottom. Plots with zero response result from Mitral cells which remain silent for these particular weight values. The time constants of both the ORN and mitral cells were set to $\tilde{\tau}_m \approx 10$ ms, with a threshold potential, $V_{th} = 50000$. The time constants of the excitatory synapses were set to $\tilde{\tau}_E \approx 4$ ms, whereas for the inhibitory synapses the time constants were set to $\tilde{\tau}_I \approx 16$ ms. For the ORNs, constant values randomly selected in a range between 500 and 1000, were used to represent a constant concentration of each odor stimulus. The total running time in terms of biological values is equivalent to 5 seconds at a sampling frequency of $f_{smp} = 10$ kHz. Although the clock frequency was set to $f_{clk} = 10$ MHz thus each run lasted for 5 ms of the FPGA processing time.

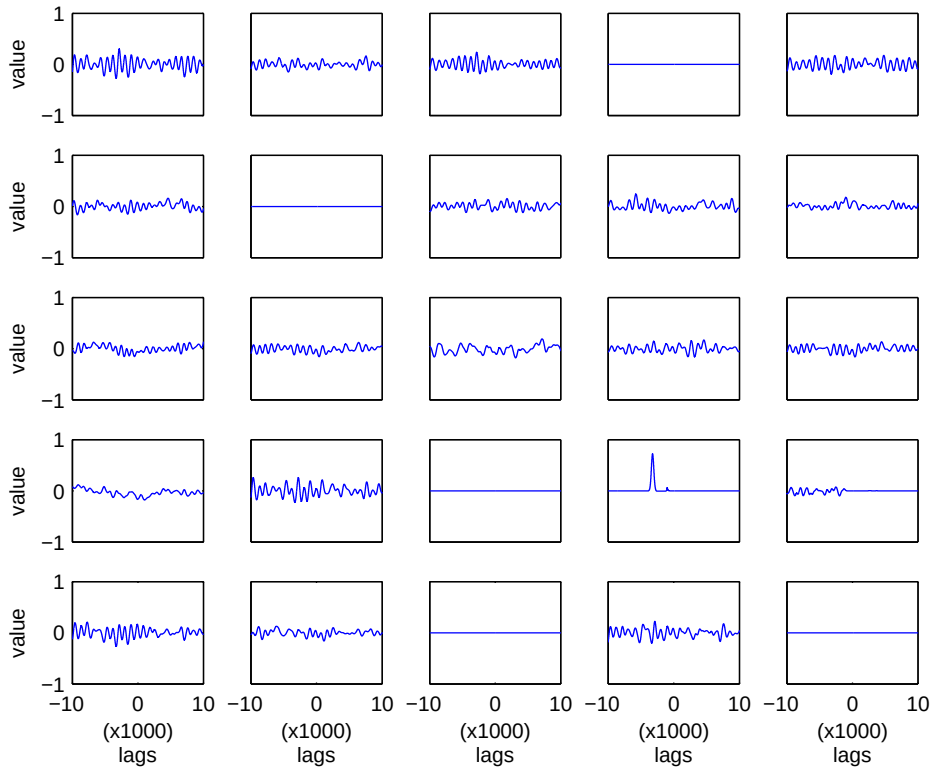

Figure H.65: Cross-correlation analysis for odour 5: trained weights vs. +80% difference weights. The Cross-correlation analysis was carried out between the response of the olfactory bulb of the trained weights and the weights minus a percentage of the difference between weight values and the limit range for the weights. Plots are sorted from left to right and from up to down, starting from the cross-corelation between for the first mitral cell (the first column and first row) up to the 25th mitral cell in the last column at the bottom. Plots with zero response result from Mitral cells which remain silent for these particular weight values. The time constants of both the ORN and mitral cells were set to $\tilde{\tau}_m \approx 10$ ms, with a threshold potential, $V_{th} = 50000$. The time constants of the excitatory synapses were set to $\tilde{\tau}_E \approx 4$ ms, whereas for the inhibitory synapses the time constants were set to $\tilde{\tau}_I \approx 16$ ms. For the ORNs, constant values randomly selected in a range between 500 and 1000, were used to represent a constant concentration of each odor stimulus. The total running time in terms of biological values is equivalent to 5 seconds at a sampling frequency of $f_{smp} = 10$ kHz. Although the clock frequency was set to $f_{clk} = 10$ MHz thus each run lasted for 5 ms of the FPGA processing time.